INFORMATION TO USERS

While the most advanced technology has been used to photograph and reproduce this manuscript, the quality of the reproduction is heavily dependent upon the quality of the material submitted. For example:

- Manuscript pages may have indistinct print. In such cases, the best available copy has been filmed.
- Manuscripts may not always be complete. In such cases, a note will indicate that it is not possible to obtain missing pages.
- Copyrighted material may have been removed from the manuscript. In such cases, a note will indicate the deletion.

Oversize materials (e.g., maps, drawings, and charts) are photographed by sectioning the original, beginning at the upper left-hand corner and continuing from left to right in equal sections with small overlaps. Each oversize page is also filmed as one exposure and is available, for an additional charge, as a standard 35mm slide or as a 17"x 23" black and white photographic print.

Most photographs reproduce acceptably on positive microfilm or microfiche but lack the clarity on xerographic copies made from the microfilm. For an additional charge, 35mm slides of 6"x 9" black and white photographic prints are available for any photographs or illustrations that cannot be reproduced satisfactorily by xerography.

Order Number 8727922

Asymptotic giant branch populations in composite stellar systems

Cook, Kem Holland, Ph.D.

The University of Arizona, 1987

U·M·I
300 N. Zeeb Rd.
Ann Arbor, MI 48106

PLEASE NOTE:

In all cases this material has been filmed in the best possible way from the available copy. Problems encountered with this document have been identified here with a check mark __✓__.

1. Glossy photographs or pages _____
2. Colored illustrations, paper or print _____
3. Photographs with dark background __✓__
4. Illustrations are poor copy _____
5. Pages with black marks, not original copy __✓__
6. Print shows through as there is text on both sides of page _____
7. Indistinct, broken or small print on several pages __✓__
8. Print exceeds margin requirements _____
9. Tightly bound copy with print lost in spine _____
10. Computer printout pages with indistinct print _____
11. Page(s) _____ lacking when material received, and not available from school or author.
12. Page(s) _____ seem to be missing in numbering only as text follows.
13. Two pages numbered _____. Text follows.
14. Curling and wrinkled pages _____
15. Dissertation contains pages with print at a slant, filmed as received _____
16. Other _____

_____

_____

University
Microfilms
International

ASYMPTOTIC GIANT BRANCH POPULATIONS IN COMPOSITE STELLAR SYSTEMS

by

Kem Holland Cook

A Dissertation Submitted to the Faculty of the

DEPARTMENT OF ASTRONOMY

In Partial Fulfillment of the Requirements
For the Degree of

DOCTOR OF PHILOSOPHY

In the Graduate College

THE UNIVERSITY OF ARIZONA

1 9 8 7

THE UNIVERSITY OF ARIZONA
GRADUATE COLLEGE

As members of the Final Examination Committee, we certify that we have read the dissertation prepared by Kem Holland Cook

entitled Asymptotic Giant Branch Populations in Composite Stellar Systems

and recommend that it be accepted as fulfilling the dissertation requirement for the Degree of Doctor of Philosophy.

P. A. Strittmatter	6 May 1987 Date
James W. Liebert	6 May 1987 Date
Raymond F. White	6 May 1987 Date
Edward W Olszewski	6 May 87 Date
S. White	6 May 1987 Date

Final approval and acceptance of this dissertation is contingent upon the candidate's submission of the final copy of the dissertation to the Graduate College.

I hereby certify that I have read this dissertation prepared under my direction and recommend that it be accepted as fulfilling the dissertation requirement.

Marc Aaronson by PAS Dissertation Director	May 6, 1987 Date

STATEMENT BY AUTHOR

This dissertation has been submitted in partial fulfillment of requirements for an advanced degree at The University of Arizona and is deposited in the University Library to be made available to borrowers under rules of the Library.

Brief quotations from this dissertation are allowable without special permission, provided that accurate acknowledgment of source is made. Requests for permission for extended quotation from or reproduction of this manuscript in whole or in part may be granted by the head of the major department or the Dean of the Graduate College when in his or her judgment the proposed use of the material is in the interests of scholarship. In all other instances, however, permission must be obtained from the author.

SIGNED: Ken Holland Cook

To Jeanne and Keegan

ACKNOWLEDGEMENTS

It is with sorrow and a deep sense of loss that I write these acknowledgements— my dissertation advisor and friend, Marc Aaronson, died six days before my oral defense of this dissertation. Marc's enthusiasm for science and his joy for doing astronomy guided me through many periods of doubt about the wisdom of pursuing a second Ph.D. I would like to acknowledge his scientific guidance, his help and encouragement, his technical skill, his humor and warmth. Marc's broad knowledge of astronomy and his meticulous observing skills will be a constant example for me. I miss Professor Marc Aaronson, the astronomer and Marc, my friend.

I owe special thanks to Mike Keane and Ed Olszewski. These two, more than others, have had to put up with my foibles. They were always there with a helping hand and the final production of this dissertation is due in no small part to their help.

I would like to thank the Steward Observatory community for its supportive atmosphere and friendship. I would like to particularly thank Roc Cutri, Dave Dearborn, Jill Bechtold, Steve West, Jim Liebert, Craig Foltz, Bill Latter, John McGraw, Mark Cornell, Mike Lesser, and Chris McAlary for their personal and scientific enrichment of my graduate experience. Jim Liebert deserves special acknowledgement for his friendship, encouragement and teaching. Peter Strittmatter and Charlie Lada were tolerant advisors and friends throughout my constant petitions for changing the system.

Considerable credit must be given to the National Optical Astronomy Observatories for the use of their facilities for the collection and reduction of essentially all of the data in this dissertation. Particular thanks and recognition are due Jeannette Barnes for her unflagging devotion in making sure that not just I, but all observers get their data reduced.

Mount Wilson and Las Campanas Observatories provided a stimulating atmosphere in which to finish this dissertation. I thank its staff and director for their support and understanding. I would also like to acknowledge Steward Observatory, the University of Arizona Summer Research Awards program and the National Science Foudation Grant AST 83-16629 for financial support.

Finally, I thank my family, Jeanne and Keegan, my parents and Bobbie Cook, and Ed O. for their personal support and understanding of what many might consider a frivolous endeavor—a second Ph.D.

TABLE OF CONTENTS

LIST OF ILLUSTRATIONS viii

LIST OF TABLES xii

ABSTRACT xiii

1. THE ASYMPTOTIC GIANT BRANCH: THEORY AND OBSERVATIONS 1

Stellar Evolution Theory of the Asymptotic Giant Branch 2
Observational Studies of AGB Evolution 11

2. DATA COLLECTION AND REDUCTION 20

Photoelectric Photometry 23
CCD Photometry 30
Synthetic Aperture Photometry 36
Broad-Band Transformations 39
Intermediate-Band Transformations 48
Bright Star CCD Photometry 51
Globular Cluster Photometry 51
Point-Spread Function Photometry 53
Completeness Tests 58
Reddening 59
Summary 60

3. THE 77–81 INTERMEDIATE-BAND PHOTOMETRIC SYSTEM . . 61

Theoretical Analysis 64
Defining the System 69
Extinction 70
Standards 72
Field Giants 80
Globular Cluster Giants 90
M 15 96
M 92 96
NGC 4147 101

M 3 101
M 5 106
M 4 106
NGC 6402 109
NGC 6712 112
M 107 116
NGC 6366 121
M 69 121
M 71 125
The Metallicity Calibration 128
Baade's Window 135
Blanco's Results 146
Summary 154

4. THE SAGITTARIUS DWARF IRREGULAR GALAXY 157

Completeness 167
Differential Luminosity Function 171
Bright Blue Stars 184
Bright Red Stars 193
Carbon Stars in Sagdig 199
Distance 213
Summary 214

5. CONCLUSIONS 216

APPENDIX A: 222

APPENDIX B: 234

APPENDIX C: 242

REFERENCES 247

LIST OF ILLUSTRATIONS

Figure Page

1. Color Residuals of the Photoelectric Photometry Transformation . 28
2. Color Residuals from the Night of August 30, 1984 49
3. Color Residuals from the Night of June 9, 1985 50
4. The Position of the 77 and 81 Passbands 63
5. Theoretical Color-Color Diagram of a Black Body 67
6. Color-Color Diagram of Bright Stars on the 77–81 System 79
7. The 77–81 Color Compared to the Carbon Richness Class 81
8. Color-Color Diagram of Solar Neighborhood Giants 84
9. Comparison of D(7120) to 77–81 86
10. The 77–81 Color as a Function of M Type 89

11a. Color-Magnitude Diagram of M 15 97
11b. Color-Color Diagram of M 15 98
12a. Color-Magnitude Diagram of M 92 99
12b. Color-Magnitude Diagram of M 92 100
13a. Color-Magnitude Diagram of NGC 4147 102
13b. Color-Color Diagram of NGC 4147 103
14a. Color-Magnitude Diagram of M 3 104
14b. Color-Color Diagram of M 3 105
15a. Color-Magnitude of M 5 107
15b. Color-Color Diagram of M 5 108

Figure Page

16a. Color-Magnitude Diagram of M 4 110

16b. Color-Color Diagram of M 4 111

17a. Color-Magnitude Diagram of NGC 6402 113

17b. Color-Color Diagram of NGC 6402 114

18a. Color-Magnitude Diagram of NGC 6712 117

18b. Color-Color Diagram of NGC 6712 118

19a. Color-Magnitude Diagram of M 107 119

19b. Color-Color Diagram of M 107 120

20a. Color-Magnitude Diagram of NGC 6366 122

20b. Color-Color Diagram of NGC 6366 123

21a. Color-Magnitude of M 69 126

21b. Color-Color Diagram of M 69 127

22a. Color-Magnitude Diagram of M 71 129

22b. Color-Color Diagram of M 71 130

23a. $(V-I)_{0.2}$ as a Function of [Fe/H] on Webbink's Scale 131

23b. $(V-I)_{0.2}$ as a Function of [Fe/H] on Zinn and West's Scale . . . 132

24. I band CCD Frame of Baade's Window Field 137

25. Completeness as a Function of I Magnitude in Baade's Window . 138

26. Color-Magnitude Diagram of the Baade's Window Field 140

27. Color-Color Diagram of the Baade's Window Field 141

28a. I Luminosity Distribution for the Baade's Window Field 142

28b. I Luminosity Distribution of Baade's Window
Stars with $77-81 > 0.21$. 143

29. Mean TiO Tracks for 4 Systems with Extended TiO Tracks . . . 147

30. Comparison of I Photometry in Baade's Window 151

Figure Page

31. 77−81 as a Function of Blanco's M type in Baade's Window . . 153
32. Comparison of V Photometry in Baade's Window 155
33. V Band Image of Sagdig 161
34. The Sagdig Field with the Stellar Images Subtracted 162
35. V band CCD frame of the CF1 Field 163
36. Completeness as a Function of Dereddened V mag. 165
37. Color-Magnitude Diagram of the South Galactic Cap 170
38a. V−I Distribution of Stars in Sagdig and CF1 172
38b. V−I Distribution of Stars in the South Galactic Cap 173
39a. Dereddened V, V−I Color-Magnitude Diagram for Sagdig 174
39a. Dereddened V, V−I Color-Magnitude Diagram for CF1 175
40a. Dereddened I, V−I Color-Magnitude Diagram for Sagdig 176
40a. Dereddened I, V−I Color-Magnitude Diagram for CF1 177
41b. Dereddened Color-Color Diagram of Sagdig 178
41b. Dereddened Color-Color Diagram of CF1 179
42. V Luminosity Distribution of the Sagdig and CF1 Fields 180
43. I Luminosity Distribution of the Sagdig and CF1 Fields 181
44. V−I Distribution fo the Sagdig and CF1 Fields 183
45. Dereddened, Differential, V Luminosity Function of Sagdig 185
46. Corrected Differential I Luminosity Function of Sagdig 186
47. Positions of Blue Stars in the Sagdig Field 189
48. Positions of the Brightest Blue Stars in Sagdig 190
49. $< M_B(3) >$ as a Function of Parent Galaxy Luminosity 192
50. $15M_\odot$ Evolutionary Track Compared to the Sagdig Data 194

Figure Page

51. $< M_V(3) >$ as a Function of Parent Galaxy Luminosity 196

52. Color-Color Diagram for the Brightest Red Stars in Sagdig . . . 197

53. Positions of the Brightest Red Stars in the Sagdig Field 200

54. The Color-Color Diagram of the Likely Carbons Stars in Sagdig . 203

55. The Color-Color Diagram of Possible Carbon Stars in CF1 . . . 204

56. Positions of the Carbon Stars in the Sagdig Field 206

57. Color-Magnitude Diagram of the Sagdig Carbon Stars 207

58. Luminosity Distribution of the Sagidg Carbon Stars 209

59. Luminosity Distribution of all Carbon Stars in Sagdig and CF1 . 211

60. V−I Distribution of all Carbon Stars in Sagdig and CF1 212

LIST OF TABLES

Table Page

1. Journal of Observations 22
2. Summary of Broad-Band Transformations 46
3. Summary of Intermediate-Band Transformations 52
4. Black Body Colors 66
5. Bright Star Data from all Runs 74
6. Solar Neighboorhood Giants 83
7. Dereddend Colors of Cluster Giant Branch Tip Stars 92
8. Adopted and Derived Cluster Parameters 95
9. Late-M Giants in the Baade's Window Field 148
10. Bahcall and Soneira Simple Model 168
11. Sagdig Brightest Blue Stars 187
12. Sagdig Carbon Stars 205

ABSTRACT

This dissertation presents a technique for the identification and classification of late-type stars and for the estimation of M star metallicities. The technique uses broad-band, V and I, CCD images to identify red stars and two intermediate-band CCD images to classify these as carbon or M types. One of the intermediate passbands is centered on a TiO absorption band at 7750Å and the other is centered on a CN absorption band at 8100Å. Color-color plots of $V-I$ versus the intermediate-band index, $77-81$, clearly distinguishes carbon from M stars. Observations of both early- and late-type stars were used to define the 77-81 system based upon the intermediate-band filters.

The TiO bandstrength deduced from the 77-81 color as a function of $V-I$ color was investigated for field giants and giants in 12 globular clusters. A linear correlation between [Fe/H] and the $V-I$ color at a given TiO bandstrength was found. This correlation can be used to estimate the metallicity of M giants. The stellar population of a field in Baade's Window was examined using this technique. Many late-M stars and no carbon stars were found. The color-color diagram for Baade's Window suggests a range of metallicities for the M giants of [Fe/H] ≈ -0.4 to $> +0.2$.

The stellar population of the Sagittarius Dwarf Irregular galaxy (Sagdig) was examined using the $77-81$ system. A method for estimating reddening based upon the color mode of foreground stars was developed

for the analysis of the Sagdig data. Sagdig is estimated to be ~ 1.3 megaparsecs distant. Bright blue and red stars in Sagdig are evidence for recent star formation. Carbon stars were identified in Sagdig. They display a bimodal luminosity and color distribution which suggests distinct epochs of star forming activity between 1 and 10 Gyr ago. The spatial distribution of carbon stars and bright red stars in Sagdig shows this galaxy to be much larger than previously thought.

CHAPTER 1

THE ASYMPTOTIC GIANT BRANCH: THEORY AND OBSERVATIONS

The asymptotic giant branch phase of stellar evolution makes otherwise faint stars very bright and so allows astronomers to examine the star formation history of lower mass stars in distant galaxies. In addition, study of the asymptotic giant branch promises to yield an increased understanding of such diverse astrophysical phenomena as the chemical evolution of stellar populations, the time evolution of stellar populations, the formation of stellar winds, mixing length theory, and the relationship between the initial stellar mass and the final remant mass. The asymptotic giant branch, or AGB, phase of stellar evolution is characterized by an electron-degenerate carbon and oxygen core and shell burning of helium, hydrogen or both and relatively rapid mass loss from the extended stellar envelope (Iben and Renzini 1983). This is the final nuclear burning stage in the evolution of stars with initial masses less than about 10 $M_{\odot}$, i.e. almost all observable evolved stars.

The observational definition of the AGB came long before any physical insight into the unique physical processes which occur during it. The term asymptotic giant branch can be traced to Sandage and Walker (1966) who demonstrated that the stars which lay on what had previously been considered a blueward bifurcation of the giant branch were a distinct class of stars based on their position in a U−B, B−V color-color diagram. The name described the approach of this sequence of stars to the main giant branch

with increasing luminosity. The discovery of the ultraviolet excess difference between these stars and giant branch stars, and thus a basis for their status as distinct from the giant branch, traces to comments made by Walker on a paper by Oke, Greenstein and Gunn (1966) in a NASA sponsored conference on Stellar Evolution in 1963. Sandage and Walker did speculate that the smaller ultraviolet excess of the AGB stars compared to giant branch stars of a similar luminosity could be due to an increased metal abundance caused by deep convection bringing processed material to the surface.

Stellar Evolution Theory of the Asymptotic Giant Branch

The evolutionary stages which lead a star to the asymptotic giant branch are fairly well understood (Iben and Renzini 1985). In the following summary of the theoretical understanding of stellar evolution onto the AGB, I will not give specific references but refer the reader to the recent reviews of Iben and Renzini (1983, 1985). The requirement that a star develop an electron degenerate carbon and oxygen core limits the initial mass to greater than about 0.8 $M_\odot$ and less than 10 $M_\odot$. Iben and Renzini point out that this mass range is composed of two distinct classes of stars distinguished by the route they take to the AGB: low mass stars and intermediate mass stars. Low mass stars develop an electron degenerate, helium core along the way and have masses less than about 2.3 $M_\odot$. The intermediate mass stars never develop an electron degenerate, helium core but ignite helium burning "non-degenerately".

The evolution of both low and intermediate mass stars onto the first giant branch proceeds in a similar manner. Once a star exhausts its core

hydrogen during its main sequence residence, it establishes hydrogen burning in a shell around the exhausted core. The core contracts (at least until the onset of degeneracy) and heats the hydrogen burning shell which becomes thinner and produces less energy. During this process, the envelope absorbs energy, expands, the outer layers cool and its opacity increases. Eventually, the increase in opacity causes the convection zone to extend inward to transport energy. There is a penetration of convection into the regions where there has been nuclear processing. The result is the enhancement of ^{14}N, a decrease in ^{12}C, an increase in ^{13}C and an almost complete loss of Li. This episode, which has been termed the first dredge-up, occurs at the base of the giant branch. Its general features are supported by observations although there may be evidence for more mixing than predicted (Iben and Renzini 1983). This extra mixing could be caused by rotation, magnetic fields and other non-classical stellar evolution effects.

Evolution up the red giant branch (RGB) is driven by the increased energy production in the hydrogen burning shell due to heating from the contracting core. This climb is terminated by the ignition of helium burning in the core. For stars with initial masses greater than about 2.3 $M_\odot$, the helium core mass at ignition depends upon the initial mass because the core temperature depends upon the mass. For stars with less than 2.3 $M_\odot$, electron degeneracy in the core becomes significant because central temperatures are not as high as in the more massive stars. This degeneracy produces an essentially isothermal core where the central temperature rises more slowly than in a non-degenerate core. This effect prolongs the RGB lifetime of the low mass stars. All stars in this mass range continue up the

RGB until they have a degenerate core mass of 0.4 $M_\odot$. At this point, the temperature becomes high enough that helium burning begins. In the low mass case, the helium core mass at ignition is a constant (0.4 $M_\odot$), and the thermal runaway caused by the rapid onset of triple-alpha nuclear burning in the degenerate core verges on being a violent event. This is called the helium core-flash. The ignition of helium signals the end of the RGB and the star rapidly becomes hotter and less luminous.

After helium is burning in the core and the degeneracy in the low mass cores is lifted, the evolution of low and intermediate mass stars once again follows a similar course. After exhaustion of helium in the core, a star will develop a thick helium burning shell which will thin and the core will contract to the point of degeneracy. This will be accompanied by the swelling of the envelope and movement onto the asymptotic giant branch. This process is analogous to that which occurs after exhaustion of hydrogen in the core and is accompanied by a similar episode of deep convection termed the second dredge up phase. The result is somewhat different in that only for stars with intial masses greater than about 3.3 $M_\odot$ does the penetration of the convective zone reach processed material and alter the surface composition of the star (Becker and Iben 1979). Once again this dredge up results in the relative enrichment of nitrogen, but this time primarily at the expense of the relative abundance of oxygen.

Iben and Renzini have divided the asymptotic giant branch into two phases. The first phase which they term the early-AGB phase (E-AGB) begins immediately after the thick shell helium burning has thinned and the star is at the base of the AGB. The thin shell of burning helium provides

almost all of the energy during this phase since the core has contracted to become degenerate and can supply no more luminosity from the release of gravitational potential energy. It is this phase for low mass stars that places them on a track extending from a region near the red end of the horizontal branch toward the RGB and gives the AGB its name. More massive stars will be more luminous during core helium burning and will never populate this "blue bifurcation" of the giant branch. The end of the E-AGB is signaled by the reignition of hydrogen burning in a thin shell outside of the helium burning shell. The confinement of the exquisitely temperature sensitive triple-α process to a shell produces a thermally unstable situation (Schwarzschild and Harm 1965) and thermal pulses begin. This phase of the AGB is termed by Iben and Renzini the thermally pulsing-AGB or TP-AGB.

Thermal pulses are produced by the pressure increase caused by the energy deposition from helium shell burning resulting in a temperature increase in the outer portions of the shell. The pressure increase causes an expansion which results in a density drop, but the pressure increases much faster than the density is able to drop because of the overlying layers, and the temperature thus increases. An increase in energy production in the shell results in a greater increase in energy production until expansion is so great that temperatures do fall. The consequent expansion drives the hydrogen-helium discontinuity (the mass boundary of the original hydrogen depleted core, just above which hydrogen is burning) to low enough densities and temperatures that the hydrogen burning is shut off. This expansion also cools the helium burning shell so that its energy output is decreased. When the helium luminosity is reduced below the surface luminosity, the

matter which had been lifted off the helium shell falls back and heats up. This heating reignites hydrogen burning which increases until its luminosity is roughly that produced by helium burning. There follows a quiescent state until the hydrogen shell has processed a critical amount of mass through the hydrogen-helium boundary. When this is exceeded, the conditions for thermal instability are met in the helium burning shell and the pulse is repeated.

The energy flux due to shell helium burning is large enough that the radiative gradient exceeds the adiabatic gradient and convection begins. This convection zone extends from the base of the helium burning shell to the hydrogen-helium discontinuity. The strength of each pulse grows until a limit is reached after about 10 to 15 pulses (Fujimoto and Sugimoto 1979). This shell does not reach beyond the hydrogen-helium discontinuity and convection stops as the pulse shuts itself off. As the star's luminosity begins to increase when the pulse energy makes its way to the surface, the envelope convection zone moves inward to carry the excess energy flux and reaches the processed material deposited by the shell convection. This is the third dredge-up which was first demonstrated theoretically by Iben (1975).

In the powerdown phase of the thermal pulse, there is no hydrogen shell burning and the triple-alpha products from the helium shell are dredged up without further processing. The primary result of the powerdown phase is the transport of ^{12}C to the outer envelope of the star. This process will eventually result in the carbon abundance exceeding the oxygen abundance in the AGB star's atmosphere, making a carbon star. High metallicity may prevent the formation of a carbon star via this path in two ways. The

amount of dredged up carbon must be greater in a higher metallicity star in order to exceed the oxygen abundance. A higher metallicity AGB star will also have a more extended envelope with a lower gas pressure in the region where the convective zone for dredge up must develop. A lower gas pressure makes convection less likely since the radiative gradient is less likely to exceed the adiabatic gradient.

Between pulses, the helium burning products ^{12}C and ^{16}O can mix with the hydrogen burning shell and be converted to ^{14}N. This nitrogen can then be processed to ^{22}Ne during the next pulse when the convective shell extends to the region containing the freshly produced ^{14}N. During the course of a pulse, the helium burning convective shell may become hot enough to process the carbon and oxygen products of helium burning to nitrogen which in turn is processed into neon. This envelope burning is directly proportional to the stellar mass, but also depends on the mixing length and the metallicity. Renzini and Voli (1981) have shown that envelope burning slows down the enrichment of carbon in more massive stars' atmospheres. It may even prevent the carbon abundance from exceeding the oxygen abundance.

The production of neon in the intermediate mass AGB stars yields a source of neutrons for the creation of s-process elements. S-process elements are produced by the capture of slow neutrons by nuclei as massive as or more massive than iron (Cameron 1955; Burbidge et al. 1957). The burning of ^{22}Ne to ^{25}Mg in the convective zone of more massive stars produces a neutron flux capable of s-process element creation from heavy nuclei (Iben 1975). In less massive AGB stars, if ^{13}C is introduced into the helium burning shell, then its conversion to ^{16}O would provide a source of neutrons

and the production of neutron rich nuclei. The production of this ^{13}C requires the mixing of hydrogen into the helium burning convective shell. How this mixing might occur is not well understood although there have been suggestions of plumes or semiconvection (Ulrich 1973; Iben and Renzini 1982). The reason for producing neutron-rich isotopes in the low mass AGB models is the observation of these isotopes in low mass AGB stars.

The theoretical insight provided by the discovery of the third dredge-up gave astronomers an evolutionary path for both carbon and S stars to their place in the Hertzsprung-Russel diagram. Because of the lack of a mechanism to alter the surface abundance ratio of carbon and oxygen in a dramatic fashion, these late-type stars were an enigma (Wallerstein 1973) before the understanding of the third dredge-up. Both of these classes of red giant, carbon and S stars, are characterized by the presence of molecular species which point to a lowered relative abundance of oxygen. In carbon stars (C stars), the presence of C_2 and CN in measurable quantities demands that carbon be more abundant than oxygen. If this were not the case, essentially all of the carbon would be sequestered in CO. Carbon monoxide has such a high dissociation energy that essentially all of the less abundant of its two components is bound up in it. In S stars, the spectroscopic evidence suggests that carbon and oxygen are about equally abundant. Molecular equilibrium calculations show that when the carbon and oxygen abundances are about equal only the metals which form the most stable oxides can compete with carbon for oxygen (Scalo and Ross 1976). The appearance of ZrO and LaO (two, very stable oxides) in S star, visible spectra as the primary molecular features is a consequence of the carbon to oxygen ratio

being almost one. The evolutionary sequence along the AGB is predicted to be from M-type through S-type to C-type due to the enrichment of the AGB star's outer layers with carbon. This is observationally corroborated by the observations of Magellanic Cloud clusters where the sequence M-S-C is a luminosity sequence along the AGB (Bessel, Wood, and Lloyd Evans 1983; Lloyd Evans 1984).

The term carbon star as used here will always refer to a star on the asymptotic giant branch. There is, however, a class of less luminous late-type stars which have carbon enriched atmospheres which are also called carbon stars. These stars are less luminous than is required for thermal pulsing even considering the interpulse dip in luminosity; they have bolometric magnitudes that are greater than -3. McClure (1985) has summarized the current understanding of the different, carbon enriched, late-type stars. Observational evidence puts most of the lower luminosity carbon and s-process enriched field stars in close binary systems. These objects are thought to be the product of mass transfer from an evolved star to its companion in a binary system. There is still uncertainty about the origin of the unusual surface abundances in the hottest C stars (R0 - R4 in the old Morgan-Keenan classification) because these are not luminous enough to be AGB stars but are not found in a disproportionate number of binary systems. The lower luminosity carbon stars will not be considered further here.

Iben and Renzini (1983) have summarized some of the uses of theoretical AGB models in the investigation of stellar evolution and stellar populations. AGB theory makes strong predictions about the mass loss experienced during evolution to the carbon-oxygen white dwarf stage. If

mass loss is not great enough to terminate the AGB before the core mass reaches 1.4 $M_\odot$ then carbon will ignite and a thermal runaway in the degenerate core will occur. The consequence of this is that the most massive intermediate-mass stars may be expected to ignite carbon burning in their degenerate core and become supernovae. AGB theory and some theory of mass loss can be used to calculate the ages of AGB stars from the maximum AGB luminosity of a well populated AGB. In the simplest interpretation, the mere presence of AGB stars more luminous than the RGB tip demands that there was star formation less than about 10 Gyr ago (assuming the sub-solar metallicities used in the stellar evolution codes). AGB luminosity functions may help shed light on the initial mass function of their progenitors or vice versa. AGB stars are predicted to be an important site for galactic nucleosynthesis because they have potentially experienced three episodes of dredge-up and experience mass loss. These stars should also be a major source of interstellar grains whose composition will depend on the type of AGB star that produces them — silicates for M-types and carbon-rich grains for C-types (see Muchmore, Nuth, and Stencel 1987). Implicit in the predictions made from current AGB theory is the necessity for realistic models of convection under various conditions in a star and realistic mass loss rates throughout the post-main sequence life of an AGB star. Most such predictions are very sensitive to these parameters.

Theory predicts that the type-composition of the AGB will depend on both the metallicity and the age of the population producing the AGB stars. The lower the metallicity the easier it is to make a carbon star, and the bluer the AGB. This means a higher temperature AGB which makes it

is harder to make later M stars. For very old populations, there will be no carbon stars because mass loss will deplete the small envelope before it can be polluted by the third dredge-up. These differences are conveniently expressed by the ratio of carbon stars to M stars, or C/M ratio.

Observational Studies of AGB Evolution

The path to the thermally-pulsing asymptotic giant branch seems to be well understood theoretically and observations support the theory. Evolution along the AGB is not so well understood. That current theories of the AGB commit sins of both omission and commission becomes apparent when they are compared with observations of AGB stars. A glaring sin of omission, as succintly pointed out by Wood (1985), is the failure of theorists to produce neutron rich elements in stars with initial masses of 0.8 $M_\odot$ to 3 $M_\odot$. The most glaring sin of commission is the prediction that carbon stars should exist that are more than three times as luminous as any known and that most carbon stars are predicted to be more than six times brighter than they are (Cohen et al. 1981).

The spectral classification of late-type stars as M, S or C is of great use in understanding AGB evolution as can be seen from the preceeding discussion of AGB theory. The identification and classification of late-type stars has, until recently, meant the collection of spectra. Lee et al. (1940) carried out a slitless spectroscopic survey in the visual of red stars in the northern sky and identified many new carbon stars. The relatively cool nature of these objects means, however, that redder portions of the spectrum will be the most fruitful when searching for late-type stars. Nassau and van

Albada (1949) and Nassau and Colacevich (1950) developed criteria for the classification of M, S and carbon stars from low dispersion spectra in the near infrared. Nassau and Blanco (1954,1957) greatly increased the number of known carbon stars with a Schmidt survey in the near infrared of 130° along the Galactic equator. There followed many such surveys for Galactic carbon stars. Perhaps the most complete, published list is that of Stephenson (1972) which contains data on more than 3000 Galactic carbon stars. Westerlund (1960, 1964) extended this type of survey to the Magellanic Clouds.

The observational data with which to test AGB theories has most often come from studies of the Magellanic Clouds. These stellar systems are close enough so that their late-type populations are easily studied but they are far enough away that their members can be considered to be at a common distance. The low dispersion surveys of the Magellanic Clouds by Blanco, McCarthy and Blanco (1980; hereafter BMB) produced two theoretically significant results. They found that the C/M ratio (defined by them to only include M-types later than 5) for the Small Cloud was about ten times the C/M ratio found in the Large Cloud. They also found a simple, tight carbon star luminosity distribution and no very bright carbon stars.

Blanco, Blanco, and McCarthy (1978), in a preliminary report on these surveys, pointed out that the ratios of carbon to M stars (C/M) toward the Galactic center, the anticenter, the Large Magellanic Cloud (LMC) and the Small Magellanic (SMC) can be used to rank these 'systems' by metallicity in that the C/M ratio decreases with increasing metallicity. This observation provides support for the metallicity dependence of the third dredge-up theory of carbon star production if one can assume that the C/M

ratio is derived from the total AGB population. The BMB study, however, only dealt with later-M types and so a shift to bluer colors for AGB, M stars will also decrease the C/M ratio. Since there are no AGB carbon stars and many AGB M stars in the Galactic bulge (Blanco, McCarthy and Blanco 1984), metallicity effects must play some role on the third dredge-up. Blanco, Blanco, and McCarthy (1978) also found a single mode distribution of carbon star luminosities in both Magellanic Clouds with a standard deviation of 0.4 mag and a mean of $I = -4.6$. This particular discovery has not yet ceased to bedevil AGB theorists because of the relatively low luminosity of most of the observed C stars and the complete absence of observed carbon stars in the brightest magnitude of theoretical distributions. The surface distribution of late-type stars found in these surveys was examined by Blanco and McCarthy (1983). They found a reasonable correlation with the red surface brightness of the Clouds and they found a good correlation of the total number of carbon stars in each Cloud with that Cloud's luminosity. The surface C/M ratio for the Large Cloud is roughly constant while it drops by a factor of 4 from the center of the Small Cloud to its periphery. They interpreted this to mean that the stellar populations present in the LMC are the same across its surface while they vary in the SMC.

Studies of the Magellanic Cloud clusters have also proven fruitful in understanding the AGB, particularly AGB evolution as a function of mass. Aaronson and Mould (1985) have completed an infrared, photometric survey of rich, Cloud clusters for luminous AGB stars. They find a steady increase in the AGB tip luminosity with increasing turnoff mass. Carbon stars were found, but only in clusters with turnoff masses less than about

two solar masses. In younger clusters, Aaronson and Mould suggest that AGB evolution is terminated by mass loss before enough carbon can be dredged up to make a carbon star. The observational evidence pertaining to the truncation of the AGB is summarized in Mould and Aaronson (1986).

Reid and Mould (1984, 1985) have completed photometric surveys for field AGB stars in the LMC and followed this with spectroscopy of a well defined subset of their photometric AGB stars. The AGB luminosity function which Reid and Mould found demonstrated the theoretically embarrassing lack of luminous AGB stars of all types. This discovery essentially mandates more severe mass loss along the AGB than current (non-ad hoc) theories can produce. Reid and Mould also found different AGB luminosity functions at different places and suggested this is the consequence of different star formation histories. In their spectroscopic follow-up, Reid and Mould found evidence for dredge-up in the presence of s-process elements in most of the luminous AGB stars, though few were actually carbon stars. They also found no evidence for envelope burning, although their sample did not contain stars in the most crowded regions of current star formation, where the most massive AGB stars would be expected.

Grism and objective prism surveys of the seven dwarf spheroidal satellites of the Galaxy have shown that all contain carbon stars (Aaronson, Olszewski and Hodge 1983). The Draco and Ursa Minor dwarfs, however, do not contain the luminous carbon stars of the AGB (Aaronson and Mould 1985). The current understanding of the AGB in these systems is summarized in Aaronson (1986). In the seven dwarfs, observations of the AGB provide the best estimate of the most recent epoch of star formation

in the three dwarfs which have not had a main sequence turn-off measured. As in the Magellanic Clouds, the number of carbon stars scales with the dwarf spheroidal's luminosity.

Although slitless spectroscopic surveys provide the type of spectroscopic data needed for finding and classifying AGB stars, they suffer from two problems. They are unsuitable for crowded fields because spectra will overlap and they are not as sensitive as photometric techniques because of the dispersion of the image. The necessity to follow up broad band surveys with infrared photometry or spectroscopy in order to determine the classification of the late-type stars found has prompted a number of investigators to develop photometric classification techniques that can be used with area detectors (Palmer and Wing 1982; Aaronson et al. 1984; Richer Crabtree and Prichett 1984). The development of all these systems can be traced to the Wing, eight-color system. Wing (1967) developed 27 narrow passbands for the investigation of late type stars with the Wampler scanner at Lick Observatory. These passbands were refined into an eight filter system for photometry of late-type stars (Wing 1971). The central wavelengths were designed to correspond to prominent molecular absorption bands or effective continuum points. Baumert (1972) used this system for an extensive study of 362 galactic carbon stars. Wing and Stock (1973) suggested that a simplified system using only two of the filters (7806Åand 8122Å) could be used in a photographic search for carbon stars in globular clusters. This suggestion lay fallow until Palmer and Wing (1982) presented a three filter system for direct photographic identification of M and C type stars. They used this system to examine globular clusters for late-type stars because they felt it

was in such crowded fields that it would prove to be more efficient than objective prism surveys. Although they found many new M stars they found no new globular cluster carbon stars.

Aaronson et al. (1984) and Richer, Crabtree and Prichett (1984) then applied Wing-filter-based systems for the identification of late-type stars with CCDs as the detector, and applied them to external galaxies. The four filter system consisting of two Wing and two broad band filters which Marc Aaronson devised was then adopted by Richer and his collaborators over their six filter system (Richer, Prichett and Crabtree 1985; Richer and Crabtree 1985). This system, which will be more fully described in a later chapter, uses broad band colors to distinguish late-type stars and the Wing filters to distinguish those with cyanogen absorption features (carbon stars) from those with titanium oxide absorption features (M stars). The advantages of using a CCD for studying crowded fields in distant systems have allowed the identification of carbon stars in systems that are over a megaparsec away (Richer, Prichett and Crabtree 1985).

These filter based surveys have extended our knowledge of the constitution of the AGB well beyond the influence of the Galaxy. Carbon stars have been identified in the isolated Local Group dwarf irregulars: WLM, IC1613 and NGC6822; in two of M31's satellites: NGC 205 and Andromeda II; in two Local Group spirals: M31 and M33; and in the distant, Sculptor system: NGC300 (Aaronson et al. 1984; Richer, Crabtree and Prichett 1984; Richer, Prichett and Crabtree 1985; Richer and Crabtree 1985; Cook, Aaronson and Norris 1986). Beyond the simple demonstration of the existence of these intermediate-age stars in these systems, these studies

have supported the absence of the very bright carbon stars noted by Blanco, McCarthy and Blanco (1980) in the Magellanic Clouds. Richer and his collaborators have also used their data to construct full AGB luminosity functions for the fields they surveyed in M31 and NGC300, and suggest that the paucity of bright AGB stars seen in the Clouds is present in M31, but there may not be a deficiency in NGC300. These studies have also turned the carbon star luminosity distribution around and used the observed distribution to estimate distances. The survey of five Local Group members by Cook, Aaronson and Norris (1986) showed that the C/M ratio in a system is strongly correlated with its total luminosity—the C/M ratio in a system decreases as the systems total luminosity increases. The relation they found held for the Galaxy and the Magellanic Clouds as well.

Spectroscopic follow up of the Cook, Aaronson and Norris survey has shown that their system does in fact accurately discriminate between carbon and other late-type stars (Aaronson, Mould and Cook 1985; Aaronson and Mould 1986). This survey also resulted in the identification of the first S star outside of the Milky Way's outer halo. This S star was found to be somewhat bluer (hotter) than other pure S stars. Its bolometric magnitude is similar to the pure S star found in the SMC (Blanco, Frogel, and McCarthy 1981). Although the photometric technique used does not accurately discriminate between S and early M types, it does allow the identification of potential S stars.

The Cook, Aaronson and Norris survey technique is a useful method for identifying AGB stars for further study. It is able to provide type discrimination, magnitude and color information. In the early work with

this system, the Wing-type filters were used to derive an instrumental index which corresponded to a TiO band strength minus a CN band strength. The purpose of this dissertation is to create a reproducible system and calibrate this system for future investigations. Observations with the these intermediate-band filters have the potential to provide more than a simple type distinction; they can yield band strength information about CN and TiO. In conjunction with the broad band colors, this information can be used to lift the degeneracy in observed C/M ratios induced by the effects of metallicity and age. With a metallicity calibration in hand, the newly defined intermediate-band system will be used to investigate the late-type stellar population of the Galactic bulge and the recently discovered dwarf irregular galaxy in Sagittarius. This dissertation contains no previously published results, and all of observations are new. The papers by Cook, Aaronson and Norris (1986), Aaronson et al. (1984) and Aaronson, Mould and Cook (1985) present the early evolution of this system and some preliminary results which complement this work.

Chapter 2 will contain the details of the data collection and the data reduction. It will also provide estimates of the various sources of error and their magnitudes. Chapter 3 will introduce the intermediate-band filters and establish the standard "77−81" system. Chapter 3 will also provide the metallicity calibration of the TiO band strength as measured with the 77−81 system for M giants. Finally, this chapter will investigate the late stellar population of the Galaxy's bulge in Baade's Window in terms of its metallicity and its in late-type stellar content. The fourth chapter will be the investigation of the recently discovered Sagittarius Dwarf Irregular galaxy

using the 77–81 system. In Chapter 4, this dwarf will be shown to have a relatively unusual population of carbon stars as well as evidence of recent star formation. The final chapter will be a brief summary of important results of this dissertation. Chapter 5 will also present a plan for further work using the 77–81 system in the study of the AGB populations of resolved stellar systems.

CHAPTER 2

DATA COLLECTION AND REDUCTION

The goal of a system for the investigation of the AGB must be the flexibility to examine the extremely bright AGB stars found in the Galaxy as well as identify carbon and M stars in distant, crowded stellar systems. The comparison of nearby M giants with carbon stars in galaxies at the edge of the Local Group or beyond necessitates spanning 24 magnitudes.

The basic data of the 77–81 system on stars which are well characterized spectroscopically was collected as photoelectric photometry because these are nearby, bright stars. These bright stars comprised a range of types found on the AGB as well as bright (relatively unreddened) A stars in order to define the system. These data were collected on a 0.4-m telescope at Kitt Peak National Observatory. The full potential of the 77–81 system includes a metallicity calibration of the TiO band strength and this calibration was done by examining globular clusters of various metal abundances. The globular cluster photometry was ideally suited to CCD (charge-coupled device) photometry on the 0.9-m at Kitt Peak. Most of a cluster's members fit on one CCD frame and the exposures did not need to be long since the cluster stars of interest are the giants. Some of the fainter stars observed on the 0.4-m could also be observed on the 0.9-m and the primary system definition applied to the CCD data. For the study of crowded faint stellar systems, point-spread function fitting photometry of CCD image data was the

best approach. These data, on faint systems, were collected on the Cerro Tololo 4-m telescope and the 0.9-m data were used to tie the photoelectric photometry of the bright stars to the CCD photometry of AGB stars at I = 21.5.

The data presented in this thesis were collected on eleven nights of observing using the facilities of the National Optical Astronomy Observatories (NOAO) at the Kitt Peak National Observatory (KPNO) and Cerro Tololo Inter-American Observatory (CTIO) sites. A journal of the observations is presented in Table 1. The 1984 observing run resulted in a massive amount of data on Local Group galaxies most of which is not presented here. All nights of the run are listed in the journal because observations of standard stars which are reported here were made on all of the nights. The broad-band V,I system used throughout this work is that defined by Cousins (1973, 1976) as realized by Landolt (1983) and Graham (1982). The broad-band filters used during all of the observations were interference filters designed by Mould (1983) to match the passband definitions of the Cousins system as presented by Bessel (1979). In this chapter, raw, instrumental magnitudes through these two passbands will be referred to by lower case letters, v and i. The two intermediate-band filters used are referred to as 77 and 81 in reference to their central wavelengths of 7750Å and 8100Å. The properties of these filters will be more fully described in Chapter 3.

Data were collected on the mountain by instrument computers and written to magnetic tape. The photoelectric photometry data were written in KPNO Forth and were translated using the Central Computing Facilities of NOAO; printed output was used for the data reduction described below.

Table 1. Journal of Observations

Date	Site	Telescope/ Instrument	Seeing	Weather	Program
8/28/84	CTIO	4-m/PFCCD	1.2″	clear	Baade's Window, standards
8/29/84	"	"	1.2″	cirrus early	standards
8/30/84	"	"	1.1″	clear	NGC 6822 control field, standards
8/31/84	"	"	1.0″	cirrus early	Sagdig, standards
9/01/84	"	"	1.1″	clear	standards
4/28/85	KPNO	0.9-m/RCA2	1-2″	clear	standards
5/14/85	KPNO	0.4-m/GaAs PMT	2″	clear	standards, field giants
5/15/85	"	"	1-2″	clouds late	"
6/08/85	KPNO	0.9-m/RCA2	2″	clear	standards, field and cluster giants
6/09/85	"	"	2″	clear	"
6/10/85	"	"	2″	clear	"

The CCD data had various instrumental effects corrected before being written to tape in FITS format. The FITS tapes contained header information such as the exposure time, filter, telescope coordinates and the airmass of the observation. The FITS tapes were translated to the format required by the data reduction package DAOPHOT (Stetson 1983, 1987) which was used for the reductions described in detail below. The long exposures for the Sagittarius Dwarf Irregular Galaxy were averaged before reduction.

Photoelectric Photometry

Photoelectric photometry was obtained using the #4 KPNO 0.4-m with an RCA 31034A, GaAs photomultiplier, KPNO PMT #52. The photomultiplier coldbox was kept at a constant cold temperature by packing the cooling jacket with crushed dry ice. A 33 arcsec aperture was used for all of the observations. This aperture was used because all of the objects (program and standards) were bright and uncrowded. The data acquisition was controlled by an LSI 11 computer and the data was written to magnetic tape as well as being printed out for each integration. The photomultiplier output was analyzed by a Princeton Applied Research Model 1109 photon counter. The KPNO User's Manual for the system suggests that the dead time for this counter is roughly 50 to 60 nanoseconds. After an integration, the total integration time, the filter number, the Universal time, the sidereal time, an identification number and a code for object or sky was written to tape. The time was supplied by an Astro-Computer clock. The data was collected in sets of 5 second observations of the star plus sky in the sequence 81,77,I,V,V,I,77,81 generally followed by a sky only sequence of 81,77,I,V. The

sky was chosen to be a field a few arcminutes from the star which had no apparent stars within in or near its periphery. For the brightest stars only one half of a set was collected on occasion. These sets were repeated until at least 10^5 counts were collected. The dark count was measured at the beginning, and the end of the night and randomly throughout the night. It was measured as about one Hz and ignored in the data analysis. Stellar integration rates varied from 1000 Hz to over 10^6 Hz.

Two intermediate-band filter sets made at the same time were taken to the telescope to check against each other if time permitted. The coldbox was installed for the first night with the filter slide on the telescope pier side which prevented high declination observations from being made. This was changed during the intervening day and the set of intermediate-band filters not used on the first night was inadvertently installed for the second night. This was discovered well into the second night when count rates calculated for stars observed on the previous night were compared to those observed at the time. It was decided that this was a chance for a comparison of the two sets. The transmission curves which were taken to the telescope suggested no color differences but there were differences in peak transmission.

The individual integrations were examined to assess possible variations larger than would be expected from counting statistics. This procedure showed that the second night became non-photometric about an hour before data collection was stopped due to approaching clouds and the non-repeatability of integrations at the 10% level. For the observations during photometric weather, the mean airmass of a set of observations and the mean count rate for each filter for a set observations was then calculated.

Once the mean counts per second were calculated they were corrected for the photon counter's deadtime using the canonical 50 nanosecond value. (This value was also suggested by D. Hayes in lieu of an accurate measurement.) Deadtime is a refractory period which follows an image tube pulse during which further detection of pulses is eliminated. The deadtime is primarily caused by capacitance in the cabling and in the amplifier. The correction was a simple, first order correction of the form:

$$corrected\ rate = (observed\ counts)/(time - (observed\ rate) * deadtime).$$

This is a small correction since even for rates of 1 MHz, it is only 5%.

The corrected counts were then sky subtracted. Sky measurements were always taken for objects at high airmasses and for those near the beginning and the end of the night when the sky was changing relatively rapidly. Most observations of a star also included at least one set (V,I,77,81) of sky observations in the middle of the stellar observations. For the brightest stars in the 0.4-m program, a sky observation was occasionally omitted if a sky value had just been determined for the previous star in the same portion of the sky (within about 10° and near the zenith). Except for observations near evening and morning twilight, sky values were relatively constant at about 150 Hz for the intermediate-band and V filters and about 500 Hz for the I filter. There was some variation due to the 0.3 phase moon although observations were always done at least 30° away from it. Because many of the program stars had $V \lesssim 3$, a 3% neutral density filter was used for duplicate observations of eight of the program stars and five standards. These observations were done immediately before or after an observation of the same star without neutral density. Sky was measured

in the same manner as that without neutral density. The neutral density observations also provided a direct check of the detector linearity. A wide range of magnitudes was observed with the neutral density filter because of the necessity of observing the same standards as done without neutral density. When a plot of the difference in raw magnitude for stars observed with and without neutral density was made, I discovered that above 70000 Hz there was a linear decrease in the magnitude difference between the observations. This relation was measured as 0.022 mag per magnitude. This empirical correction was then applied to all observations above 70000 Hz after the deadtime correction. This was the last observing season for this phototube and this non-linearity at high count rates could have been due to some aging response of the tube.

Direct measurement of the broad-band extinction was only accomplished on the first night of the two night run. This was due to the fact that the second night was cut short by cirrus moving in as extinction measurements were being made. The measurements on the first night consisted of observations of two Landolt standards once on the meridian and once four hours over. The extinction measured in this manner was $k_V = 0.134$ and $k_I = 0.054$. These values are rather low compared to the mean extinction measured at Kitt Peak by the Standard Consortium (NOAO Newsletter 1985 #4). They found $k_V = 0.186$ and $k_I = 0.101$ for ten nights during the year and a half bracketing my run. Because I was only interested in the program star's colors, I reduced the data purely as colors and used the measured $k_V - k_I$ of 0.08 which is very close to the mean, published difference. The intermediate-band extinction was also only measured on the first night of the

run. The values obtained were $k_{77} = 0.072$ and $k_{81} = 0.057$. These values were adopted for the second night as well.

Six Landolt standards were observed on the 14th and eight were observed on the 15th. These observations were used to determine the transformation to the V,I system. Because of the expectation that the color term for the transformation would be the same for both nights (there was no detector change), the two nights were combined to solve for the coefficients in a transformation of the form:

$$(\mathrm{V} - \mathrm{I}) = (v - i)_0 * \mathrm{C} + \mathrm{C1}.$$

In this equation, V and I are the standard magnitudes, $(v - i)_0$ is the extinction corrected instrumental color and C and C1 are constants to be determined.

The two nights were combined by calculating the zero point shift from the instrumental magnitude of the four stars observed at about the same airmass on both nights. This zero point shift was the same for V and I. The least squares fit to the above relation had a correlation coefficient of 1.00 and the color term was within 0.01 mag of the color term determined for each night separately. Figure 1 is a plot of the color residuals for the Landolt standards as a function of color. The residuals scatter about the mean with a standard deviation of 0.010 mag and there is no color dependence.

The intermediate-band data were reduced by forming nightly instrumental magnitudes and then calculating any shift in color of stars observed on both nights. Because of the aforementioned change in intermediate-band filter sets, there was a mean shift of 0.201 in raw, 77−81 color from night to

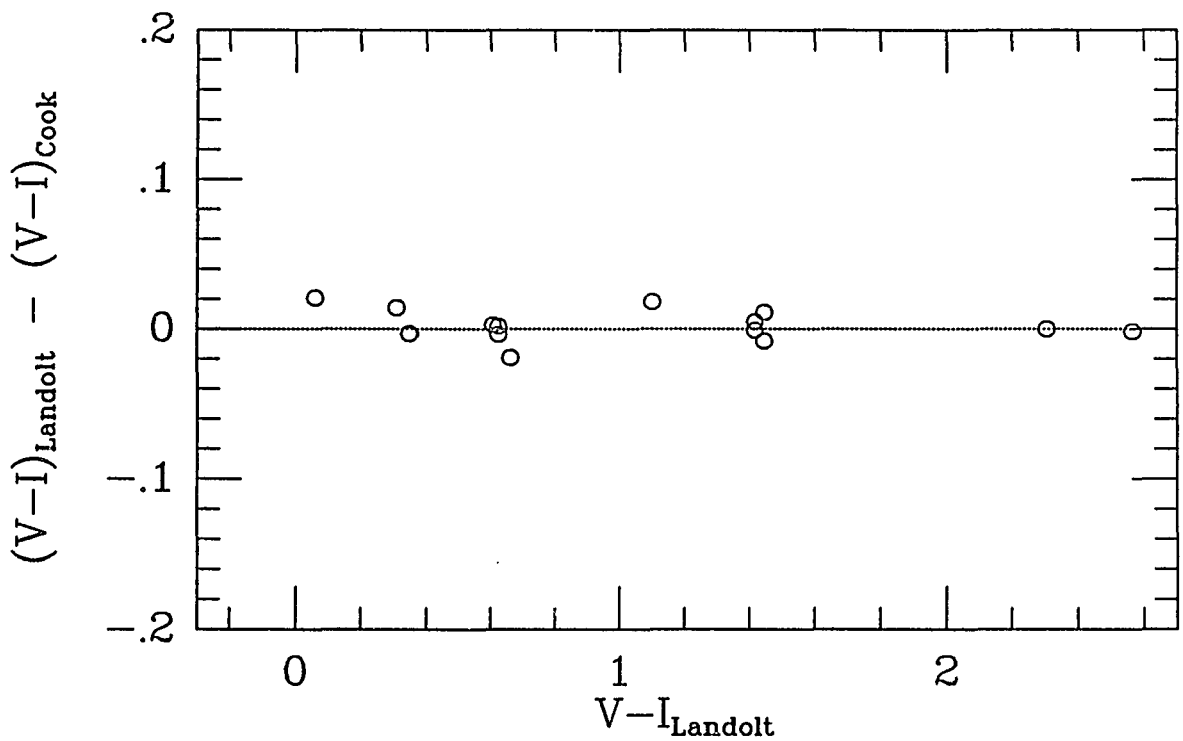

Figure 1. Color Residuals of the Photoelectric Photometry Transformation

night with no apparent color dependence. The filter set used on the second night had the most similar transmission curves to the 2″ x 2″ filters used at all other telescopes in this work so the first night was shifted to the second night's zero point. The second night was also the night when all of the A0 stars were observed in order to begin the definition of the 77−81 system. The result of that definition (see Chapter 3) was that a shift of 0.078 mag in 77−81 color was then applied to bring the instrumental colors onto the 77−81 system. The standard deviation for observations of the five stars in common to both nights was 0.014 mag.

Observations of the brighter stars were also made through a 3% transmission, neutral density (ND) filter. The same Landolt standards were observed with the ND filter, and the color transformations were checked to assure the filter's neutrality. The broad-band transformation was found to be the same, but the intermediate-band colors were shifted 0.017 mag to the red with no measurable color dependence. The ND observations were averaged with the observations without ND to obtain the values reported here.

The accuracy of the photometric observations can be estimated in various ways. The uncertainties in the measured brightness of the stars due to Poisson statistics were small for all the objects measured. Because of the minimum of 10^5 counts for each star this error was always less than about 0.003 magnitudes. For the standards and the dimmer program stars such as the Gleise and Yamashita stars up to six sets of observations were necessary to collect enough counts and the standard deviation of these sets can be measured. It was found that the variance of these sets was in the

mean 0.006 magnitudes more than that expected from the count rates. This suggests a photometric limit of about ±0.01 mag for the colors from the combination of the weather and operator. This same estimate is found in the standard deviation of the residuals of the standard star broad-band colors and the residuals of the 77−81 colors from night to night.

CCD Photometry

All of the CCD (charge-coupled device) observations reported in this thesis were made with two chips from RCA. The CTIO, prime focus RCA chip and the KPNO RCA#2 came from the same RCA production batch (Pat Seitzer, personal communication). They are both 'thinned' to enhance the blue response. These devices collect photoelectrons produced in silicon which are then detected by the potential they produce on a capacitor. The detected voltage is translated into data units by analog to digital converters. A data unit represents a fixed number of detected photoelectrons which can be adjusted for each chip to a level appropriate for the data collection computer's dynamic range. A recent review of CCD function and astronomical use is given in MacKay (1986). There are six instrumental effects which are important for the CCD data presented here: readout noise, bias structure and level, nonuniform quantum efficiency across the chip, dark count, charge transfer problems and nonuniform thickness. The readout noise is primarily a consequence of the on-chip amplifier. RCA chips typically have about 80 electrons rms readout noise. This noise sets a lower limit to the performance of the CCD. The bias level at which each well on the CCD surface is held results in an output current even when there has not been

any signal to integrate. The bias level may vary from pixel to pixel but at a very low level. Some chips are designed with a few columns shielded from exposure, termed the overscan region, to allow measurement of the bias level for each integration. Most chips are designed to read out a few virtual columns which will be at the bias level. The overscan region is not necessarily at the same bias level as the rest of the chip although the offset has been found to remain the same; it is for this reason that bias frames are collected even when they contain no detectable structure.

The bias is a zero point for each integration and needs to be subtracted before any other reductions. This was done differently at CTIO and KPNO. The method employed at CTIO was to accumulate a series of about five, 0 second integrations (biases) at the beginning of the night. These are averaged to create a bias frame which is then smoothed by a n pixel moving average. This is an acceptable procedure because the high spatial frequency bias structure has been measured to be extremely small; it is the larger, low spatial frequency bias structure that is important.

The procedure at KPNO is similar to that at CTIO except that the bias frame is not smoothed. This necessitates collecting a large number of biases. The number of biases collected is determined by the desire to add as little noise to the data in the debiasing procedure as possible. I averaged 100 to 150 biases each night to construct a bias frame. This procedure results in the addition of noise at the level of one tenth the readout noise.

To correct a data frame, the overscan region's bias level is subtracted from the bias frame on a row by row basis by averaging a set of pixel values not too near the data region-overscan region border. This transition is not

instantaneous and is often characterized by a few pixel width of abnormal bias levels. After this level is subtracted, the overscan region is eliminated. This is termed debiasing and trimming. After trimming the data frame, the bias frame is subtracted and the result is termed a debiased, trimmed and bias subtracted picture.

CCDs exhibit pixel to pixel variations in quantum efficiency. This is corrected by a procedure called flatfielding. For the results presented in this thesis, flatfield exposures were always exposures of a flat white surface on the interior of the telescope dome (flat). This surface was uniformly illuminated by an incandescent lamp through a color balance filter in order to try to mimic the sky color. Irregularities in illumination and reflection are compensated by the out of focus nature of these exposures. A number of exposures are collected through each filter; these are averaged and then bias corrected. A copy of this frame is then heavily smoothed and the averaged frame is divided by the smoothed frame to produce the flatfield frame. The flatfield retains the pixel to pixel differences in quantum efficiency but has a mean of 1. A data frame is divided by the flatfield frame after bias correction on a pixel by pixel basis to produce a flattened data frame. The result is a correction of the high frequency variations in the quantum efficiency but a retention of the linear relation of counts to image intensity. This procedure once again adds noise to the data although the level of the individual flatfield exposures is adjusted to be well above the read noise so that the flatfield readout is not contributing to the noise. The desire for a high exposure level in the flatfield exposure to beat down the sampling noise is balanced by the fact that there may be nonlinear effects in the quantum

efficiency of each pixel. Each flatfield exposure should result in a level near that expected for sky in a typical object frame if faint object photometry is the final objective. Consequently, many flats for each filter are averaged to reduce the statistical noise before preparations of a flatfield. At CTIO twenty were averaged for each filter; while at KPNO 10 were averaged for each filter. At CTIO, it was possible to roughly match the expected sky values for long exposures and be well above the readout noise. At KPNO, the program involved short exposures of bright objects and the data would have very low sky values with the program objects much brighter so flatfields were taken at relatively high levels and fewer were needed to reduce the statistical noise to acceptable levels.

There are many possible sources of dark counts. Thermal excitation is common to all CCD's and is the reason that they are operated at low temperatures. For all of my applications, the thermal dark count of a few electrons per pixel per hour is negligible. The on-chip amplifiers of some chips act as light emitting diodes and this is a significant source of a nonuniform dark count; this is the case for the CTIO prime focus CCD. The amplifier is apparently situated off the south east (as the sky is imaged) corner of the chip and contributes 150 counts in the corner pixel per thousand seconds, dropping to essentially zero counts 300 pixels from the corner. In order to correct this, the median of six dark exposures of 1000 seconds was scaled to the exposure time and subtracted for exposures longer than a hundred seconds.

The basic reduction of the two dimensional data to correct the bias, flatfield and dark count instrumental effects has been programmed into the

data collection computers for the KPNO and CTIO CCD systems. The data presented here was corrected in this manner at the time of collection. This "mountain reduced" data was examined to be sure that sky levels were flat across the chip and that the bias level had been removed but no further check of these corrections was made.

The instrumental effect of charge transfer inefficiency was only noticed for the data from the KPNO RCA#2 CCD. This chip has problems transferring charge at all illumination levels. Measurements of the curve of growth of stellar images showed that the transfer inefficiency as measured by the trailing of counts from a stellar image was a constant factor for all image intensities and background levels and image positions. This transfer inefficiency was apparent as trails in both the column direction and the row direction; it affects the shift registers as well as the data collection pixels. It would be too complex to attempt to construct a data frame with the transfer inefficiency corrected; this is not really needed to do accurate photometry. Because the trailing is a constant factor of the intensity, it can be dealt with as a kind of zero point shift for aperture photometry.

Multiple internal reflections within a CCD at long wavelengths lead to interference patterns called fringes. Some chips suffer this problem more than others and this is probably due to the uneven thinning process used to enhance the blue sensitivity. The interference pattern due to the non-planar geometry generated by uniform illumination of the chip is wavelength dependent and the fringing from the night sky continuum will average out. Night sky features will produce fringe patterns across the chip which will vary with the varying intensity of the features. Fringing was not observed

at the KPNO #1 0.9-m. Fringing is a well known problem of the CTIO prime focus RCA chip. Some of this difference may be the result of the faster beam on the 4-m.

The fringe pattern intensity can be large enough (many hundreds of electrons) and it can vary so rapidly (peak to peak in a few pixels) that it can seriously affect attempts to measure stellar image intensities. This problem is corrected by creating a frame which only contains the fringe pattern (a fringe frame) and subtracting this from the data. A fringe frame is created by collecting exposures of a relatively star free region of the sky when fringing is strong due to sky conditions. Each exposure is offset a few tens of pixels relative to the others so that a frame constructed from their median will not contain stellar images. It will contain the fringe pattern. The mean sky level of this frame is subtracted from the frame to create a zero mean level. Because the fringing is due to essentially monochromatic skylines, it is purely additive. A fringe frame must be created for each passband because the pattern is wavelength dependent. Unfortunately, the relative intensities of the sky features within a passband can change so that the fringe pattern seen through a particular filter is not always the same. This variation is generally small and it would require an inordinate amount of telescope time to correct it. As it is, creating a fringe frame requires quite a bit of telescope time. Since it is the fringing of the night sky which must be corrected, twilight sky emission features do not produce a good match. This means real observing time must be used to create fringe frames. A high signal to noise fringe frame requires a lot of observing time — "and we all hate to take good data if it means wasting observing time."

(E. Olszewski 1987, personal communication).

A library of broad-band fringe frames has been created at CTIO so that these do not need to be constructed by each observer. I did, however, need to construct fringe frames for the intermediate-band filters. The broad-band fringe frames were constructed from four exposures of 600 seconds. The 77 fringe frame was constructed from four exposures of 500 seconds and the 81 fringe frame was constructed from four exposures of 450 seconds. These exposures were taken of the relatively star free field at high airmass. This enhanced the fringing because of the atmospheric pathlength and yielded high signal to noise fringe frames with a smaller expenditure of time.

The procedure used to defringe data frames requires some human judgement. The appropriate fringe frame is scaled to a range of levels wide enough to include the likely best value and subtracted from the data. The results are examined to establish the interval of scale values which contains the minimum residual fringing. The process is then repeated over this smaller interval. Because the fringe frame pattern may not exactly match the data frame pattern and because images on the data frame cause confusion, the best value for scaling the fringe frame could not be determined to better than 5 per cent with this set of fringe frames. This may introduce relatively slow variations of a few per cent from the real sky value in the data which will not affect stellar photometry. Fringing was not detectable for the standard star exposures or for the Baade's Window exposures because they were so short.

Synthetic Aperture Photometry

Synthetic aperture photometry was performed using Peter Stetson's program DAOPHOT (Stetson 1983, 1987). This program consists of 12 relatively independent subroutines which I will refer to by name in describing my use of the program. Rough image centers are found using the subroutine FIND. This routine needs an estimate of the full width at half maximum for the images on the frame; it then convolves the data with a modified Gaussian and identifies local maxima in the convolved data's brightness enhancement. The routine rejects as stellar images those which are too elongated in either the row or column dimension (bad columns). It also rejects as stellar images those which are too peaked (hot pixel) or those generated by holes (cold pixels). The rejection limits are set by the user. It also rejects maxima that are less than a specified value. Its output is a list of image centers, rough magnitudes relative to the brightness threshold and the two parameters used for image rejection, Sharp and Round. The image center is not a centroid and may be offset from the true centroid by a few tenths of a pixel.

The PHOTOMETRY subroutine of DAOPHOT computes the magnitude within a synthetic aperture centered on a coordinate which must be supplied. When large apertures will be used, the centers from the FIND output are suitable. The routine does intrapixel interpolation to find the intensity in partial pixels. The sky value is determined by calculating the mode within an annulus specified by the user. The routine returns a magnitude relative to a user specified zero point and an error estimate which is the quadratic sum of the poisson errors for the sky and star pixel intensities. These errors are calculated with a user supplied value of the number of

electrons (photons) per data unit. The routine will calculate magnitudes for up to twelve apertures for each center.

The magnitudes for the standard stars and the globular cluster member magnitudes were measured using these two DAOPHOT subroutines. These magnitudes are a good approximation to true aperture photometry. Some of the same types of errors will occur as do in photoelectric photometry. There will be an error due to the inaccurate center from FIND, when apertures are small compared to the stellar image. There will be an error due to the fact that the true sky under the aperture is not measured. This error should be subject to less systematic error than the photoelectric measure of sky because the sky is sampled in an annulus about the aperture. The DAOPHOT sky value may also be systematically lower than a photoelectric estimate because of the use of the mode in estimating the sky. There is also quantization error in the sky pixels for short exposures.

In CCD photometry, a total magnitude is generally calculated for a stellar image which is then compared to the total magnitude of a standard star's image. This requires the measurement of a growth curve for both of the images. This is quite different from the procedure for photoelectric photometry where a fixed aperture is used to measure both program and standard stars in rapid succession. This works because the time averaged seeing over a photoelectric integration will not change more rapidly than the alternation between standards and program stars in reasonable weather. The total magnitude measurement is necessary for CCD exposures because of the much longer exposure times and the time spans between program and standard observations.

Broad-Band Transformations

The broad-band system used in this thesis is that defined by the set of equatorial standards of Landolt (1983). These standards were designed to yield the usual Johnson UBV and the Cousins RI. The advantage of the Landolt standards is that they comprise a single set of standards which can be used throughout the year and in both hemispheres. For the observations at Cerro Tololo, the standards developed by Graham (1982) in the E-regions were also used. This was done as a time saving measure. Two to five standards from the Eregions could fit onto one CCD frame. These two set of standards were developed from the same set of bright E-region standards of Cousins (1973, 1976) and used the same instrumental setup and filters and should represent the same system. The procedure used to reduce the data from the KPNO #1 0.9-m and the RCA#2 CCD to determine standard star magnitudes was different than that used for the CTIO data because of the charge transfer inefficiency problem of RCA#2.

Instrumental magnitudes for the standards observed at CTIO were found using the synthetic aperture photometry routines described above. Growth curves for a standard frame were determined by examining the results of using increasingly larger apertures to determine the magnitude. This was done in one pixel steps. As the aperture radius is increased, the uncertainty in the magnitude increases due to two factors. One factor is that the larger number of pixels increases the noise due to sampling and readout; this effect increases the error linearly with the aperture radius since the pixel number increases as the square of the radius and the error increases as the quadratic sum of the individual pixel errors. The magnitude for larger

apertures is also less certain due to the uncertainty in the sky level. This uncertainty increases as the area of the aperture since it is the sky value for the whole aperture which must be subtracted to determine the image brightness. The result is that the signal to noise decreases for large apertures because the image brightness is rapidly decreasing in the outer regions of a stellar image. The Landolt, VI, standards are generally the brightest objects in the CCD field which contains them so that their total magnitudes were measured directly. This was done with the smallest aperture which contained the total magnitude for the reasons just mentioned. The aperture containing the total magnitude was determined to be the aperture beyond which the mean magnitude change for a change in aperture was a small constant. This constant was not always zero because of the uncertainty in the determination of the sky level. This is seriously affected by quantization error for the low sky levels in the short standard exposures. This small constant was always less than ± 0.003 mag and no attempt was made to correct the standard magnitude for the sky error.

Some of the standards in the E-regions are much fainter than the brightest stars on a frame. In this case, the brightest stars were used to measure an aperture correction from a 3.6 arcsec aperture (3 pixel radius) to the smallest aperture which contained the total magnitude. The standard star's total magnitude was then constructed from the aperture correction and the standard's magnitude through a 3.6 arcsec aperture. The 3.6 arcsec aperture magnitude is much less uncertain than the full aperture, but still contains about 80%-90% (depending on the seeing) of the image intensity. The CTIO magnitudes were calculated with a sky annulus extending from

8.4 to 21 arcsec.

The above procedure would not work well for the Kitt Peak data because the tail due to the charge transfer inefficiency of RCA#2 is easily measurable 35 pixels from the center of a bright stellar image. To measure a total magnitude with a 70 pixel aperture (60 arcsec), would introduce very large uncertainties into the magnitude. From an examination of stellar image profiles for all the nights of Kitt Peak data, it was determined that, except for the tail, all of the image brightness on all the nights was contained in a 16 pixel aperture. This corresponds to a 14 arcsec aperture. Magnitudes measured through this aperture suffer a loss that is a constant fraction of the image total due to the trailing and this can be thought of as a simple loss of quantum efficiency. This procedure will work as long as the seeing for the standards is not so bad that the images grow beyond the 8 pixel radius. This was not the case. Sky was determined in an annulus from 9.5 to 23 arcsec around the image. This annulus is contaminated by the charge transfer trail, but the modal nature of the sky determination eliminates most of its effects.

Once instrumental magnitudes for the standards were collected a package of programs for the reduction of CCD standard data was used to calculate transformation coefficients. This package, CCDCAL, was written by Peter Stetson and was available at the NOAO computers. This program computes coefficients for a user supplied transformation equation by a weighted least squares fit to the data. The user may also specify values for coefficients which may be known, a priori, or independently determined. The error analysis done by the program allows an examination of the

significance of various terms in a transformation. The program returns estimated errors for the coefficients determined from the standard value errors, the observational errors and the goodness of fit to the transformation as well as an estimate of observational scatter which is due to residuals larger than those expected from the observational errors. This program makes the clear distinction between the standard photometric indices which are generally produced from photoelectric photometry and the magnitude data from CCD observations. This distinction is due to the variability of weather effects (such as seeing and thin cirrus) which change slowly with respect to serial, photoelectric measurements but rapidly with respect to CCD photometry.

Transformations of the form:

$$v = \mathrm{V} + \mathrm{A0} + \mathrm{A1} * \mathrm{X} + \mathrm{A2} * (\mathrm{V} - \mathrm{I}) + \mathrm{A3} * (\mathrm{V} - \mathrm{I}) * \mathrm{X}$$

and,

$$i = \mathrm{I} + \mathrm{B0} + \mathrm{B1} * \mathrm{X} + \mathrm{B2} * (\mathrm{V} - \mathrm{I}) + \mathrm{B3} * (\mathrm{V} - \mathrm{I}) * \mathrm{X}$$

were tested to describe the transformation of the CTIO data to the standard system. In these equations, A0 through A3 and B0 through B3 are coefficients to be determined. V and I are standard magnitudes and v and i are raw, instrumental magnitudes and X is the airmass. The zero indexed terms are the photometric zero points for each filter; A1 and B1 are the first order extinction coefficients (k_V and k_I respectively); A2 and B2 are the color terms for the detector system; and A3 and B3 are second order extinction terms. The significance of each term was estimated by its uncertainty, its ability to decrease the residuals of the observations and by its ability to decrease the uncertainty of the other coefficients. These tests called for the inclusion of the second order extinction term. In a fit to the

above transformation, this coefficient had the same significance as the first order color term. If this coefficient is set to zero the observational scatter about a solution essentially doubles. (The exact increase varies with the night.)

Roughly 20 observations of standard stars were made each night except the instrument and cloud shortened night 8/29/84. There were not many data points to pin down four free parameters so an iterative procedure was employed. It was noted that the value of the zero point, the color term and the second order extinction term did not vary more than a few per cent from night to night in the full solutions for all parameters. Thus it would be a reasonable procedure to set one or more of these coefficients to its mean value for the run in order to determine another coefficient's value for a particular night.

The mean extinction for the five nights was estimated from a fit to all of the coefficients for each of the five nights. This mean extinction was then fixed and a rough mean for the color extinction was evaluated for the five nights. With these two coefficients fixed, a rough color term was calculated which was the mean of that measured on the five nights. Although the second order extinction term might be expected to change with time, its absolute value of a few per cent made it extremely unlikely that any change could be meaningfully measured. Hardie (1962) points out that variation in the second order extinction coefficient is found to be less than variations in the first order extinction coefficient. Thus, its value was fixed as the mean of its observed value on the five nights of the run. This was done using the rough, mean color coefficient and the mean extinction.

The color term was not expected to have changed over the course of the run. Any change in the color term would indicate a change in the functional form of the quantum efficiency of the CCD in the affected passband and this is unlikely to have happened. The value of the color term was fixed by calculating the mean value measured on the five nights using transformations with the fixed second order extinction term, and a mean zero point. The mean zero point was used because it was found to vary less in all of the different solutions than the extinction.

Once the two color-dependent terms were fixed, the behavior of the other two coefficients was examined under a variety of assumptions. Mean CTIO extinction values were fixed from the work of Landolt (1983) and this did not work very well. The mean measured extinction was fixed and this did not work well. Various mean extinction values within the observed range were fixed and the solutions were not that good. On the other hand, if the zero point was fixed then the solutions had the lowest scatter and the lowest uncertainties for the coefficients. The mean zero point for each transformation was determined by fixing the extinction at the value determined from a solution with the zero point and the extinction free. This gave a value for the zero point which varied from night to night by less than ± 0.002 mag. Fixing the zero point is not unreasonable for modern CCD dewars because the temperature regulation can be quite good. It also should be noted that the CCD had been on the telescope for the observing run before mine so that it had apparently had a few days to stabilize before these data were taken.

After the other three coefficients had been calculated, the extinction

was solved for each of the five nights of the run. Because of the observed weather changes during the five nights, it is not unreasonable to find that there were changes in the extinction from night to night. A summary of the transformations and extinctions determined for this run is found in Table 2 which includes error estimates for the coefficients and residual scatter about the solution.

The transformations for the KPNO data were calculated using CCDCAL in a manner similar to that used for the CTIO data. The same form for the transformations was investigated. The second order extinction term for the transformation, however, was set to zero because the mean value estimated for the three night run was less than 0.006 in both transformations. The extinction had been measured directly for three to five stars on each night, and its nightly value was fixed at the observed value. These extinctions measures were made by observations of stars at roughly one airmass and roughly two airmasses. These values were in reasonable agreement with values returned by the CCDCAL package when the extinction was a free parameter. By fixing the extinction, the program could not compensate for observational errors by varying the extinction in concert with the other parameters. The color term for the transformation was determined from the mean nightly color terms calculated with the color term and the zero point as free parameters. I obtained the color terms: $A2 = 0.0075$ and $B2 = -0.0050$. These are relatively close to the values reported by the KPNO Standards Consortium in the NOAO Newsletter #4 (1985) of $A2 = 0.013$ and $B2 = 0.000$ where A2 is the coefficient for a B-V index. These small color terms mean that the filter-CCD-telescope combination is a close match to the Landolt

Table 2. Summary of Broad-Band Transformations

All broad-band transformations were of the form:

$$\text{observed mag} = \text{standard mag} + C0 + C1 * (V - I) + C2 * X + C3 * (V - I) * X$$

Band: V

Date	C0	C1	C2	C3
8/28/84	2.3079	0.0578	0.1755 ± 0.0023	−.0214
8/29/84	"	"	0.1842 ± 0.0041	"
8/30/84	"	"	0.1801 ± 0.0013	"
8/31/84	"	"	0.1925 ± 0.0020	"
9/01/84	"	"	0.1929 ± 0.0019	"
4/28/85	5.4658	0.0332	0.1800	–
5/14/85	0.853	0.032	0.180	–
5/15/85	0.593	"	"	–
6/08/85	5.5643	0.0075	0.2207	–
6/09/85	5.6033	"	0.2356	–
6/10/85	5.5658	"	0.1969	–

Table 2. (cont.) Summary of Broad-Band Transformations

Band: I

Date	C0	C1	C2	C3
8/28/84	3.8928	0.0499	0.1005 ± 0.0034	−0.0397
8/29/84	"	"	0.1021 ± 0.0055	"
8/30/84	"	"	0.0989 ± 0.0027	"
8/31/84	"	"	0.1122 ± 0.0023	"
9/01/84	"	"	0.1033 ± 0.0018	"
4/28/85	6.7058	−.0043	0.1000	–
5/14/85	1.549	0.032	0.1000	–
5/15/85	1.289	"	"	
6/08/85	6.7637	−.0050	0.1055	–
6/09/85	6.7482	"	0.1357	–
6/10/85	6.7127	"	0.1292	–

system. The color residuals for a typical CTIO night's transformations are shown in Figure 2; a typical KPNO night's color residuals are shown in Figure 3.

The data for the weather shortened night of 4/28/85 contained no observations at high airmass and so very little information to constrain the extinction. Values close to the mean KPNO extinction were adopted of $k_V = 0.18$ and $k_I = 0.10$. The zero points and the color terms were then calculated. The color terms were A1 = 0.033 and B1 = −0.0043. These could have been set to the values obtained during the later run but this increased the uncertainty in the transformation so the measured values were used. The KPNO transformation and extinction results are listed in Table 2 as well.

Intermediate-Band Transformations

The instrumental magnitudes in the intermediate-bands for the standard and the late-type program stars were calculated in the same way as the broad-band instrumental magnitudes. Nightly extinction measures were then used to correct the measured 77−81 color. If the measured extinction did not vary by more than about 10% from night to night of a run a mean extinction was calculated for all nights and adopted as the extinction for the run. A zero point shift was used to bring this color onto the intermediate-band system as defined in Chapter 3. This shift could vary from night to night of a run. The shift could be the result of an instrumental zero point change — an occurrence which was never noticed to a significant degree in the broad-band transformations. This shift could also be produced by the weather due to saturation of some of the telluric water bands in the

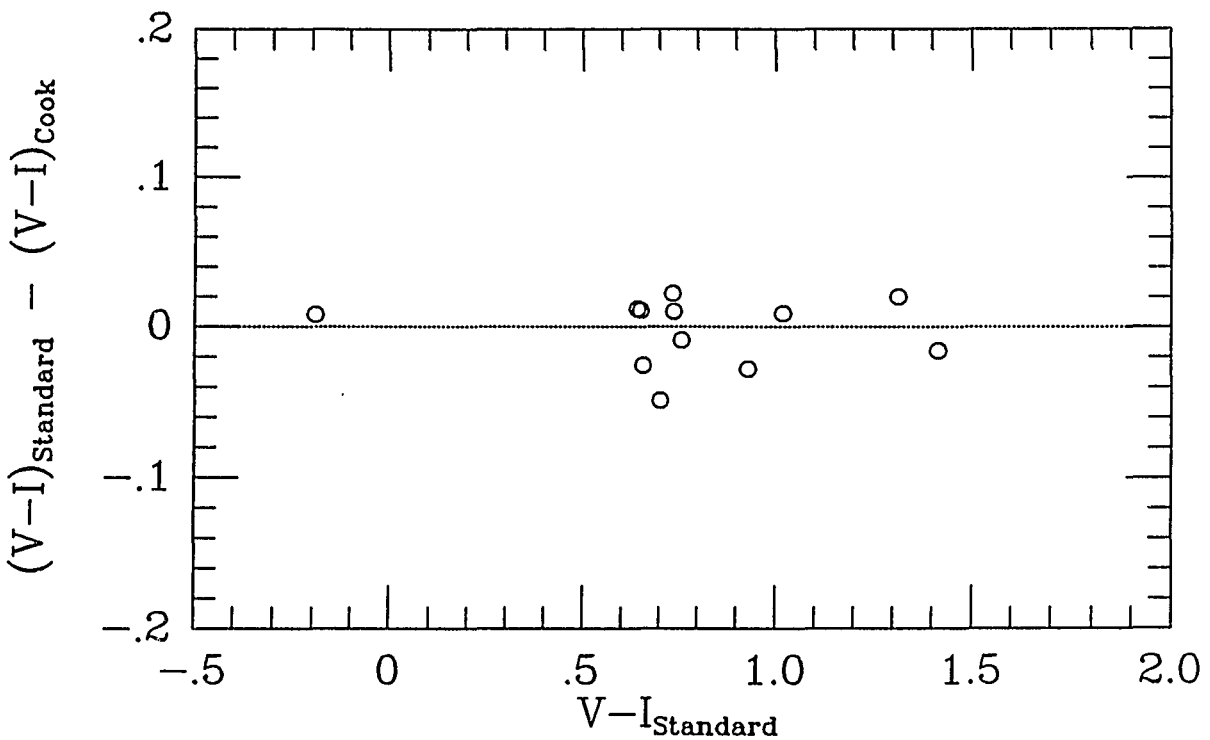

Figure 2. Color Residuals from the Night of August 30, 1984

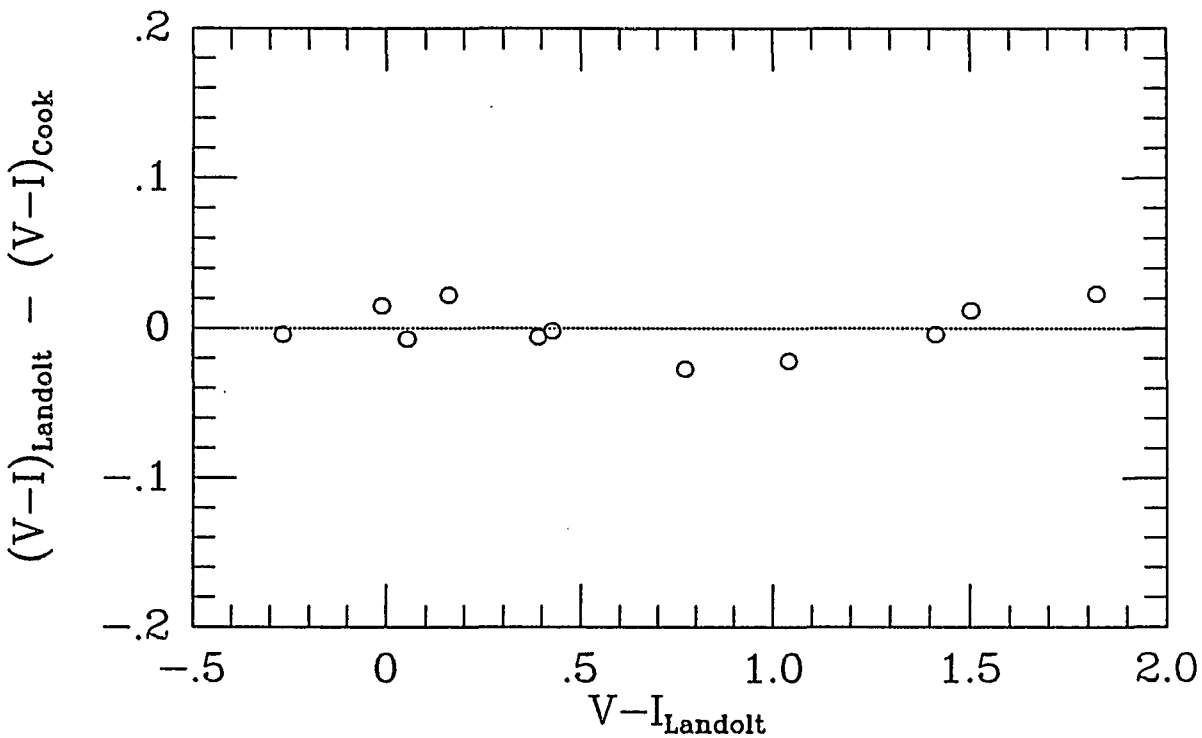

Figure 3. Color Residuals from the Night of June 9, 1985

81 passband. This effect is discussed in more detail in the third chapter because of its relation to the definition of the 77−81 system. It was found that a color term was never required to bring the data from the three different, instrumental systems used in this work onto the same standard system. The 77−81 transformations are summarized in Table 3.

Bright Star CCD Photometry

Bright ($V < 12$) program stars were photometered in the same manner as standard stars. There was also a series of observations on 6/10/85 of some of the field giants which had been observed at the 0.4-m. These were observed through a three per cent transmission, neutral density filter. Standard stars were also observed through the ND filter to check that the transformation was the same as without the ND filter. The broad-band transformation was the same as that without the ND filter except for the zero point. The intermediate-band transformation also required a color shift of 0.015 mag to bring the ND colors into agreement with the observations without the ND filter. This was the same result as that found using an ND filter for the photoelectric photometry.

Globular Cluster Photometry

Stars were identified in frames of globular clusters obtained at KPNO which were roughly five standard deviations above the sky level. Photometry was performed on these stars using a six pixel aperture (5.16 arcsec). This small aperture was used to reduce the effect of crowding in these crowded fields. The magnitudes were corrected to the 13.76 arcsec aperture used for

Table 3. Summary of Intermediate-Band Transformations

All 77-81 transformations were of the form:

$$\text{observed } (77-81) = \text{system } (77-81) + C0 + C1 * X_{77} - C2 * X_{81}.$$

Color: $77-81$

Date	C0	C1	C2
8/28/84	−.060	0.075	0.051
8/29/84	−.066	"	"
8/30/84	"	"	"
8/31/84	−.032	0.062	0.051
9/01/84	−.039	"	"
4/28/85	−.024	0.103	0.124
5/14/85	0.122	0.072	0.057
5/15/85	−.078	"	"
6/08/85	−.021	0.103	0.124
6/09/85	"	"	"
6/10/85	"	"	"

the transformation to the standard system by identifying isolated, bright stars on the frame and measuring their mean magnitude difference between the two apertures. The crowded nature of the fields and the low sky levels limited the accuracy of this aperture correction to ±0.005 mag for a frame.

Point-Spread Function Photometry

The point-spread function (psf) is a description of the stellar image produced by a convolution of the seeing and the telescope optics. This function is certainly not constant in time; it must be determined for each data frame. The PSF may not be constant across the frame. The optical design of the CTIO 4-m (only CTIO 4-m data was analyzed by psf fitting) was optimized for a much larger field than used by the CCD so that the image shape in the focal plane would not be expected to vary. The irregular surface of the CCD in the $f/2.7$ beam might cause a position dependent psf but a brief analysis of the results presented later did not show a correlation of the coordinate within a frame and the fitting error of an empirical psf.

The primary purpose of the DAOPHOT program is to calculate magnitudes for stellar images by simultaneously fitting an empirical point spread function to all of the stellar images in a defined group. This procedure produces good photometry of crowded fields and blended images. The main user input is in the construction of the point spread function which is done in an interactive manner. My use of DAOPHOT followed the general precepts laid out in the manual (Stetson 1983, 1987).

Stellar images were identified using the FIND routine with the threshold set to reject brightness enhancements less than three standard

deviations above the local sky. Magnitudes were estimated from aperture photometry using a relatively small aperture. Bright stars with less than 15,000 data units in their peak were examined as psf candidates. Stars with more than 15,000 data units in their peak pixels were considered to be too close to the reputed nonlinear regime of the chip. A psf candidate was rejected if it was too crowded, near any chip defects or cosmic ray events, near the edge of the frame, or obviously a blended image. All remaining stars within one magnitude of the top candidate were then used to construct a point spread function. The restriction on brightness is suggested by Stetson because of noise considerations. A star one magnitude fainter than the brightest psf star will add as much noise in the wings of the psf as signal in the core. Two to four images were used to construct the psfs used here. The procedure is iterative and produces an empirical point spread function. For the CTIO plate scale of 0.6 arcsec per pixel, the data was undersampled for most of the seeing which was encountered. The undersampling mandated the use of more than one star to create the psf so that the vagaries of the undersampling did not seriously affect the constructed psf.

The first approximation to the psf is found by summation of the observed psf stars' intensities. The result should be a fairly accurate point spread function within a few arcsec radius of its center because the candidates were chosen to not be crowded. The stellar images near the psf stars are then fit with this approximation and subtracted from the frame to produce a frame with the psf stars in a less cluttered environment. A second approximation is created from this new frame. This procedure is repeated with the radius of the fit increased, reflecting the elimination of neighbors from the psf stars'

neighborhood and so from the outer portions of the psf. It is useful to examine the results of subtracting the psf stars themselves from the frame during this construction to ensure that each one is being well fit by the sum. The iterations are continued until a psf is constructed from a frame in which all the neighbors of the psf stars are cleanly subtracted. The psf radius must be large enough to include all of the stellar image.

After a psf was derived for each frame, it was fit to all of the stellar images identified in the frame one by one. The fitted images were subtracted and the resultant frame was searched for images which had not been previously identified by FIND. Rough magnitudes were derived for the newly found images using synthetic aperture photometry at their positions in the original frame and they were added to the star list for the frame. This star list was then broken into groups of stars which would be simultaneously fitted with the psf. These groups were defined by the fact that all members of the group are separated by less than a set amount from at least one other group member. Ideally, this separation would be the full magnitude aperture radius for the frame plus the radius over which the psf would be fit to an image. This would ensure that a group would contain all the stars which affected the psf fit of any of its members. This was not practical for this data because of computing limitations. The cpu time required to perform a simultaneous fit to a group of stars increase as the cube of the number stars in the group. The group size in this work was always 30 or less. Groups within the size limitation were derived by taking all oversize groups with the ideal separation and regrouping the stars with successively smaller separations until all images were members of groups with 30 or less

members. The minimum separation used was never less than 2.7 arcsec (4.5 pixels), a separation which cracked even the most stubborn amalgamation of images into manageable groups.

The output of the multiple psf fitting for each stars is an accurate centroid for the image, a magnitude relative to the psf, an estimate of the goodness of the fit (CHI), an error estimate, the modal sky value used, the number of iterations required for the fit and a measure of the image peculiarity. The peculiarity measure, SHARP, is essentially the difference of the fitting residuals in the outer and inner portions of the fit. A crowded image will have a large positive SHARP value as will an extended image such as that of a galaxy. A cosmic ray or a hot pixel in the inner portion of the fit will yield a large negative value for SHARP. Photometry of images which had abnormally high or low SHARP values was rejected.

The magnitudes derived for the fitted stars are relative to the magnitude of the point spread function. This is just the sum of the psf stars aperture magnitudes. The aperture chosen, 2.4 arcsec, was small enough that it would not be contaminated by adjacent stars. It was large enough to be a good measure of the psf stars' brightnesses since the full width at half maximum was always less than 1.2 arcsec. To obtain the total magnitude for the photometry, an aperture correction for the frame must be measured. This is the difference between the magnitude in the small aperture used to set the psf magnitude and the total magnitude. This correction was measured for twenty to forty of the brightest stars which are still within the linear range of the chip by subtracting all of the other fitted images from the frame. Aperture photometry was performed on the resultant frame in the

same way that total magnitudes for the bright standards were determined and the mean of the best growth curves was used to define an aperture correction for the psf photometry in that frame. This aperture correction was compared to that for the most isolated stars in the original frame and always found to be close to the best estimate without cleaning the frame. The corrected magnitudes were then put on the defined system by applying the transformations determined for the night the data was obtained.

The uncertainty of the final magnitudes is due to four main sources. There is an uncertainty in the instrumental magnitude reported by DAOPHOT due to measurement of the sky. There is uncertainty due to psf scaling. The psf uncertainty arises from uncertainty in the empirical form of the psf and in its fit to a particular star. These uncertainties are calculated by DAOPHOT using Poisson statistics to estimate the uncertainty due to the relatively small number of photons per pixel in the sky and the psf. After properly accounting for the statistical errors DAOPHOT arbitrarily adds 0.0075 mag of uncertainty because experience had led Stetson to find that this produced a more realistic error estimate. There is also an uncertainty in determining the aperture correction for each frame which is primarily composed of the uncertainty in sky values because of the need for large apertures. The final source of uncertainty is the transformation to a defined system. For the broad-band system, the formal uncertainty in the various coefficients as estimated in the least squares minimization of CCDCAL was ± 0.002 to ± 0.004 mag, but the observational scatter of the standards about this solution was about ± 0.01 mag. The uncertainty in the transformation to the intermediate-band system is simply the uncertainty in measuring the

relative extinction coefficient of the 77 band with respect to the 81 band. In summary, the external and errors are estimated to be the quadratic sum of the reported DAOPHOT errors, errors in the transformation, and errors in the aperture correction. The formal uncertainty for the transformation is small and the uncertainty in the aperture correction is about equal to the arbitrary 0.0075 mag added by DAOPHOT to its error estimate. Thus the DAOPHOT reported errors are reasonable estimates of the total error.

Completeness Tests

DAOPHOT is designed to allow for the addition of artificial stars into frames of real data. This procedure will produce estimates of the star finding efficiency and the photometric accuracy of the multiple star psf fitting procedure. The user chooses the number of stars to be added to the frame and the magnitude range within which they will all lie. The program uses the host computer's random number generator (DEC's VMS 4.1 random number generator for these tests) to select positions and magnitudes from the specified range. For the tests done in this thesis, ten separate additions of different sets of 100 stars were examined. This was done so that each set of additions would not significantly affect the crowding in the frame. The artificial star images were in the form of the defined, empirical point spread function. The frame containing the additions was then reduced as a new frame, but in exactly the same manner as the original. The resulting photometry was searched for the added images. An added image was considered to have been recovered if it was found within 0.3 arcsec of the position where it had been added. The recovered image was rejected as not that of the added image

if its recovered magnitude differed from its added magnitude by more than 1.4 times the recovered's magnitude's uncertainty. The error distribution of the recovered stars was essentially the same as that estimated for the real stars in the magnitude ranges that these tests were done except for a small number of widely discrepant points. These points were due to overlapped images or "recovery" of the wrong star. The "loss" of these stars gave a direct measure of the incompleteness in a given magnitude range due to crowding.

Reddening

Reddening corrections were calculated from the work of van de Hulst (1949). Van de Hulst's curve #15 was used to derive the ratio of the intermediate-band color excess, E(77−81), and the broad-band color excess, E(V−I), to E(B−V). These ratios were determined to be 0.134 and 1.35 respectively. This analysis does not take into account the effective wavelength change for the passbands produced by the interstellar extinction. Dean, Warren and Cousins (1978) have examined the wavelength dependence of reddening on the Cousins V−I. Their theoretical analysis used Nandy's reddening law rather than van de Hulst's. For a star with a $(B - V) = 1.6$, which is the color of essentially all stars of interest in this thesis, the ratio was found to be:

$$E(V - I)/E(B - V) = 1.25 * (1.096 + 0.012 * E(B - V)).$$

This formula yields ratios of 1.37 to 1.38 for all of the reddenings encountered in this work. The color dependence is insignificant. The ratio of the total absorption to the color excess in the V passband was assumed to be 3.05.

Summary

The foregoing techniques were used for the reduction of the data in the following chapters. If there were deviations from the general procedures presented here they will be noted in conjunction with the data they to which they apply. There are two appendices which present the psf photometry for the Baade's Window field and the Sagittarius Dwarf. The errors presented are those calculated by DAOPHOT. The CCD photometry for the reddest cluster giants is presented in the body of Chapter 3. Chapter 3 also contains the photoelectric photometry results. In anticipation of the results, I will note that due to all of the factors noted here and some which will be mentioned later, the cluster photometry and the photoelectric photometry are good to only about ± 0.01 mag even though the program stars were quite bright.

CHAPTER 3

THE 77–81 INTERMEDIATE-BAND PHOTOMETRIC SYSTEM

Late type stars are best studied at longer wavelengths because they are much brighter there. Nassau and van Albada (1948) showed that even at dispersions of 3400Å mm^{-1} carbon and M stars could be spectroscopically identified due to the prominent molecular bands of CN and TiO. Wing (1967) developed a set of 30Å "band passes" for the study of late type stars in the near infrared which were situated to take advantage of some of these molecular absorption bands. He found that a band centered at 7812Å was very sensitive to TiO absorption and that a pair of bands at 8116Å and 8140Å were sensitive to CN absorption in carbon stars. It is interesting to note that these bands were in his program primarily as continuum points. The fact that a useful continuum point for M stars (8140Å) is situated on top of a region of CN absorption and that a useful continuum point (7812Å) for carbon stars is located in a region of strong TiO absorption suggested to Wing and Stock (1973) that a simple two filter system for the discrimination of C from M type stars could be developed. Although the C_2, Swan bands of carbon are a more direct measure of the carbon abundance in a star, and there are stronger TiO bands than those near 7750Å, the complementary nature of the 77 and 81 passbands with respect to continuum determination and their red central wavelengths should make them an efficient system for the determination of C and M types.

The spectral region near 7812Å contains the (0,1), (1,2), (2,3), and (3,4) band heads for the red, gamma system of TiO (Pearse and Gaydon, 1963). This group of band heads causes a large trough of absorption to extend from the atmospheric A band redward as can be seen in the spectrum of the M6 III star, BS6146, shown in Figure 4. The spectral region near 8100Å contains the (2,0) and (3,1) band heads of the cyanogen, red system. These bands also degrade to the red as can be seen in Figure 4 where the spectrum of UX Dra, a C7,3 carbon star, is also shown. From a consideration of the widths of these features it can be seen that band passes of a few hundred angstroms would be useful. In fact, Wing (1967) combined his measurements at 8140Å and 8116Å to create a useful CN index.

The suggestion of Wing and Stock (1973) was not acted upon until Palmer and Wing (1982) applied a three filter modification to the photographic examination of globular clusters for carbon stars. Shortly thereafter Marc Aaronson (Aaronson et al. 1984) and Harvey Richer (Richer, Crabtree and Prichett 1984) designed filter systems based upon Wing passbands for use in CCD imaging. The filters used in this thesis were designed by Marc Aaronson and were purchased from Spectro-Optics in Sylmar, California. These filters are interference filters which are anti-reflection coated on one side. The central wavelength of the 77 filter is 7752Å and the full width at half maximum transmission is 284Å. The central wavelength of the 81 filter is 8104Å and the full width at half maximum transmission is 365Å. Both filters have a broad flat maximum which is at about 86% transmission and 120Å wide in the 77 filter and 89% transmission and 160Å wide in the 81 filter.

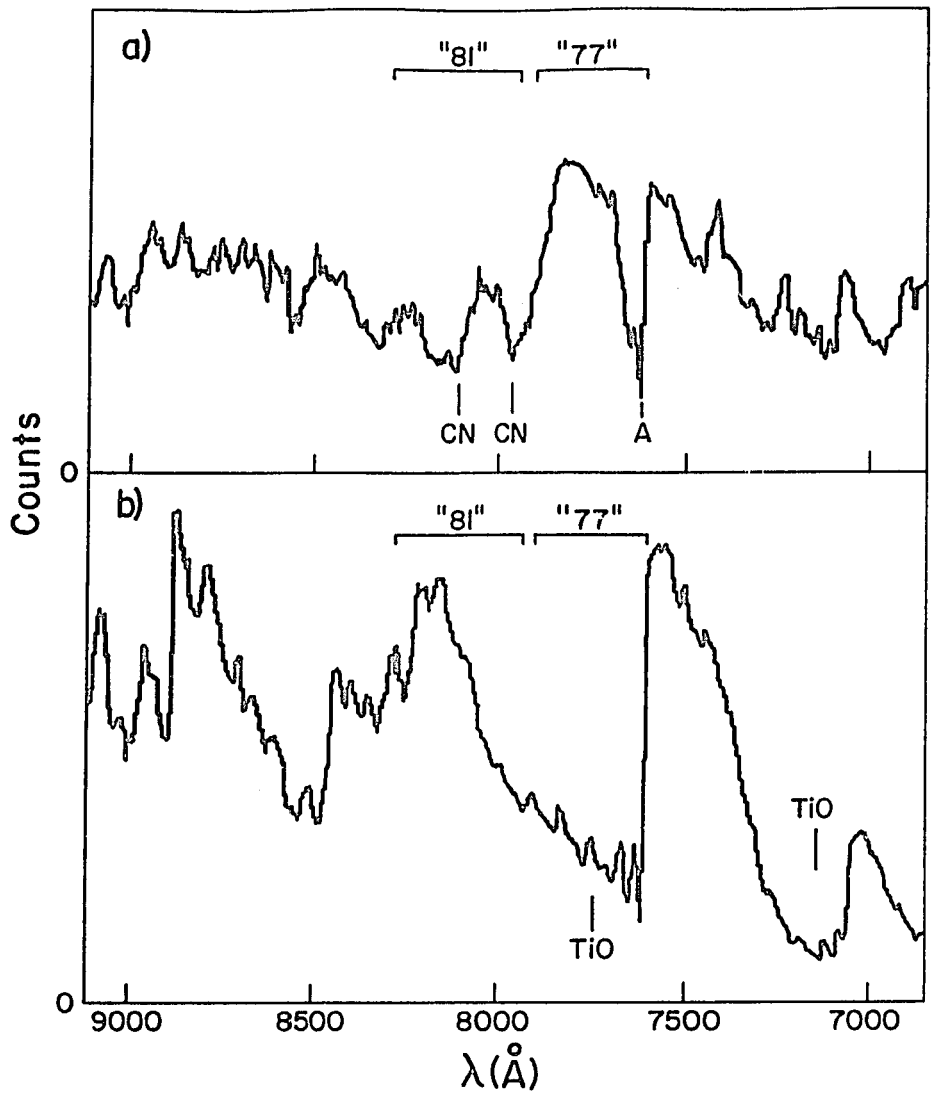

Figure 4. The Positions of the 77 and 81 Passbands

Raw spectra of (a) UX Dra an C7,3 carbon star and (b) BS 6146 an M6 III star are shown with the 77 and 81 passbands indicated.

Theoretical Analysis

The passbands of the intermediate-band filters are in regions which are relatively free of strong, atomic absorption lines. In fact, this is one of the reasons that these passbands were chosen. Consequently, a simple theoretical analysis of the expected flux through each filter from a blackbody should be applicable to observations of early type stars. The flux from a black body at a given wavelength, lambda, is given by the formula

$$F_\lambda = \frac{2\pi hc^2\lambda^{-5}}{e^{hc/\lambda kt} - 1}$$

Using central wavelengths of 7750Å and 8100Å, passbands of 284Å and 365Å, and considering the passbands to be small with respect to the central wavelengths, the total flux emitted from a blackbody within each filter's passband is

$$F = \frac{2\pi hc^2\lambda^{-5}}{e^{hc/\lambda kt} - 1}\Delta\lambda$$

The detectors used for observations at these wavelengths are all photon detecting devices and so the observable is directly related to the photon flux which is given by

$$77 - 81 = -2.5\log\frac{F_{77}\lambda_{77}}{hc} + 2.5\log\frac{F_{81}\lambda_{81}}{hc}$$

This formula can be used to calculate the expected photon flux from a blackbody of a given temperature. For this simple analysis, I will just consider the relative quantum efficiency at the central wavelengths of an idealized RCA CCD. The chips used at KPNO and CTIO came from the same batch and should have similar quantum efficiency curves (P. Seitzer, personal communication). There is a drop from 42 to 33 per cent efficiency from 7750Å to 8100Å as estimated from the curves published in the NOAO

Newsletter # 8. This is a 21 per cent drop in efficiency which translates the above curve 0.22 mag to the blue when the relative transmissions of the filters are also considered in the calculation of the number of photons detected. In order to apply these calculations to stellar observations, it is necessary to transform the blackbody temperature to an observable color index. The V−I color is a good index for late type stars because of the wide separation of the V and I central wavelengths and the red central wavelength of the I passband. I have used the transformation of Bessel (1979) for the transformation to Cousins V−I . Table 4 lists temperatures, broad band colors and intermediate-band colors calculated from the above equation and the noted corrections. Figure 5 plots this data in a color-color diagram. As would be expected, the intermediate-band color shows a weak dependence upon temperature. When plotted against V−I color this theoretical track shows the loss of sensitivity of the V−I index at high temperatures and its extreme sensitivity at low temperatures. If a star emits less energy in the 77 filter's passband, as would be expected for an M star with significant TiO absorption, then the star's observed colors should place it on the red side of the blackbody track. If a star has significant absorption in the 81 filter's passband, as would be expected for a carbon star and CN were present, then the stars colors would place it to the blue of the blackbody curve. These molecular band tracks would separate from the blackbody track at red V−I colors since low temperatures are necessary for the formation of molecules.

There are a number of reasons for considering this track in the color-color plane rather than on the simpler, one dimensional, 77−81 color line. The blackbody region of the 77−81 color line is almost 0.2 mag wide

Table 4. Black Body Colors

°C	77 − 81	V − I	System[a]
13000	−.0314	−.120	0.002
12000	−.0273	−.085	0.016
11000	−.0224	−.055	0.011
10000	−.0164	−.020	0.017
9500	−.0128	.015	0.021
9000	−.0088	.072	0.025
8500	−.0042	.155	0.030
8000	.0010	.250	0.035
7500	.0071	.330	0.041
7000	.0141	.415	0.048
6500	.0223	.515	0.056
6000	.0322	.625	0.066
5500	.0440	.760	0.078
5000	.0585	.930	0.092
4750	.0671	1.000	0.101
4500	.0767	1.110	0.110
4250	.0875	1.280	0.121
4000	.0997	1.530	0.133
3750	.1137	1.970	0.147
3500	.1299	2.760	0.164
3250	.1486	3.800	0.182

Notes:

(a) The calculated 77−81 colors were shifted to match the observed colors of the mean G0 star.

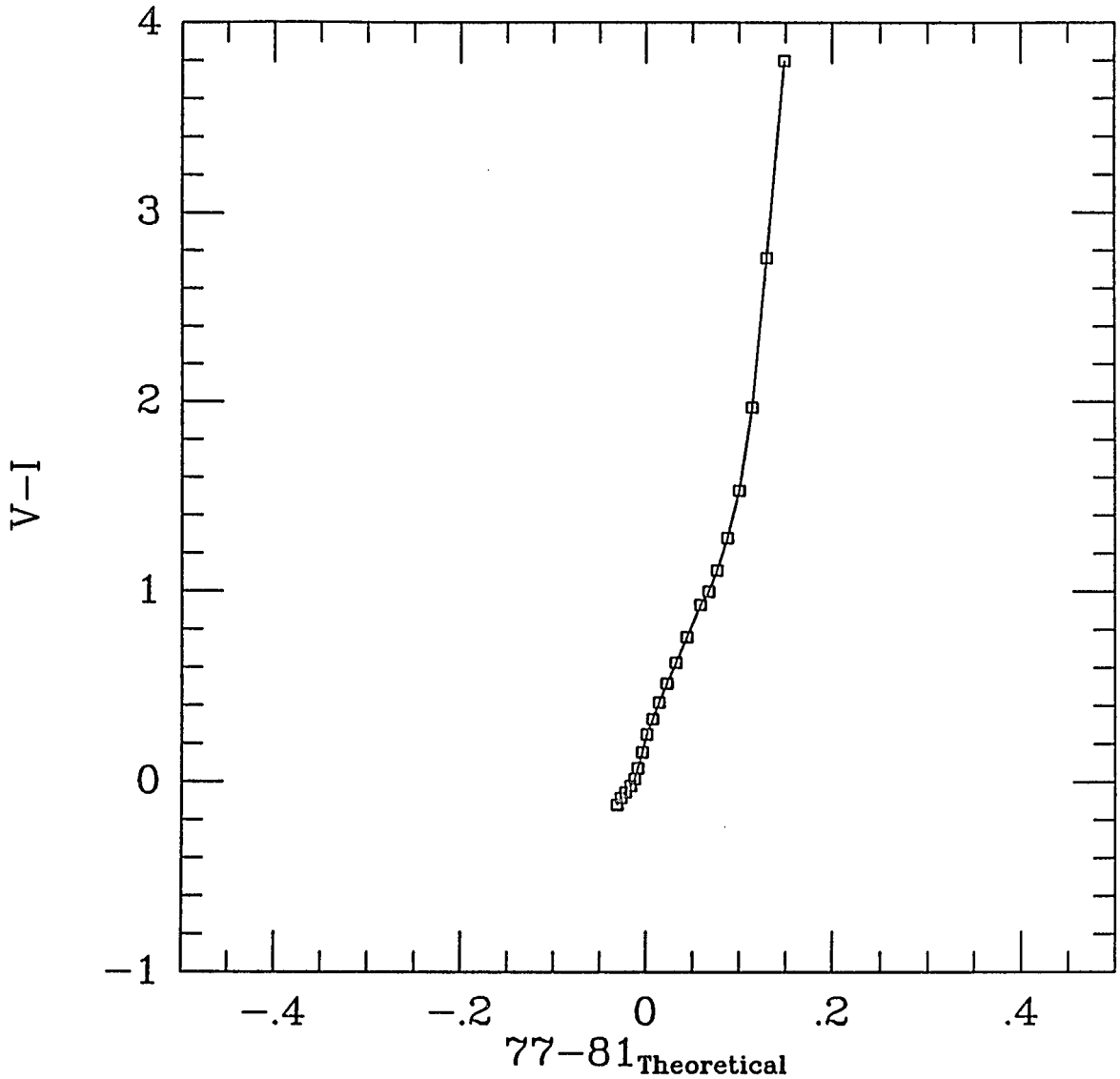

Figure 5. Theoretical Color-Color Diagram of a Black Body

because of the weak temperature dependence of this index. This width destroys discrimination of deviations from a blackbody unless some function of temperature is also measured. There is at least one atomic feature which could confuse measurements of 77−81 only. Na I absorption at 8183,8195Å can be strong in dwarfs. For cool dwarfs, this absorption becomes rapidly swamped by molecular band absorption although it could reduce a very early M star's 77−81 color. The primary problem this Na I absoprtion is expected to cause is the placement of stars, which are not carbon rich, on the carbon star side of the blackbody curve. With the addition of the broad band color this is not such a problem. If the dwarf is cool, it will show enough molecular absorption so that if [O] > [C] it will still appear on the red side of the blackbody curve (where [X] is defined as log[(number density of X)/(solar number density of X)]). If [C] > [O], then it will be in the carbon star region where it belongs. Carbon stars do, however, appear at higher temperatures than M stars (R type carbon stars are the temperature of K stars) and there may be K dwarfs with strong Na I at these temperatures as well as metal poor, halo, subdwarf K stars with very strong atomic lines. But, without the V−I color, such dwarfs would pollute the whole carbon star region. With the V−I color, these stars only confuse the region where the early type carbon stars will be found. Thus the blue, 77−81 side of the blackbody curve which is redder than a K star's colors (V−I> 1.7), will be free from this contamination. Wing (1967) found easily measurable CN in essentially all K and M giants with the mean CN band strength increasing with luminosity class. Wing (1967) also found that his CN index in K and M giants showed a high dispersion which he attributed to different [N] for

these stars. This CN is a result of the stability of the CN molecule and is not due to an overabundance of carbon. Its presence sets the boundary of the carbon star region quite a bit to the blue at the V−I color of a K star.

Another contaminant of the carbon star region in a simple one dimensional technique could be from A type stars due to the Paschen continuum. The Paschen limit is at 8203Å and can be expected to give A stars abnormally blue 77−81 colors because the 81 filter extends to about 8275Å.

Defining the System

The primary purpose of the intermediate-band filters is to measure the presence of CN or TiO absorption with the 77−81 color. This simplifies the definition of the intermediate-band system since it is only needed to set up a group of color standards. Because the passbands are relatively narrow, color terms are not expected in transforming from observations made with one system to another. A color term only arises from a variation in the effective wavelength due to detector differences or energy distribution differences. This is one of the clear advantages of making these passbands as broad as they are rather than a few tens of angstroms wide. Because the filters are interference filters, there is a shift in effective wavelength in non-parallel light. This shift is small compared to the passbands even for the relatively fast beam of the CTIO prime focus CCD system ($f/2.66$). For a $f/2.66$ beam, the wavelength shift is calculated to be about 16Å (Corion Corp. catalog 1985). The approximately 300Å passbands are small with respect to continuum slope changes in stars and they are also small with respect to

detector, quantum efficiency slope changes. Consequently, over these spectral ranges, such small differences which do exist should not produce significant shifts in the effective wavelength. This means that an instrumental color will require only a constant to bring it onto a defined system. If magnitude standards were defined, it would require the measurement of two constants.

Astronomical magnitude systems are usually defined so that an A0 star has a zero color index for all indices. Conforming to this convention, I have defined an A0 star's 77−81 to be zero. Currently, this means that for a trio of bright (not too reddened) A0 stars whose mean V−I = 0.002, 77−81 has been set to 0. Photometry for these stars was obtained using a photoelectric photometer on a single run of two nights and so the system must be considered provisional. These measurements do provide a standard so that observations at different times and with different instruments can be compared and that is what a system is designed to do. Because of the scarcity of standards, a number of secondary 'standards' were developed from observations on two CCD runs which bracketed the photoelectric run. In practice, it is these secondary standards which are used to determine the transformation to the system.

Extinction

Perhaps the most vexing problem encountered in the use of the intermediate-band filters has been the determination of the extinction. At first glance, the actual value of the extinction would not seem to be important since the intermediate-band measurements are usually made at low airmasses and at almost the same time. Thus, because of the small

difference in effective wavelength and the likely low extinction because of the long wavelength, the 77−81 color should not be greatly affected. This has not been the case.

The 81 filter includes within its passband a number of atmospheric water features. The H_2O (1,2,1) band has its origin at 8227Å and extends from 8161Å to 8287Å with many distinct features but no clear band head (Pearse and Gaydon 1963). It is also possible that the extinction for the 77 passband be affected by atmospheric oxygen because it slightly overlaps the A band. The extinction was noted by Wing (1967) to be variable from night to night using his 30Å scanner passbands. Wing (1967) found the extinction at 7812Å to vary from 0.045 to 0.100 mag/airmass with a mean of 0.072 in his thesis data which comprised 35 good nights. The extinction at 8116Å varied from 0.055 to 0.120 mag/airmass with a mean of 0.082, while the extinction at 8140Å varied from 0.070 to 0.150 mag/airmass with a mean of 0.112 during these same nights. Baumert (1972) reported similarly wide variations for 56 photometric nights using the Wing (1971) eight-color system. He found the extinction at 7809Å to vary from less than 0.00 to 0.11 mag/airmass and the extinction at 8122Å to vary from less than 0.00 to 0.15 mag/airmass. Baumert (1972) adopted an acceptable range of extinctions which included more than two thirds of his nights at each wavelength which were 0.020 to 0.085 at 7809Å and 0.025 to 0.095 at 8122Å. The mean extinction for the acceptable nights was 0.053 mag/airmass at 7812Å and 0.060 mag/airmass at 8122Å. Hayes (1970) determined extinction values for 30Å passbands which were not supposed to be seriously affected by atmospheric features. He found extinction values of 0.076 mag/airmass at 7780Å and 0.080 mag/airmass at

8090Å. Table 3 (in chapter 2) lists the extinction values which I have adopted for the various observing runs as described in Chapter 2. It is important to note that the difference between the 77 and 81 extinction coefficient can change by a few hundredths of a magnitude.

Wing (1967) also found that in order to determine absolute fluxes it was necessary to analyze his data assuming that some of the water absorption lines were saturated. He found this to be the case in both his 8116Å and 8140Å bands. A simplified analysis which considered the extinction to be composed of an airmass dependent and an airmass independent term was sufficient to account for this saturation. The airmass independent term is variable and its determination would require the measurement of zero point terms for the intermediate-band magnitude transformations. This saturation effect does not affect the determination of the color extinction coefficient; it merely serves as a zero point shift to the zero airmass color. I have accounted for it by the use of a zero point term in the color transformation which does not arise from shifts in detector sensitivity.

Standards

The set of stars which currently serve as standards for the 77−81 system were picked because they were observed several times during the spring of 1985. The primary standards used for tying this set of observations together were: the A0 Landolt standard, 102-58, the M 5 dwarf, Gleise 581, and the carbon star, Yamashita 237. They provided a broad range of 77−81 values in order to check for possible color terms in the transformations. These stars were observed during each of the spring runs at least once and

102-58 was observed on all nights expect the first night of photoelectric photometry. Because of the desire to set $77 - 81 = 0$ for an average A0 star, the three A0 stars observed during the photoelectric photometry run were used to determine an average instrumental 77−81 for an A0 star. The instrumental colors were very close to that of the desired system, i.e. these A0 stars had an instrumental $77 - 81 = -.077 \pm 0.008$. These stars also have an average $V - I = 0.00$ and the 77−81 color was put on the system by adding a small constant. The values so determined for 102-58's, Y237's and G581's colors then became the primary standards.

Table 5 lists stars whose 77−81 color can be considered to be relatively well determined because of multiple observations often on different nights. These stars fall into two groups, those which were observed in the north and those observed in the south. The problem of tying the southern observations into the northern system has been discussed in the data reduction chapter, but it is likely that there is about 0.010 mag uncertainty in the 77−81 zero point. Figure 6 shows all standard stars and late type stars plotted in a color-color diagram which also contains the blackbody line. This figure contains photometry from four observing runs on three, different telescope-instrument systems. The relatively tight locus followed by all but the carbon stars demonstrates that all of the observations have been brought onto the same system. The blackbody curve has been shifted by the addition of a constant to the 77−81 values from that predicted above so that the predicted 77−81 of an G0 star matches the mean observed 77−81 (0.065). The reason for this shift is that the Paschen continuum does affect the colors of A stars and if the curves were matched at the A0 point, then the

Table 5. Bright Star Data from all Runs

Id	77−81	V−I	Run[a]	Type	Source[b]	Comments[c]
127	−.165	1.854	6	C3,5ch	Yamashita	
130	−.170	1.138	6	C3.3	Yamashita	
131	0.017	0.944	6	C3,0	Yamashita	
146	0.063	9.999	6	C0,0	Yamashita	
147	−.149	3.447	6	C5,5	Yamashita	
149	−.111	3.264	6	C5,5	Yamashita	
237	−.239	2.029	6	C4,4	Yamashita	
"	−.241	1.993	5	C4,4	Yamashita	
"	−.236	2.005	4	C4,4	Yamashita	
239	−.054	1.473	6	C1:,1ch	Yamashita	
"	−.027	1.443	5	C1:,1ch	Yamashita	
249	−.233	1.958	6	C3,5J	Yamashita	
"	−.235	1.923	4	C3,5J	Yamashita	
255	−.043	3.580	6	C8,1	Yamashita	
581	0.336	2.536	6	M5 V	Gliese	
"	0.340	2.711	4	M5	Gliese	
"	0.349	2.499	5	M5	Gliese	
587.1	0.164	1.883	6	M0 V	Gliese	
"	0.045	0.059	4	M0 V	Gliese	
"	0.167	1.902	5	M0 V	Gliese	
589A	0.298	2.405	6	M4	Gliese	
589B	0.466	3.091	6	M6	Gliese	
629.1	0.143	1.624	5	M0 V	Gliese	
4567	0.006	−.016	5	A0 V	BS	
4781	−.009	−.049	5	A0 V	BS	
5859	0.021	0.040	5	A0 V	BS	
5858	−.015	−.047	6	A0 V	BS	
6627	0.011	−.011	6	A1 V	BS	
70272	0.113	1.640	5	K4.5III	MS	(Id ?) III−IIIb
79097	0.250	1.928	4	M2 III	Landolt	(Variable ?)
89056	0.185	1.858	6	M1.5	MS	
"	0.163	1.859	5	M1.5III	MS	IIIab
98118	0.141	1.701	5	M0 III	MS	III−IIIab
99196	0.086	1.383	5	K4 III	BS	
10089	−.044	−.073	5	B9 V	MS	(Oke & Hayes)
101282	0.068	0.527	4	F5	Landolt	
101281	0.139	0.860	4	G3:	Landolt	
102212	0.168	1.746	5	M1 III	MS	IIIab
102466	1.265	1.068	4	K0 III	Landolt	
102472	0.160	0.980	4	G9 III	Landolt	
10258	0.002	0.071	5	A0	Landolt	
"	0.004	0.054	4	A0	Landolt	
"	0.002	0.060	6	A0	Landolt	
104216	0.239	1.945	5	M2 III	BS	(Var?, R−I=1.04 gives V−I)

Table 5. (cont.) Bright Star Data from all Runs

Id	77−81	V−I	Run[a]	Type	Source[b]	Comments[c]
105205	0.101	1.419	6	M0	Landolt	
"	0.100	1.434	5	M0 III	Landolt	
10528	0.068	1.039	5	G9 III	Landolt	
105214	0.066	0.622	5	G0	Landolt	
105448	0.028	0.325	5	A3	Landolt	(Id ?)
105663	0.044	0.429	6	F2	Landolt	
107595	0.068	0.611	5	G0 V	Landolt	
107970	0.430	2.567	6	M7 III	Landolt	(Variable)
"	0.422	2.588	4	M7 III	Landolt	
107970	0.425	2.565	5	M7 III	Landolt	
108475	0.059	1.254	5	K0 III	Landolt	(Id ?)
108702	0.061	0.612	4	G2 V	Landolt	
109231	0.077	1.492	6	K2 II	Landolt	(TiO may be present)
109747	0.060	0.396	6	A0	Landolt	
110353	0.222	2.306	5	M0 III	Landolt	(K5 III Herbig)
110340	0.045	0.346	5	A4	Landolt	
110471	0.102	1.450	5	M0 III	Landolt	
110441	0.082	0.644	5	F3	Landolt	
111775	0.163	1.815	4	?	Landolt	
111773	0.061	0.267	4	B9	Landolt	
112142	0.248	2.129	5	M3 III	MS	IIICa−1
112595	0.153	1.800	6	K2:III:	Landolt	
112636	0.071	0.799	6	G7:	Landolt	
112769	0.147	1.719	6	M1 III	MS	IIIb
112822	0.064	1.064	6	G8 III	Landolt	
112805	0.021	0.138	6	A1	Landolt	
113996	0.142	1.721	5	K5 III	MS	
117675	0.218	2.049	6	M2 III	MS	
"	0.212	2.011	5	M2 III	MS	
118246	0.003	−.105	5	B5	Landolt	(Variable ?)
119228	0.192	1.952	6	M2 III	MS	IIIabBa0.7
"	0.200	1.942	5	M2 III	MS	IIIabBa0.7
120477	0.123	1.585	5	K5 III	MS	IIIv
"	0.113	1.590	6	K5 III	MS	IIIv
127665	0.075	9.999	5	K3 III	MS	
"	0.073	1.209	6	K3 III	MS	
141477	0.158	1.791	6	M0.5III	MS	IIIab Var?BS
141992	0.129	1.599	6	K4−5III	MS	Var?BS
"	0.118	1.588	5	K4−5III	MS	Var?BS
142574	0.148	1.696	6	M0 III	MS	
"	0.134	1.716	5	M0 III	MS	
143107	0.074	1.162	6	K2 III	MS	IIIab
148349	0.260	2.193	5	M2.5	MS	
149382	−.006	−.264	6	B5n	Landolt	
"	−.017	−.244	4	B5n	Landolt	

Table 5. (cont.) Bright Star Data from all Runs

Id	77−81	V−I	Run[a]	Type	Source[b]	Comments[c]
154143	0.251	2.098	5	M3 III	MS	
"	0.240	2.089	6	M3 III	MS	
160233	0.012	−.026	6	B1 V	Landolt	
163588	0.080	1.102	6	K2 III	MS	
167006	0.280	2.119	5	M3 III	MS	
"	0.250	2.133	6	M3 III	MS	
168720	0.159	1.810	5	M1 III	MS	
169414	0.046	1.113	6	K2.5III	MS	IIIab
205556	0.008	−.053	6	B9	Landolt	
e2o	0.078	0.638	9		Graham	
e2s	0.075	0.713	9		Graham	
e2I	0.086	0.958	9		Graham	
e3e	0.067	0.693	9		Graham	
e3k	0.077	0.660	9		Graham	
e3o	0.082	0.662	9		Graham	
e3v	0.072	0.659	9		Graham	
e7m	0.083	1.295	9		Graham	
e7s	0.077	0.768	9		Graham	
e9k	0.083	0.629	9		Graham	
e9n	0.061	0.683	9		Graham	
e9q	0.074	0.727	9		Graham	
93424	0.081	1.059	9	G8	Landolt	
94251	0.088	1.243	9	K1	Landolt	
94702	0.110	1.431	9	K2:	Landolt	
f11	−.012	−.260	9	A0p,Bp	Landolt	
f22	−.048	−.201	9	DA	Landolt	
192	−.116	9.999	9	C4,3	Yamashita	
193	0.054	9.999	9	C3,0ch	Yamashita	
208	−.212	9.999	9	C4,4	Yamashita	
212	−.252	9.999	9	C5,2	Yamashita	
237	−.282	9.999	9	C4,4J	Yamashita	
249	−.223	9.999	9	C3,5J	Yamashita	
173	0.261	9.999	9	M1	Gliese	
179	0.424	2.676	9	M4e	Gliese	
203	0.368	2.666	9	M5	Gliese	
204.2	0.333	2.421	9	M5	Gliese	
206	0.347	9.999	9	M4e	Gliese	
629.1	0.138	9.999	9	M0	Gliese	
642	0.155	9.999	9	M1.5	Gliese	
643	0.446	3.000	9	M4	Gliese	(V−I) from (R−I)$_J$=1.22

Table 5. (cont.) Bright Star Data from all Runs

Notes:

(a) Run 6 is the 6/8-10/85, KPNO observing run;
Run 5 is the 5/14-15/85, KPNO observing run;
Run 4 is the 4/28/85, KPNO observing run;
Run 9 is the 8/28-9/1/84, CTIO observing run.

(b) Yamashita carbon stars are taken from the list of Yamashita (1972, 1976); Gliese stars are high proper motion dwarfs from the list of Gliese (1969); Landolt stars are V and I standards from the list of Landolt (1983); BS stars are from the list of Hoffleit (1982); Graham E-region stars are taken from Graham (1982).

(c) The comments list finer typing available for BS stars, notations from the source regarding variability, and the source of the broad band color if not measured here.

blackbody curve would be too blue. This could be considered a defect of the passbands or of the definition of the system, but the A0 color convention was followed.

In addition to the deviation of A stars from the blackbody curve, there are three other regions where there is an obvious departure. The straight band of stars going to the red of the blackbody curve at V−I $\approx$ 1.5 is the result of TiO absorption; I will refer to this as the TiO track. The sprinkling of stars to the blue of the main track of stars (and to the blue of the blackbody line) are due to CN absorption in carbon stars. There is also a region at $V - I = 1$ to 1.5 where the main track of stars is vertical and lies on the blue side of the blackbody curve before TiO absorption pulls it redward. This region is due to CN absorption in K giants and I will refer to this feature as the K giant hump.

It is interesting to note that the decrease in CN absorption as evidenced by the redward turning of this track which starts at $V - I \approx 1.4$ or at a late K type, appears to follow the same slope as the redward TiO track. Both of these changes depend on [O] as well as temperature since it is the shift of carbon from CN to CO that moves the track redward with decreasing temperature in the late K types and it is the increase in [TiO] with decreasing temperature, due to excess oxygen, that moves the track redward in the M-type.

The 77−81 value for a carbon star is a measure of the CN abundance. This may be related to both the carbon and nitrogen abundances (Wing 1967). Yamashita (1972) classifications of carbon stars on the Keenan-Morgan system (Keenan and Morgan 1941) which are used throughout this work use

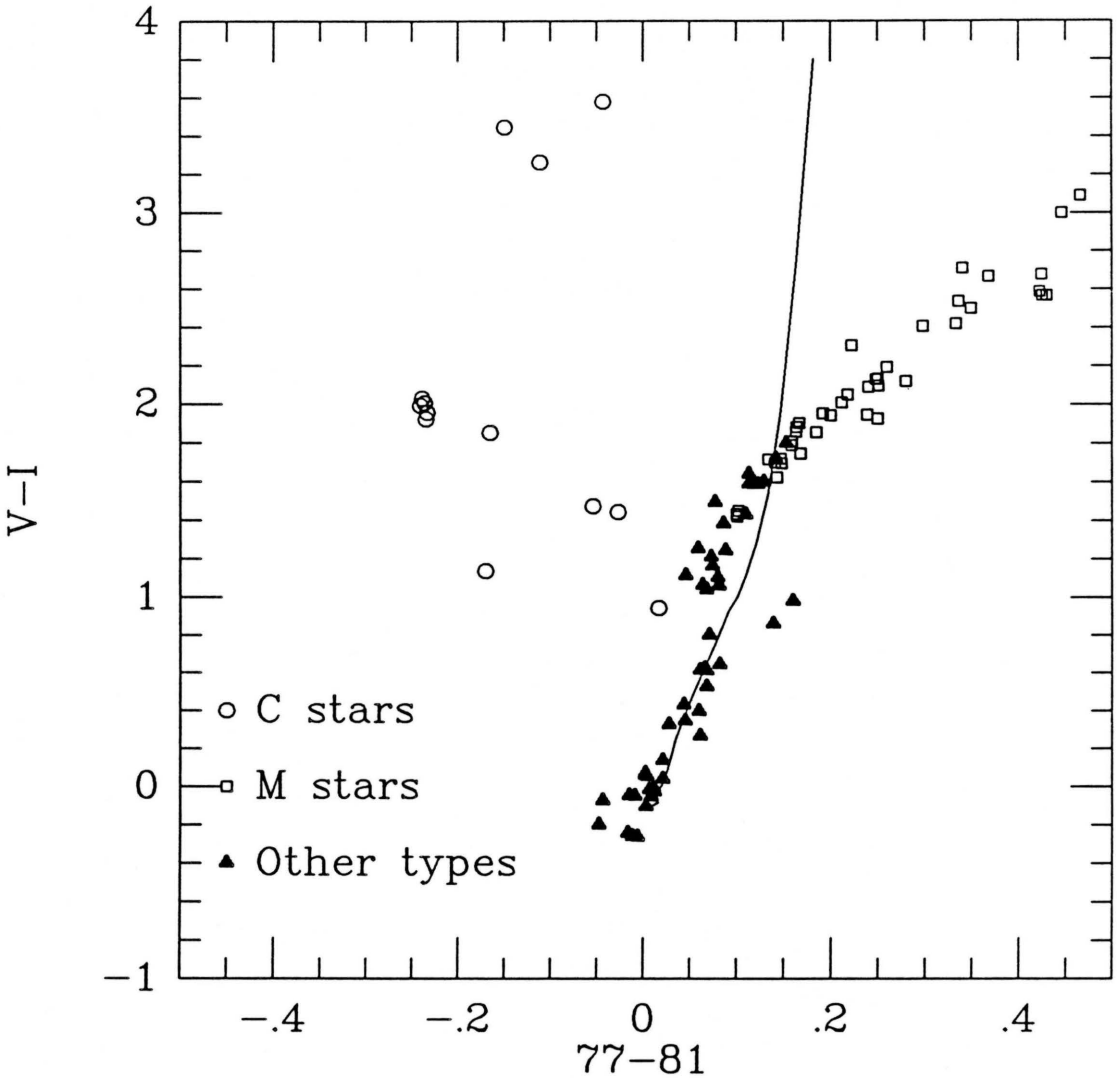

Figure 6. Color-Color Diagram of Bright Stars on the 77−81 System

The black body locus shifted to the system is shown for reference. This plot includes all V and I standards as well as bright C and M stars.

the Swan C_2 band intensities as the carbon abundance parameter. Figure 7 is a plot of the Yamashita carbon class versus 77−81 color for the carbon star measured in this work. There is a good correlation for carbon classes up to 4 but at class 5, the richest class, the 77−81 points all seem low. This may be because the most carbon rich stars have effectively used all available nitrogen in CN and it is no longer a measure of the total free carbon.

The relation of 77−81 to M-type will be more fully developed in the next section but it is clear that the 77−81,V−I color-color diagram allows the clear discrimination of C and M type stars. Carbon stars are seen to occupy a distinct, but broad, region in the color-color diagram. The tight track followed by the M type stars in Figure 6 suggests that the 77−81 color of an M star may be directly related to some function of V−I. In particular, 77−81 should correlate well with the M-type and/or the TiO band strength since the 77 filter is a measure of TiO absorption. If this is true, then a bonus of the 77−81 system would be the estimation of metallicities in M stars as a function TiO band strength and V−I .

Field Giants

In order to determine the relation between the 77−81 color and the TiO absorption a comparison was made with the work of Mould and his collaborators on the 7120Å TiO band strength in M giants (Mould and McElroy 1978; Mould, Stutman and McElroy 1979; Johnson, Mould and Bernat 1982; Mould and Siegel 1982; Mould and Bessel 1982). This body of work established that the onset of TiO absorption was a function of

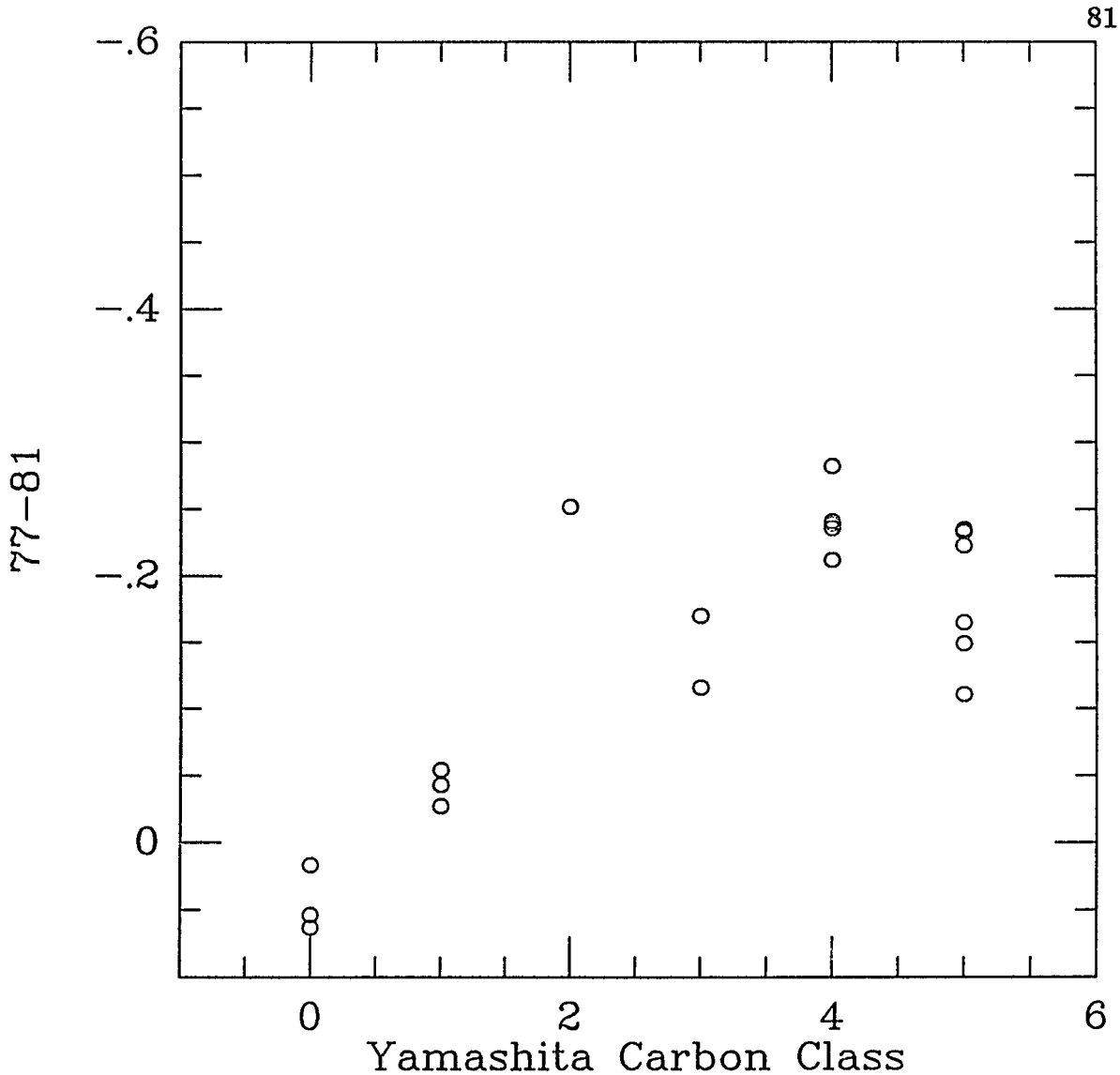

Figure 7. The 77-81 Color Compared to the Carbon Richness Class

both temperature and metallicity. As the metallicity of a star increases, the temperature at which TiO will form also increases which provides the basis of using a TiO band strength as a metallicity indicator. In order to use the TiO band strength in this way requires a measure of the temperature which is independent of the TiO absorption. An early calibration of the 7120Å band strength as a function of continuum slope for field giants (Mould and McElroy 1978) was followed by a more extensive investigation by Mould and Siegel (1982). They chose 26 bright field giants which had Galactic latitudes greater than 15°. The combination of latitude and magnitude was chosen so that these stars would form an unreddened sample of essentially solar metallicity. For this set of stars, they determined the 7120Å TiO band strength using the 7120Å Wing filter (Wing 1971). The Wing 7540Å filter and an intermediate-band filter at 10175Å were used to estimate the continuum so that they could calculate the 7120Å band strength as a depression in magnitudes, D(7120). They also used the 7540Å and 10175Å measure of the continuum slope as a temperature indicator. I observed 20 of these stars. These observations were obtained using a photoelectric photometer on the KPNO 0.4-m and a CCD on the KPNO 0.9-m.

Table 6 lists the colors of these stars where the values obtained on the different systems have been listed separately. The CCD observations were obtained through a 3% transmission neutral density filter since these are very bright stars. Table 6 also contains the 7120Å band strength in magnitudes, D(1720), obtained by Mould and Siegel (1982). As was discussed in Chapter 2, the reduction of data taken through neutral density may have introduced some small (less than 2%) systematic color shifts. Figure 8 is a

Table 6. Solar Neighboorhood Giants

Id	77−81	V−I	D(7120)[a]	Run[b]	Type	Source[c]	Comments[d]
70272	0.113	1.640	0.20	5	K4.5III	MS	(Id ?) III-IIIb
89056	0.185	1.858	0.39	6	M1.5	MS	
"	0.163	1.859	0.39	5	M1.5III	MS	IIIab
98118	0.141	1.701	0.32	5	M0 III	MS	III-IIIab
10089	-.044	-.073	-.03	5	B9 V	MS	(Oke & Hayes)
102212	0.168	1.746	0.34	5	M1 III	MS	IIIab
112142	0.248	2.129	0.65	5	M3 III	MS	IIICa-1
112769	0.147	1.719	0.34	6	M1 III	MS	IIIb
113996	0.142	1.721	0.14	5	K5 III	MS	
117675	0.218	2.049	0.59	6	M2 III	MS	
"	0.212	2.011	0.59	5	M2 III	MS	
119228	0.192	1.952	0.48	6	M2 III	MS	IIIabBa0.7
"	0.200	1.942	0.48	5	M2 III	MS	IIIabBa0.7
120477	0.123	1.585	0.22	5	K5 III	MS	IIIv
"	0.113	1.590	0.22	6	K5 III	MS	IIIv
127665	0.075	9.999	0.03	5	K3 III	MS	
"	0.073	1.209	0.03	6	K3 III	MS	
141477	0.158	1.791	0.30	6	M0.5III	MS	IIIab VAR?BS
141992	0.129	1.599	0.17	6	K4-5III	MS	VAR?BS
"	0.118	1.588	0.17	5	K4-5III	MS	VAR?BS
142574	0.148	1.696	0.26	6	M0 III	MS	
"	0.134	1.716	0.26	5	M0 III	MS	
143107	0.074	1.162	0.02	6	K2 III	MS	IIIab
148349	0.260	2.193	0.59	5	M2.5	MS	
154143	0.251	2.098	0.65	5	M3 III	MS	
"	0.240	2.089	0.65	6	M3 III	MS	
163588	0.080	1.102	0.01	6	K2 III	MS	
167006	0.280	2.119	0.67	5	M3 III	MS	
"	0.250	2.133	0.67	6	M3 III	MS	
168720	0.159	1.810	0.34	5	M1 III	MS	
169414	0.046	1.113	0.02	6	K2.5III	MS	IIIab

Notes:

(a) D(7120) from Mould and Siegel (1982).

(b) Run coded as in Table 5.

(c) Source as in Table 5.

(d) Comments as in Table 5.

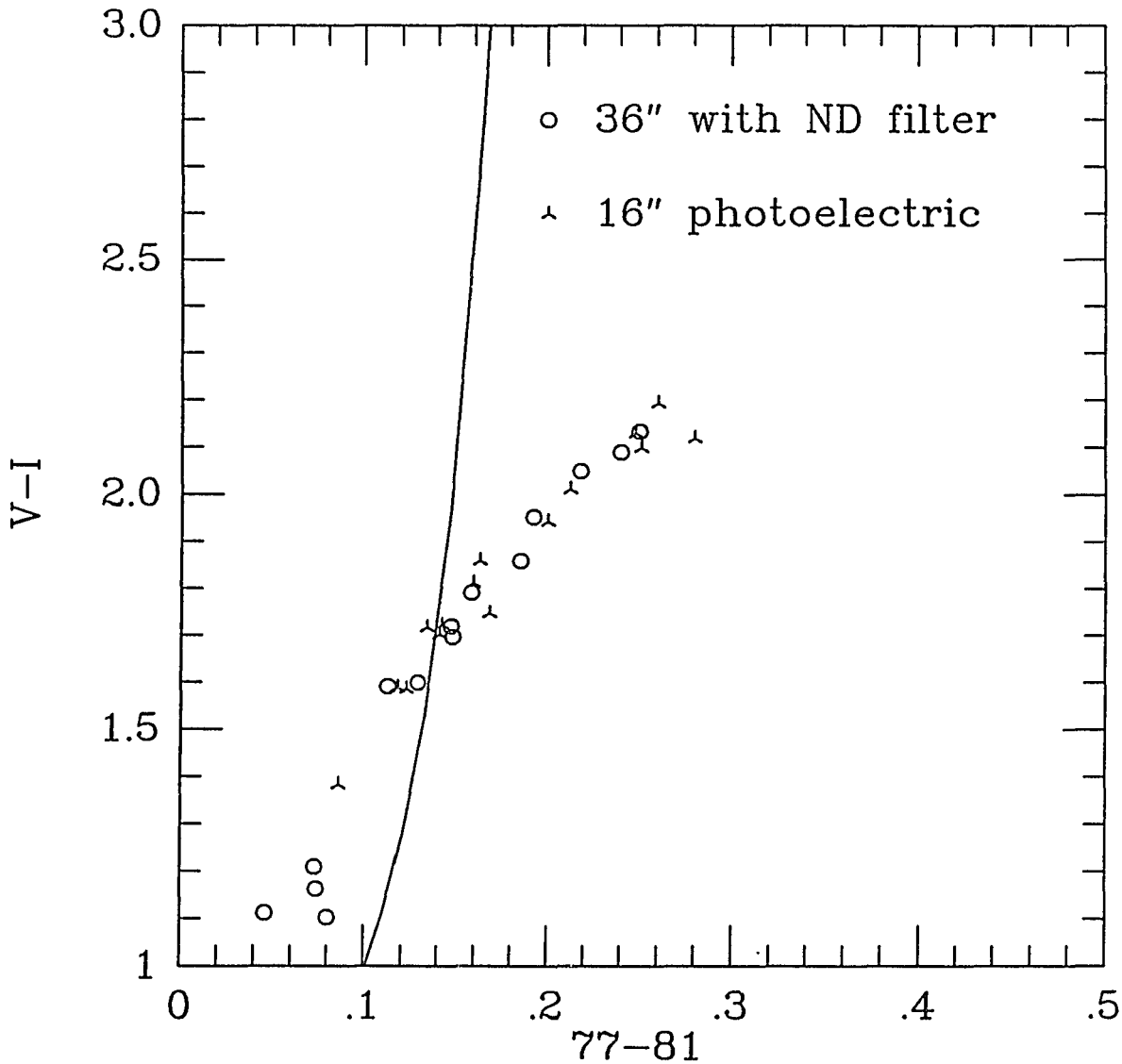

Figure 8. Color-Color Diagram of Solar Neighborhood Giants

color-color plot of these observations along with a theoretical blackbody line calculated as described in the preceding section. Figure 9 is a comparison of the 7120 band strength in magnitudes and the 77–81 colors.

The 77–81 color is well correlated with the 7120Å TiO band strength. This correlation is essentially linear from the region where the field giant colors cross the blackbody curve ($77 - 81 = 0.1$) to the strongest values measured by Mould and Siegel (1982; hereafter MS). In fact the relation seems to hold to essentially zero band strength, i.e. well into the region where CN is evident in K giants. This means that the 81 passband is only a pseudo-continuum point, but it works. Johnson, Mould and Bernat (1982) point out that the continuum measure used in Mould's investigations of the 7120Å band strength developed by Mould and McElroy (1978) may also be contaminated by CN. This may be the reason for the excellent agreement between the methods even in regions where the 77–81 color must be contaminated by CN. In less metal rich systems, the onset of TiO absorption will occur well after the disappearance of CN absorption due to the increase in CO. Such systems should follow the blackbody relation redward to the onset of TiO absorption. A least squares fit of a straight line to the data in Figure 9 yields a slope of 3.4 D(7120)/(77–81) both for all stars with $7120 > 0.0$ and for the set of stars with $77 - 81 > 0.10$. The intermediate-band D(7120) measures are clearly more sensitive than the broader 77 values in terms of magnitude change per TiO concentration change. There are probably two reasons for this: the 7120Å TiO band is the strongest of the TiO red system and the 77 filter is quite broad. Though the 7120Å filter has roughly one fifth the effective passband of the

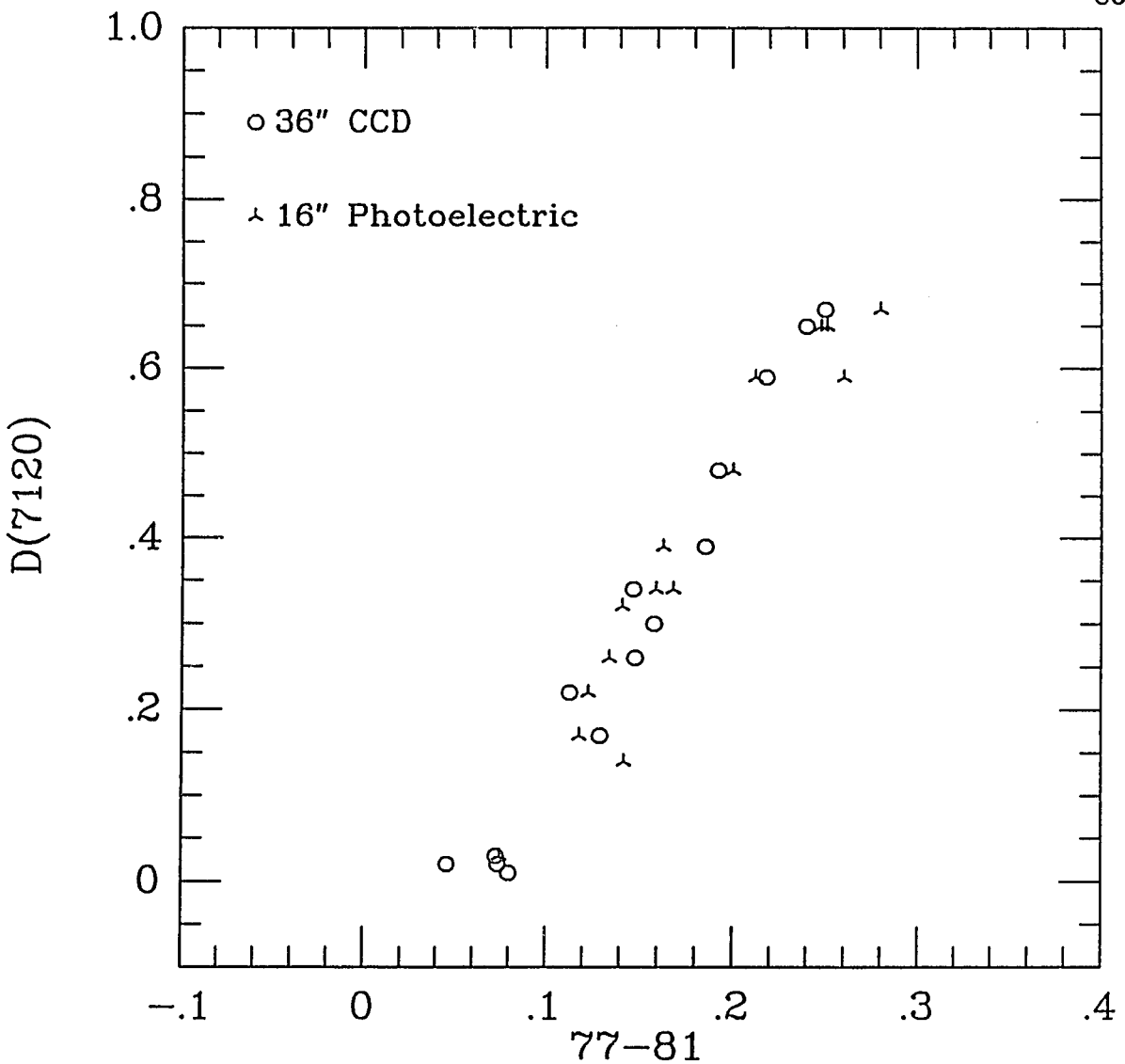

Figure 9. Comparison of D(7120) to 77-81

77 filter, the 77 filter's bandpass includes four TiO bandheads and so it is more than one fifth as sensitive to TiO even at the smallest levels measured with the narrower passband. There may also be a hint at the higher band strengths that the D(7120) is losing sensitivity as its passband is saturated while the broader 77 passband continues to correlate with increasing TiO absorption. Of course the real reason for the choice of the 7750Å region was the combination of detector sensitivity, the fact that AGB stars are very red and the symmetry of the 77 and 81 filters for the determination of M and C types.

MS find that the relation of D(7120) to their continuum gradient is best fit by a second order polynomial. This empirical relation is reasonably born out by the calculations of Johnson, Mould and Bernat (1982). For all the stars in Figure 8, it is clear that the relation between 77−81 and the V−I color is not a straight line. For the stars to the red, 77−81 side of the blackbody curve, however, the relation is quite linear. For the purposes of the empirical calibration which I am presenting, modeling this relation as linear over the region of $V - I \gtrsim 1.6$ will not introduce great errors. This excludes points which are clearly to the CN side of the blackbody relation. A least squares fit of a straight line to the observations of the field giants with $V - I > 1.6$ gives:

$$V - I = 1.215 + 3.604 * (77 - 81).$$

The scatter about this relation is about 0.03 mag and this is larger than would be expected from observational errors. Mould and Siegel note this scatter also and suggest that it is due to the dispersion in metallicity in this sample of stars. For all of the bright stars including Landolt standards

and Gleise-catalog-late-type dwarfs which I observed (see Table 5), the mean relation is:

$$V - I = 1.211 + 3.628 * (77 - 81).$$

One of the stars in this sample fell well off the mean relation for the field stars in the investigation of Mould and Siegel. This star is HD148349 which has according to MS an orbital eccentricity greater than 0.42 and should be considered a halo star. This star represents the most discrepant point in the correlation between 77−81 and D(7120) in Figure 8. It does fall exactly on the mean V−I vs 77−81 relation of the other field giants. Apparently, either Mould and Siegel's or my photometry is in error for this star.

This sample of unreddened giants also provides the best calibration of M-type versus 77−81 . Wing (1967) showed that the TiO absorption as measured by his band strength system correlated well with M-type even though MK M-typing uses TiO strengths in blue spectra and the Wing measures are in the red. Figure 10 is a plot of M-type versus 77−81 for the field giants and observations of three later type stars from the Gleise catalog.

These are nearby dwarfs which are not likely to be reddened. Though Wing (1967) found M dwarfs to have stronger TiO band strengths than giants at a given M-type in his scanner spectra, it seems that the 77−81 colors do not distinguish dwarfs from giants since they fall along the same line in the color-color diagram. A least squares fit of a line for all measured giants and dwarfs of types later than M0.5 yields:

$$(77 - 81) = 0.099 + 0.053 * (\text{M-type}).$$

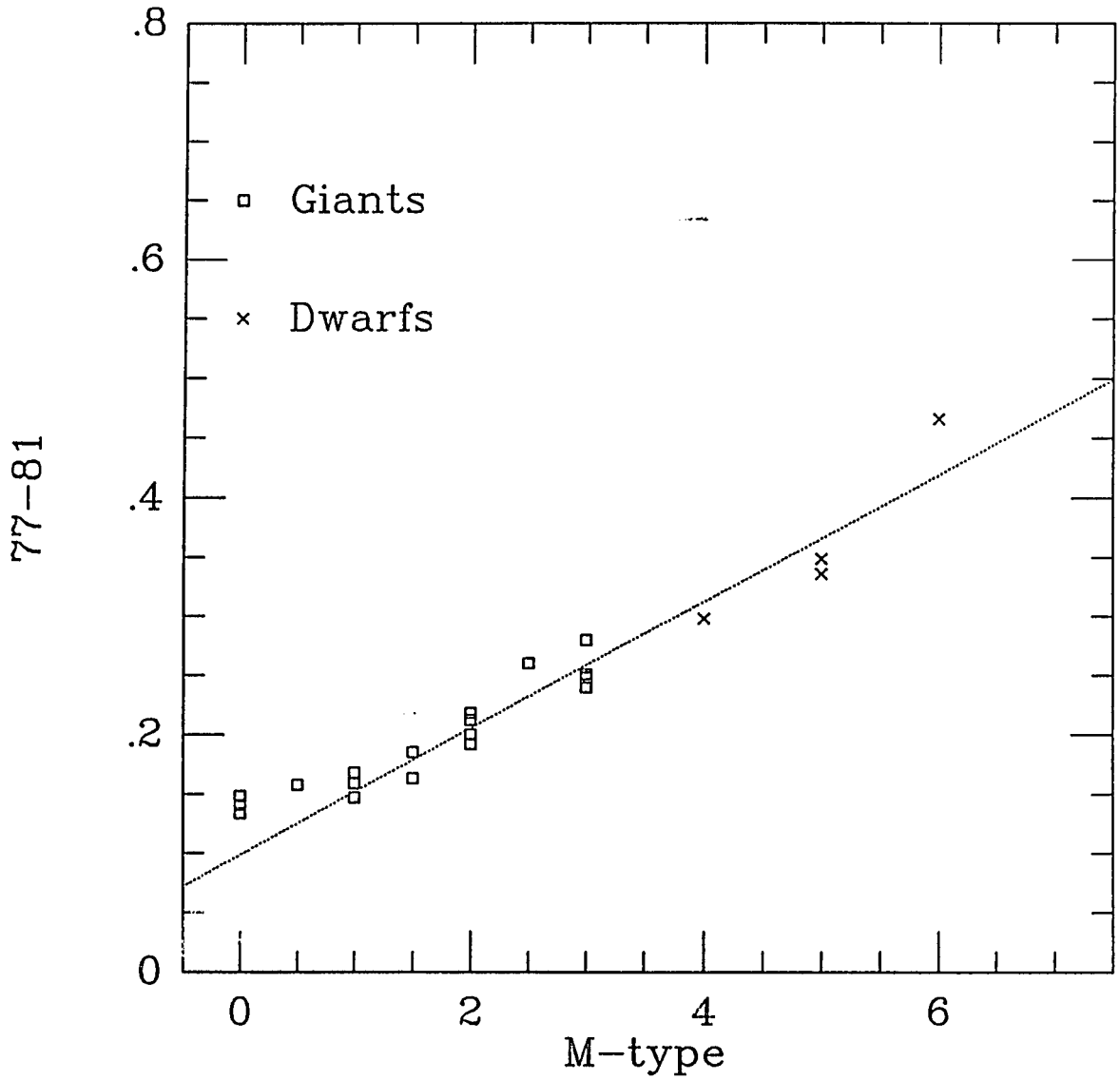

Figure 10. The 77-81 Color as a Function of M-Type

If only giants later than M0.5 from the Mould and Siegel (1982) sample of unreddened field giants are fit, then the relation is almost the same:

$$(77 - 81) = 0.106 + 0.050 * (\text{M-type}).$$

The weak band strengths at M0 and M0.5 are measured as too large in the 77–81 system compared to the MK type if there should be a linear transformation. This may be because M0 represents the onset of TiO absorption (Morgan, Keenan and Kellman, 1943) and the broad nature of the 77–81 system is primarily measuring the continuum slope at these small band strengths. It may also be due to the fact that the MK system is based upon the weaker, blue TiO absorption system and the 77 filter is more sensitive to the onset of TiO absorption.

Globular Cluster Giants

The calibration of the V–I color at the onset of TiO absorption as a function of metallicity requires observations of late-type stars with a broad range of known metallicities. Globular clusters provide a range of metallicities which are reasonably well known and they often contain giants of as late a type as would be consistent with their metallicity. Eleven globular clusters were examined using the intermediate-band system. These were chosen to span a wide range of metallicities and to be north of −30° declination. Six of these were observed by Mould and McElroy (1978) or Mould, Stutman and McElroy (1979) in their investigation of the TiO band strengths in metal-rich globular clusters.

I will briefly discuss each cluster separately, but there are certain

common features which deserve mention. Because this study was only concerned with the brightest stars in each cluster, the exposure times were too short for good photometry of the fainter stars, particularly those which were not red. In fact, since the data is synthetic aperture photometry, and the globular clusters are generally crowded, the errors for the faint stars are greater than those expected from simple photon statistics and the normal transformation errors. The result is a broadening of the less red portions of the giant track in the color-color diagram due to the scatter in the photometry.

The data for each cluster is presented in a combination figure. Part (a) of this figure consists of a color-magnitude diagram of all the stars photometered in the frame; part (b) is a color-color diagram of the reddest fifty stars (if there were fifty) which were within two magnitudes of the giant branch tip and had intrinsic, V−I, colors greater than 1. Dereddened data for stars at the tip of the giant branch for all of the clusters are presented in Table 7. This table also lists identifications made by previous investigators of these stars and the 7120Å TiO band strength measured by Mould and McElroy (1978) or Mould, Stutman and McElroy (1979) if they measured that star.

In order to estimate the effect of the metallicity on the color of the TiO track in these clusters a fiducial point on the TiO track was established. This is the V−I value where the track has a 77−81 color of 0.20, $(V-I)_{0.2}$, which is the color of a solar metallicity M2 star. This point was primarily chosen to lie on a linear region of the TiO track (see Figure 8). This point does not require more than an extrapolation of 0.1 in 77−81 even in

Table 7. Dereddend Colors of Cluster Giant Branch Tip Stars

CLUSTER	KHC#[a]	ID[b]	V−I	77−81	D(7120)[c]	REFERENCE
M 15	1	S4	1.35	0.07		Sandage (1970)
M 92	1	—	1.37	0.11		
	4	122	1.28	0.08		Sandage and Walker (1966)
NGC 4147	1	—	1.47	0.08		
	2	30	1.21	0.06		Sandage and Walker (1955)
M 3	1	—	1.61	0.10		
	2	—	1.58	0.09		
	10	I109	1.43	0.08		Sandage (1953)
	25	IV77	1.31	0.07		"
M 5	1	—	1.71	0.10		
	4	—	1.54	0.09		
	13	IV47	1.41	0.07		Arp (1955)
	24	III56	1.27	0.05		"
M 4	1	515	1.78	0.11	0.12	Alcaino (1975)
	2	516	1.74	0.10	0.14	"
	3	571	1.48	0.07	0.04	"
	4	398	1.27	0.06		"
NGC 6402	1	E	1.96	0.16	0.20	Kogon, Wehlau and Demers (1974)
	2	M	1.93	0.15	0.47	"
	3	K	1.78	0.18	0.17	"
	4	N	1.73	0.13	0.05	"
	5	—	1.72	0.08		
	6	H	1.68	0.05	0.10	Kogon, Wehlau and Demers (1974)
	7	F	1.66	0.11	0.29	"
	8	D	1.64	0.10	0.11	"
	9	O	1.53	0.10	0.11	"
	10	J	1.51	0.11	0.09	"
NGC 6712	1	D16	3.12	0.59		Lloyd Evans and Menzies (1977)
	2	V7	2.33	0.28		Sandage, Smith and Norton (1966)
	3	V10	2.16	0.21		"
	4	—	2.02	0.22		
	5	V8	1.85	0.15		Sandage, Smith and Norton (1966)
	6	—	1.75	0.17		
	7	V2	1.73	0.16		Sandage, Smith and Norton (1966)
	8	B27	1.59	0.10		"
	9	—	1.58	0.08		
	10	V21	1.70	0.09		
	11	B50	1.58	0.11		Sandage, Smith and Norton (1966)
	12	A41	1.52	0.08		"
	13	B140	1.45	0.06		Lloyd Evans and Menzies (1977)
	14	LM5	1.44	0.06	0.29	"
	15	LM10	1.40	0.04	0.07	"
	16	LM8	1.35	0.04	0.11	"
	17	B108	1.35	0.07		Sandage, Smith and Norton (1966)
	18	—	1.35	0.04		
	19	—	1.34	0.06		
	20	B66	1.30	0.07	0.155	Sandage, Smith and Norton (1966)
NGC 6366	1	IV50	1.78	0.12	0.32	Pike (1976)
	2	—	1.62	0.08		"
	3	III8	1.37	0.07		"

Table 7. (cont.) Dereddend Colors of Cluster Giant Branch Tip Stars

CLUSTER	KHC#[a]	ID[b]	V−I	77−81	D(7120)[c]	REFERENCE
M 107	1	217	1.93	0.16	0.265	Sandage and Katem (1964)
	2	E	1.70	0.09	0.105	"
	3	273	1.63	0.09	0.085	"
	4	F	1.49	0.08		"
	5	243	1.44	0.08		"
	6	245	1.43	0.08		"
	7	102	1.44	0.08		"
	8	162	1.37	0.05		"
M 69	1	I43	3.48	0.60	0.81	Hartwick and Sandage (1968)
	2	II37	2.58	0.34	0.91	"
	3	—	2.52	0.59		
	4	IV11i	2.43	0.37	0.72	Hartwick and Sandage (1968)
	5	I12i	2.22	0.35	0.36	"
	6	III43	2.00	0.18		"
	7	IV27i	1.910	0.15	0.46	"
	8	III42	1.88	0.17	0.40	"
	9	—	1.89	0.19		
	10	—	1.83	0.20		
	11	I40?	1.77	0.13	0.68	Hartwick and Sandage (1968)
	12	—	1.75	0.13		"
	13	II14i	1.67	0.11	0.22	"
M 71	1	29	3.10	0.51		Arp and Hartwick (1971)
	2	27	2.89	0.47		"
	3	H	1.81	0.19		"
	4	—	1.80	0.13		
	5	—	2.08	0.18		
	6	113	1.73	0.11	0.205	Arp and Hartwick (1971)
	7	30	1.68	0.11		"
	8	46	1.64	0.09	0.16	"

Notes:

(a) The KHC number ranks the stars in the giant branch by 77-81.

(b) The ID is the previous identification from the reference in column seven.

(c) The D(7120) values for M 71, M 107, M 3 and NGC 6712 are from Mould and McElroy (1978). The D(7120) values for M 4, NGC 6402, M 69 and NGC 6366 are from Mould, Stutman and McElroy (1979).

systems where the metallicity is so low that the latest giants are late K. For systems with higher metallicities, the determination of this point may require an interpolation within the observed TiO track because it may not be well populated. In systems where the TiO track is not well enough populated to allow a line to be fit to it, the mean TiO track slope measured for the field giants was used for the extrapolation or interpolation. Table 8 lists the measured $(V-I)_{0.2}$ for the clusters and the TiO track slope which was measured or adopted. Table 8 also lists the adopted metallicity and reddening for each cluster.

Two values for each cluster's metallicity are listed: one from Webbink (1985) and one from Zinn and West (1984). The reddenings are all adopted from Webbink (1985). The derived E(V−I) is listed for convenience in Table 8 also.

Each cluster was roughly centered on the CCD frame for this study. This meant that some of the outlying stars may not have been measured and these sometimes included giant branch tip members. The metal poor clusters which I observed will be discussed first. For five of these, I did not detect TiO absorption in the fields I observed. For these five clusters, a lower limit for $(V-I)_{0.2}$ was calculated assuming their TiO tracks would begin just above the greatest V−I observed, and that their TiO tracks would have the same slope as the field giant track (3.6). In the metal rich clusters, there was often the problem of possible field star contamination since these clusters tend to be more concentrated toward the plane of the Galaxy. I will discuss the effects of various membership assumptions on the measured TiO track for these clusters.

Table 8. Adopted and Derived Cluster Parameters

Cluster	E(B−V)[a]	E(V−I)[b]	[Fe/H][c]	[Fe/H][d]	$(V-I)^{e}_{0.2}$	Slope[f]	Obs[g]
M 15	0.10	0.135	−2.06	−2.15	≥1.82	(3.60)	5
M 92	0.02	0.027	−1.89	−2.24	≥1.65	(3.60)	2
NGC 4147	0.02	0.072	−1.68	−1.80	≥1.90	(3.60)	2
M 3	0.00	0.000	−1.30	−1.66	≥1.97	(3.60)	3
M 5	0.03	0.041	−1.60	−1.40	≥2.07	(3.60)	2
M 4	0.36	0.486	−1.09	−1.33	2.14	(3.60)	2
NGC 6402	0.58	0.783	−1.01	−1.31	2.10	(3.60)	1
NGC 6712	0.48	0.648	−1.26	−1.01	2.01	2.91	3
					2.06	3.58	
					1.97	3.06	
NGC 6366	0.65	0.878	−.71	−.99	2.06	(3.60)	2
M 107	0.33	0.446	−.88	−.99	2.10	(3.60)	2
M 69	0.17	0.230	−.92	−.59	1.98	3.41	2
					2.05	3.61	
M 71	0.19	0.257	−.45	−.58	2.01	3.40	5
					2.03	3.33	

Notes:

(a) E(B−V) adopted from Webbink (1985).

(b) $E(V-I) = 1.35 * E(B-V)$

(c) Column 4 lists metallicity from Webbink (1985).

(d) Column 5 lists metallicity from Zinn and West (1984).

(e) The different assumptions which lead to multiple $(V-I)_{0.2}$ values can be found in the section on the appropriate cluster.

(f) Column 7 lists the measured slope of the TiO track unless the field giant value was adopted which is then listed in parentheses.

(g) Column 9 lists the number of separate sets of V,I,77,81 observations used to determine the colors.

M 15

This cluster has a giant branch whose tip is only 0.6 mag redder than the horizontal branch intersection even though it is four magnitudes brighter than the intersection as seen in Figure 11a. The color-color diagram in Figure 11b shows a well populated zero TiO strength track redward in V−I of the K giant hump. The tip of the color-color diagram is Sandage's (1970) star S4. This star, listed in Table 7, has been dereddened assuming $E(B-V) = 0.10$ and the identification is that of Sandage(1970). Table 8 lists the lower limit for $(V-I)_{0.2}$ for M 15. It is interesting to note that the tip is so blue that the lower limit is 0.10 magnitude below the roughly solar metallicity field giant point.

M 92

M 92 is a high latitude cluster which has a giant branch whose tip is about 0.6 mag redder than its intersection with the horizontal branch. The tip is about 3.5 mag above the horizontal branch. M 92's color-color diagram is presented in Figure 12a and its color-magnitude diagram is Figure 12b. The color-color tip is extremely blue; there are no stars with measurable TiO absorption. The colors for the first and fourth reddest stars at the tip are given in Table 7. These are the averages of two sets of observations on two nights and assume an E(B−V) to this cluster of 0.02. Table 8 lists a lower limit of $(V-I)_{0.2}$ for M 92 which is extremely blue since there are not even any late K giants in this field.

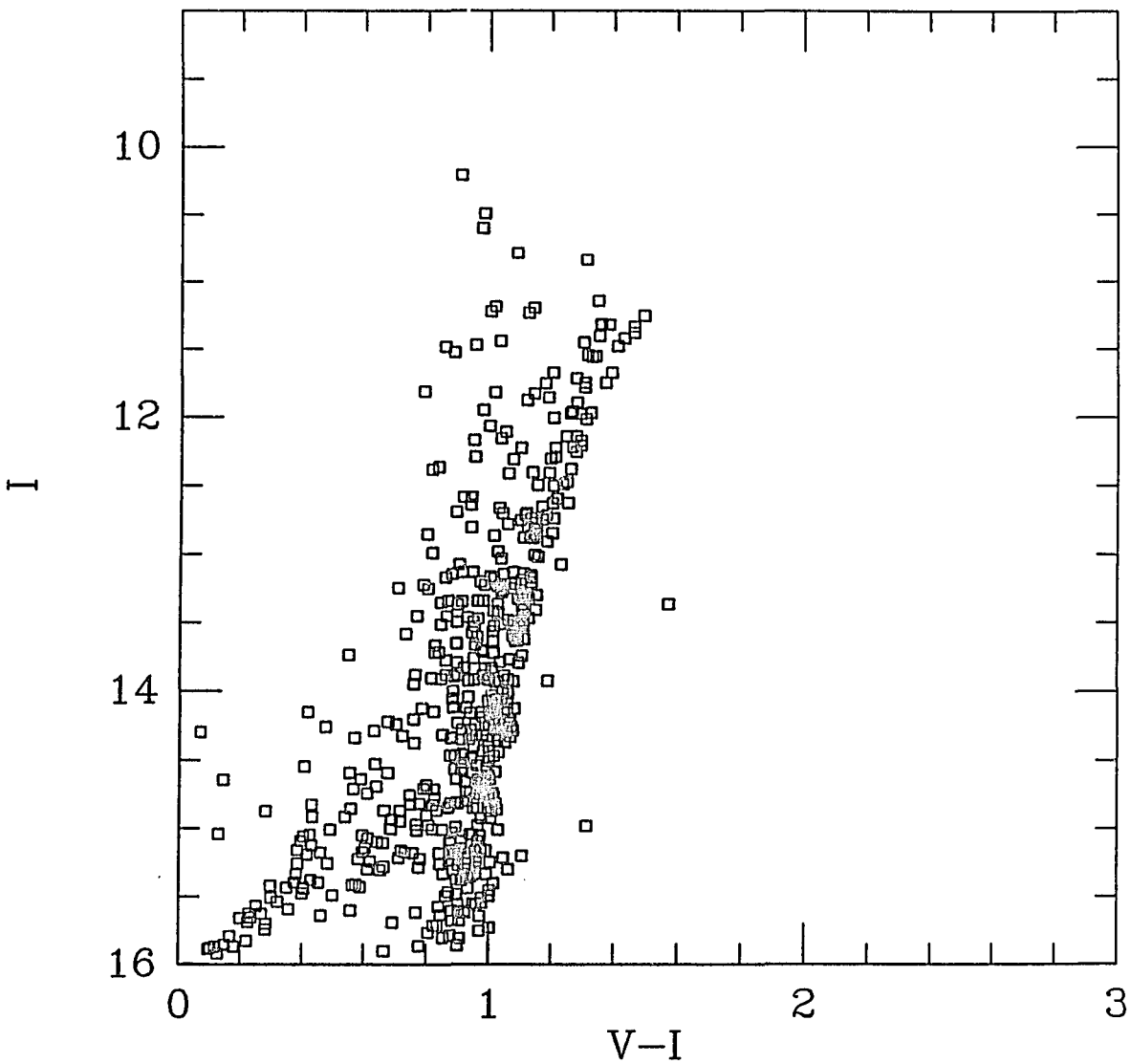

Figure 11a. Color-Magnitude Diagram of M 15

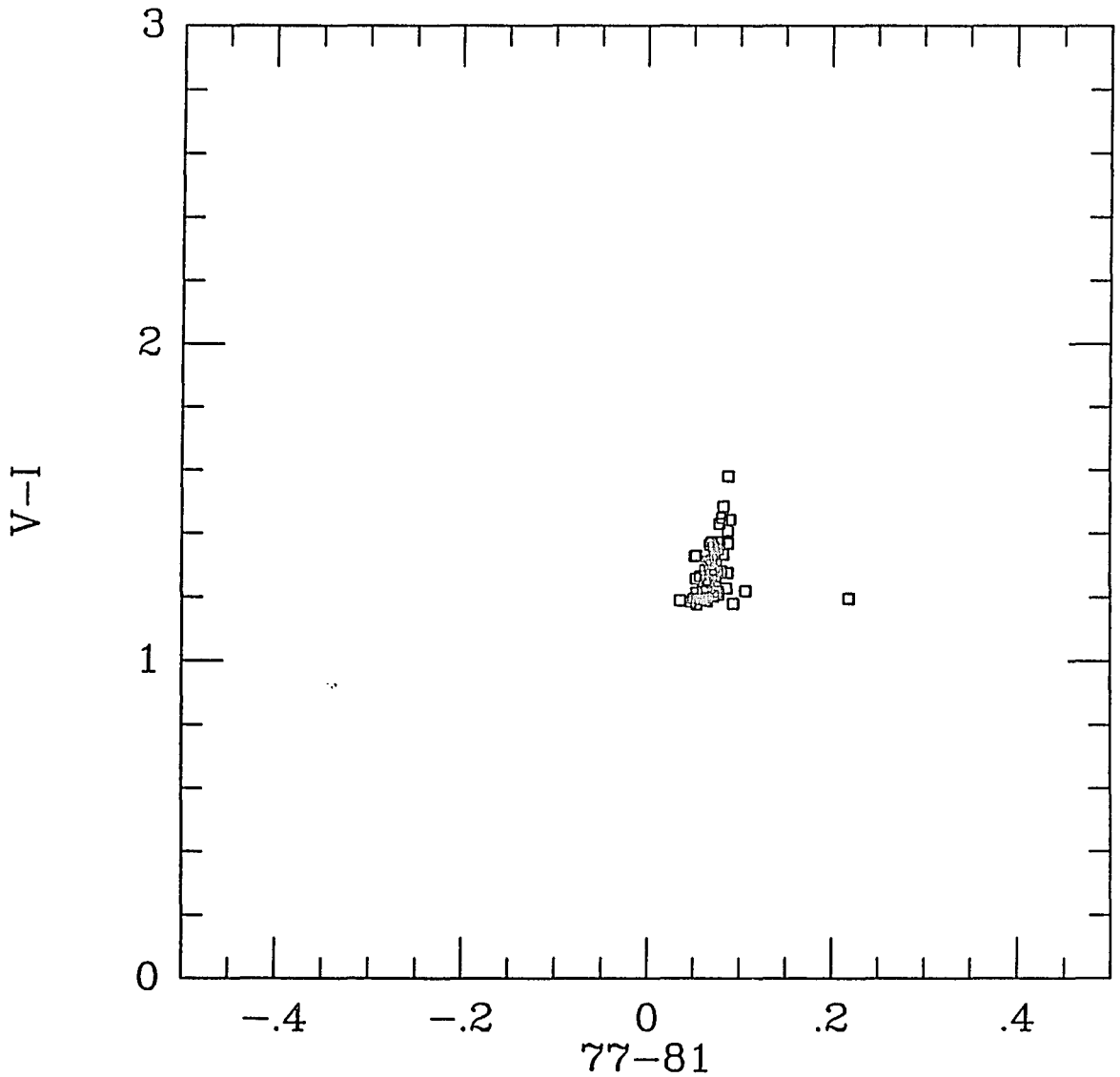

Figure 11b. Color-Color Diagram of M 15

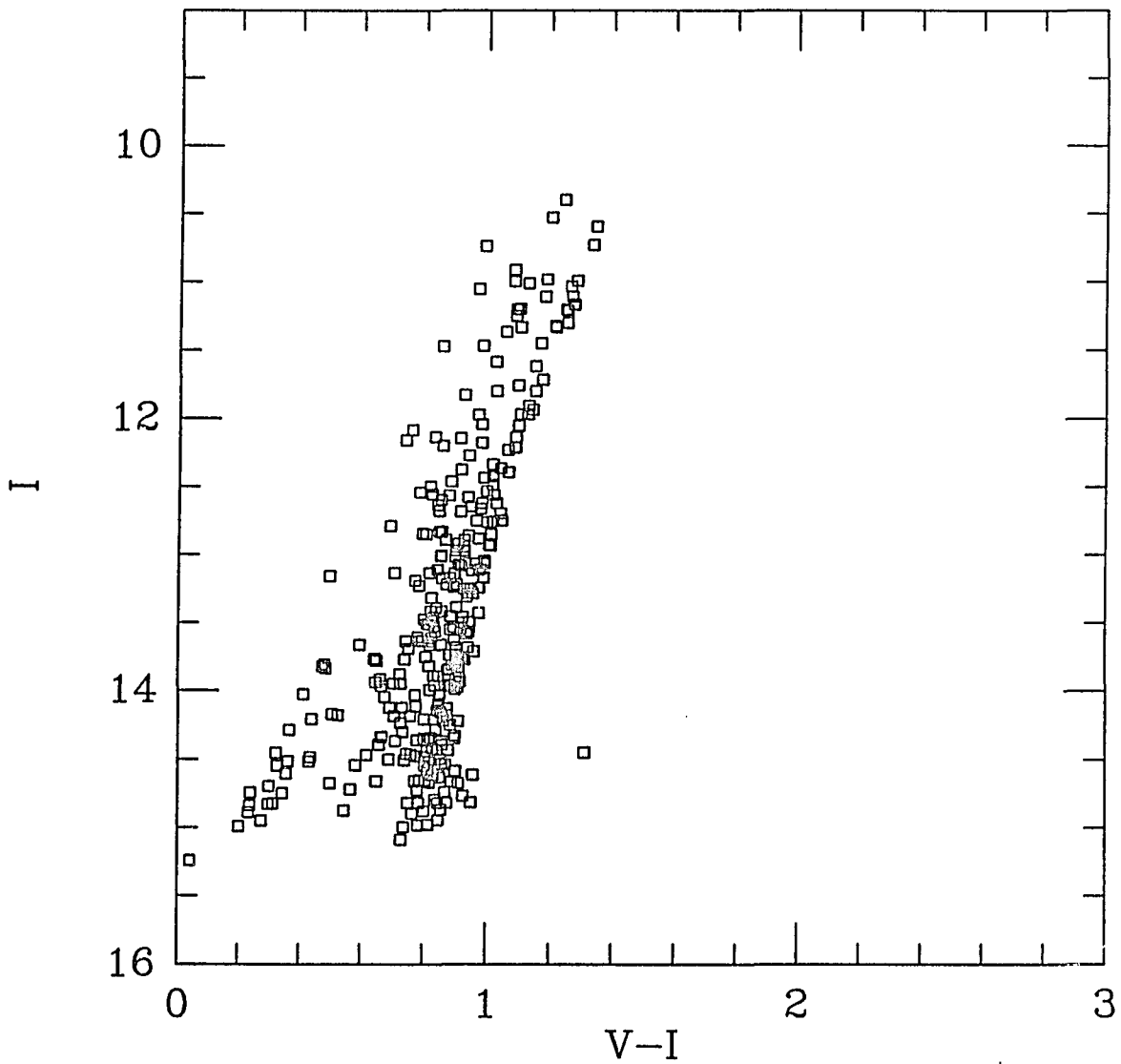

Figure 12a. Color-Magnitude Diagram of M 92

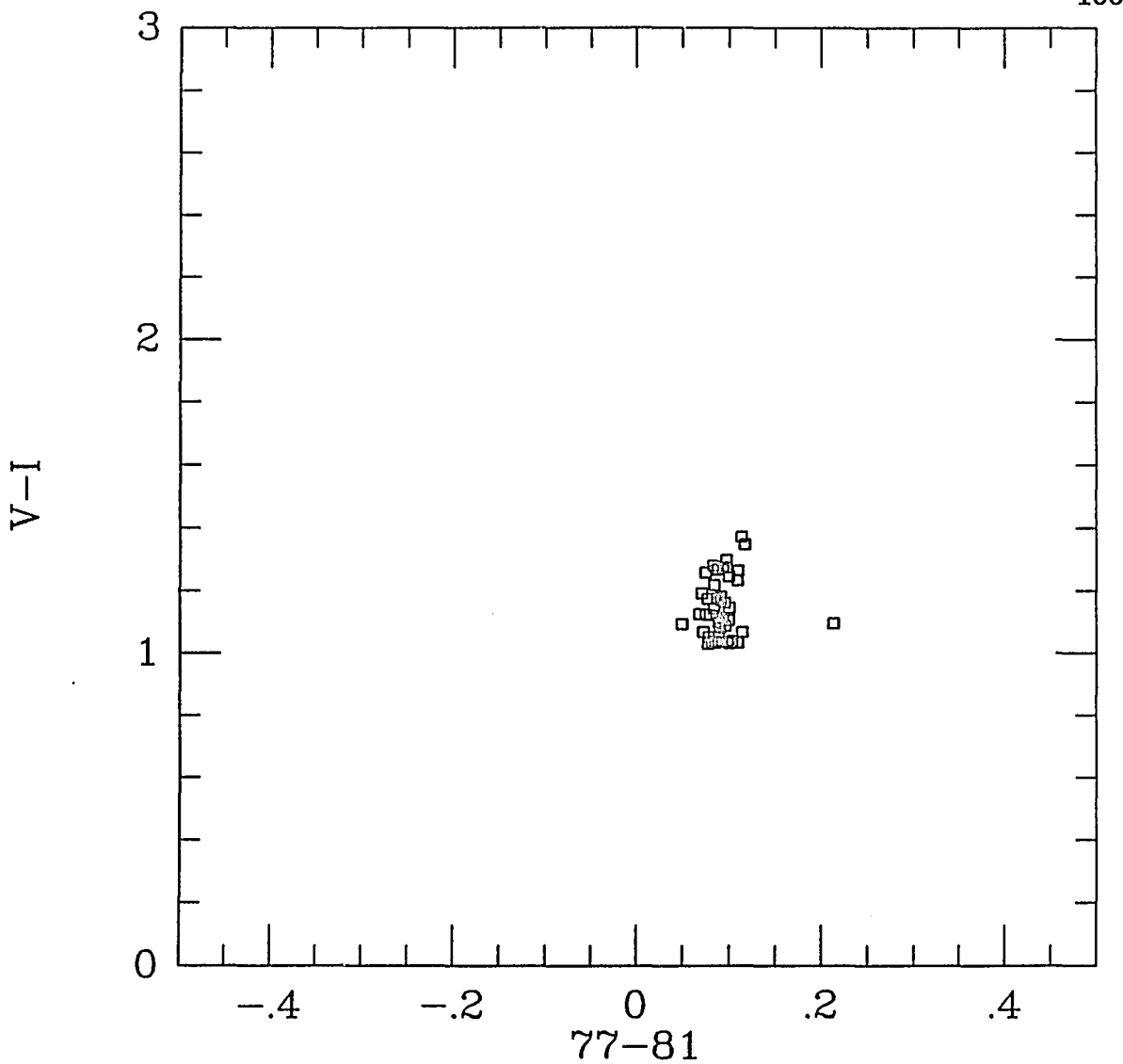

Figure 12b. Color-Magnitude Diagram of M 92

NGC 4147

This is a sparse, high latitude globular cluster whose color-magnitude diagram from my photometry is not well populated. The giant branch tip is 0.8 mag redder and four magnitudes brighter than the intersection with the horizontal branch. The color-color diagram for this cluster shows one star well up the zero TiO band strength track from the K giant hump. The color-color and color-magnitude diagrams for NGC 4147 are Figures 13a and 13b. The colors for the two reddest giant branch tip stars are given in Table 7 where the identifications is from Sandage and Walker (1955). The assumed reddening to NGC 4147 was $E(B-V) = 0.02$, and the values are an average of two sets of observations on one night. The lower limit for $(V-I)_{0.2}$ for this cluster is given in Table 8.

M 3

This dense cluster has a well populated giant branch which extends less than a magnitude to the red and four magnitudes brighter than the horizontal branch intersection. M 3's color-magnitude and color-color plots are presented in Figures 14a and 14b. The color-color diagram shows that there are no stars for which I obtained photometry which exhibit measurable TiO absorption. The reddest two stars and two other red stars for which there are identifications from the work of Sandage (1953) are listed in Table 7. These are the average of three sets of observations on two nights and have not been dereddened assuming an $E(B-V) = 0.00$. Table 8 lists a lower limit for the $(V-I)_{0.2}$ assuming that the TiO track could start just to the red of the observed stars with the slope of the field giant track.

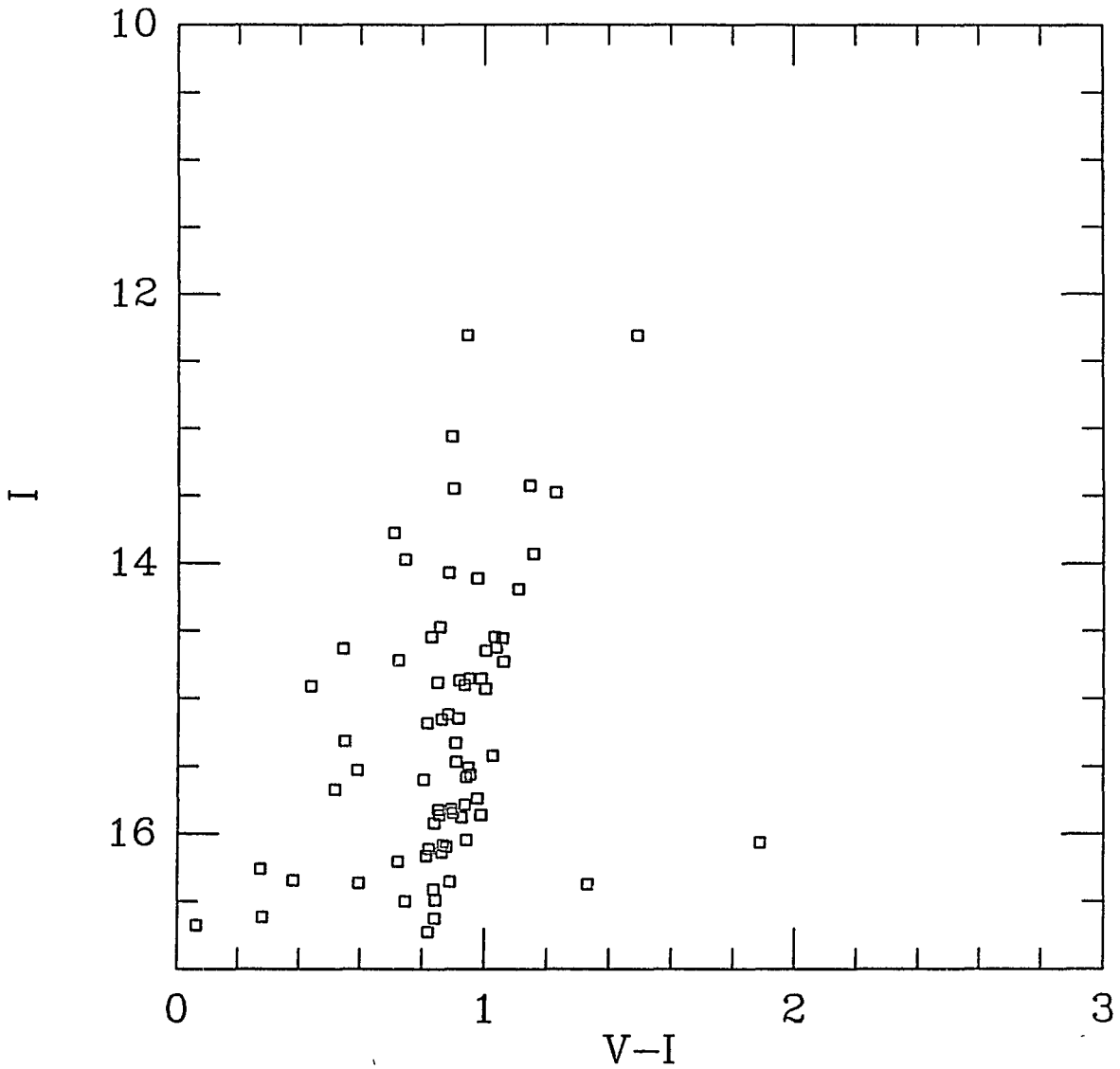

Figure 13a. Color-Magnitude Diagram of NGC 4147

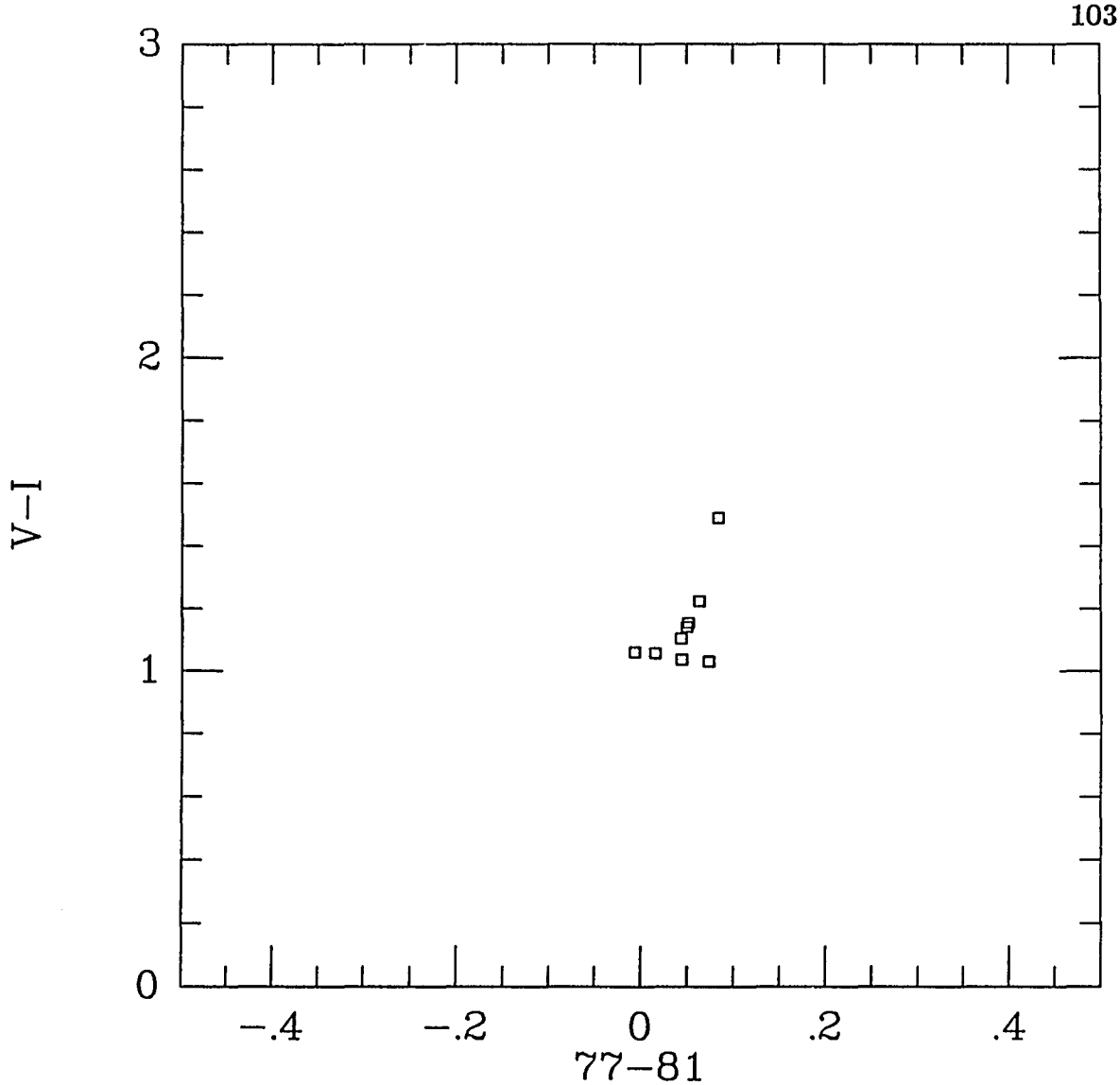

Figure 13b. Color-Color Diagram of NGC 4147

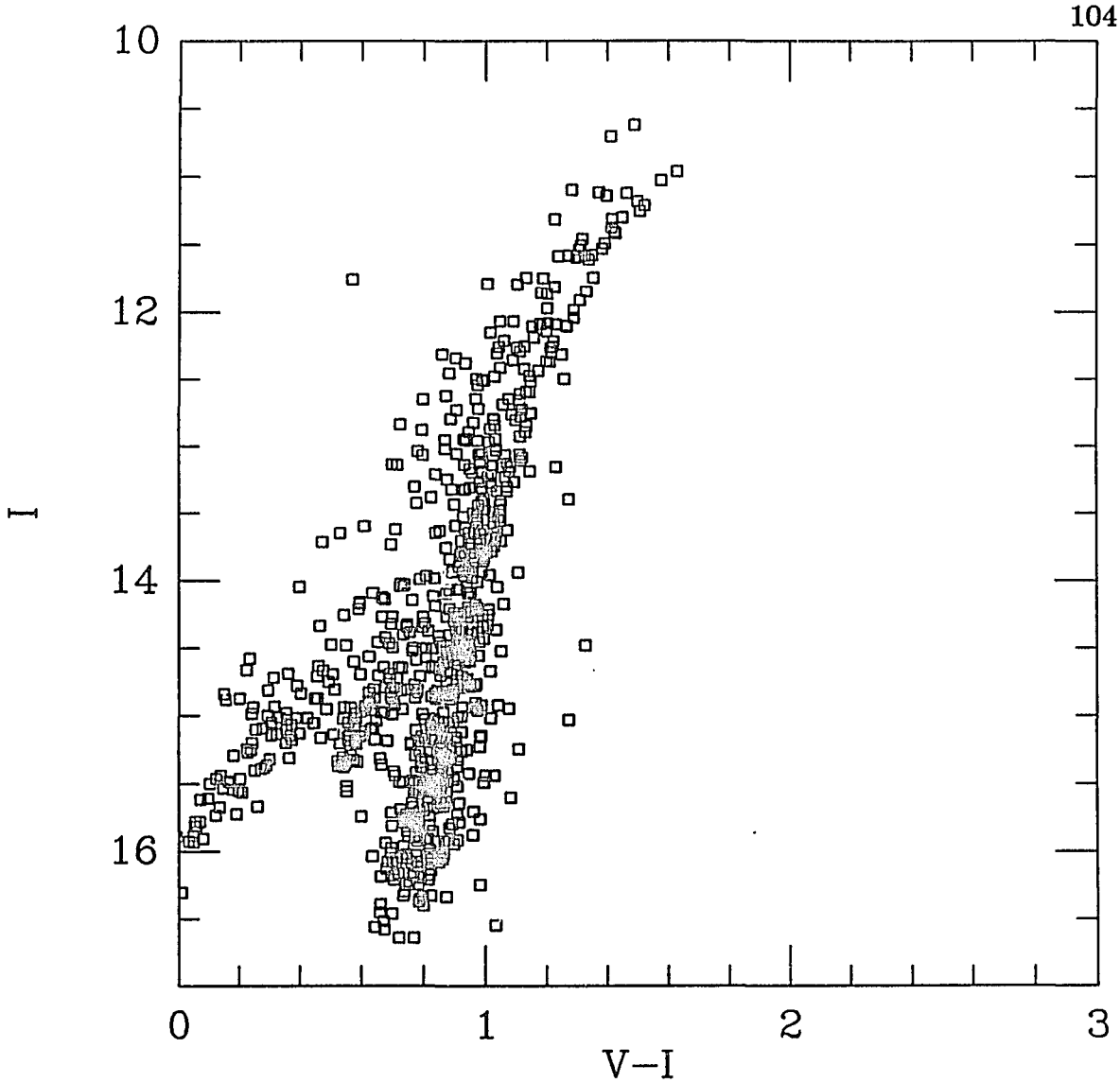

Figure 14a. Color-Magnitude Diagram of M 3

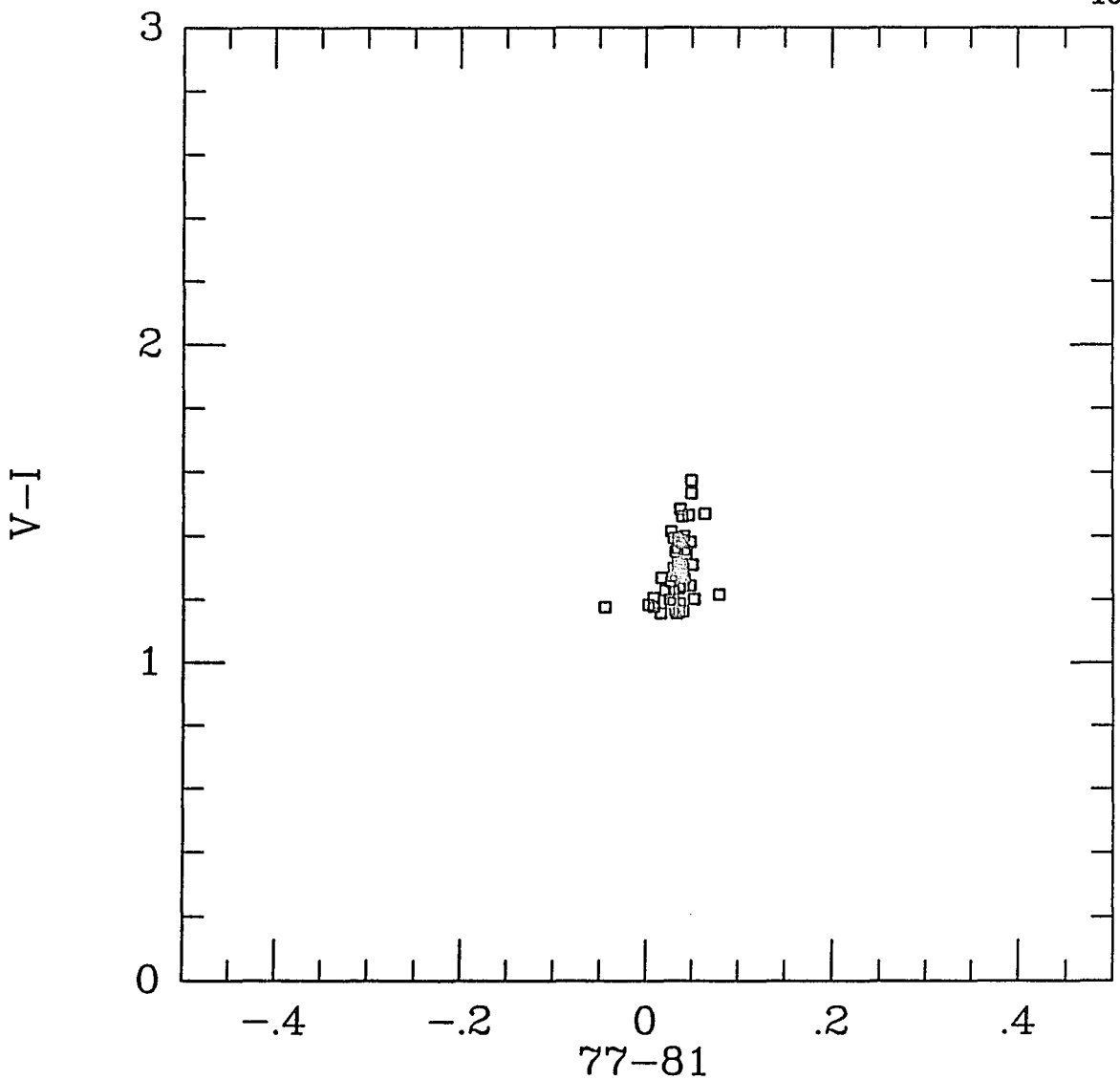

Figure 14b. Color-Color Diagram of M 3

M 5

This cluster has a color-magnitude diagram that is very similar to that of M 3 as can be seen in Figure 15a. The color-color diagram in Figure 15b of this cluster also indicates no stars with TiO absorption although the zero TiO strength track is populated to redder values above the K giant hump. The dereddened values in Table 7 assume an E(B−V) of 0.03 and are the average of two sets of observations on one night. The table lists colors for the first and fourth reddest stars and two of the reddest stars from the photometry of Arp (1955). Table 8 lists the lower limit for the $(V-I)_{0.2}$ for this cluster assuming a TiO track slope the same as that for the field giants which begins just to the red of the observed tip.

M 4

This is the closest globular cluster and it is not particularly crowded. The color-magnitude diagram (Figure 16a) shows a giant branch tip about one magnitude to the red of the horizontal branch intersection and less than two magnitudes brighter. The color-color diagram presented in Figure 16b shows that there are perhaps two stars which are on the TiO side of the zero TiO track. The colors of the four reddest stars are presented in Table 7 where the interstellar extinction to M 4 has been assumed to be $E(B-V) = 0.36$. These values are averages of two sets of observations obtained on one night. These stars are identified by the numbers given them by Alcaino (1975). An $(V-I)_{0.2}$ was estimated by passing a line which has the mean field giant TiO track slope through the mean position of stars 515 and 516. These stars have only slightly large 77−81 values than the

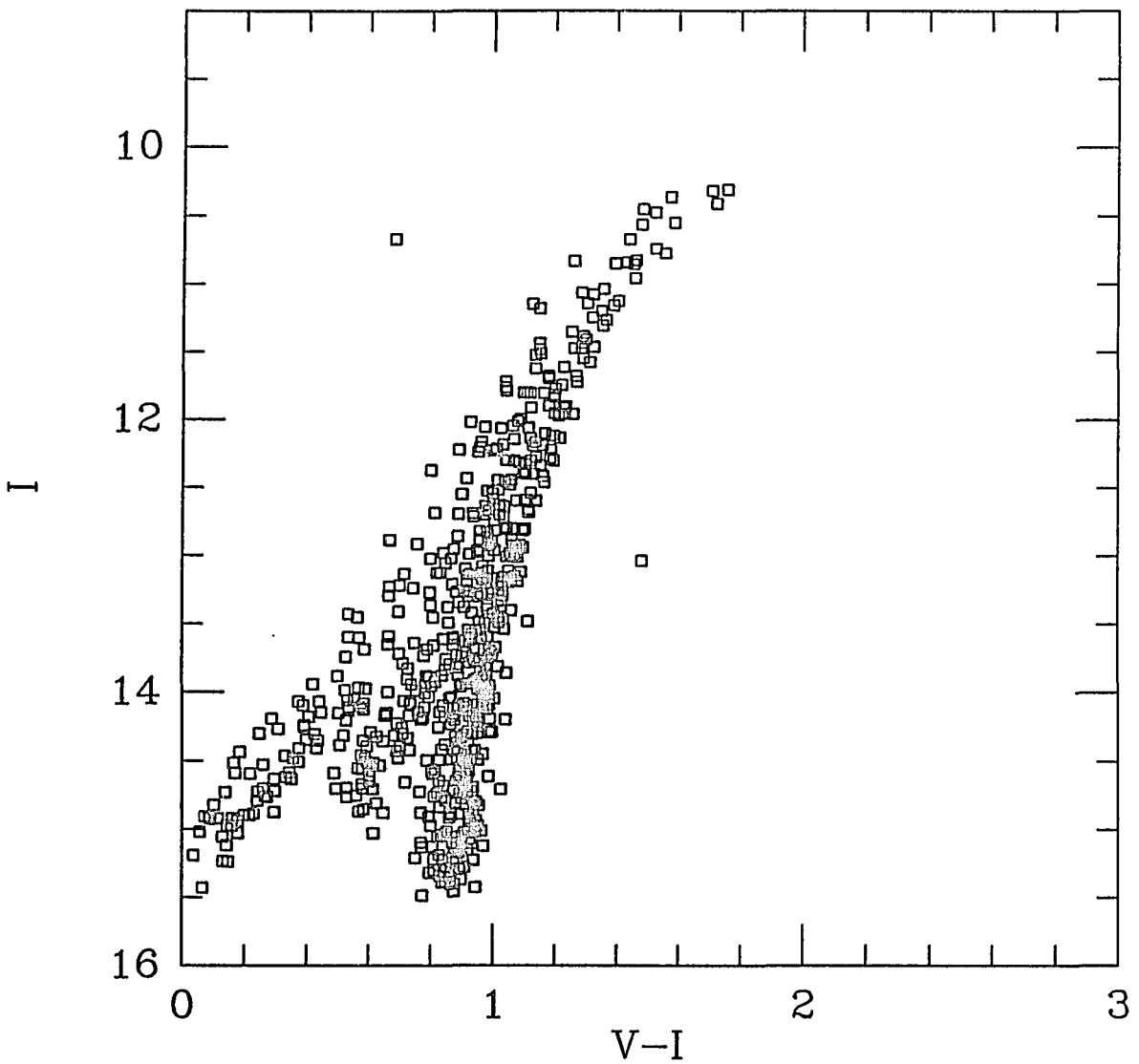

Figure 15a. Color-Magnitude of M 5

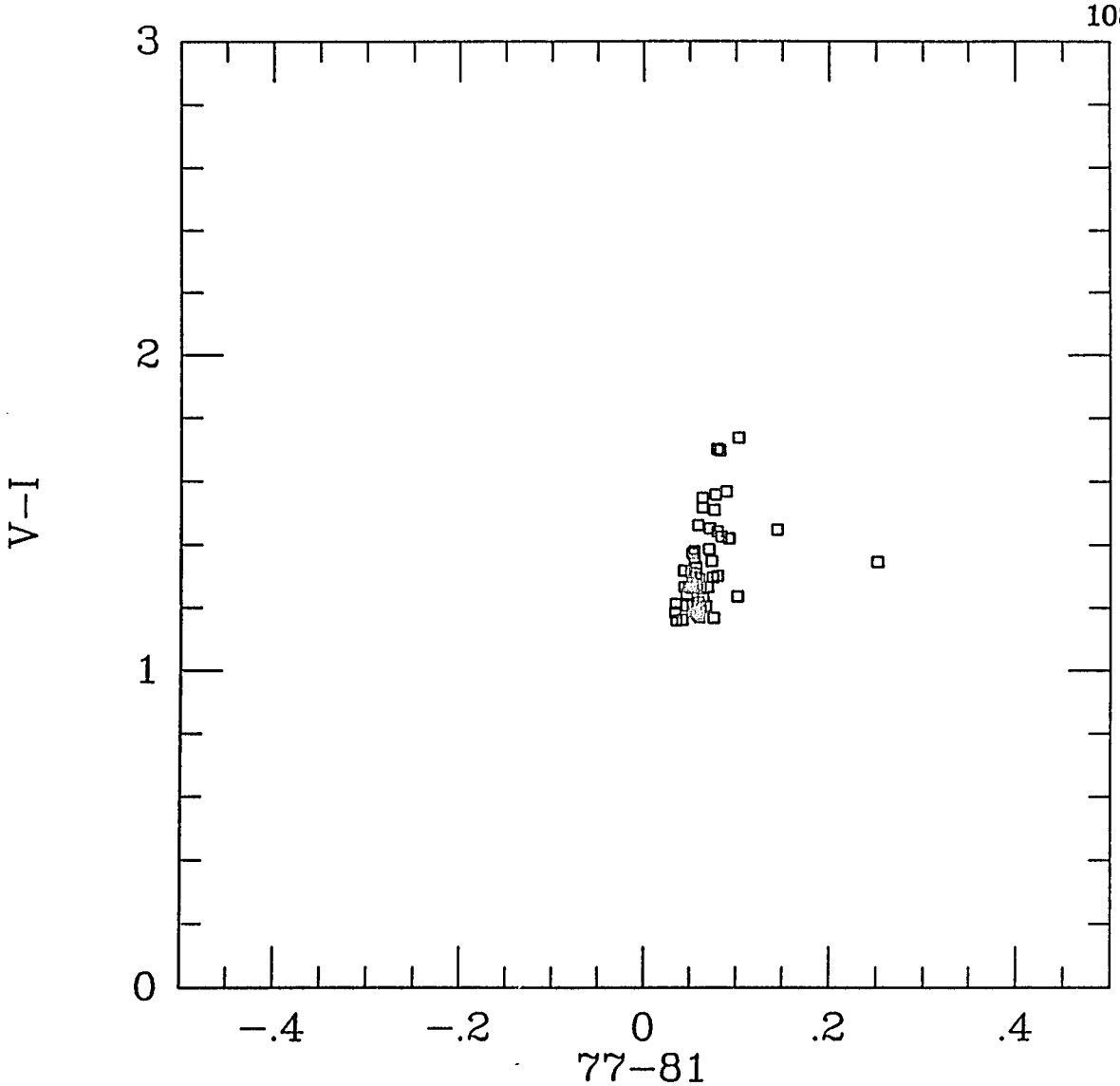

Figure 15b. Color-Color Diagram of M 5

previous cluster's reddest stars, but they are more clearly to the TiO side of the mean 77−81 color of the tip than the previous clusters.

NGC 6402

NGC 6402 (M 14) exhibits a relatively thick giant branch which extends about one magnitude to the red from the horizontal branch intersection. The color-color diagram determined from one set of observations shows quite a bit of scatter near the point where the TiO track might be intersecting the track of giants too hot to exhibit TiO. NGC 6402 data is shown in Figures 17a and 17b. The dereddened colors for the ten reddest stars in the NGC 6402 field are presented along with the identifications of Mould, Stutman, McElroy (1979). The assumed reddening was $E(B-V) = 0.58$ mag. The fifth reddest star lies in Kogon, Wehlau, and Demers (1974; KWD) E ring which they felt contained significant field star contamination. It may be 0.25 mag faint to be a member of M 14's giant branch tip. KWD do, however, find almost one half magnitude of tip width and they also find variables at the tip, but variability usually causes scatter to brighter magnitudes. Ratnatunga and Bahcall (1985) predict that there will be less than one field star in this field with a V−I greater than 1.5 within a magnitude of the giant branch tip. Star N, which is in KWD's C ring and so is almost certainly a member is about one half a magnitude above the main portion of the giant branch tip. Upon inspection Star K's photometry is contaminated by a close companion and so its colors are suspect. Star H lies in the core of the cluster and has a number of close companions and its colors must be considered suspect also. The determination of $(V-I)_{0.2}$

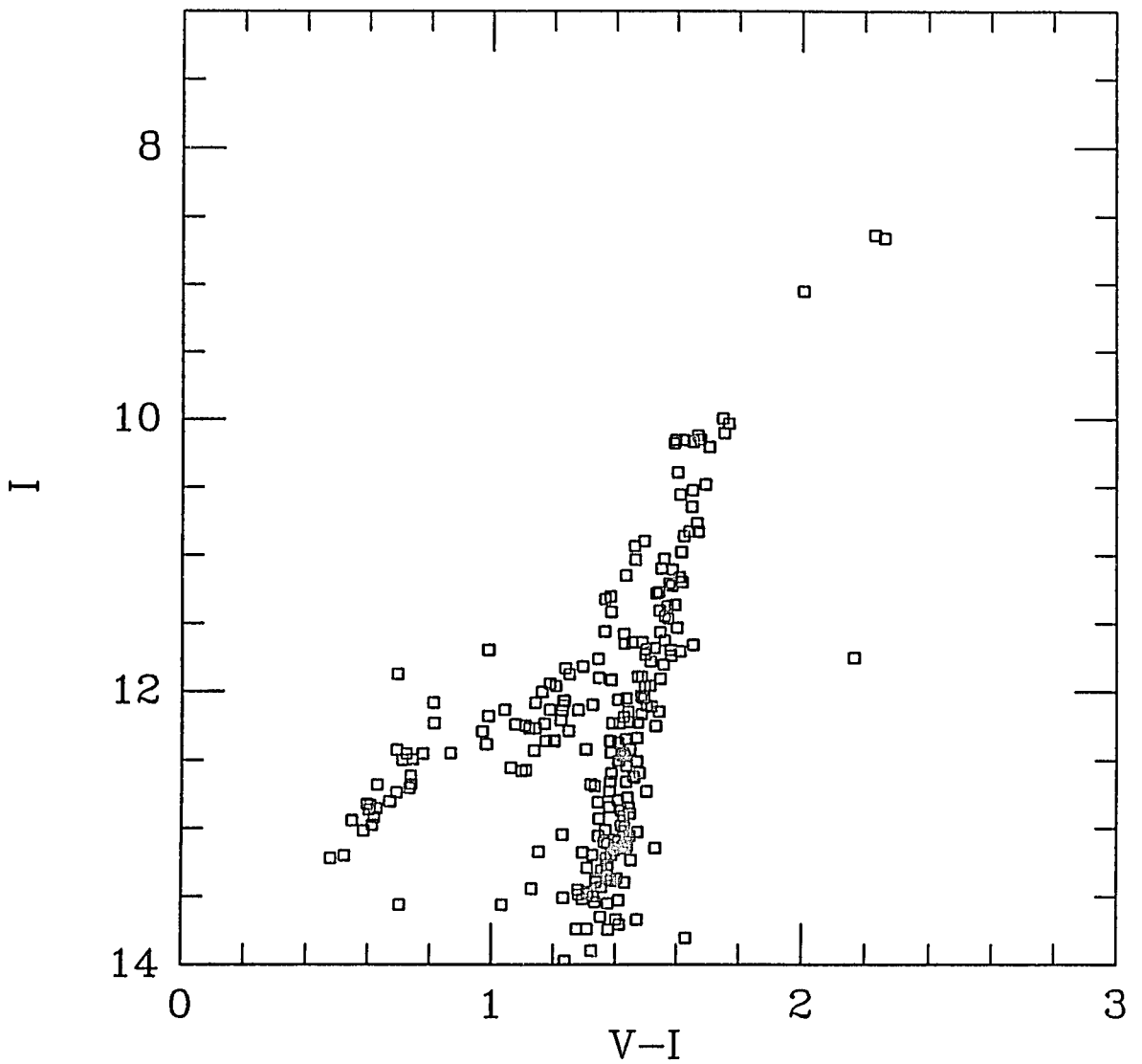

Figure 16a. Color-Magnitude Diagram of M 4

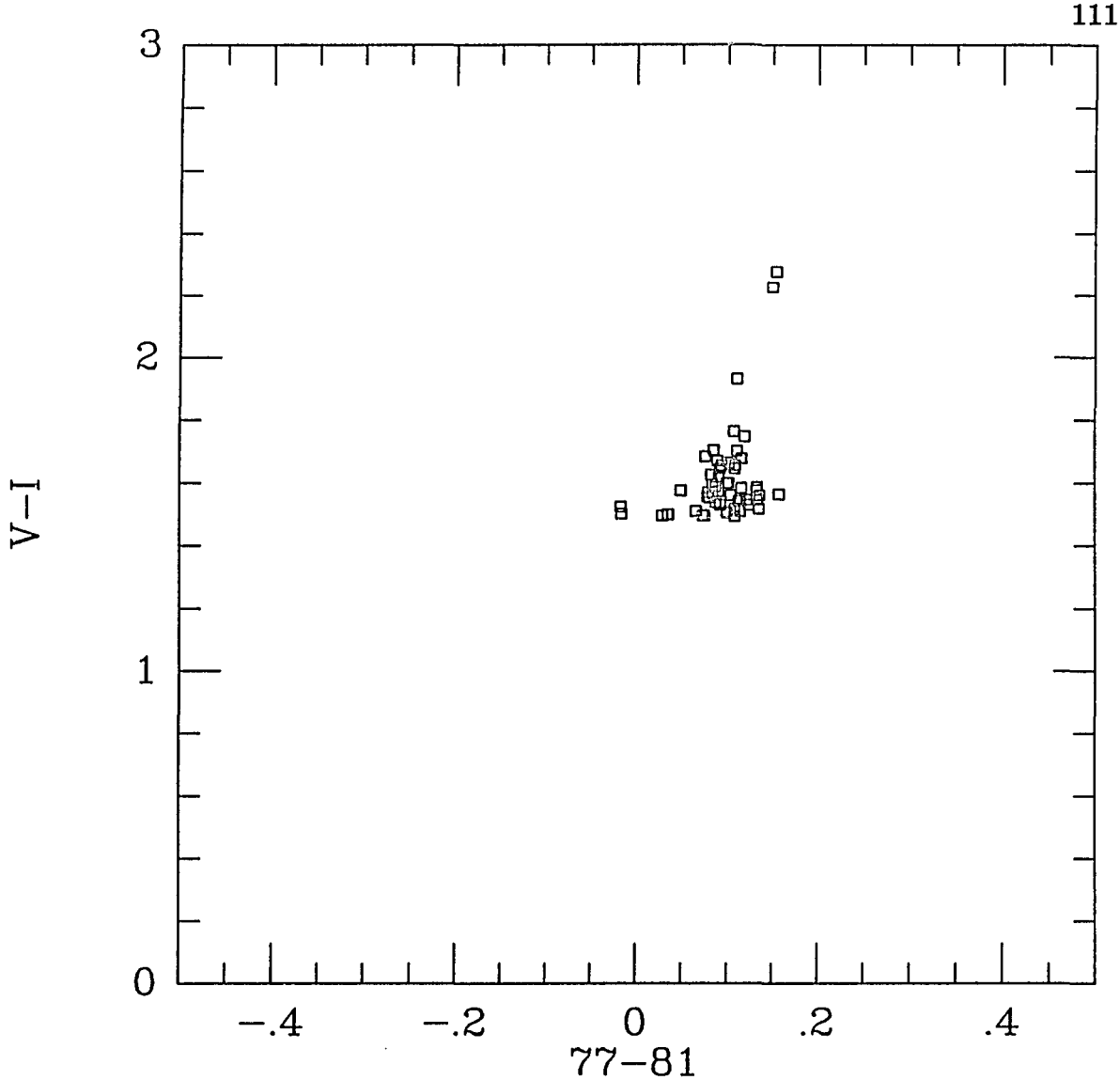

Figure 16b. Color-Color Diagram of M 4

when there is so much scatter is less certain. The first value in Table 8 is found by passing a line of the field giant slope through the mean color of stars E and M. These are the two reddest stars and they are clearly the tip of the color-magnitude giant branch and they are quite isolated. The second value is found by fitting a line to stars E, M and N. The slope of this line is so much larger than any other observed TiO track's that it results in an appreciably higher $(V-I)_{0.2}$ than the first estimate. The final value is found by fitting a line of the mean field giant slope to E, M and N.

NGC 6712

NGC 6712 lies within 4° of the Galactic plane and this field is quite contaminated with field stars. The giant branch tip is about one magnitude to the red of the horizontal branch intersection (see Figure 18a). The color-color diagram shown in Figure 18b reveals a TiO track which is at least 0.2 mag wide in V−I and extends to very strong TiO band strengths. The data for the twenty reddest stars at the giant branch tip in Table 8 assumes $E(B-V) = 0.48$ mag. These values are an average of three sets of observations on three nights. Four of the reddest stars were identified by Sandage, Smith and Norton (1966; hereafter SSN) as Mira variables and SSN's variable numbers are given. The brightest star lies about 2 arcmin from the center of the cluster and so is within SSN's cluster radius of 2.3 arcmin. It is, however, extremely red and lies within the region surveyed by SSN for variables. If it were a cluster member, such a red giant would be expected to be a variable and to have been found as such. Lloyd Evans and Menzies (1977) found this star, which they called D15, to be variable.

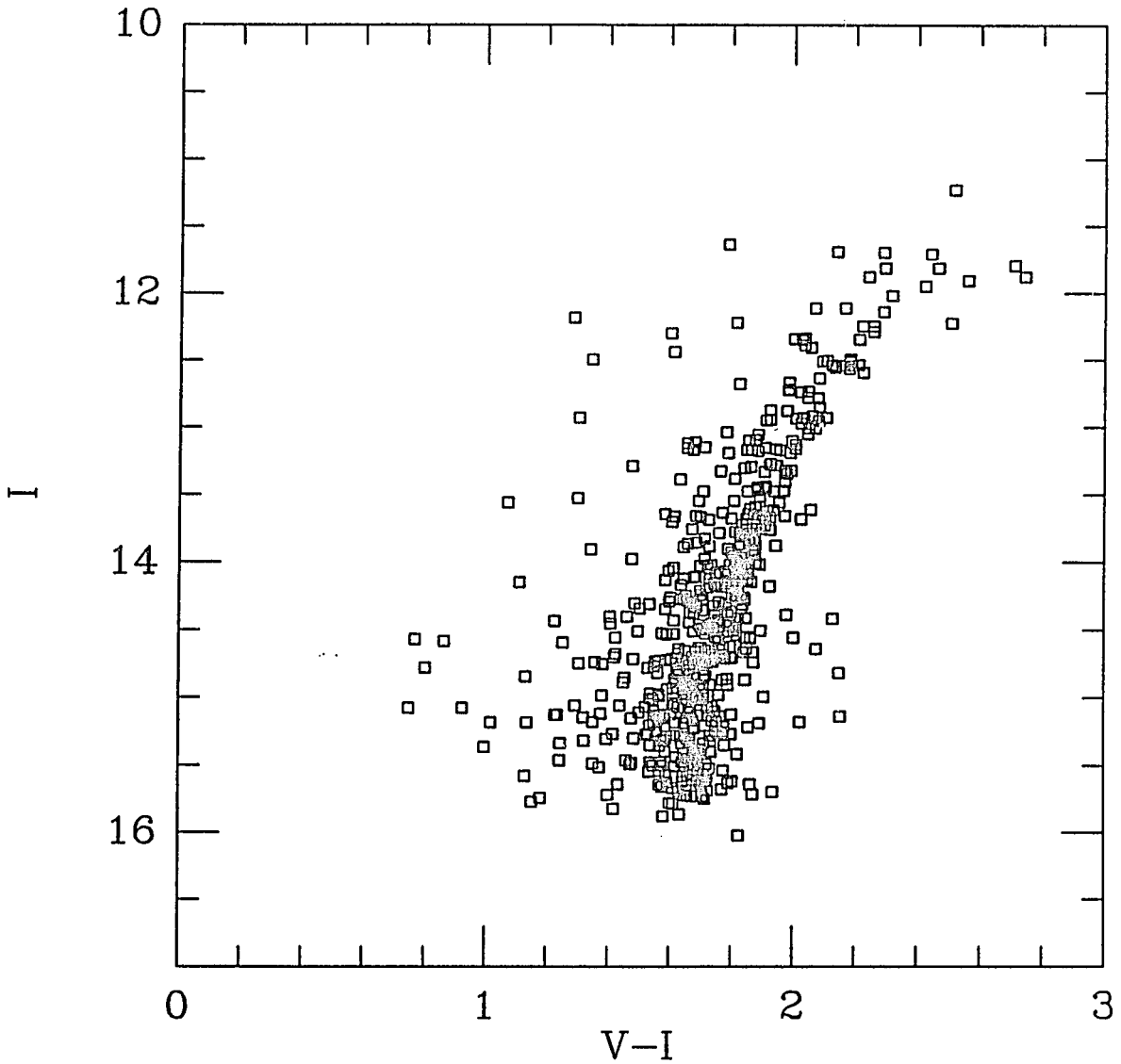

Figure 17a. Color-Magnitude Diagram of NGC 6402

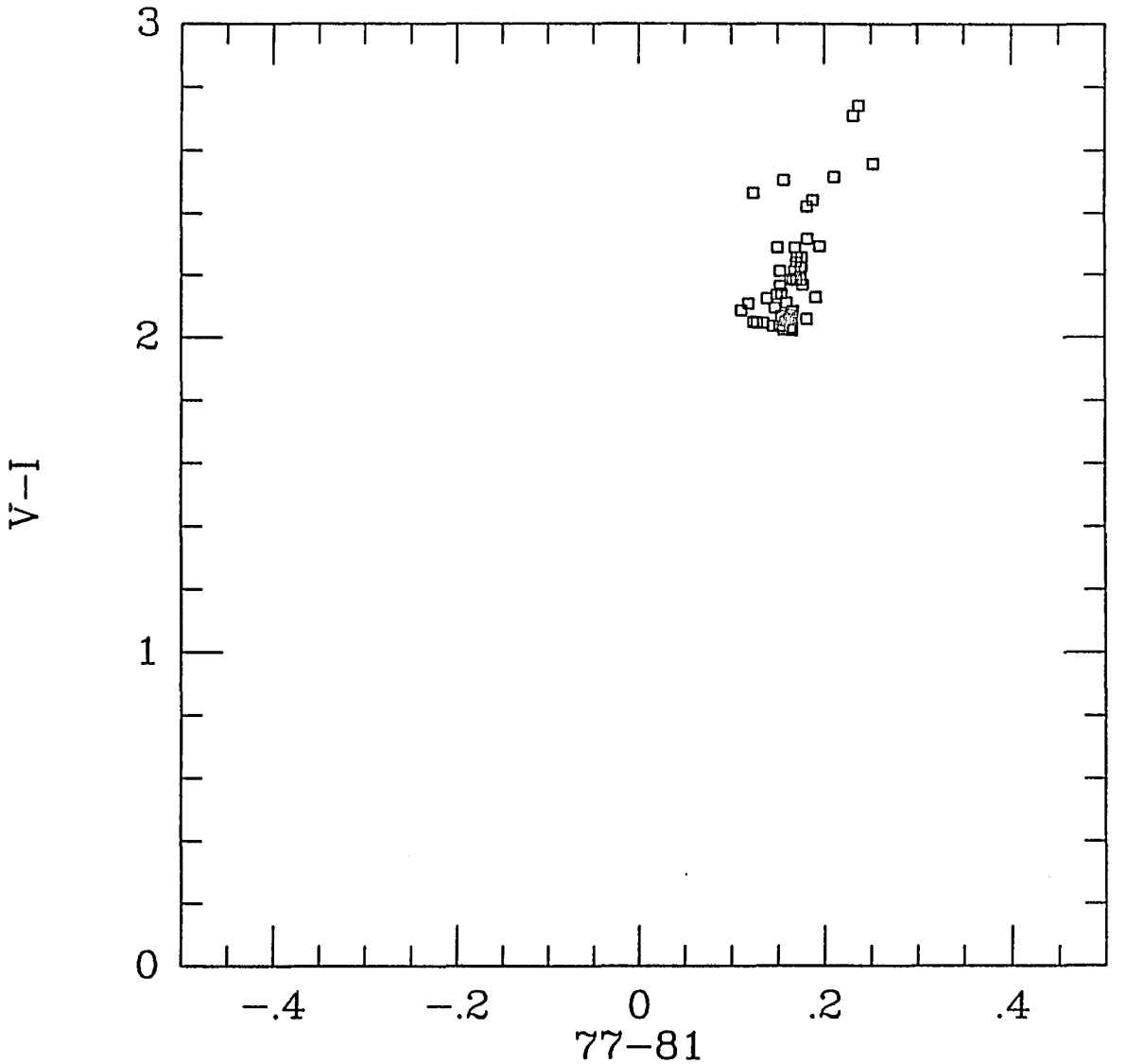

Figure 17b. Color-Color Diagram of NGC 6402

They point out that there is a high density of red variables in the Scutum cloud and so the fact that a star seems to be a variable at the tip of NGC 6712's giant branch does not guarantee its membership. The fourth reddest star is probably not a member because it is about a magnitude too faint for the giant branch tip. SSN decided that V2, V8, and V10 were members of NGC 6712, but that V7 was too bright. They found periods of 105, 117, 174 and 190 days respectively for these stars. They argued that an M_V of -4.4 for a 190 day period Mira was too bright by two magnitudes. A more modern analysis of Mira absolute magnitudes (Clayton and Feast 1969) suggests that $M_V = -3 \pm 0.4$ for this period. Thus V10 is 1.3 mag fainter than the average and V7 is 1.4 mag brighter than the average and both are about three standard deviations from the mean. V2 and V8, on the other hand are both 1.6 mag brighter than the Clayton and Feast (1969) average, $M_V = -1.6$, for their period range. It is interesting to note that V10's amplitude as measured by SSN is less than a magnitude. As such, V10 must be classified as a semiregular variable (Hoffmeister, Richter and Wenzel 1985). If this analysis is correct, then the three bona fide Miras in NGC 6712 are all overluminous by about 1.5 magnitudes. Feast (1967) showed that V7 is a radial velocity member of NGC 6712. The sixth reddest star is certainly not a member since it lies over 4 arcmin from the cluster center and is over one magnitude too bright for the giant branch tip. The problem of membership is quite severe for this cluster. The $(V-I)_{0.2}$ values presented in Table 8 all were dervied assuming that stars 4 and 6 are not members of NGC 6712. The first value presented is a least squares fit of the five stars redder than $(V-I) = 1.6$. The second value is a fit to stars

V7, V10 and V8 which lie on a line that is the same slope as the mean field giant TiO track. These are identified on the color-magnitude and color-color diagrams by circles around their points. The third value is obtained from a least squares fit to all stars with 77−81 greater than 0.11 which is a lower limit for TiO absorption. These values span a rather large range, but it is suggestive that V7, which at least has the correct radial velocity to be a member of NGC 6712, is a member of the trio of variables which form a line of the expected slope. Because these Miras are at roughly the same distance and one is radial velocity member of NGC 6712, the $(V-I)_{0.2}$ estimate which only uses their data is most likely to refer to NGC 6712.

M 107

M 107 has a giant branch which extends about one magnitude to the red of the intersection of the horizontal and red giant branches. The color-color diagram shows that there is only one star in my photometry which clearly exhibits TiO absorption. Two sets of broad-band colors but only one set of intermediate-band colors were obtained for this cluster and used to generate Figures 19a and 19b. The colors of the reddest six stars on the M 107 giant branch given in Table 7 along with the identifications of these stars from Sandage and Katem (1964). These colors have been corrected for an assumed reddening of E(B−V) of 0.33 mag. The $(V-I)_{0.2}$ value in Table 8 was determined by passing a straight line with the slope of the observed field giant TiO track slope of 3.6 through the position of star 217. Star 217's dereddened 77−81 color is quite near 0.2 and so the exact value of the slope of the TiO track does not greatly affect $(V-I)_{0.2}$.

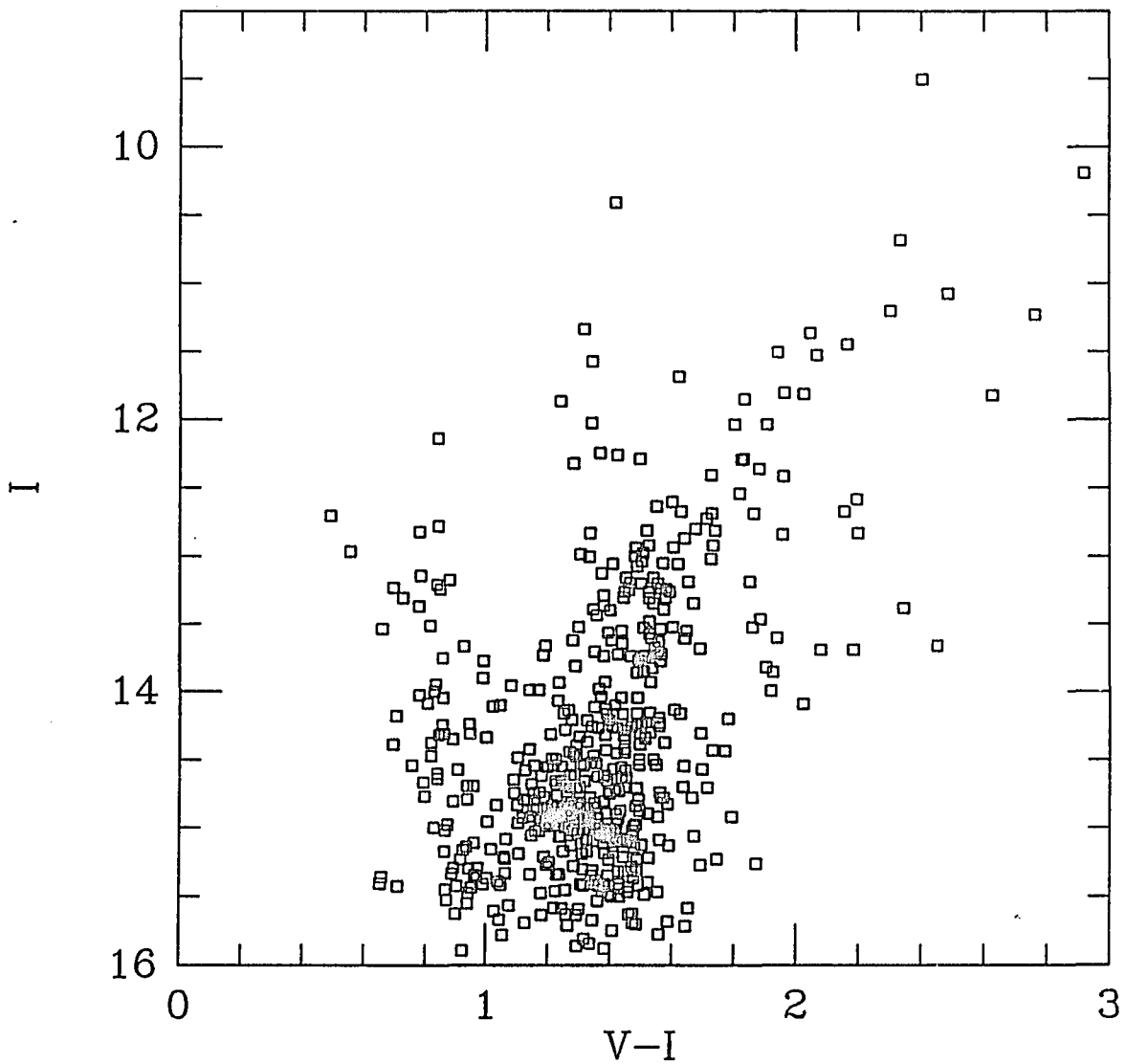

Figure 18a. Color-Magnitude Diagram of NGC 6712

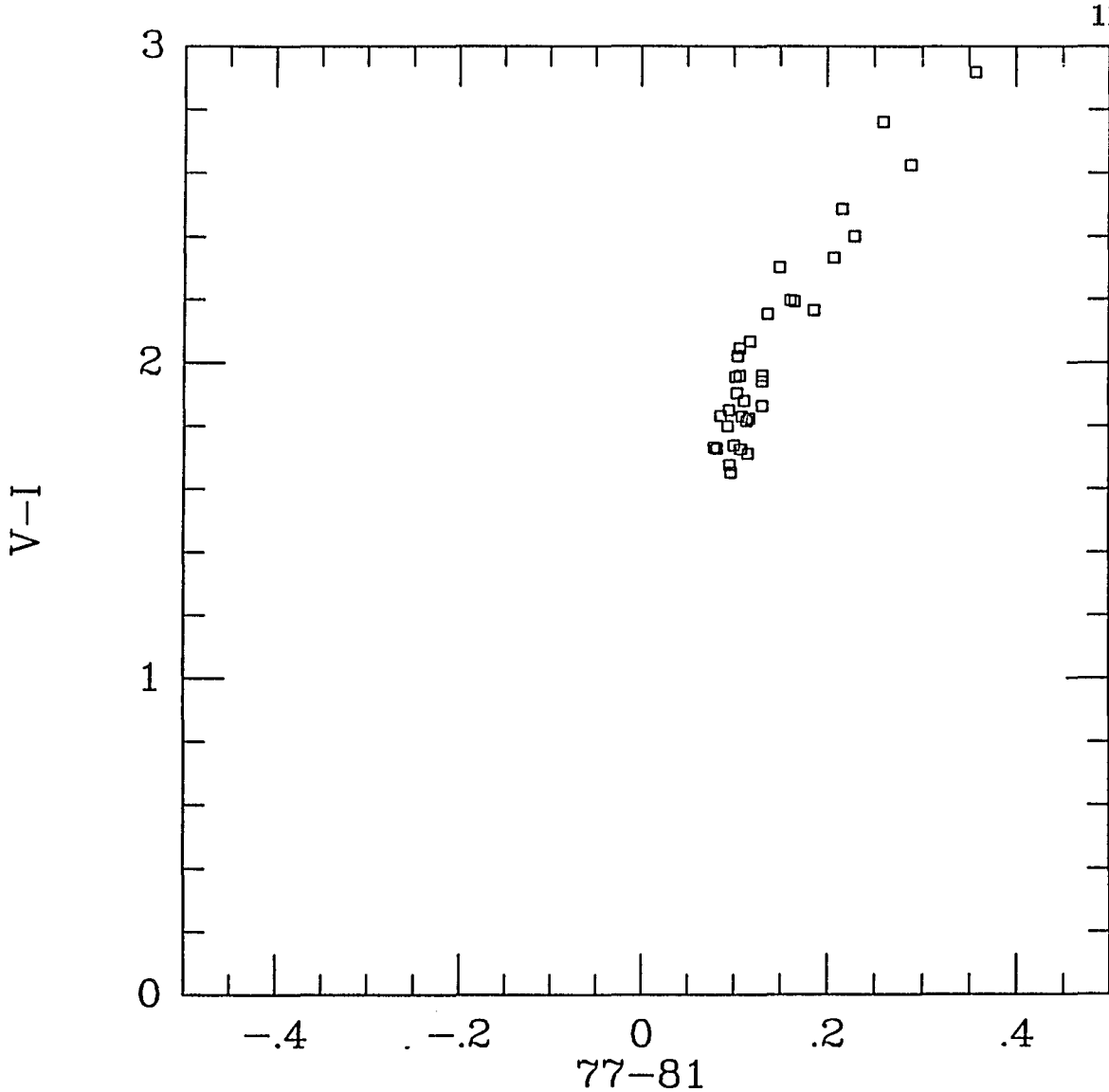

Figure 18b. Color-Color Diagram of NGC 6712

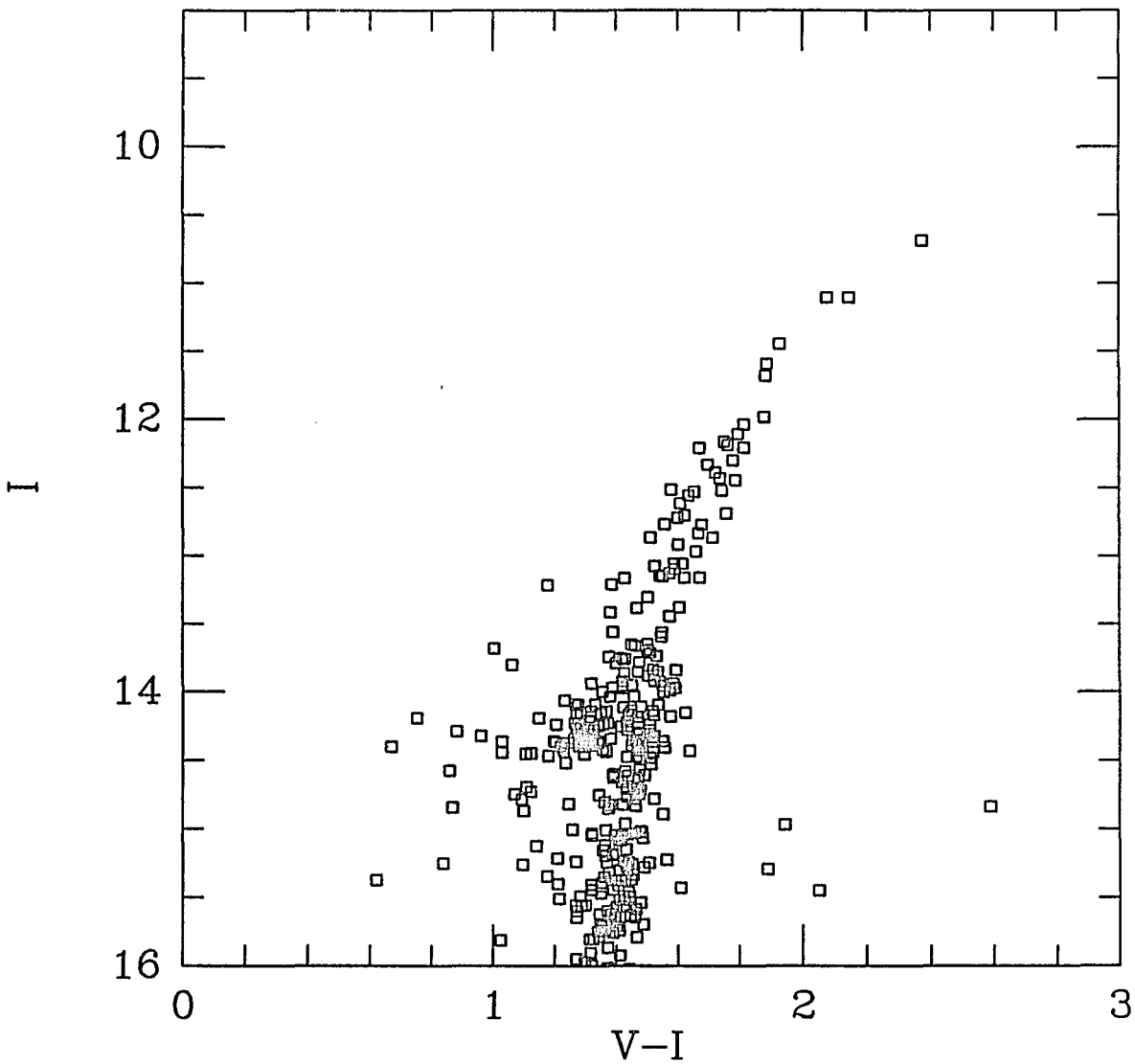

Figure 19a. Color-Magnitude Diagram of M 107

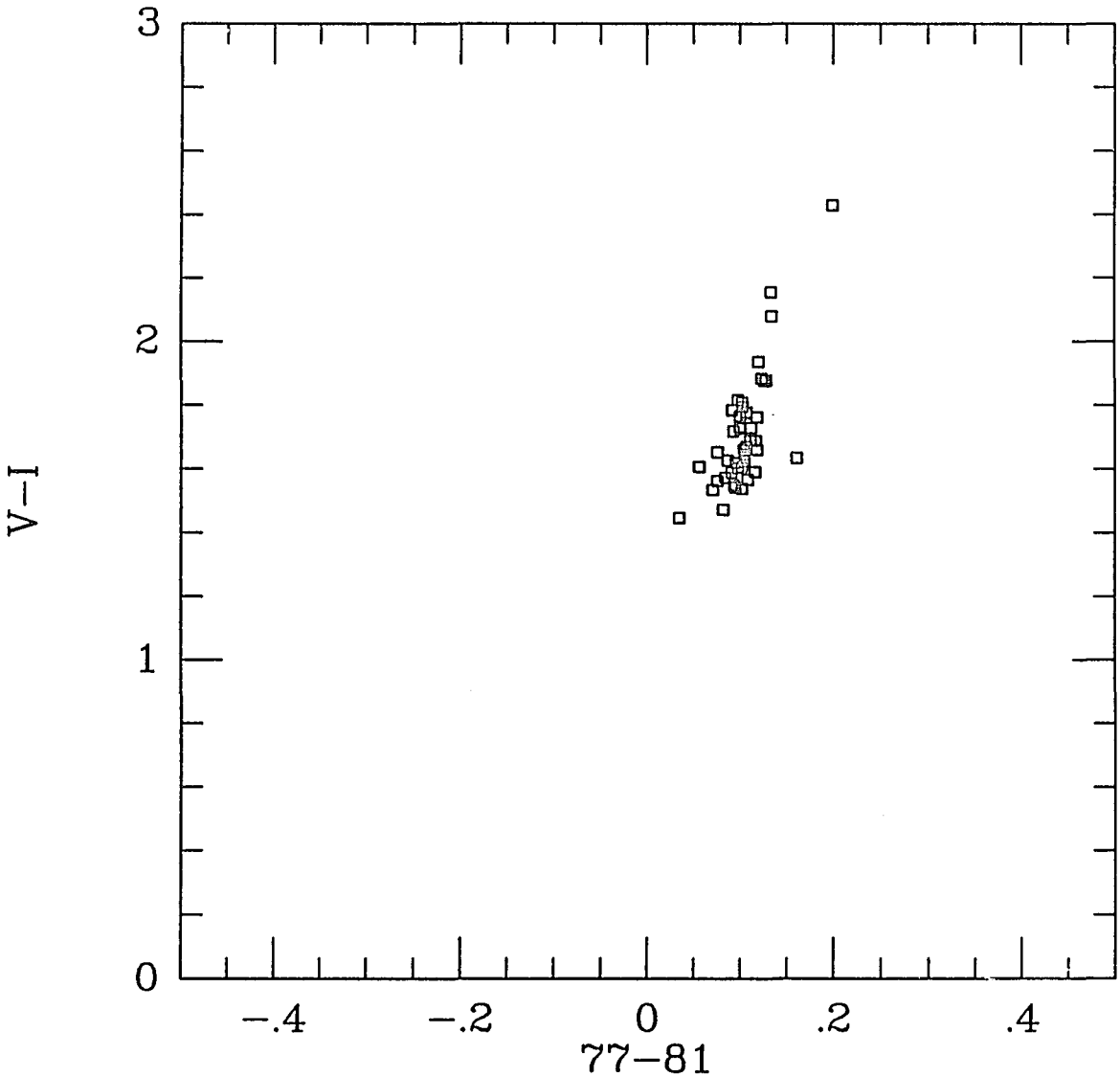

Figure 19b. Color-Color Diagram of M 107

NGC 6366

NGC 6366 is a relatively sparse globular cluster whose giant branch extends less than a magnitude to the red of its intersection with the horizontal branch as seen in Figure 20a. The color-color diagram (Figure 20b) of this cluster shows one star that is clearly to the red of the zero TiO track. The dereddened colors for the three brightest stars are given in Table 7. These are averages of determinations on two nights. The identification of two of these is from Pike (1976); the unidentified star is part of a relatively close pair and was not measured by Pike. The assumed reddening to NGC 6366 was 0.65 mag E(B−V) and though the colors of this star are less certain than for stars 50 and 8 its 77−81 color does not place it on the TiO track. The $(V-I)_{0.2}$ presented in Table 8 was again determined by passing a line with the field giant TiO track slope through the position of star 50. This value should not be too sensitive to the exact slope of the line since star 50 has $(77-81) \approx 0.2$ mag.

M 69

This cluster has a well developed giant branch shown in Figure 21a, which extends about 1.5 mag redward of the horizontal branch intersection and five magnitudes brighter. The color-magnitude diagram of stars in my field for this cluster shows quite a bit of scatter which is probably due to field contamination. Ratnatunga and Bahcall (1985) predict that there will be about four stars in this field which are not cluster members but are intrinsically redder than $(V-I) = 1.5$ and within about a magnitude of the giant branch tip. All of my field is within a four arcmin radius which

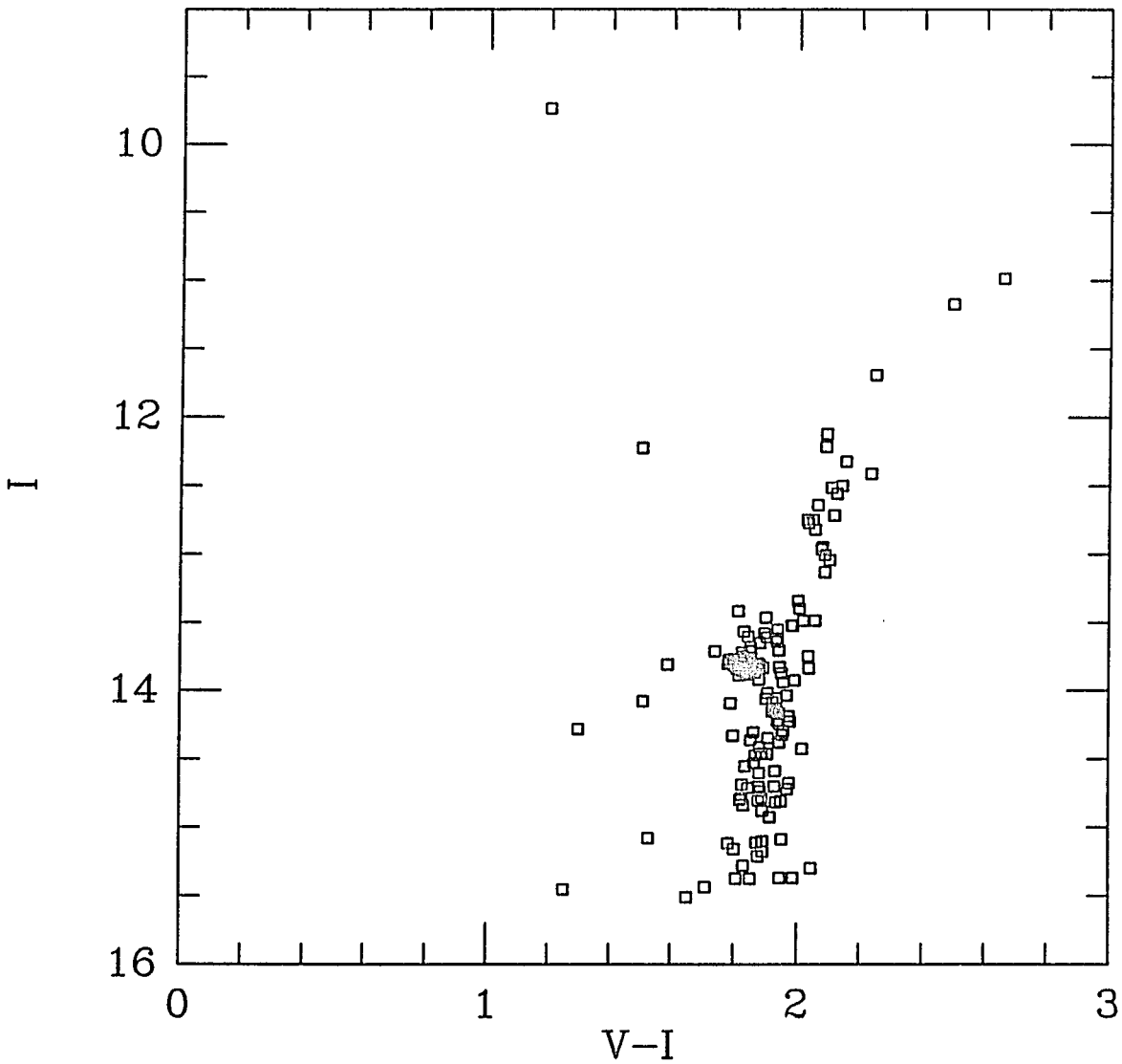

Figure 20a. Color-Magnitude Diagram of NGC 6366

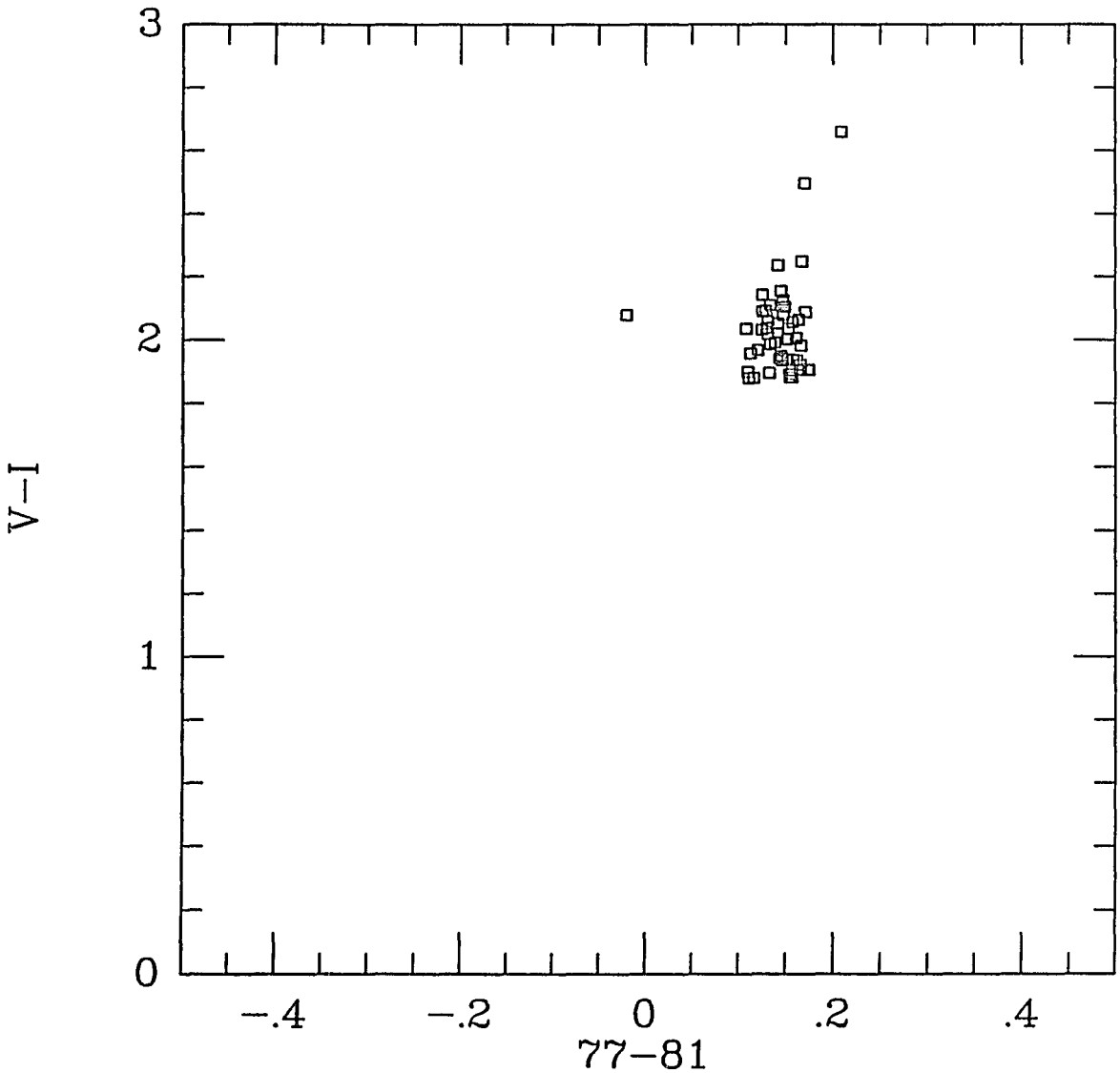

Figure 20b. Color-Color Diagram of NGC 6366

Hartwick and Sandage (1968) used as an absolute outer limit for M 69, but they only used stars within two arcmin of the cluster for their study. The color-color diagram in Figure 21b also shows a great deal of scatter. There are a number of stars which show TiO absorption. The colors of the fourteen reddest stars from the region of the giant branch tip are listed in Table 7 where $E(B-V) = 0.17$ has been assumed. The data is from an average of two sets of observations made on one night. HS's identifications are also listed for most of these stars. They divided their study into the inner one arcminute (stars labelled i for inner) and an annulus from one to two arcminutes. The third reddest star is in the core of the cluster and its colors are not well determined by this aperture photometry study. The star III35i is a magnitude below the giant branch and is probably not a member. I43o, IV12i and I40o are variables which HS consider to be cluster members. The spread in the width of the TiO track may be due to the fact that there is a lot of crowding, particularly for the stars in HS's inner arcminute. If the image of a late type star were crowded by an earlier type then the V−I color would be affected more than the 77−81 because the difference between the V−I colors would be much larger than the small differences seen in the 77−81 colors. The $(V-I)_{0.2}$ is not particularly sensitive to this scatter if the core star is not considered. This is because the scatter is most at quite red 77−81 values and the TiO track near the tip of the zero TiO branch is not as wide. The first value listed in Table 7 is for a least squares fit to the twelve acceptable giant branch stars. The second value is determined from a line fit to stars identified by HS in the outer region and so are not so crowded except that the eleventh reddest star is not used since it has a

very close neighbor and it is on the boundary of the inner region. These stars form the upper boundary of the TiO track and shift the $(V-I)_{0.2}$ almost 0.10 mag to the red. Most other assumptions about good photometry of cluster membership yield $(V-I)_{0.2}$ values near the first. Because M 69 is at $l^{II} = 1°$ and $b^{II} = -11°$, there is considerable field contamination by both the disk and the bulge populations. Although disk dwarfs of the late type seen at the tip of the giant branch are extremely unlikely at such a bright magnitude, bulge M giants are a distinct possible contaminant. If there are field stars in this photometry, they are likely to be more metal rich than M 69. For this reason, I think that the higher $(V-I)_{0.2}$ value is the most representative of the metallicity of M 69, particularly because its slope is closest to the field giant TiO track slope.

M 71

M 71 exhibits a well developed giant branch which has a tip that is at least two magnitudes redder in (V−I) than its intersection with the horizontal branch which is seen clearly in Figure 22a. This provides a number of stars on the TiO branch in the color-color diagram. The color color diagram presented in Figure 22b is from the data of 6/8/85. Five sets of observations (V,I,77,81) were made on the three nights of the 6/85 run and the average colors observed for six reddest stars are given in Table 7. These values have been dereddened using an E(B−V) value of 0.19. Two stars from the M 71 field have not been included in these data because they lay well below the M 71 giant branch. This cluster lies about 5° out of the Galactic plane and there are many field stars in the field which

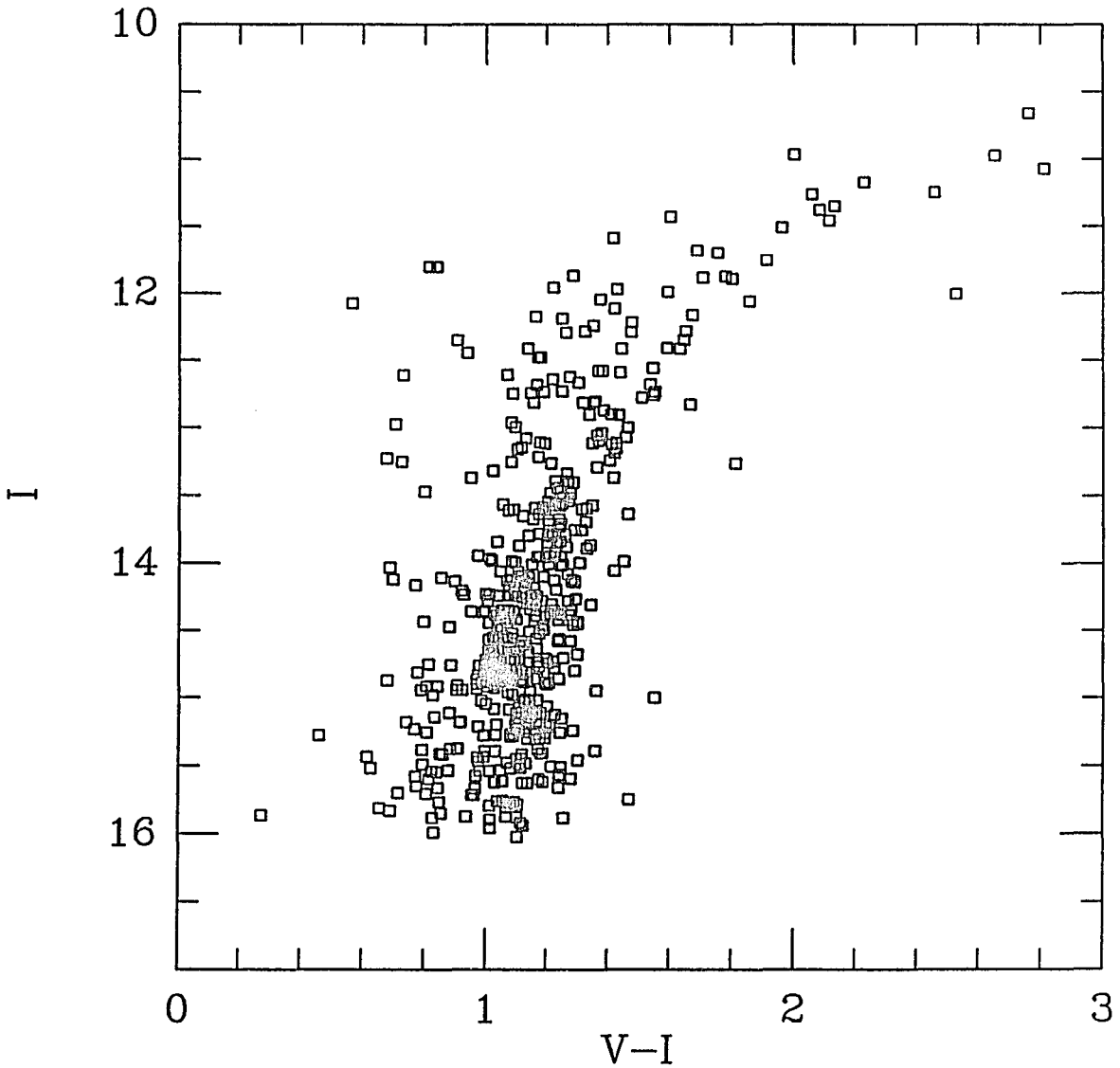

Figure 21a. Color-Magnitude of M 69

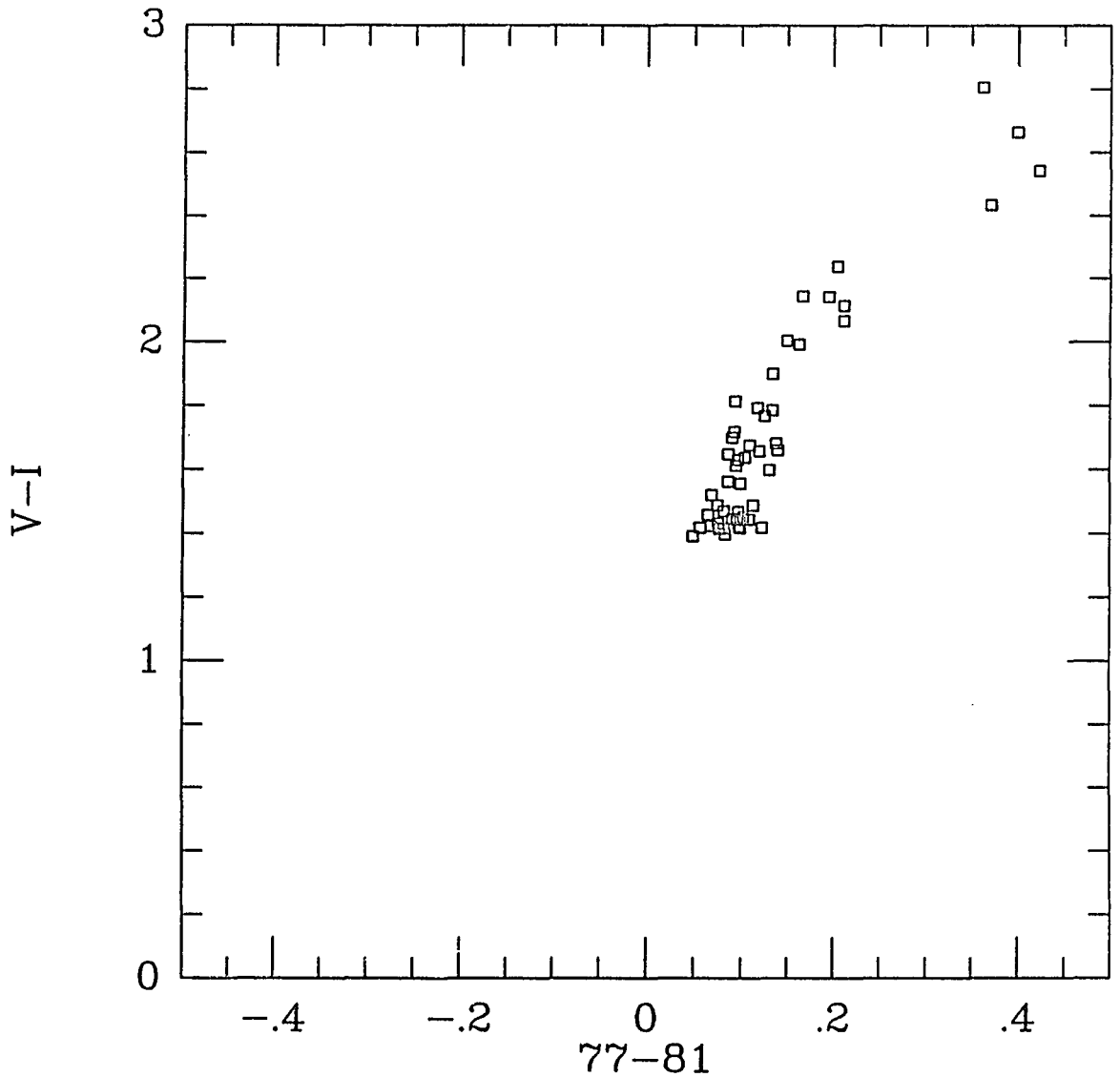

Figure 21b. Color-Color Diagram of M 69

contains M 71. Table 7 also provides the identification given to stars by Arp and Hartwick (1971). Table 8 presents the $(V-I)_{0.2}$ values. There are two values for M 71: the higher value includes star H in the determination of the least square fit to a straight line; the lower value comes from a fit which excludes star H. Star H lies in the center of the cluster and is quite crowded so that its aperture photometry may be less accurate. Cudworth (1985) has determined proper motions for M 71. He finds that all but stars 27 and 30 have membership probablilities greater than 80%. Star 27 is a variable (Sawyer Hogg 1973) and is a likely member with a probability of 60%. Cudworth (1985) does not list a proper motion for star 30. Table 8 also provides the slope and intercept $(77-81=0)$ value for the fitted lines and the correlation coefficient of the fit.

The Metallicity Calibration

Figures 23a and 23b are plots of the adopted metallicities of the clusters and the field giants versus the parameter $(V-I)_{0.2}$. The field giant value is that adopted by Mould and Siegel (1982). They based their value on the metallicity of nearby G dwarfs by Pagel and Patchett (1975) measured relative to the Hyades and the metallicity of the Hyades measured by Branch, Lambert and Tomkin (1980). None of the lower limits for $(V-I)_{0.2}$ determined for the metal poor clusters are included in this diagram.

For the metallicity scale of Webbink (1985), five of the clusters fall on a straight line with the field giants (Figure 23a). Of these, however, only M 71 has a well developed TiO branch in the color-color diagram. If a straight line is fit to these six points, the result is:

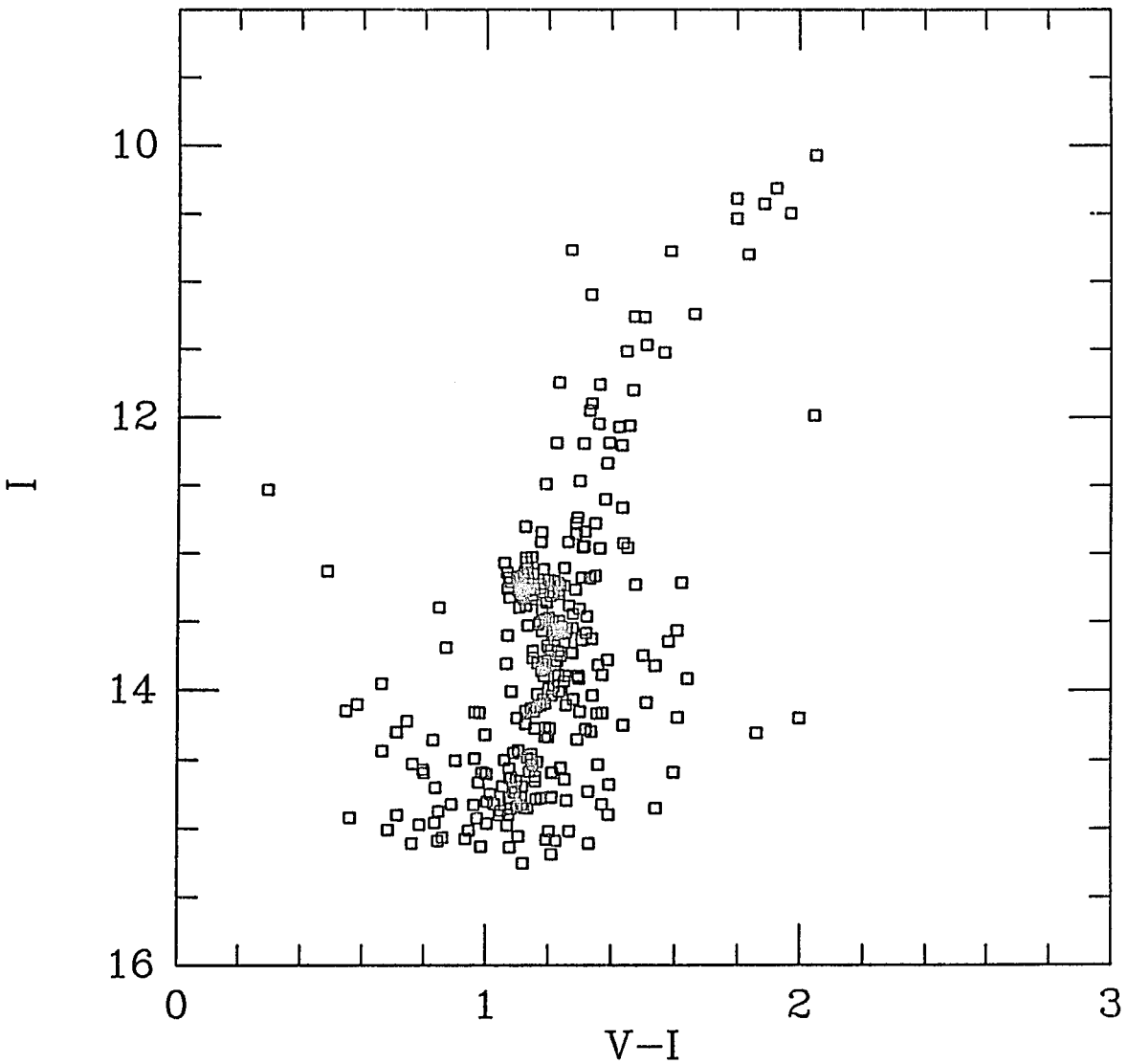

Figure 22a. Color-Magnitude Diagram of M 71

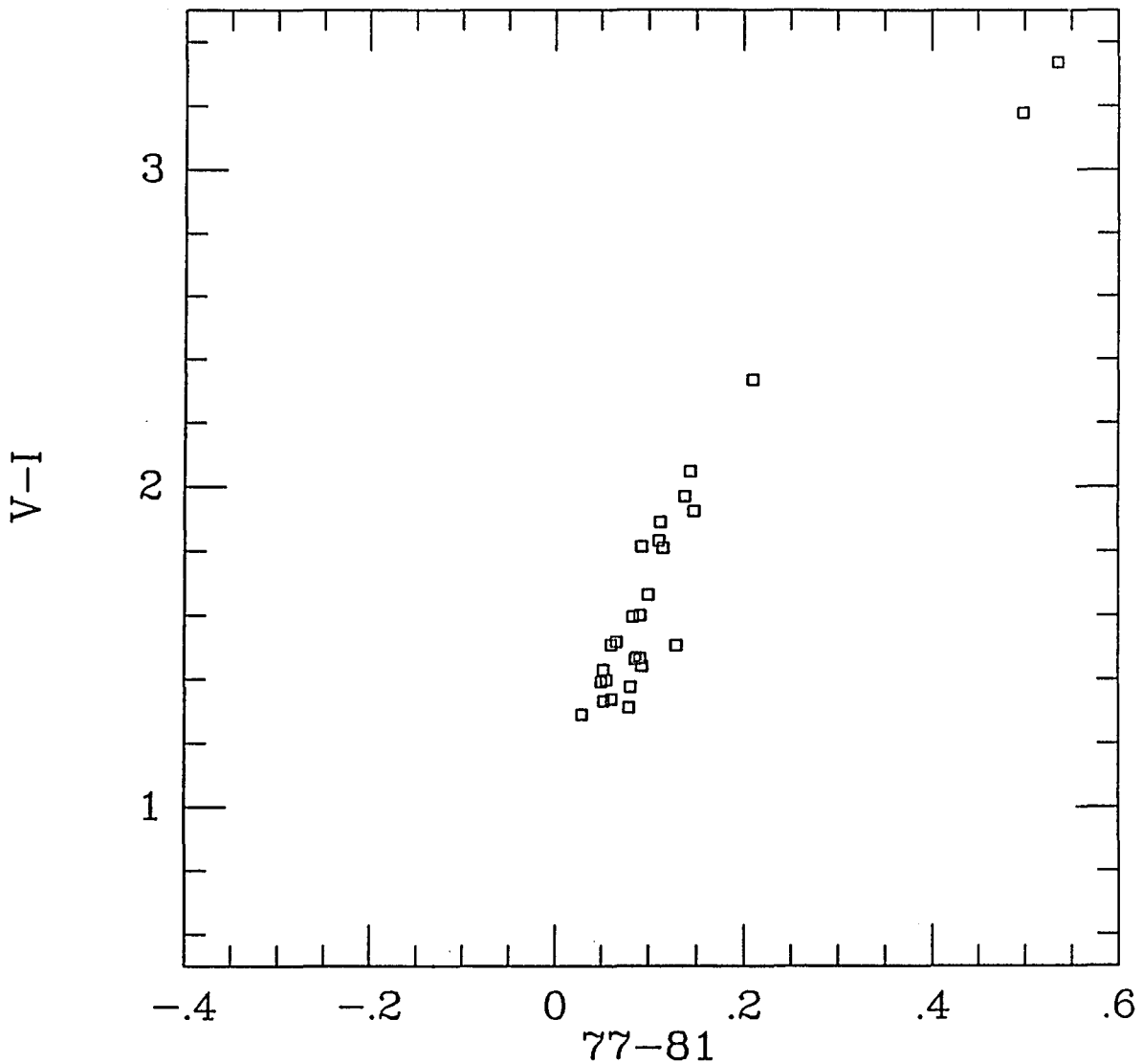

Figure 22b. Color-Color Diagram of M 71

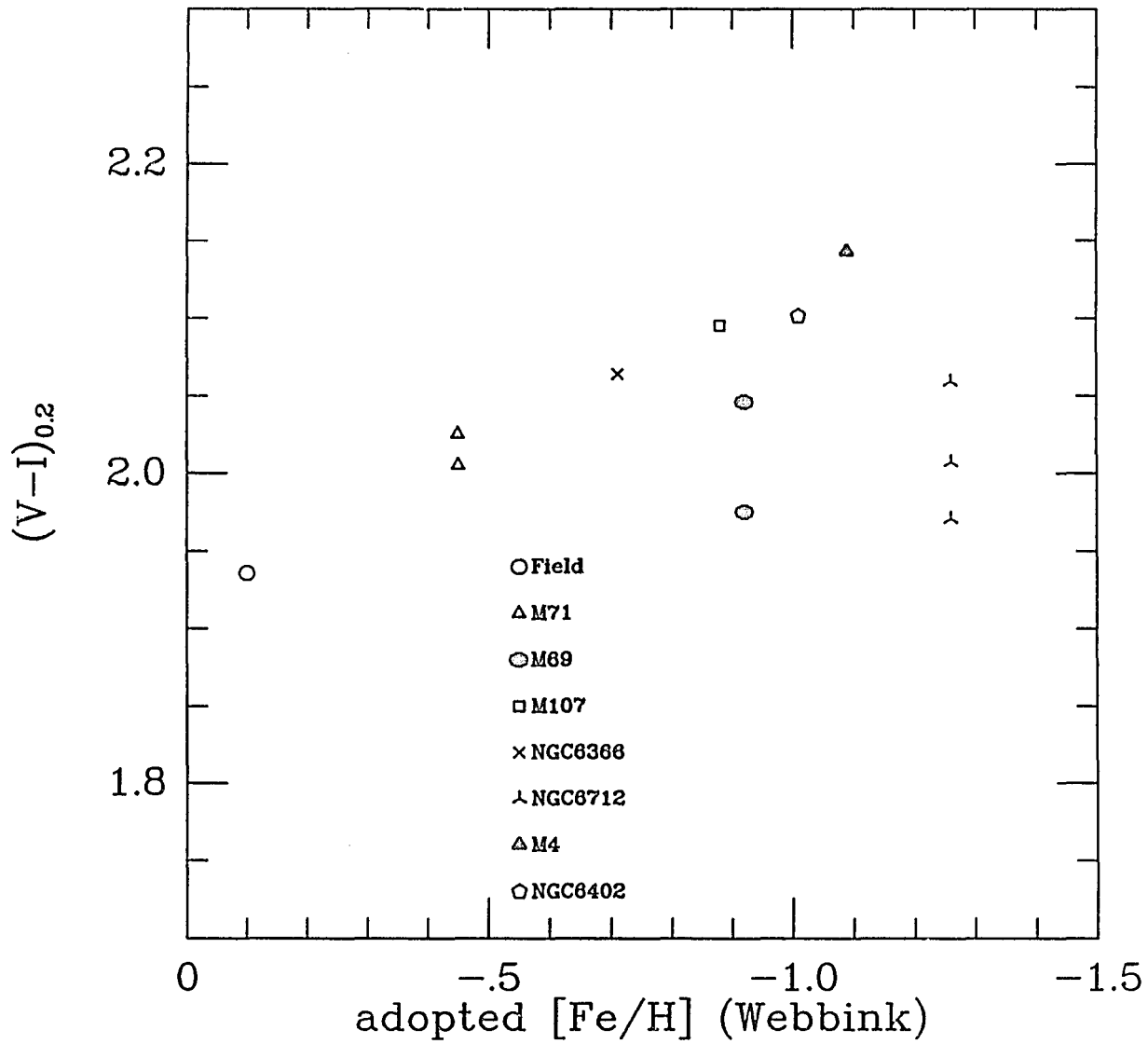

Figure 23a. $(V-I)_{0.2}$ as a Function of [Fe/H] on Webbink's Scale

The presence of multiple points of a single symbol type represent different assumptions detailed in the text.

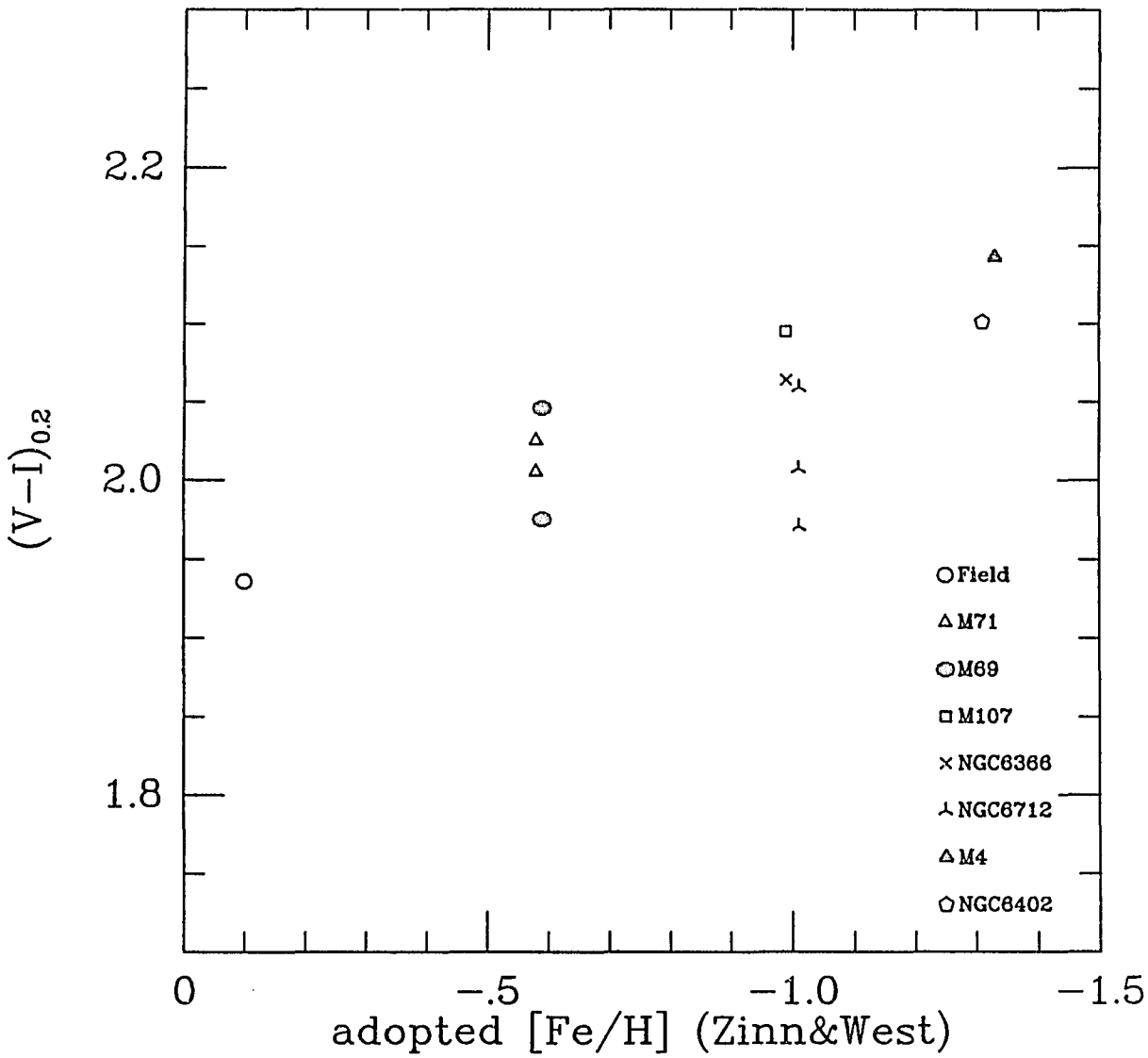

Figure 23b. $(V-I)_{0.2}$ as a Function of [Fe/H] on Zinn and West's Scale

The presence of multiple points of a single symbol type represent different assumptions detailed in the text.

$$(V-I)_{0.2} = 1.92 - .195 * [Fe/H] \qquad r = -.99.$$

If one includes the reddest point for M 69 (see the M 69 discussion above), then the correlation is not quite as good and the result is:

$$(V-I)_{0.2} = 1.92 - .182 * [Fe/H] \qquad r = -.95.$$

An unbiased least squares fit of a line to the mean $(V-I)_{0.2}$ for all the clusters using the Webbink scale yields:

$$(V-I)_{0.2} = 1.96 - 0.11 * [Fe/H] \qquad r = -.65.$$

The metallicity values used here are derived by Webbink (1985) from a correlation between dereddened subgiant colors and high-dispersion spectroscopy. He does not claim a high accuracy for this correlation. If his metallicities are compared to those of Zinn and West (1984) for the 5 clusters not including M 69 or NGC 6712, the mean difference is -0.21 ± 0.09 where Webbink is more metal rich. Webbink, however, finds M 69 and NGC 6712 to be 0.33 and 0.25 dex more metal poor than Zinn and West. If these two clusters are put on the system of Webbink using the relative ranking of Zinn and West then they will be about a half a dex more metal rich. This would put M 69 on the mean relation for the other clusters and NGC 6712 would be slightly below.

Adopting the first relation as the calibration of the $(V-I)_{0.2}$ parameter with respect to metallicity, I find the metallicity of M 69 to be $-.47$ and that of NGC 6712 to be -0.49. These values are obtained using the mean NGC 6712 and M 69 $(V-I)_{0.2}$ values. If the only the reddest estimate for each is used, then they both become ~ 0.18 dex more metal poor. The rationale for such a choice is that field stars will always serve to make

contaminated clusters appear more metal rich and crowding will also make them appear more metal rich so the reddest estimate is probably the least affected.

The Zinn and West (1984; hereafter ZW) metallicity scale seems to be more consistent with a ranking of the cluster metallicities using the $(V-I)_{0.2}$ parameter as is apparent in Figure 23b. If a line is fit to all of the clusters using the ZW scale and the mean $(V-I)_{0.2}$ for M 69, M 71 and NGC 6712 the result is:

$$(V-I)_{0.2} = 1.922 - 0.145 * [Fe/H] \qquad r = -.91.$$

If one only uses the Mira value for NGC 6712 and all the other points, then the relation becomes:

$$(V-I)_{0.2} = 1.923 - 0.151 * [Fe/H] \qquad r = -.97.$$

Although these two metallicity scales are not the same, it seems that the color of the TiO track does a reasonable job in ordering the metallicities of the globular clusters and the field giants. The tightest relation is that found for five clusters and the field giants using the Webbink scale. If one then uses this scale to estimate the metallicity of M 69 and NGC 6712, the ranking is the same as that found in the Zinn and West scale. The calibration, as it stands, depends on a very few stars which are lower metallicity than the field giants. It also does not extend below about [Fe/H] = −1.3 on the Zinn and West scale because of the absence of M stars on the giant branch at low metallicities. A true test of the calibration would be an investigation of a metal rich population. If the calibration is useful, the TiO track color of a metal rich population will be bluer than the field giants and much bluer than any of the clusters.

Baade's Window

Baade's Window is a relatively clear line of sight toward the center of the Galaxy (Baade 1946, 1951). Photometric studies of the bulge of our galaxy made in Baade's Window suggested that the late-type giants there are metal rich (Arp 1965, van den Bergh 1971). Whitford and Rich (1983) have determined spectroscopically that most bulge K giants are more metal rich than the Sun. Whitford (1986) has recently reviewed the M giant population of the bulge and feels that the late-type M giant population has evolved naturally from the metal rich K giants. The luminosities of the M giants place them above the tip of the first giant branch and so they are probably AGB stars (Frogel and Whitford 1982). Although there is a large, well studied AGB population in the bulge, it was not until Azzopardi, Lequeuex, and Rebeirot (1985) applied their green Grens technique to survey the bulge that any carbon stars were found. These carbon stars are quite blue and not luminous enough to be AGB stars ($M_V = -1.5$) as the AGB is currently understood. Thus the bulge offers an interesting population to examine with the 77–81 system. The M giants may be metal rich and there may be an uncommon class of blue, carbon stars present.

A field was chosen which is just north of NGC 6522. This field is in Blanco, McCarthy and Blanco's (1984; hereafter BMB) region A which is less obscured by intervening interstellar material than other portions of the "window". This region is very crowded in a rather uniform manner. Exposures times were 30 seconds at 77, 25 seconds at 81, 12 seconds at V and 6 seconds at I. Figure 24 is the I band exposure of this field. Over 4,000 stellar images were found in the I and the intermediate-band frames.

This crowding necessitates some estimate of the completeness to be made. If stellar images cannot be resolved when they are separated by less than the seeing, and the seeing was about 1 arcsec, then this number of images covers almost 23% of the field. This suggests that about one quarter of the images are confused to some extent. Of course, about one half of these images are so faint that they cause negligible problems with the photometry since they are four to five magnitudes fainter than any of the M giants in the Baade's Window field.

A quantitative measure of the completeness was obtained by adding artificial stars to the I frame. One hundred stars were added to the I frame ten different times and these were reduced as the original I frame was. The stars were added in a magnitude range which was thought to span magnitudes where incompleteness due to crowding would become important. Figure 25 is a histogram of the percent of the artificial stars recovered as a function of I magnitude. The details of the completeness test are given in Chapter 2. It can be seen that there is a slow decline in completeness from about 96% at I = 13.3 to about 87% at I = 15 and then a more rapid decline begins. Stars brighter than $I \approx 13$ are so rare (there are only 32 of them), and so bright that they suffer essentially no incompleteness.

Stars were chosen for study whose color errors were less than ± 0.10 mag for both colors. Appendix A contains the positions, I magnitudes, V−I colors, 77−81 colors and estimated errors for these stars. Figure 26 is a color-magnitude diagram for these stars and Figure 27 is a color-color plot for them. Figure 28a is the I magnitude distribution of stars in this field with well measured colors, and Figure 28b is the I magnitude distribution of

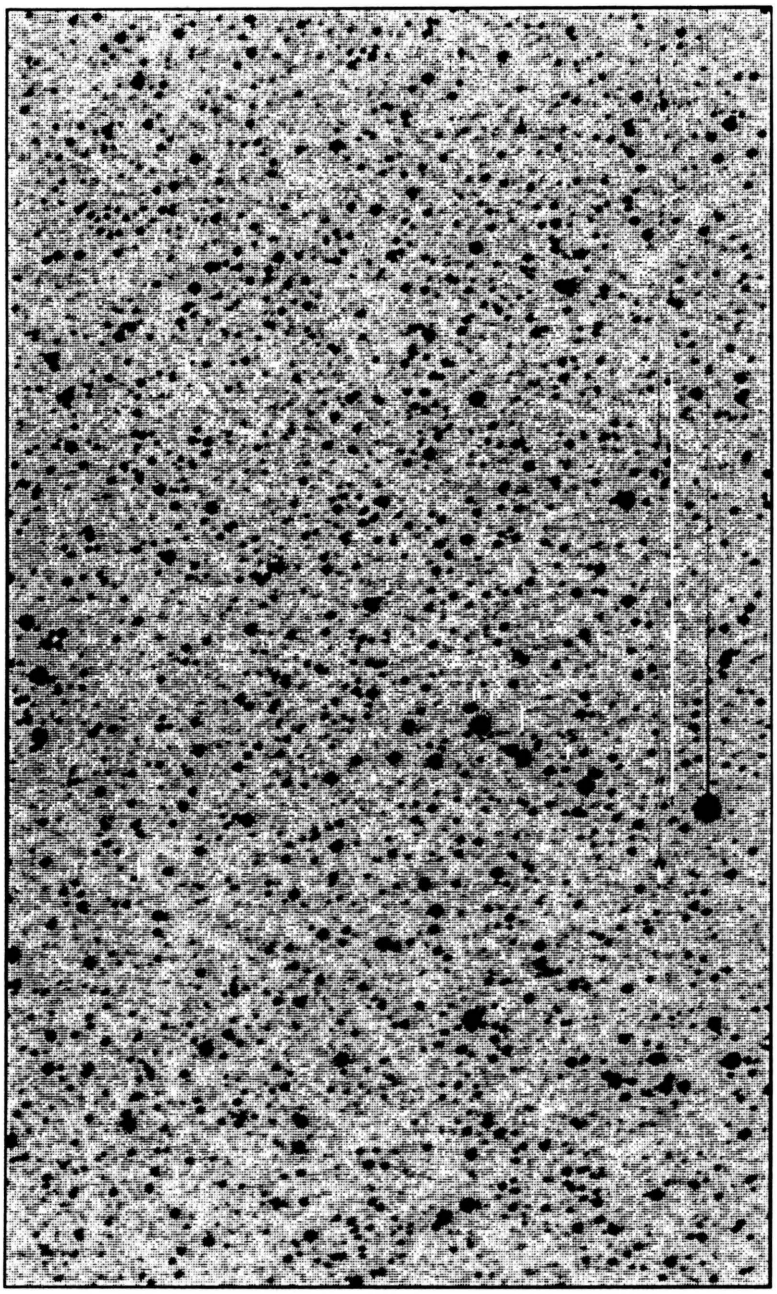

Figure 24. I band CCD Frame of Baade's Window Field

This frame is centered on Blanco, McCarthy, and Blanco's (1984) star 140. North is to the right and east is at the top; the field is 3 arcmin N-S and 5.08 arcmin E-W; and the frame is 300 by 508 pixels.

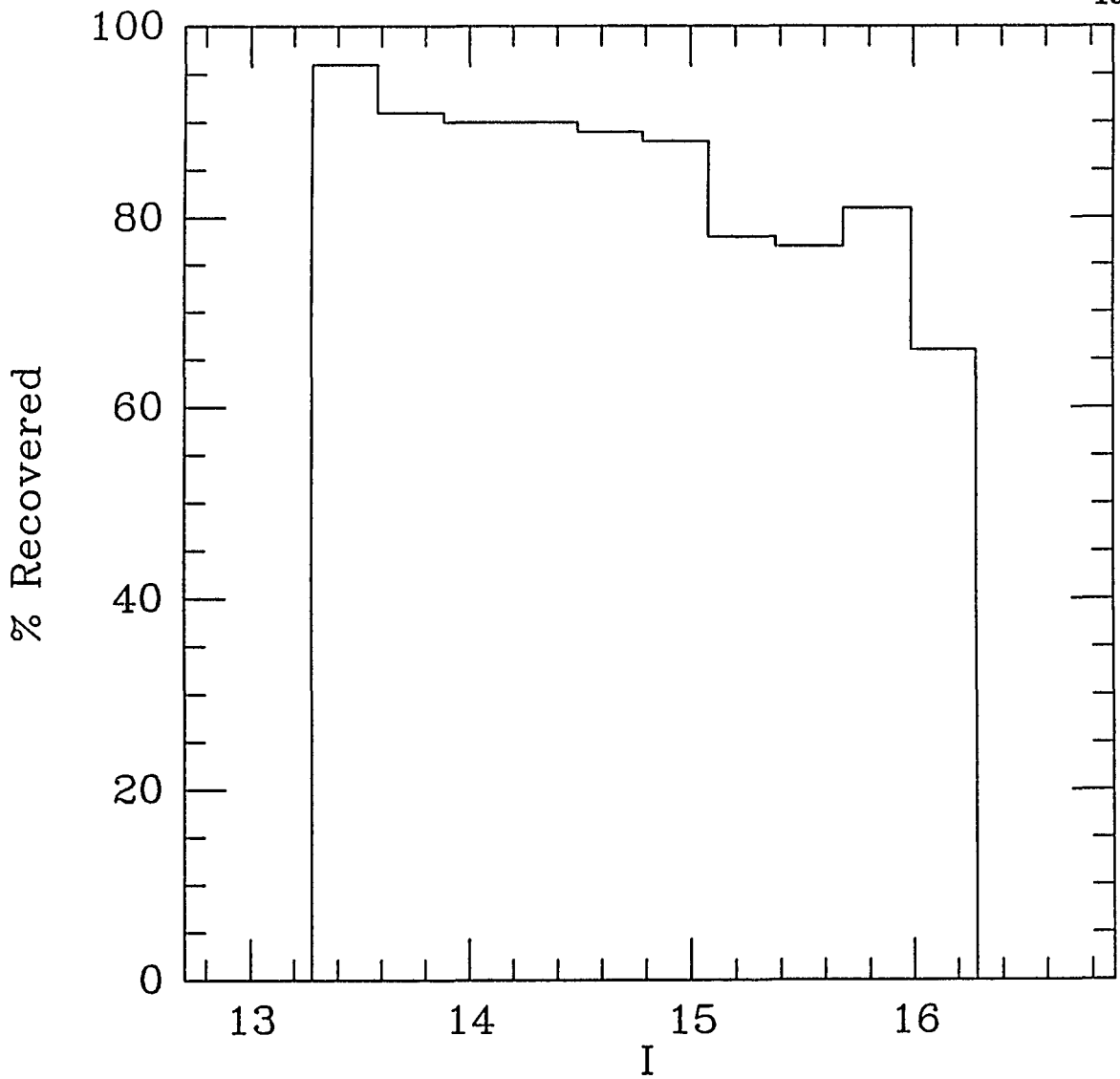

Figure 25. Completeness as a Function of I Magnitude in Baade's Window

stars with 77-81 > 0.21 which would be the color of an M1 star reddended by the measured interstellar extinction to this field of $E(B-V) = 0.46$ (Blanco, McCarthy and Blanco 1984). The peak of stars near $I = 13$ is caused by the presence of the nuclear bulge population of M giants. The increase in numbers at around $I \approx 15.5$ is probably due to foreground contamination by dwarfs.

The color-magnitude diagram for this field shows an extraordinarily well developed asymptotic giant branch. It is apparent that for stars as red as these stars I,V−I color-magnitude diagrams are not the best approximation to an HR diagram. This is seen from the fact that the AGB becomes nearly horizontal at the reddest colors since the I passband is too blue to be well correlated with the total luminosity. There is almost a two magnitude spread in the width of the AGB. A few tenths of this spread may be a distance effect because of the relatively large line of sight depth for the bulge compared to its distance. A spread in metallicity would also produce a broad AGB, but this spread would be more in color than magnitude (Whitford 1986). An age spread could easily produce a broad AGB. Two other effects may be adding to the spread of the AGB. Some of these stars may be in the process of shrouding themselves in dust and so their I magnitudes do not rise as quickly as their bolometric magnitudes and many of these stars are likely to be quite variable.

The color-color plot shows a well developed TiO branch. This branch extends a full magnitude to the red of the zero band strength line and exhibits an interesting twist. For very late giants, TiO and VO absorption becomes so strong that the TiO track stops moving as rapidly redward because

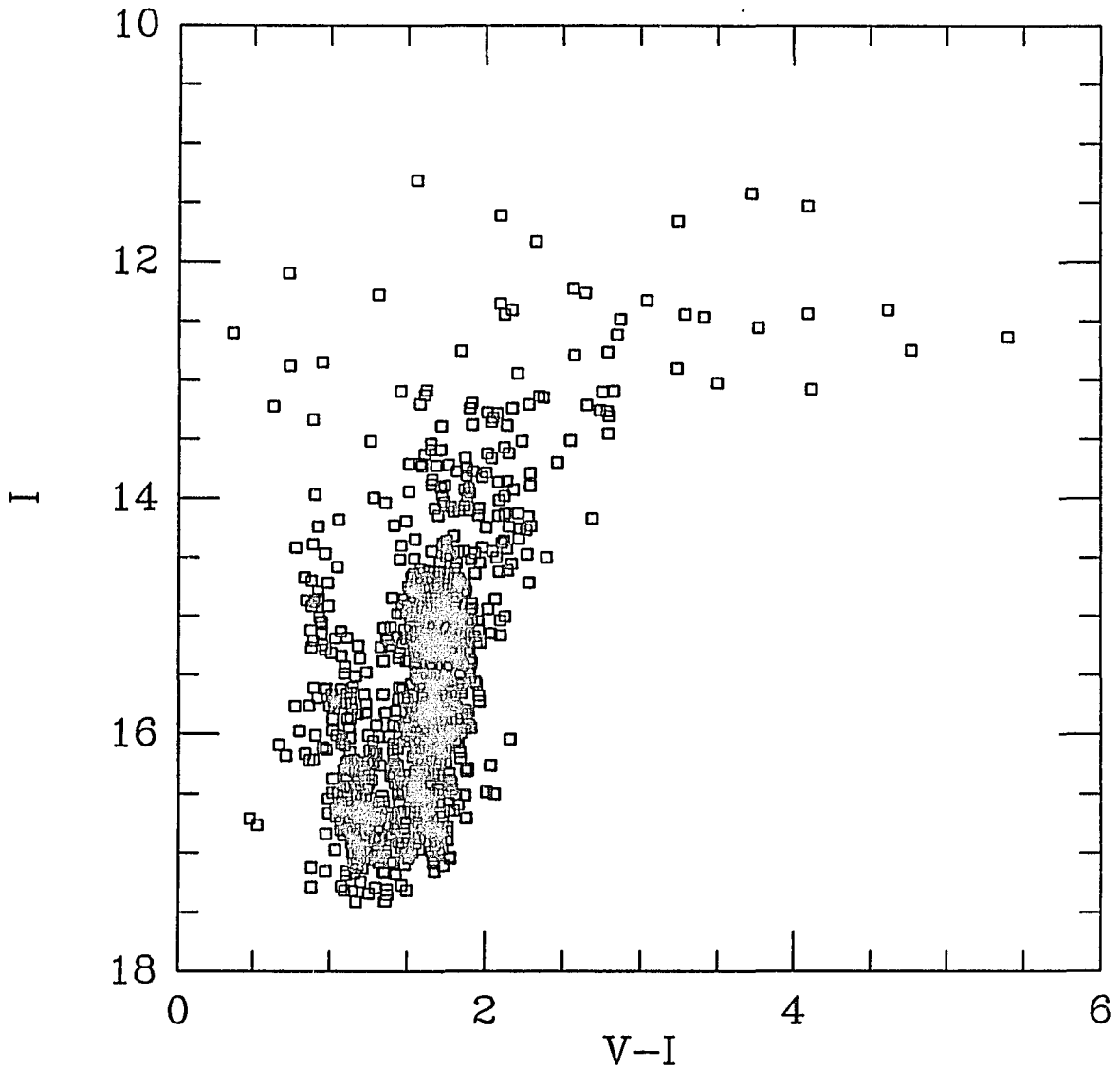

Figure 26. Color-Magnitude Diagram of the Baade's Window Field

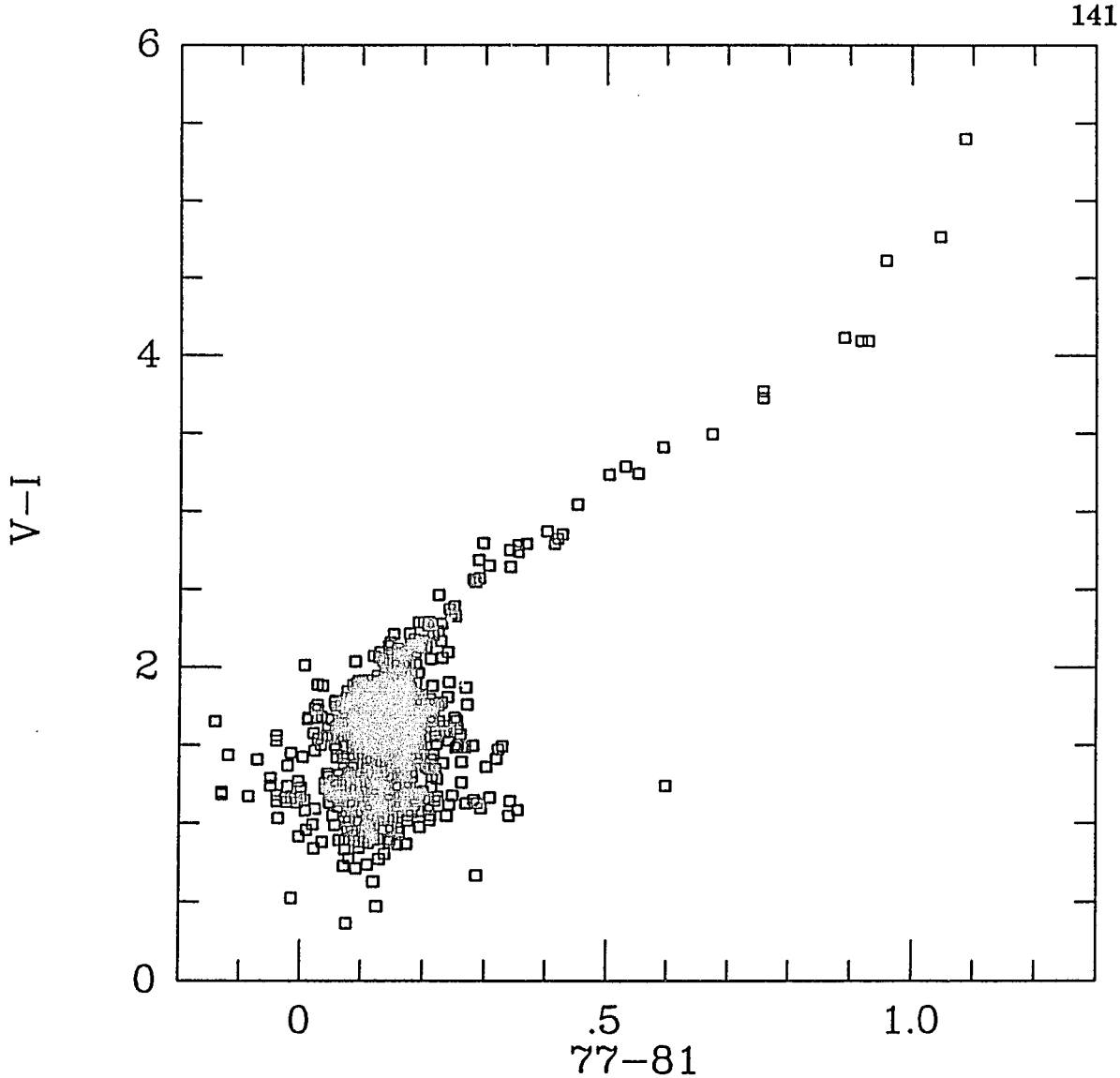

Figure 27. Color-Color Diagram of the Baade's Window Field

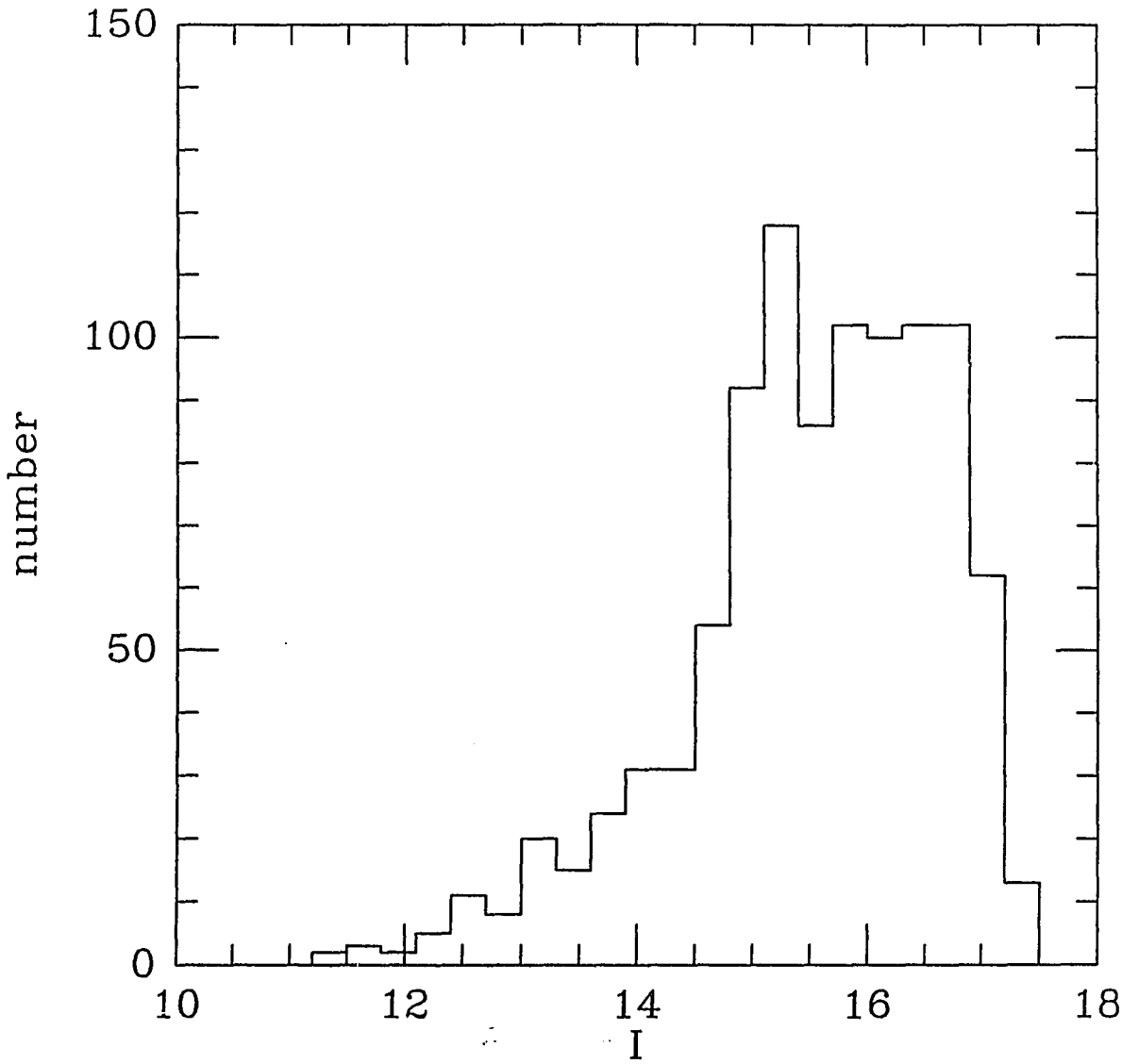

Figure 28a. I Luminosity Distribution for the Baade's Window Field

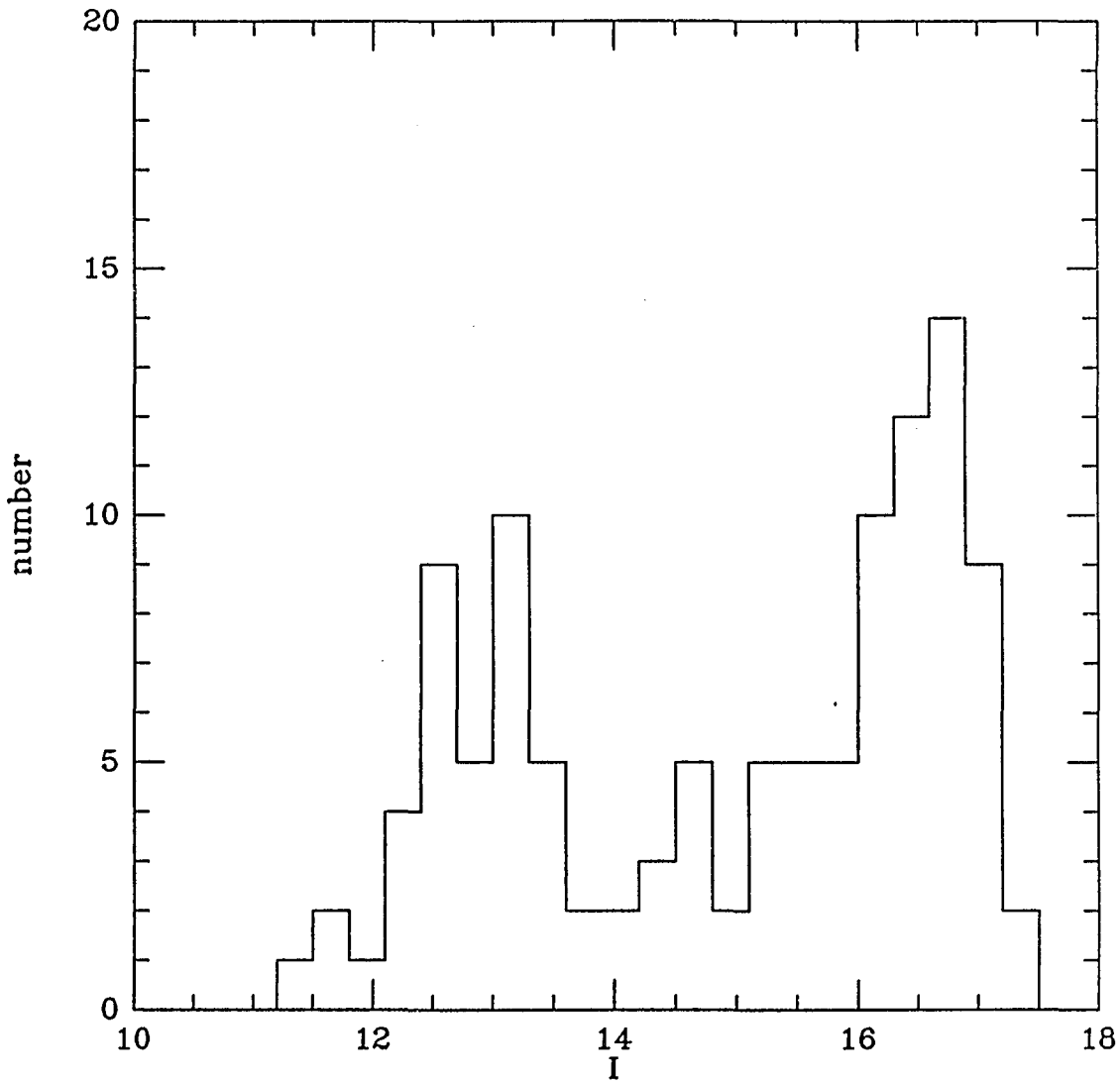

Figure 28b. I Luminosity Distribution of Baade's Window Stars with $77 - 81 > 0.21$.

the bandpass of the 81 filter is seriously contaminated by TiO and VO. Another possible explanation of this apparent upturn is that it is due to low metallicity stars. This is not very likely because low metallicity stars are not expected to become M8 giants. Finally, it is possible that even though line blanketing should be decreasing the sensitivity of V−I to temperature, the V−I sensitivity to temperature is really increasing. This could be because both passbands are on the blue side of the blackbody maximum.

There are four stars in the color-color diagram which fall well to the blue 77−81, side of the main body of stars. The 77−81 errors for these stars are all less than 10% and it is possible that these are carbon stars. The dereddened colors for these stars range from 0.6 to 1.0 which are extremely blue for carbon stars. Their magnitudes range from I = 16.4 to 17.3 and so they are not likely to be carbon stars because even at the distance of the bulge, $(M-m)_0 \approx 14.2$ their magnitudes would be that of dwarfs. Their magnitudes are also well below the completeness limit of $I \approx 15$ which is due to crowding. Although these stars could be CH stars, since these can be this quite faint and blue, confusion in the photometry of these relatively faint stars in such a crowded field is the most likely source of the carbon star colors. BMB found no carbon stars in this field in their grism survey (1984).

The well defined TiO track observed in Baade's Window allows a good estimate to be made of the metallicity of the M giants there. A least squares fit of a straight line to stars with color errors less than ±0.05 in both colors yields a slope of 2.66 with a correlation coefficient of 0.984. This value is not very close to the mean field giant slope, it is much flatter.

This may be because there is a clear spread of 77−81 at a given color and this is pulling the fit up at the blue, 77−81 end or down at the red, 77−81 end. This is best seen in the clump of stars points in Figure 27 where the TiO track is beginning to pull away from the zero band strength region. There is a spread of 0.4 mag in V−I over which this occurs and this is present out to about 77-81 = 0.30. To estimate the mean metallicity of the bulge giants a straight line fit to all stars with color errors less than 0.10 in both colors and with V−I greater than 2.278 (intrinsic $(V - I) = 1.6$) gives a slope of 2.87 and a correlation coefficient of 0.99. These two estimates give dereddened $(V - I)_{0.2}$ values of 1.88 and 1.84 respectively. Both of these lines have significantly flatter slopes than any other observed TiO tracks. If a line of slope 3.6 is fit to the data for all points $(V - I) > 2.278$ then $(V - I)_{0.2}$ is 1.69 and the dispersion about the line is ~ 0.1 mag. Using the metallicity calibration for the Webbink metallicity scale, these three estimates of $(V - I)_{0.2}$ yield metallicity estimates of +0.21, +0.42, and +1.18! If the scatter observed in the V−I direction is indicative of a range of metallicities, the 0.4 mag V−I width of the TiO track suggests metallicities ranging from +1.6 to -0.4 for [Fe/H]. That is, if the upper and the lower bounds of the observed TiO track are due to differences in metallicities then this color difference represents 2 dex in metallicity. Of course, these estimates of the metallicty depend upon an extrapolation of the relation found for the globular clusters and the field giants. This calibration contains no high metallicity points and is probably wrong at the high metallicity end since [Fe/H] $\approx +1.6$ for a star would mean about 80% (by weight) heavy elements. One thing, however, is quite clear—many of the late-M giants in Baade's

Window are quite blue in (V−I) for the amount of TiO measured with the 77−81 system. This is most likely indicative of super-solar metallicity. This is clearly demonstrated in Figure 29 where the mean TiO tracks found in NGC 6712, M 71, field giants and Baade's Window are plotted. The range of metallicity from NGC 6712 to the field giants is about 1 dex. The Baade's Window TiO track lies roughly as much below the field giants as NGC 6712 lies above.

Blanco's Results

This study is an interesting contrast to the grism study of BMB and the supplemental study of Blanco (1986). BMB determined a complete sample of late M giants in Baade's Window from a study of grism plates taken with the CTIO 4-m telescope. In a smaller field around NGC 6522, Blanco reported a complete sample of giants of type M1 or later. My field is completely within the late type study and about two thirds contained in the earlier type study.

BMB found 12 giants which they classified as M6 or later in my field. These stars are listed in Table 9. Using 77−81 to classify M types I found 10 of these. The BMB star 61 would have been classified as M5 rather than M6. The BMB star 57 would not have been found in a study of this type because there is a close blue companion which results in a confused V image. Consequently, the V image would not have been matched with the redder passbands because its centroid is shifted out of the acceptable range of 0.3 arcsec from the mean shift between filters. If a 77−81 color is evaluated for the relatively clear, red image, it would indicate an M6III

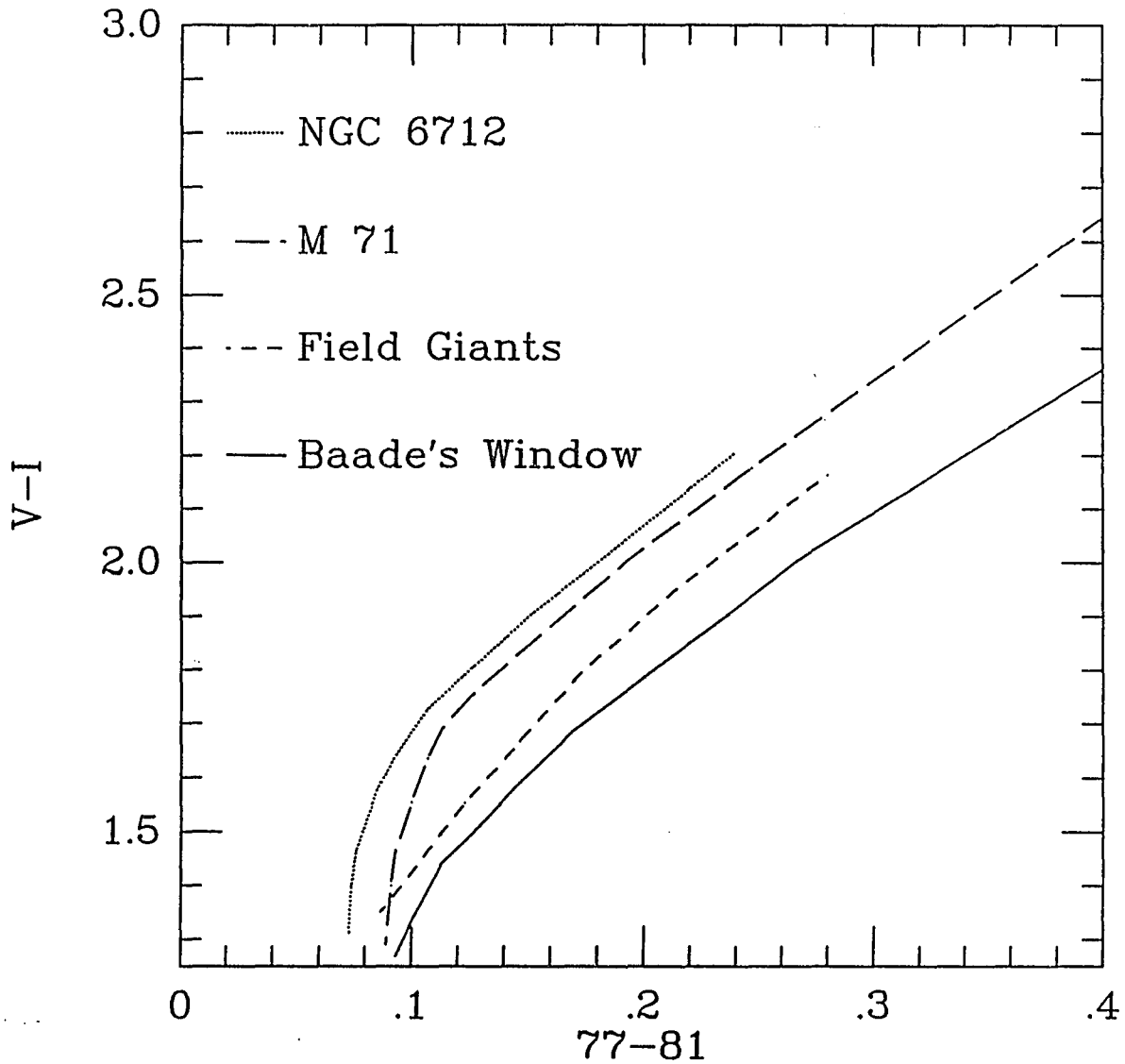

Figure 29. Mean TiO Tracks for Four Systems with Extended Tracks

Table 9. Late-M Giants in the Baade's Window Field

Blanco's Results[a]				This Dissertation		
Number	V	I	Type	V	I	77−81
31	16.33	13.3	6.5	16.32	15.31	0.08
36	16.37	12.7	6	16.33	12.56	0.76
38	16.52	12.7	6	16.54	12.44	0.93
39	15.44	11.5	6	15.62	11.52	0.92
57	16.65	13.1	7	16.69	14.93	0.70
65	17.81	13.2	7	17.51	12.75	1.05
69	15.45	11.7	6	15.15	11.42	0.76
76	16.08	12.9	6.5	17.02	12.40	0.96
81	17.60	12.9	8	18.04	12.64	1.09
92	17.00	13.4	6.5	17.19	13.08	0.89
1137	-	13.1	6	16.14	12.90	0.50
1096	-	12.5	6	15.88	12.47	0.59

Notes:

(a) V magnitudes, numbers and types for stars with identification numbers less than 100 are from Blanco (1986); all I magnitudes, and information for the two stars 1137 and 1096 are from BMB (1984).

star. The 77−81 technique is thus seen to be a valid method of examining the composition of late-type populations.

There is a noticeable discrepancy between the BMB photometry and the CCD photometry. Figure 30 shows a comparison of the ten common stars. The BMB I values are in the mean 0.24 mag fainter than mine. The difference is not correlated with color but it does show a small positive correlation with magnitude. The slope of the points in Figure 30 is 1.1, and this suggests that the problem lies in the iris photometry of BMB in this extremely crowded region where sky is hard to find. A too high value for the sky would result in fainter magnitudes which would be relatively fainter for dimmer images. If BMB's values are too faint this decreases the difference that suggested to BMB that Bulge giants are intrinsically fainter than solar neighborhood late-M giants or those in the Magellanic Clouds. Blanco and Blanco (1984) presented a list of stars which they had calibrated in a variety of ways for use in their study of the Baade's Window RR Lyrae stars. Of these stars three were in my field. There were two whose magnitudes were determined by photoelectric photometry, BB4 and BB21, and one, BB43 determined by a PDS scan of plates. My V value (12.83) for the bright standard BB4 is 0.08 mag too faint. However, because this star is relatively blue, my photometry of it may not be as accurate because the counts in the central two pixels are both about 20,000 adu which may not be in the linear range of the chip. Another confounding factor is the fact that BB4's centroid is less than 6 pixels from the edge of the chip; this is too close to the edge for good photometry. For BB21, my V value of 15.48 is 0.24 mag too bright and for BB43, my V of 17.09 is 0.25 too

faint. Walker and Mack (1986) have examined the BB stars using VI, CCD photometry and generally agree with the Blanco and Blanco V values for bright stars. The only star which I have in common with Walker and Mack is BB4 for which they obtain V = 12.77 and (V − I) = 0.63 as a primary photoelectric standard for their CCD photometry. My value for BB4's V−I is 0.73. This means that I am 0.06 mag fainter at V and 0.04 mag brighter at I subject to the caveat that BB4 is not a well determined star because it lies near the edge and may be too bright at V to be well measured. Van den Bergh (1971) studied Baade's Window and established his values for a photoelectric sequence with which I have 6 six stars in common. I am 0.07 mag fainter in the mean with a standard deviation of 0.03. This is not particularly good agreement, but crowding must affect the photoelectric photometry more than the point-spread function photometry.

Walker and Mack (1986) have analyzed their results and those of Blanco and Blanco (1984), van den Bergh (1971) and Arp (1965). They find that their CCD results are brighter than van den Bergh's photoelectric photometry by about 0.1 mag at V = 16 but agree well for V < 14. Their results are fainter than Blanco and Blanco's by about 0.03 mag from V = 14.5 to 16.5. Walker and Mack used a set of the five brightest Blanco and Blanco stars as secondary standards to calibrate their CCD photomery. They determined the magnitudes and colors of these stars by synthetic aperture photomery and then proceeded to fit Lorentzian profiles to stars in their CCD frames calibrated by the aperture photometry on the bright stars. This is the most likely source of the difference between my photometry and theirs. My magnitude transfers are made using a frame which has been

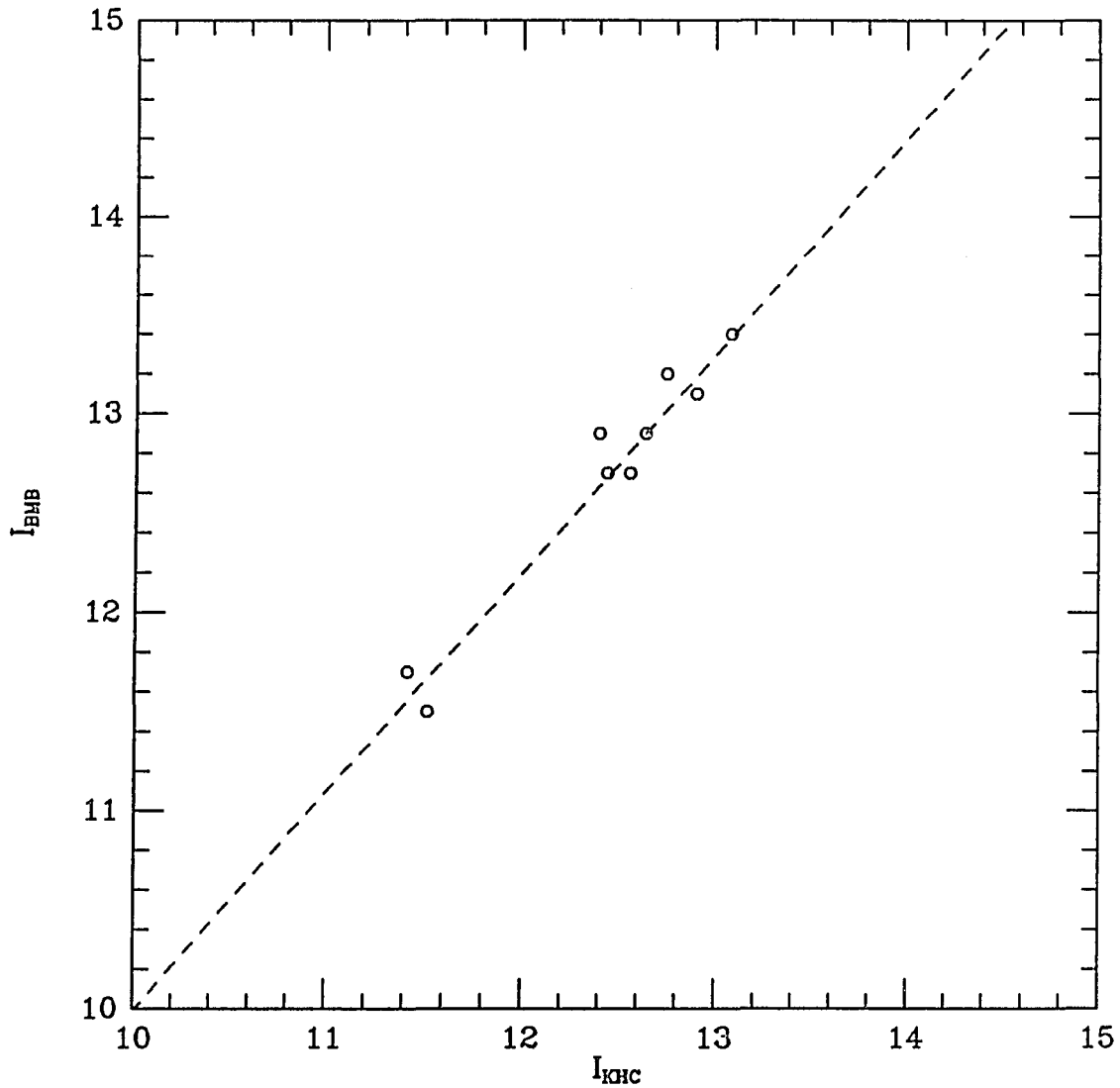

Figure 30. Comparison of I Photometry in Baade's Window

The I magnitudes for M6 and later giants obtained in this work compared with that of Blanco, McCarthy, and Blanco (1984).

cleaned of all resolved stellar images except those for which a total aperture magnitude is to be measured. This procedure results in a 0.01 to 0.02 magnitude shift in my own mean aperture magnitudes compared to my fitted magnitudes. This partly explains my fainter V values. The question of my I magnitudes and V−I colors must remain open. The overlap between the various investigators listed above and my photometry has allowed an estimate to be made of the relative V values but there is only one too bright, blue star on the edge of my frame to base any comparison of I photometry. If the comparison of the values for BB4's color is valid and Walker and Mack's (1986) value is correct, then my V−I colors are 0.10 mag too red. This assumption would result an even higher estimate of the M giant metallicities.

Blanco (1986) has presented the results of typing stars as early as M1 in a region around NGC 6522. About two thirds of my survey field is covered by his analysis. All of the stars which Blanco classified as M1 or later are in the color-color diagram presented, but using the correlation of 77−81 with M-type developed from the field stars and assuming all stars to suffer the same interstellar extinction I would classify 19 of the 43 stars as earlier than M1. Of these 19, 15 are type M1. If a ±0.02 mag error is allowed in the 77−81 color for typing then 7 of the 15 could be classified as M stars using 77−81 . Figure 31 is a plot of the M-type of Blanco versus the 77−81 measured in this work. The line is the correlation found from the unreddened field stars shifted to reflect the reddening toward Baade's Window. This correlation is really only based on stars of type 3 or less since there were few stars later than 3 in the standard sample. Three of the four stars later than 3 were dwarfs and giants may not follow this

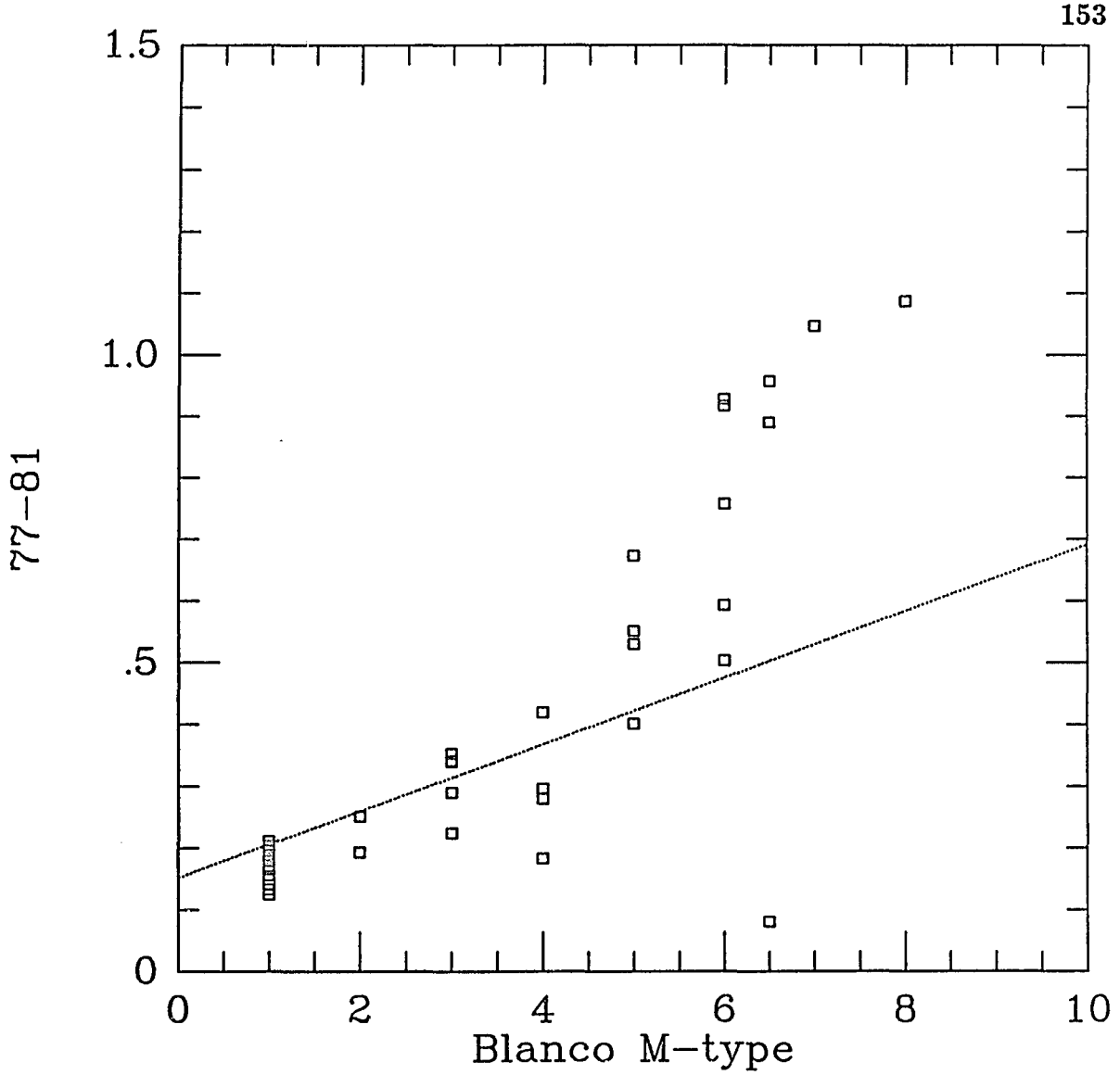

Figure 31. 77−81 as a Function of Blanco's M-type in Baade's Window

relation. From Wing's (1967) work, however, one would expect the giants to fall below the dwarfs in such a plot. The later Baade's Window giants all fall above the field correlation which means that the 77−81, TiO band strength is increasing faster than at earlier types. This could be due to the broad nature of the 77 filter. At these late types there may be additional absorption due to vanadium oxide. This will increase 77−81 more rapidly than the simple increase in TiO. This effect must somehow be corrected for in the visual inspection of the grism spectra for Blanco's typing.

Blanco has also estimated magnitudes for his M stars from plate material. The relation of his V values and my V values is plotted in figure 32. There is a very small magnitude dependence, in that Blanco is relatively fainter at faint magnitudes. Excluding the widely discrepant points, my V values average 0.09 mag fainter and the slope of a straight line fit to the relation in Figure 32 is 1.02.

The AGB population of the Galactic bulge has been found to be metal rich. There is also evidence of a large spread in metallicity for the M stars. The 77−81 technique does not reveal any new carbon stars in the field which I have surveyed–one where the grism survey of BMB found none also. My photometry is somewhat at odds with previous authors in that I am generally fainter, but previous efforts have always been based to some extent on photoelectric photometry in this extremely crowded field.

Summary

The 77−81 system has been established well enough to allow direct comparison of data from different systems in different hemispheres. The

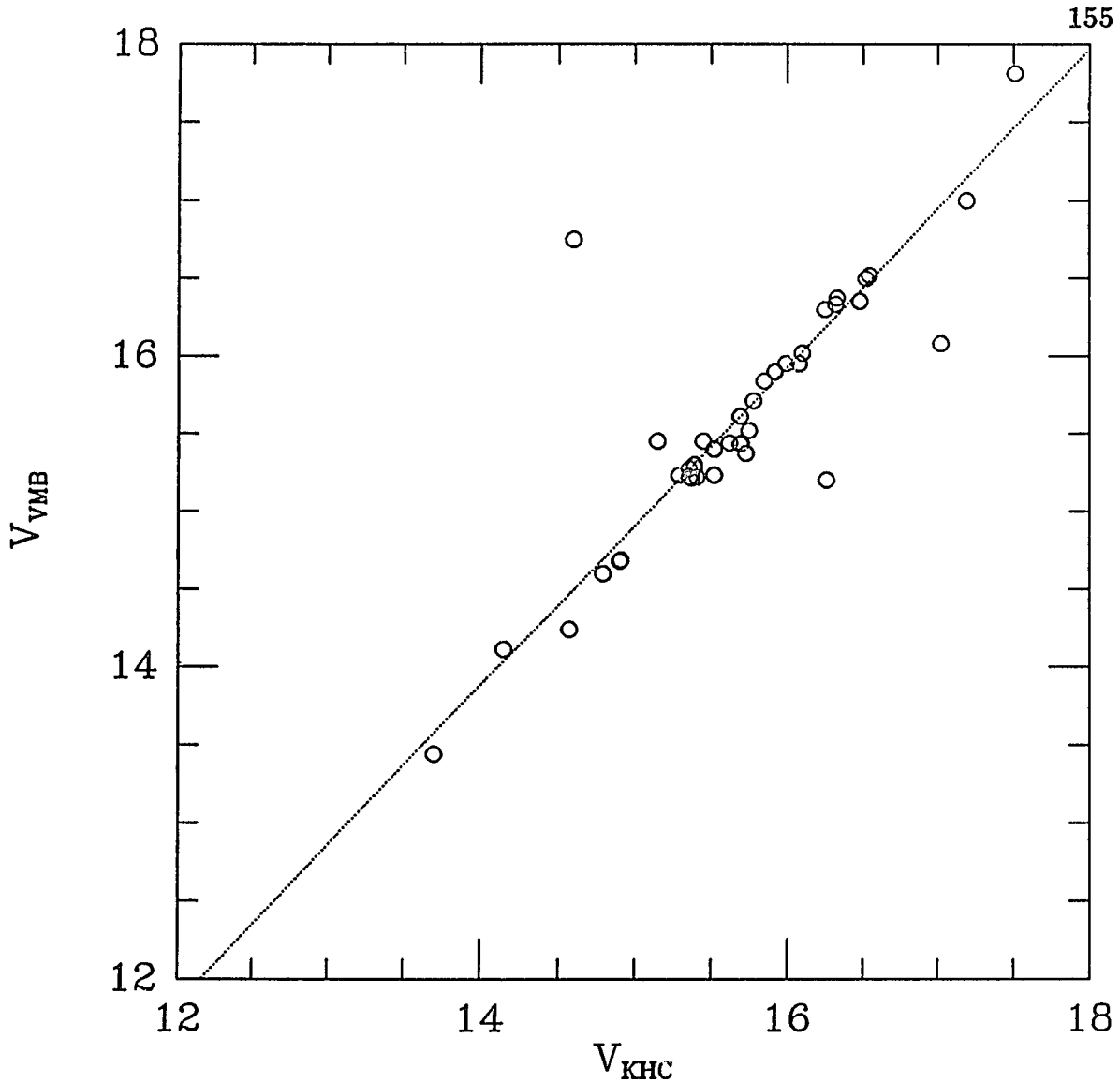

Figure 32. Comparison of V Photometry in Baade's Window

Comparison of Blanco's (1986) V photometry with the photometry in this work for the M stars in the Baade's Window field.

77−81 color is well correlated with M-type and reasonably correlated with carbon richness class. The 77−81,V−I color-color diagram clearly distinguishes M and C types from other stars. A correlation of the V−I color of the TiO track in the 77−81, V−I color-color diagram with metallicity is sensitive enough to clearly distinguish the metallicities of systems differing by 0.5 dex. This metallicity correlation has been applied to the late-type stellar population of the Galaxy's bulge, which has been found to be metal rich.

CHAPTER 4

THE SAGITTARIUS DWARF IRREGULAR GALAXY

The Sagittarius dwarf irregular galaxy (Sagdig) was discovered in 1977 by Cesarsky et al. (1977; hereafter CLLSW) on photographic plates from the ESO Schimdt telescope, and at about the same time by Longmore et al. (1978; hereafter LHWM) on plates from the UK Schmidt. A follow-up plate taken by CLLSW at prime focus of the ESO 3.6-m showed the galaxy to have a very large number of resolved stars. Both groups found the system to be roughly elliptical and estimated the apparent total magnitude to be about $B_0 = 15.5$. The system was found to be quite blue by both groups. Neither group, however, found HII regions. Both groups followed the optical detection with detection at 21 cm. The color, the detection of neutral hydrogen at 21 cm, and the amorphous appearance resulted in their classification of this galaxy as a dwarf irregular.

The distance estimates by the discovery reports were based upon eye estimates of the magnitudes of brightest blue stars. CLLSW found the brightest blue stars to be about $m_B = 18.5$ while LHWM found them to be about $m_B = 19.6$. The heliocentric velocity found for Sagdig by CLLSW (-58 kms^{-1}) suggested to them that it may be associated with NGC 6822 which is only about 4.6° away and has the same heliocentric velocity. Using the brightest blue stars as a distance indicator following the precepts of Sandage and Tamann (1974), the two discovery groups thus found Sagdig

to have a distance modulus of $(m - M)_0 \approx 25$ (LHWGM) or $(m - M)_0 \approx 24$ (CLLSW).

The property that made Sagdig immediately stand out from other dwarf irregulars was the 21 cm measurement of neutral hydrogen mass. Both groups found the mass(HI)/L_B to be about 4, which is independent of the assumed distance. This is a very high value even for a dwarf irregular (see Fisher and Tully 1975). A study by Sargent and Lo (1986) of faint dwarf galaxies has emphasized this finding. These authors also find that the HI velocity structure is chaotic and the projection of the HI contours on the optical image of the galaxy leave about one half devoid of detected HI.

Sagdig is an interesting system to study from a number of points of view. It is a system which has apparently undergone recent star formation as evidenced by the presence of blue stars. It is also a system which has a great reserve of HI compared to its current luminous mass. It is intrinsically faint and is an excellent test case for models of late-type galaxy evolution and the regulation of star formation. It is also of interest as a test of the brightest star distance indicators. The use of the brightest stars to estimate distances has a long and checkered history (Humphreys 1983; Sandage 1983) It is exactly for low luminosity systems such as Sagdig that the methods has been found most wanting (Sandage 1986). But, it is also for systems such as Sagdig where there are few if any other methods available for estimating distance that the brightest star analysis is most often performed. An examination of Sagdig's AGB population should provide a measure of its star formation activity prior to the most recent burst which produced the bright blue stars. An investigation of its AGB may also constrain Sagidg's

distance. If Sagdig is as intrinsically faint as the discovery reports suggest, then its AGB population may provide a bridge between those seen in the Magellanic Clouds and those seen the dwarf spheroidals.

A photometric study of this galaxy is complicated by the fact that it lies at a low galactic latitude and there is not only significant foreground stellar contamination but there is also unknown, but probably quite high interstellar extinction toward it. The discovery papers assumed an extinction similar to that toward NGC 6822 of $A_B \approx 1$. Because of time constraints at the telescope, and the apparent small size of Sagdig, I thought that a single 3′ x 5′ field would provide both a field sample and the galaxy data. Reduction of the data, however, suggested that even though the galaxy had been situated in one corner of the field, it does extend across the whole frame. Consequently, a control field which was obtained for a study of NGC 6822 was pressed into service as a control for Sagdig. The field is about 3 degrees away but most importantly it is almost two degrees higher in Galactic latitude than Sagdig. I will argue that this difference is not significant to the current study and that the expected differences from star-count models of the Galaxy for the two fields do not bear on any of the conclusions in this chapter.

The details of the reduction of the data and its transformation to the standard system are given Chapter 2. Two long exposures and at least one short exposure were made through each filter. The long exposures were 450 s at V, 400 s at I, 1000 s at 77, and 900 s at 81. The short exposures were one tenth the duration of the long. The long exposures were averaged before reduction. The average of the two, long V exposures is shown in

Figure 33. Figure 34 shows the field after all of the stellar images fit by DAOPHOT have been subtracted from Figure 33. Although the bright, foreground stars which are saturated do not subtract out well, the majority of the stars subtract out cleanly. The result is a smooth background with the central body of the galaxy clearly visible. The positions, I magnitudes, V−I and 77−81 colors and estimated errors for the stars in the Sagdig field are listed Appendix B. Figure 35 shows the average of the two, long V exposures of the NGC 6822 control field, CF1. The positions, I magnitudes, V−I and 77−81 colors and estimated errors for the stars in CF1 are listed in Appendix C.

Initial exposures centered on Sagdig showed that there were two extremely bright field stars just to the south (one east and one west) of the galaxy which were saturating and bleeding even on the short exposures. The galaxy was then positioned on the frame so that these stars would not destroy the long integrations and also to offset the galaxy to the east side of the frame. The hope was that in this manner Galactic field star contamination could be accounted for using the portions of the frame distant from the body of the galaxy. This seemed a reasonable thing to do since Sagdig had a reported Holmberg diameter of only 180 arcsec (LHWGM). There was concern at the start of integrations on Sagdig whether the night was photometric because there had been some thin cirrus earlier in the evening. But, at the beginning of the long exposures for Sagdig the sky was checked and appeared to be clear. Reductions of standards taken just before moving to the Sagdig field showed 2% variability and about 1% extra extinction due to some passing high cirrus. Though there was no apparent cirrus at

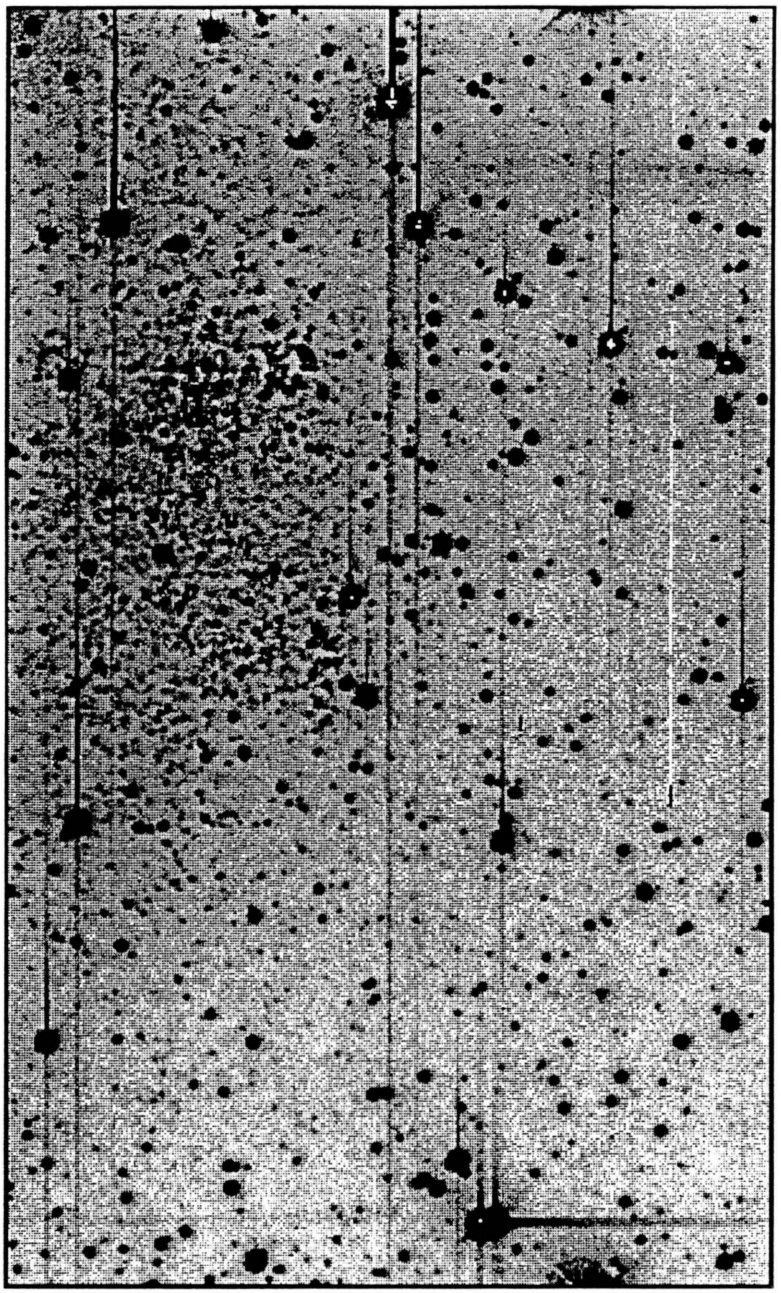

Figure 33. V Band Image of Sagdig

This is the average of two 450 s V exposures. North is to the right and east is up: the frame is 3 arcmin by 5.08 arcmin and 300 by 508 pixels.

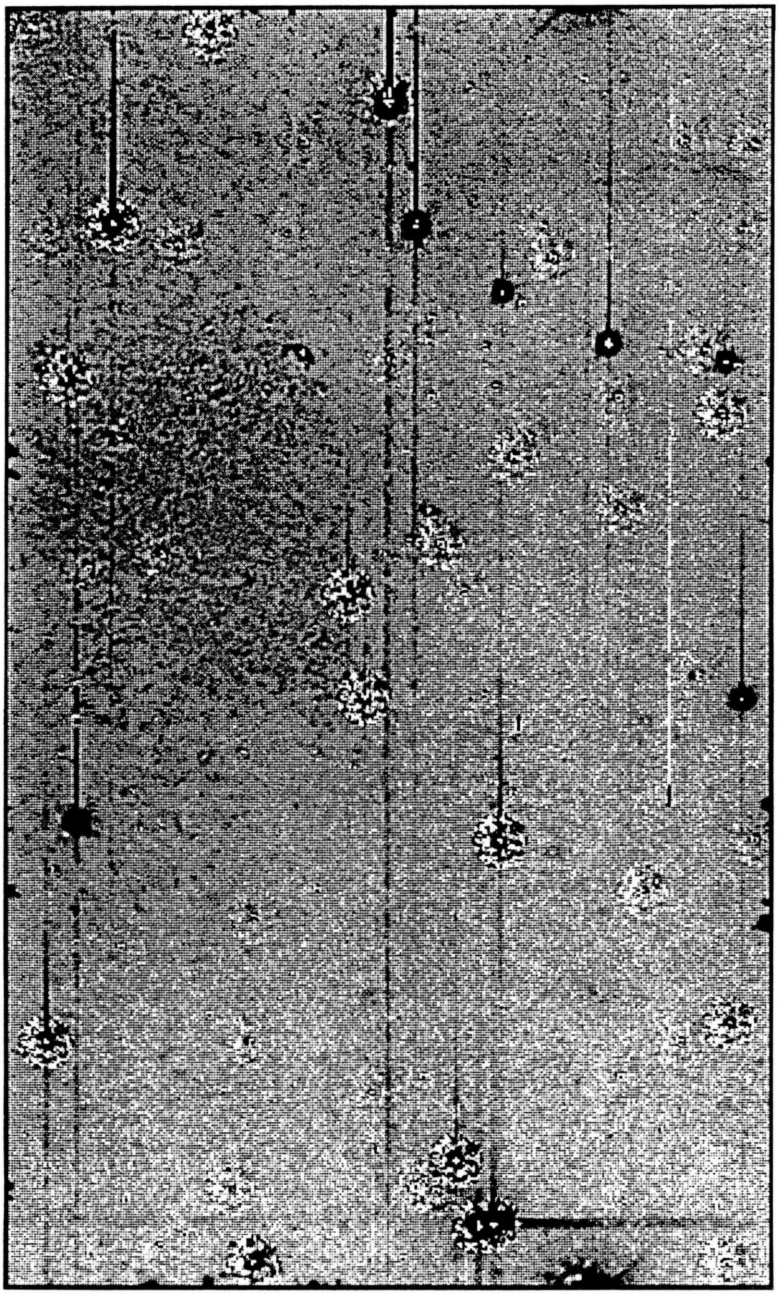

Figure 34. The Sagdig Field with the Stellar Images Subtracted

The images fit with the psf for the V band frame of Figure 33 were were subtracted from Figure 33 to produce this frame. Saturated images of foreground stars do not subtract out well.

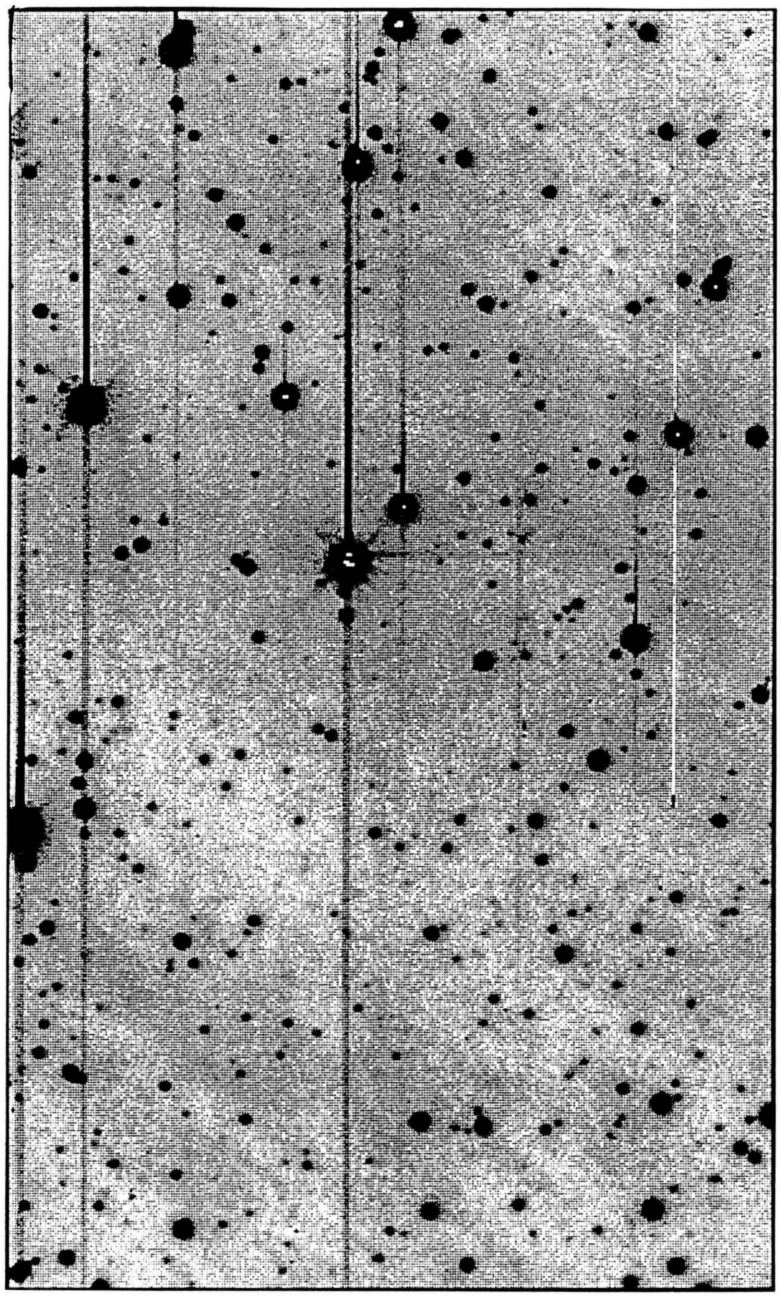

Figure 35. V band CCD frame of the CF1 Field

This frame is the average of two 450 s V band exposures of the CF1 field—a field 1° in Galactic latitude from NGC 6822. The size and orientation are the same as for Figure 33.

the beginning of the long integrations, the first two bands (V and I) were repeated for short integrations at the end of the intermediate-band exposures as a photometric check. The I integrations yielded the same magnitudes. The sum of the two long V integrations proved to be 0.012 mag too faint when compared to the final V integration. When the final short V exposure and the initial, short V exposure with the galaxy appropriately positioned, were compared stellar magnitudes were found to be the same to within the errors. Consequently, I have concluded that though the weather was rapidly becoming photometric during the V exposures the long integrations suffered some extinction due to residual cirrus and the observed magnitudes have been corrected by −0.012 mag. After the long V integrations (which were the first long integrations on this field), it was photometric.

Completeness

Completeness studies were performed to assess the effects of crowding on finding stellar images and accurate photometery of these images in a magnitude range relevant to the asymptotic giant branch (AGB) in Sagdig. These tests were only done on the V frame because it was the most crowded and so the most likely to suffer incompleteness due to crowding. Artificial stellar images were added in the range of 16,000 ADU above sky to 1,000 ADU above sky. This corresponded to V magnitudes of 19.2 to 22.2 which was expected to be the range where incompleteness would become significant from visual inspection of the CCD frames. This range also contains the upper limit of the expected V magnitudes for Sagdig AGB stars. The results for ten different additions of 100 stars each are shown in Figure 36.

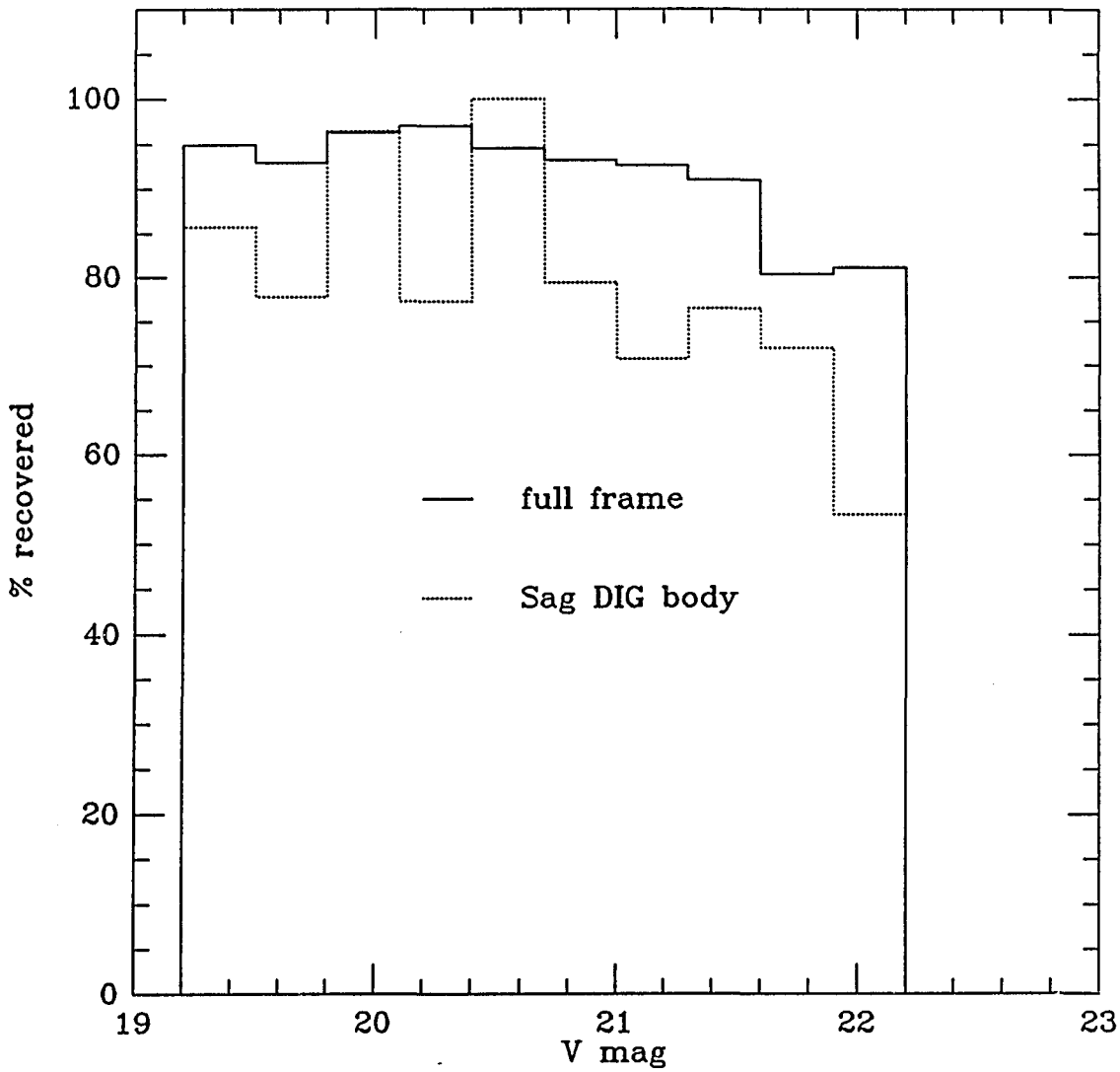

Figure 36. Completeness as a Function of Dereddened V mag

The solid line represents all of the artificial stars added to the frame; the dotted line represents stars added to the body of Sagdig (see text for a definition of body).

This histogram shows that there is not much of a dependence of completeness on magnitude in this range although there seems to be a drop in completeness in the two faintest bins. For the whole frame, 91.3the 1000 added stars where recovered within 0.3 arcsec of their added position and within the estimated error for their magnitude of their added magnitude. More relevant to the study of the blue stars is the completeness in the main body of the galaxy. Of the stars added, 228 were added to the region $0 <$ xpixel# < 141 and $180 <$ ypixel# < 241. This is the most crowded portion of the frame and 183 stars were recovered (80.3%). In the body of the galaxy, the general level of completeness is less and the decrease for the faintest magnitude bin is much greater. The completeness at I is undoubtedly better because there are about 75% the number of stars as in the V frame. The brightness of the added stars would correspond to I magnitudes of 17.7 to 20.7. From these tests it is possible to estimate that this data set is 90complete for stars brighter than $V = 22.2$ mag and $I = 20.7$ outside of the galaxy body. Within the body of the galaxy, crowding results in only about 80% completeness to $V = 21.9$ with a rapid fall at fainter magnitudes.

Color-color plots were constructed from the reduced data and a number of stars were noted to occupy the carbon star region. Since there is only one known dwarf carbon star (Dearborn et al. 1986), there are not expected to be any foreground carbon stars in this field and all the carbon stars belong to Sagdig. The positions of the carbon stars on the frame (see Figure 56) suggested that there might not be an appropriate region to use to correct for foreground contamination. Thus, another method was needed

to estimate the number of foreground stars. During the same observing run data were obtained for a intermediate-band analysis of NGC 6822 and a control field at NGC 6822's Galactic latitude was also obtained. Since NGC 6822 is only 4.6°from Sagdig on the sky, the NGC 6822 control field was pressed into use as a control for the Sagdig field. Table 10 shows the Galactic coordinates for Sagdig and the control field (CF1).

It also shows the theoretical appropriateness of CF1 as a control for foreground contamination. The simplified, Bahcall and Soneira model (1980; hereafter BS, see their Appendix B) for the stellar distrubution of the Galaxy was used to calculate the expected differences in the Galactic star counts in these two fields. Though CF1 is not the ideal control field for Sagdig, it does contain roughly the same contaminating foreground populations so that by correcting the number of stars an appropriate control can be constructed. There is another problem because of the low latitudes involved–variable reddening. The Burstein and Heiles (1982) reddening maps of this region suggest that E(B−V) should be about 0.03 mag higher toward Sagdig than CF1. These maps also show that the reddening toward NGC 6822 to be E(B-V) $\approx$ 0.18 mag when it is known that it is really about twice that (McAlary et al. 1983). Without any other information the Burstein and Heiles values could be used.

The data from the control field were reduced as described in chapter two. In order to directly compare these fields, some reddening must be adopted. As an additional estimate of the reddening, the standard star and field giant color-color plot (see Chapter 3) was shifted to best match the TiO branch and G and K star regions apparent in the data from these

Table 10. Bahcall and Soneira Simple Model

Star Counts at V per magnitude			
V	Sagdig[a]	CF1[b]	Sagdig/CF1
15	4.5	3.4	1.33
16	10.1	7.4	1.36
17	20.4	14.6	1.39
18	37.6	26.3	1.43
19	64.1	43.3	1.48
20	103.3	67.2	1.54
21	120.4	78.9	1.53
22	136.6	90.1	1.52
23	152.3	101.1	1.51
24	168.3	112.3	1.50

Notes:

(a) The coordinates of the Sagdig field are $l^{II} = 21.1°$and $b^{II} = -16.3°$.

(b) The coordinates of the CF1 field are $l^{II} = 21.1°$and $b^{II} = -16.3°$.

fields. This produced reddening estimates of 0.26 mag E(V−I) for CF1 and 0.08 mag for Sagdig, and 0.025 mag E(77−81) for CF1 and 0.006 mag for Sagdig. It was also noted that the vertical, ridge line of field stars in the color magnitude diagrams for CF1 was 0.15 mag redder in V−I than for Sagdig. This ridge line is probably produced by the superposition of main sequences at different distances and has the color of the local main sequence turnoff. This ridge should serve as an accurate fiducial point to estimate the reddening if there were a measure of the unreddened value. Paul Schecter and John Caldwell (1987) kindly provided the data necessary for this estimate. They have obtained V and I, CCD photometry for 20,000 stars at the south Galactic cap to a limiting magnitude of I = 16. This sample should be composed of unreddened field stars and a color-magnitude diagram of this data is shown in Figure 37.

The ridge line for these stars is $V - I = 0.77$, which immediately produces estimates of $E(V-I) = 0.09$ for Sagdig and $E(V-I) = 0.30$ for CF1. The difference may seem large, but at this latitude the interstellar extinction is quite patchy. The similar reddening estimates produced by matching the color-color diagram features and the matching the unreddened field stars argues that those values are near the true value. I will adopt an E(V−I) toward CF1 of 0.30 and a value of 0.09 toward Sagdig. Figures 38a and 38b show the color distribution of the dereddened data for the Sagdig and CF1 fields compared to the south Galactic cap data. Figure 38a presents a magnitude range from CF1 and Sagdig which should be brighter than all Sagdig stars. This is matched in Figure 38b by a magnitude range which should sample the same disk population (same height above the plane of the

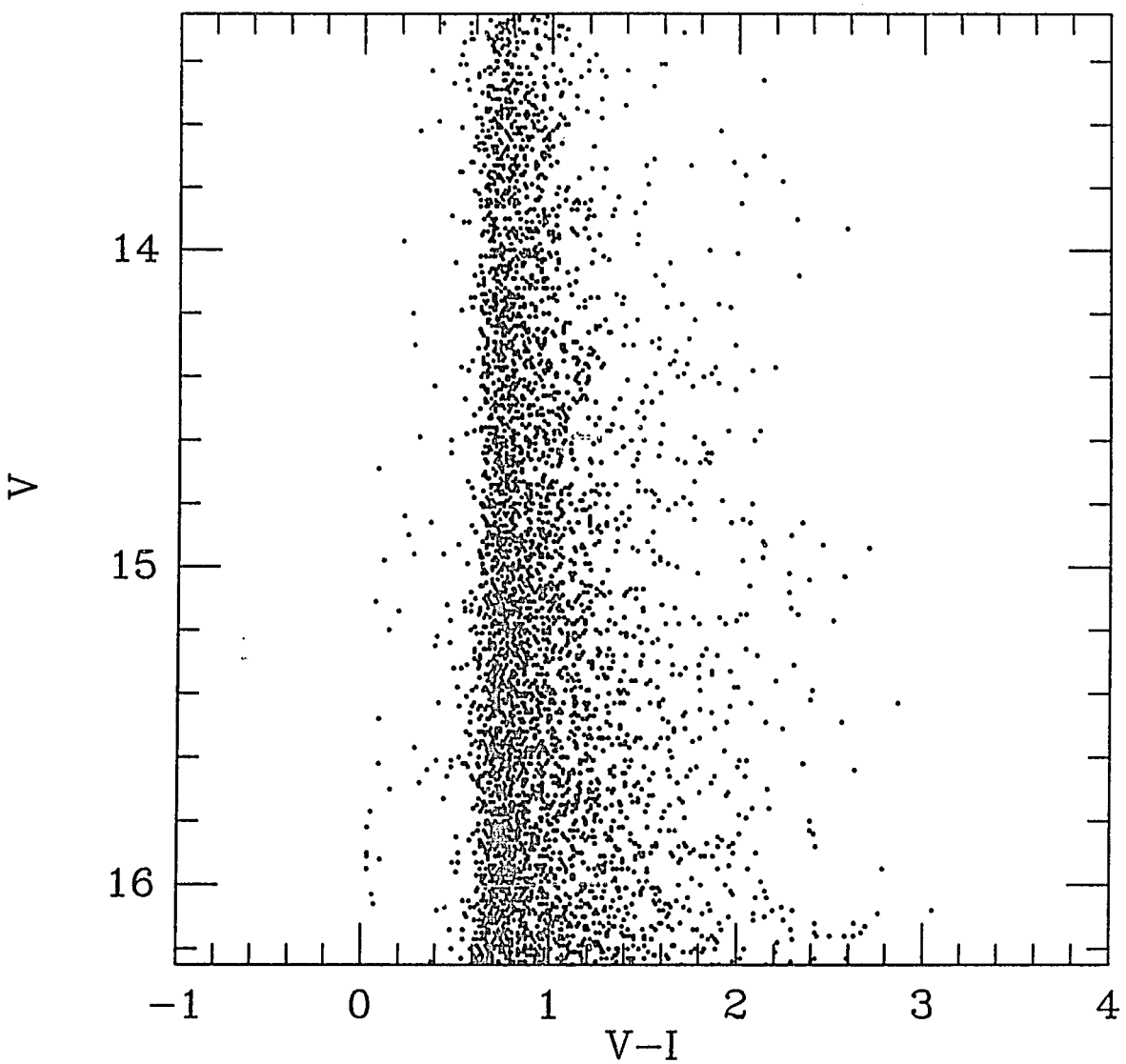

Figure 37. Color-Magnitude Diagram of the South Galactic Cap

Magnitudes and colors for 4366 stars in the South Galactic Cap from Schechter and Caldwell (1987).

disk) as estimated by cosec b.

The intermediate-band color excess estimated from shifting the color-color diagrams is roughly what would be expected from the E(V−I) values. I will adopt E(77−81) values calculated from E(V−I) because it is easier to estimate E(V−I) since it is ten times larger and it can be estimated with two different methods. The dereddened data for Sagdig and for CF1 is presented in Figures 39, 40 and 41.

The color magnitude data includes all stars which were matched in the V and I frames, while the color-color diagrams include stars which were matched in all four bands. Note that the foreground stars form a ridge at about $V - I \approx 0.77$ in the color magnitude diagrams; this was the feature used to help determine the reddening.

Differential Luminosity Functions

Figures 42 and 43 present the dereddened V and I luminosity functions for Sagdig and the NGC 6822 control field, CF1. These were produced from the V and I data independently and represent a superset of the data on stars which have been matched with magnitudes for both passbands. The control field values have also been corrected for the predicted difference due to the different Galactic latitude and longitude than Sagig. This was done by correcting the CF1 counts using the ratios shown in Table 10. The BS model predicts V band star counts—the I values have been corrected using the simple assumption that the relative number of stars in the two fields would be the same at I as at V. This should not produce significant errors in the relevant magnitude ranges because the fields are so close together on the

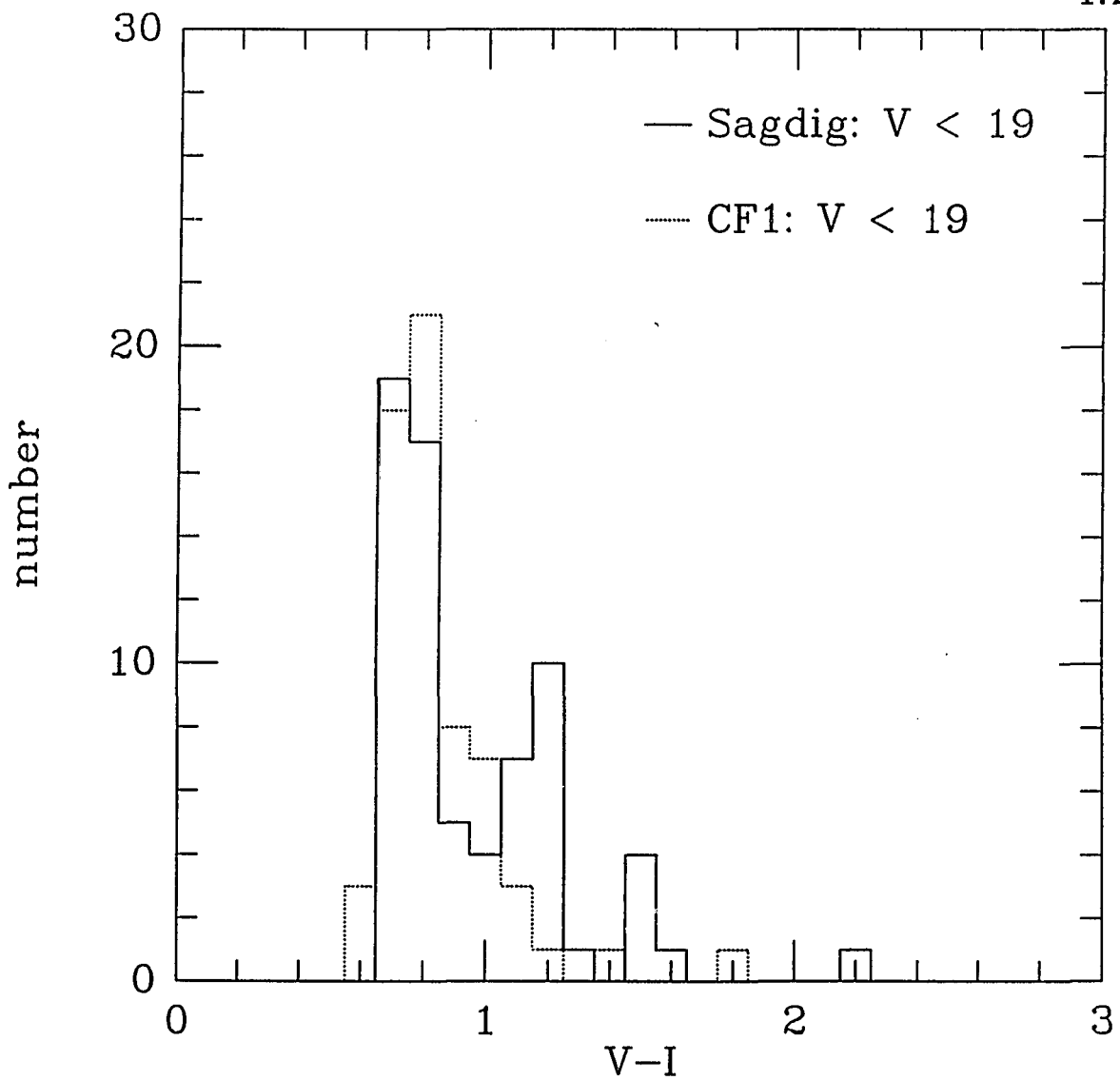

Figure 38a. V−I Distribution of Stars in Sagdig and CF1

The V−I color distribution for stars brighter than $V - I = 19$ in the Sagdig and CF1 fields.

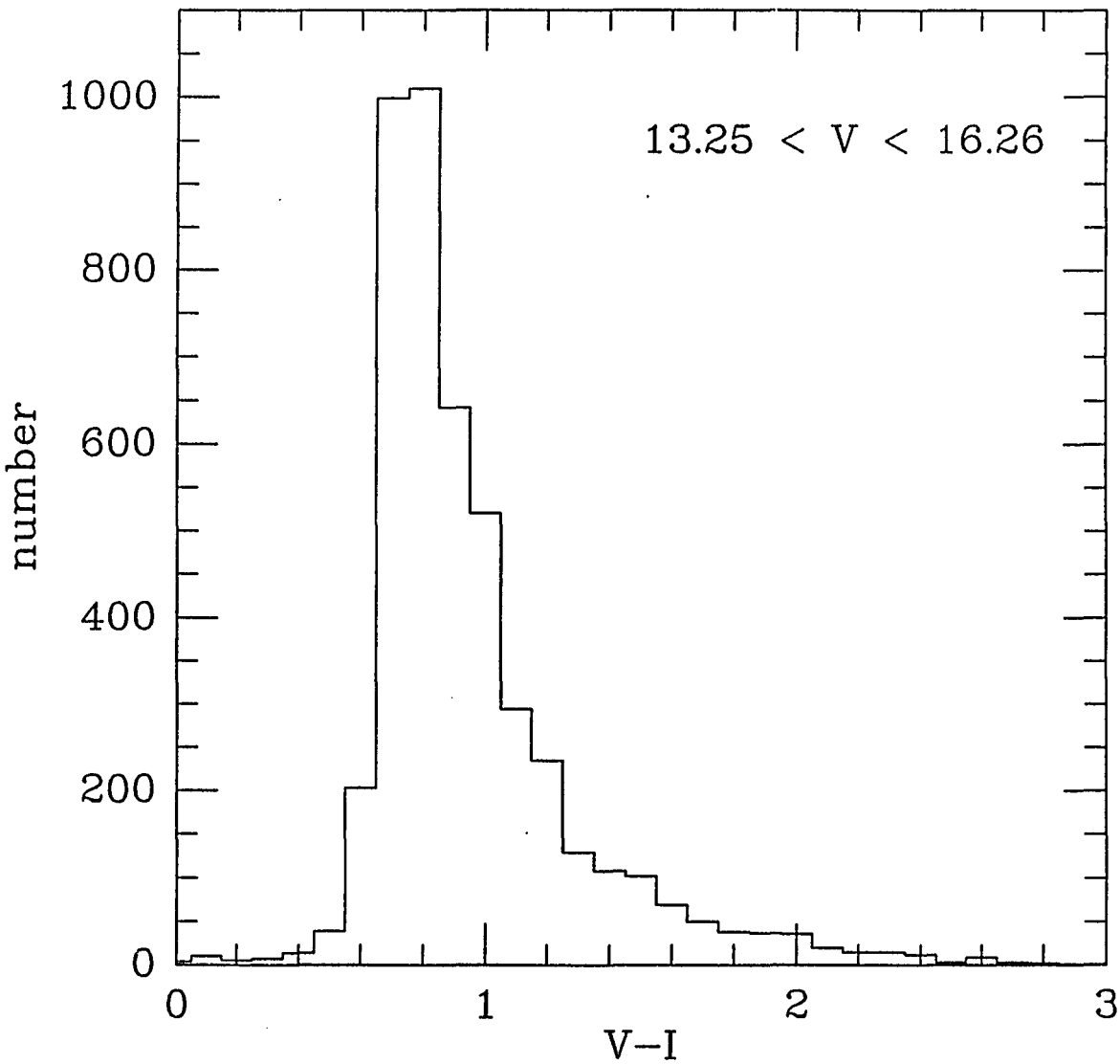

Figure 38b. V−I Distribution of Stars in the South Galactic Cap

The V−I color distribution of stars at the South Galactic Cap with $13.25 < V < 16.26$ from Schechter and Caldwell (1987).

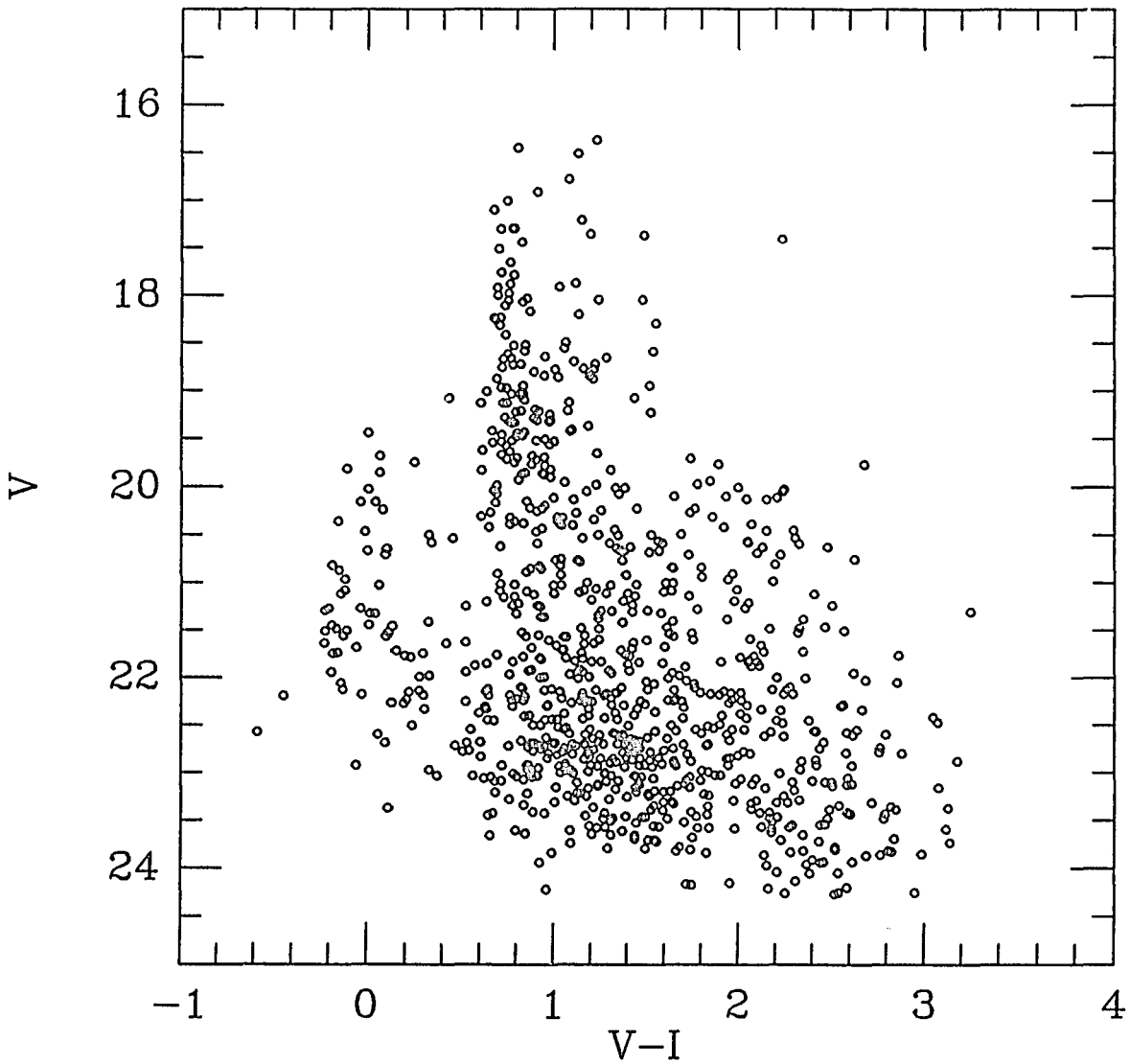

Figure 39a. Dereddened V, V−I Color-Magnitude Diagram for Sagdig

Note the absence of stars bluer than $(V - I) \sim 0.5$. This is data for stars with detections in the two broad passbands.

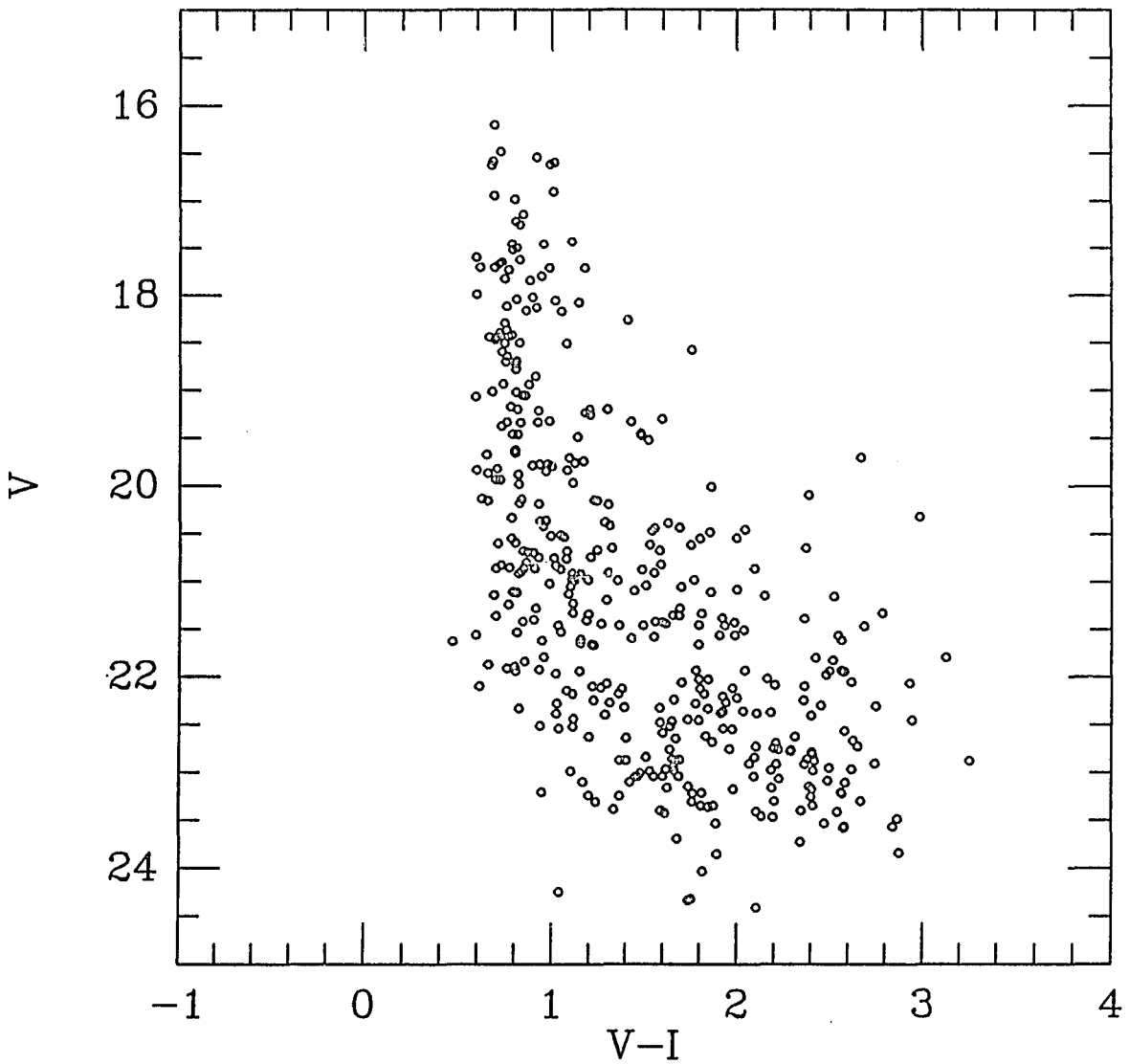

Figure 39b. Dereddened V, V−I Color-Magnitude Diagram for CF1

Note the absence of stars bluer than $(V - I) \sim 0.5$. This is data for stars with detections in the two broad passbands.

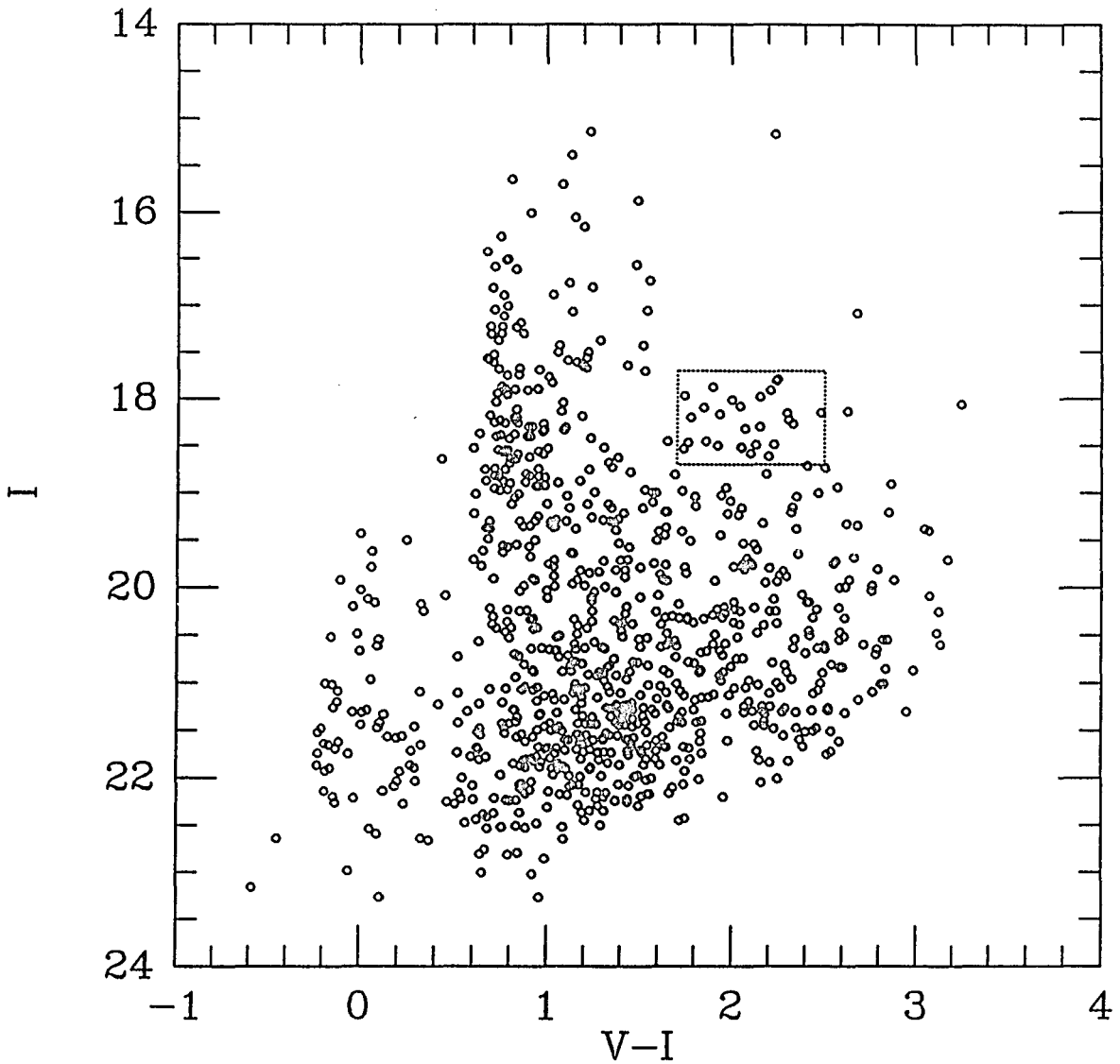

Figure 40a. Dereddened I, V−I Color-Magnitude Diagram for Sagdig

Note the presence of a significant concentration of stars in the Sagidg data in the region marked by the box. This is data for stars with detections in the two broad bands.

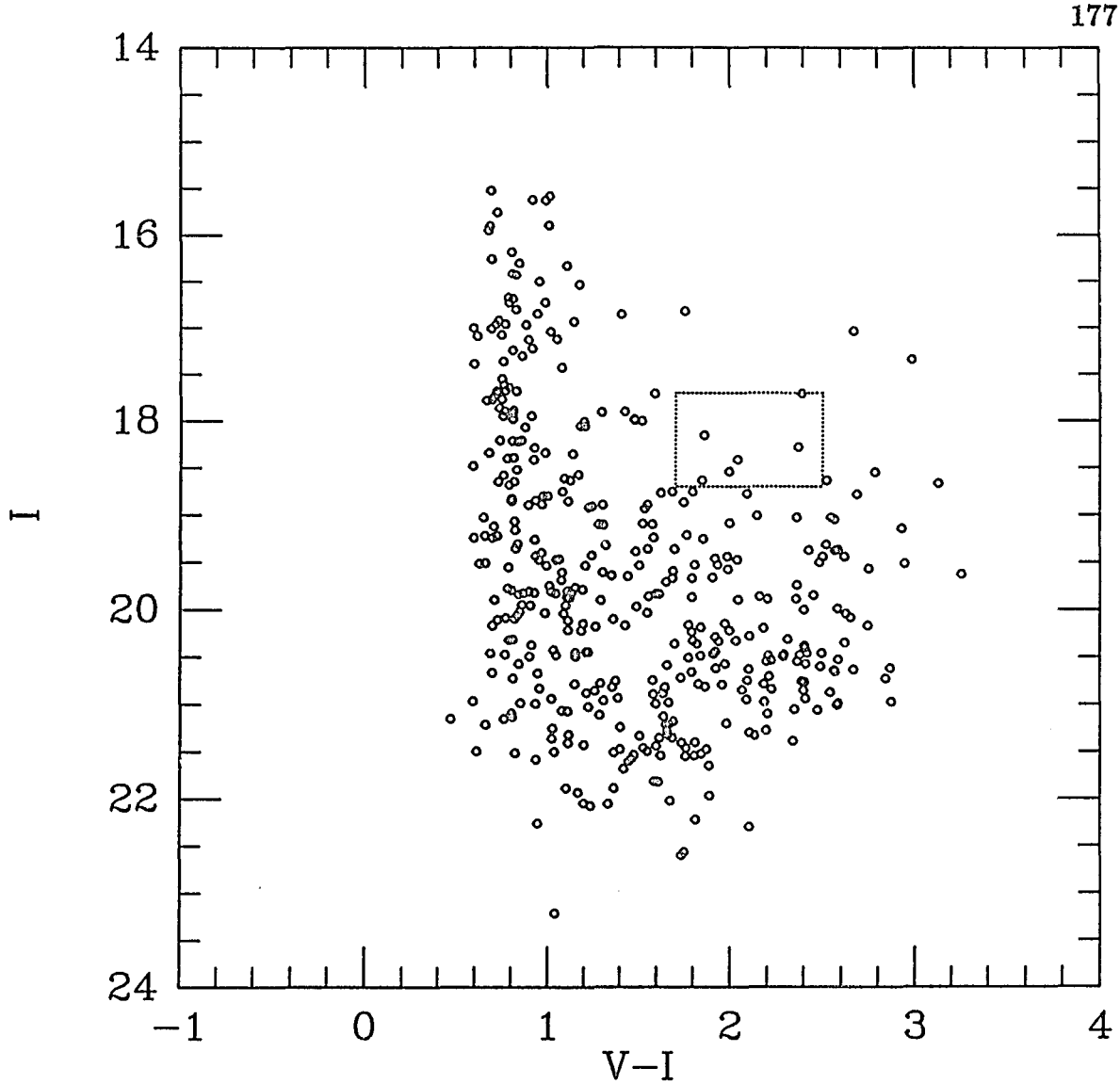

Figure 40b. Dereddened I, V−I Color-Magnitude Diagram for CF1

Note the absence of a significant concentration of stars in the CF1 data in the region marked by the box. This is data for stars with detections in the two broad bands.

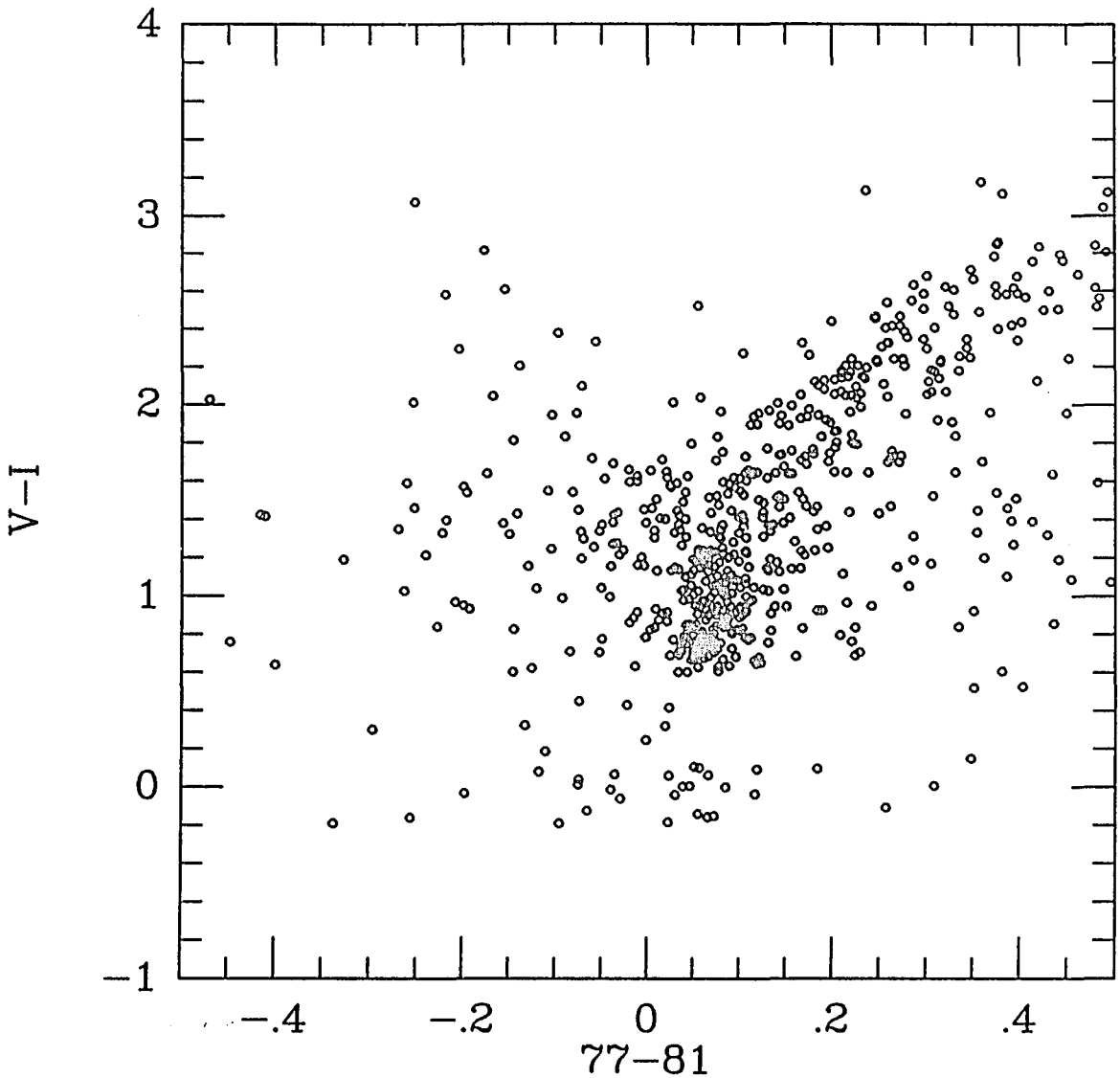

Figure 41a. Dereddened Color-Color Diagram of Sagdig
This is data for stars detections in all four passbands.

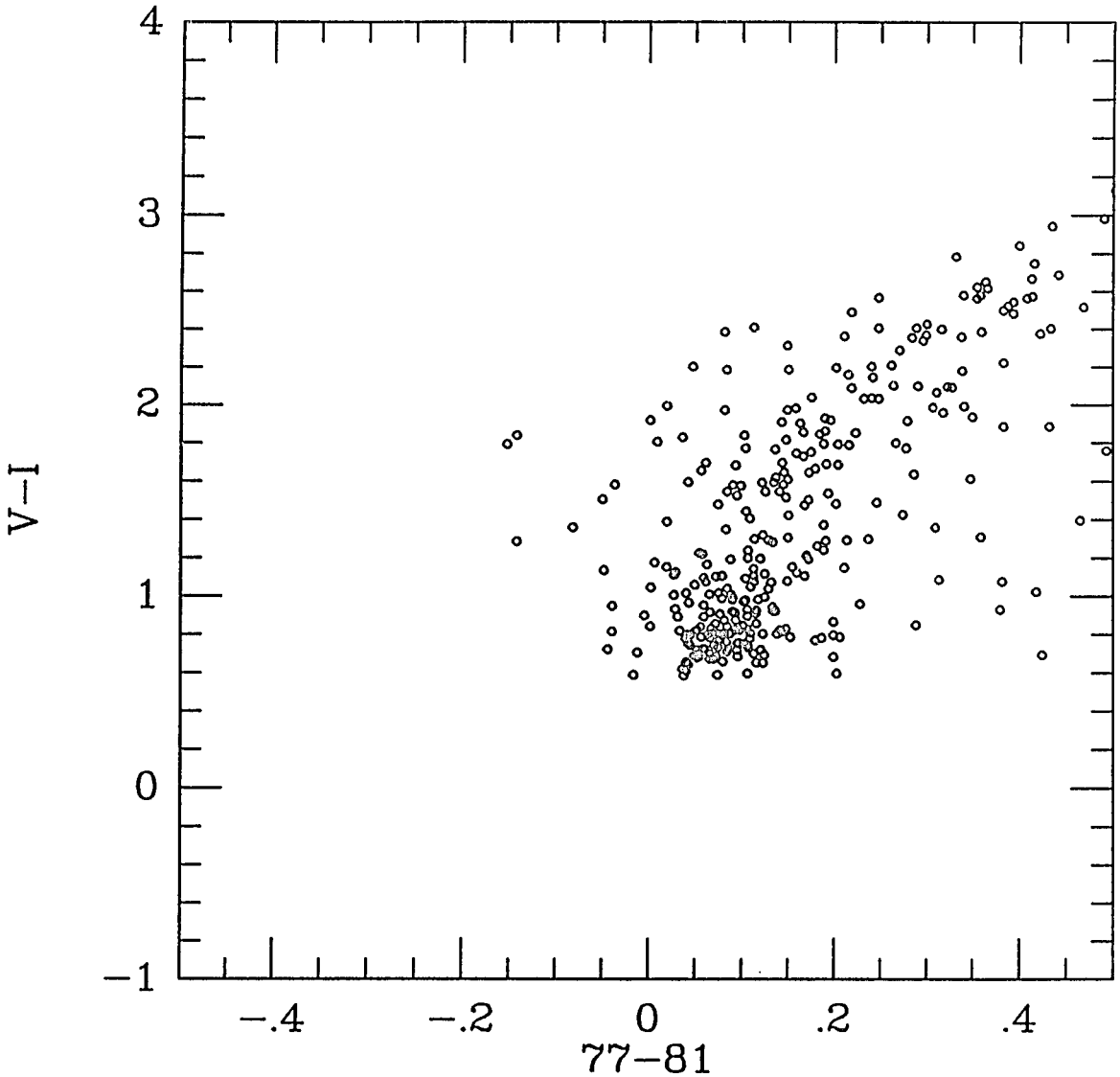

Figure 41b. Dereddened Color-Color Diagram of CF1
This is data for stars detections in all four passbands.

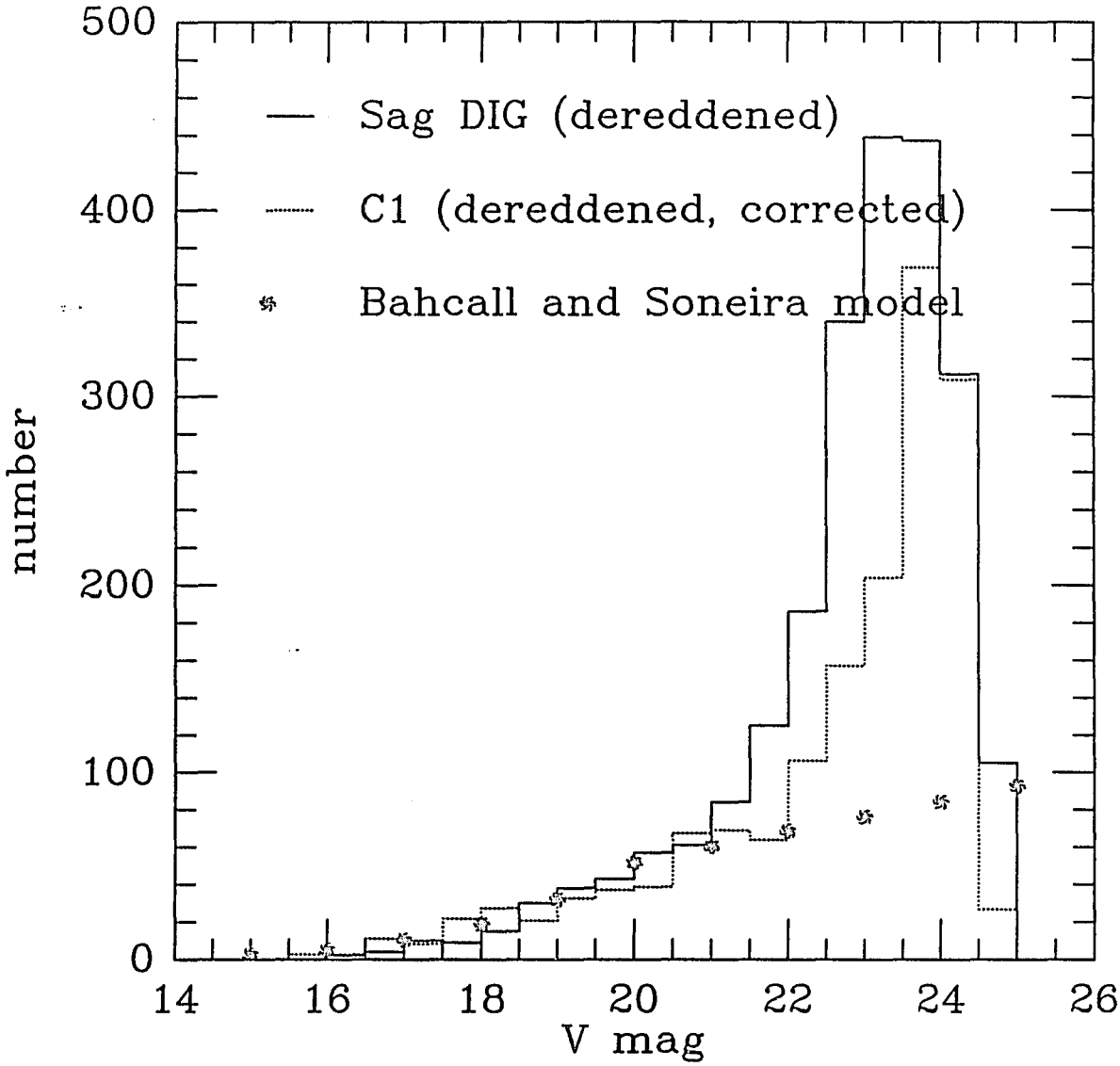

Figure 42. V Luminosity Distribution of the Sagdig and CF1 Fields

The dereddened luminosity distribution at V for the Sagdig field is compared with the luminosity distribution found in the CF1 field scaled by the ratios in Table 10 and the prediction of the star count model of Bahcall and Soneira (1980).

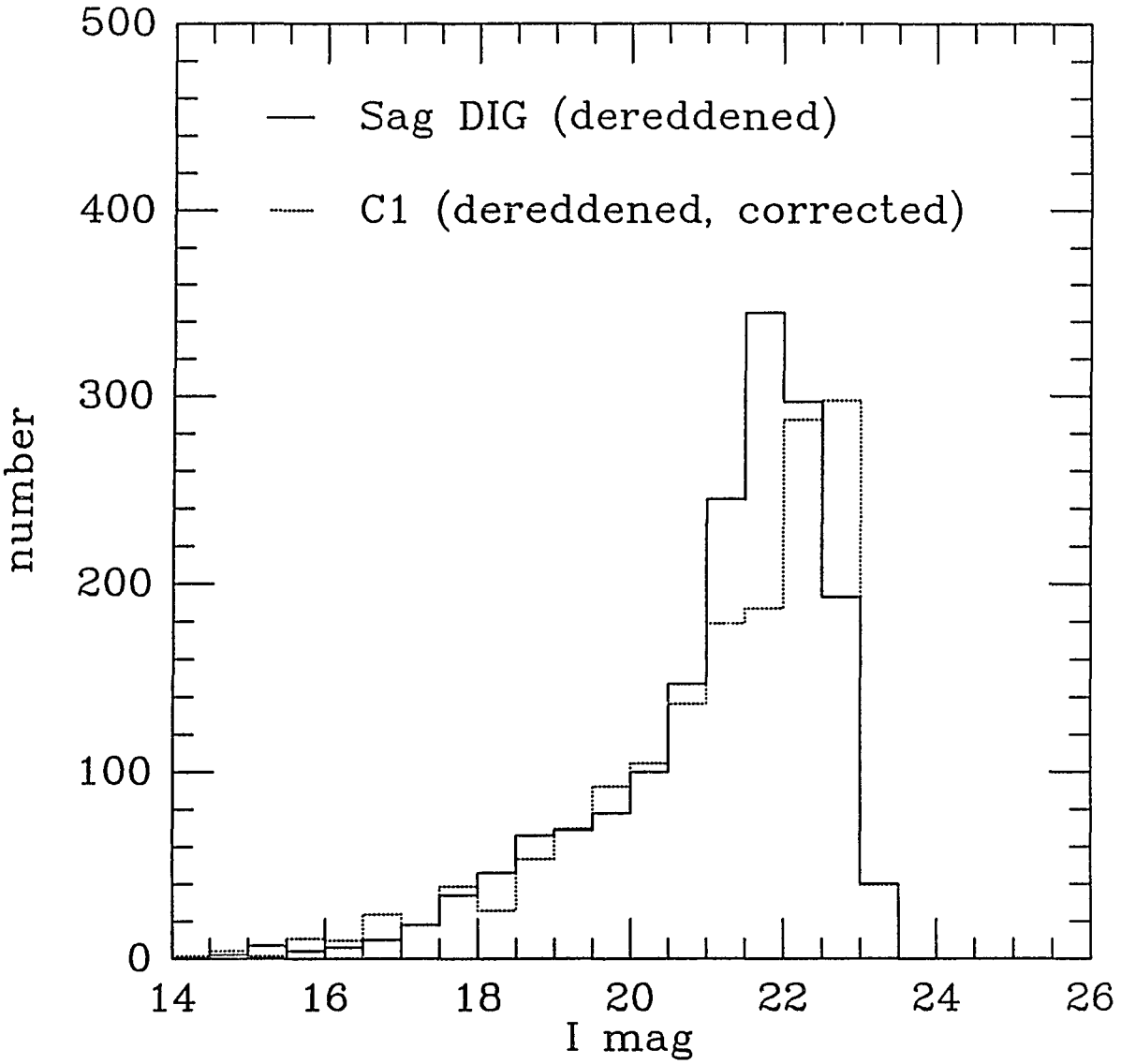

Figure 43. I Luminosity Distribution of the Sagdig and CF1 Fields

The dereddened luminosity distribtuion at I for the Sagdig field is compared with the luminosity distribution found in the CF1 field scaled by the ratios found in Table 10. The assumption is made that the relative star counts in the two fields wil be the same at I as at V.

sky that they are not sampling significantly different, Galactic populations. Plotted in Figure 42 with the data, are the absolute numbers of stars predicted by the BS model. This model seriously underestimates the number of stars fainter than V = 23 along this line of sight. Because of the low Galactic latitude, this line of sight is very sensitive to the thickness of the disk. Apparently, the BS model does not adequately account for the disk thickness in that the real disk must be thicker than that modelled. This shortcoming does not necessarily affect the use of the model to determine the relative foreground contamination toward the two fields of interest. The model has just been used to estimate the ratio of foreground stars toward CF1 so that this number may be subtracted from the Sagdig field. This procedure works fairly well as will be seen shortly.

From the completeness analysis, it is expected that the V counts would be complete beyond $V = 22.2$ and these histograms bear this out. It seems that the Sagdig data becomes seriously incomplete at $V \approx 23.5$. The I exposures were not as deep and it is seen that they become incomplete at $I = 21.5$. The control fields become incomplete at fainter, dereddened magnitudes because they are less crowded. This results in over corrections at the faintest magnitudes. Figure 44 is the color distribution of stars in the control field compared to the Sagdig field. Unique to the Sagdig field are stars bluer than $V - I \approx 0.5$. There are also two other color ranges where Sagdig contributes appreciably: $V - I \approx 1.4$ and $V - I \approx 2.2$. Figures 45 and 46 are the luminosity functions of Sagdig corrected for foreground contamination. These two histograms show that Sagdig starts significantly adding to the counts in the field at an $I = 21.5$ and V−I of about 1.5. This

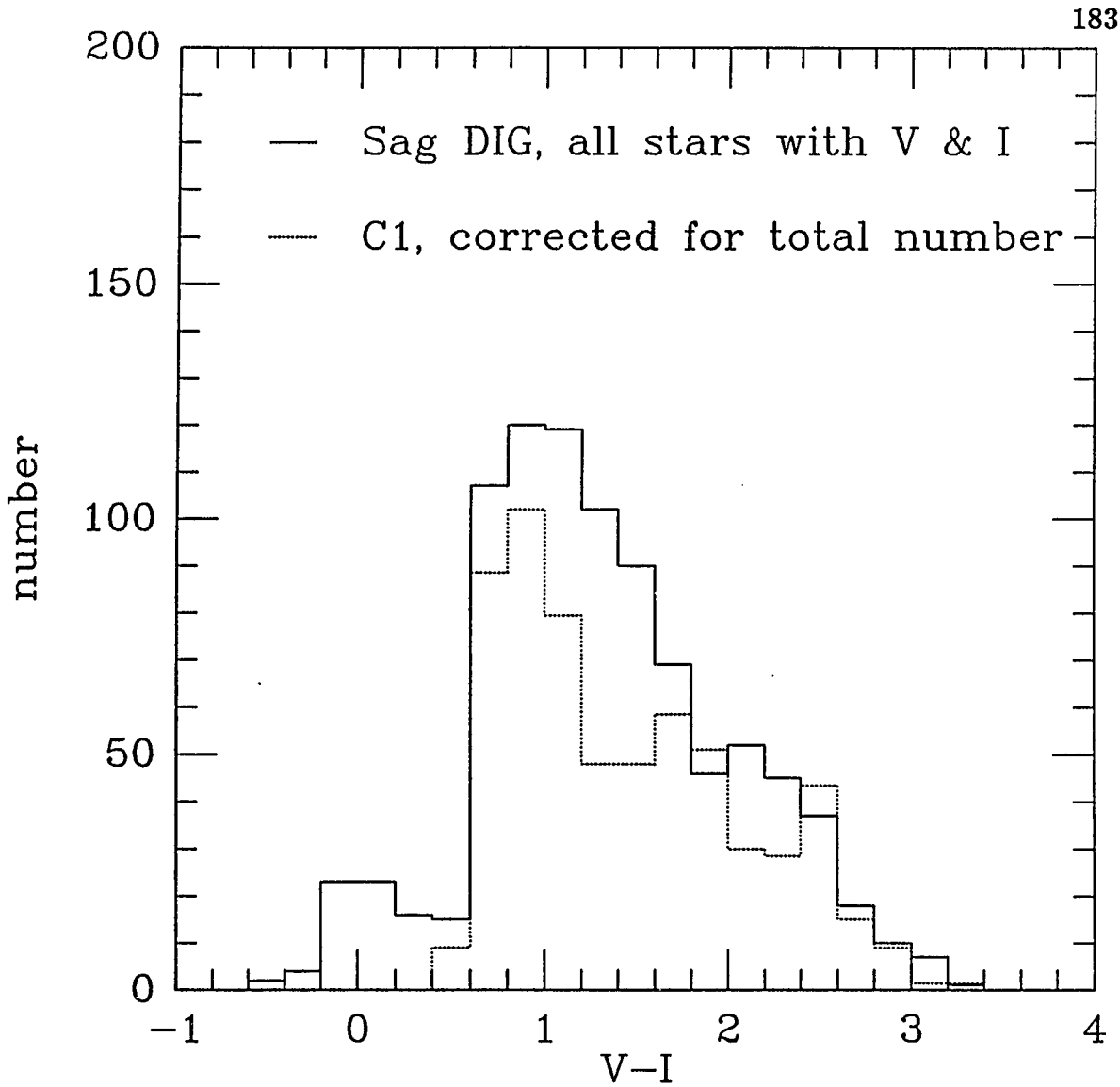

Figure 44. V−I Distribution for the Sagdig and CF1 Fields

The color distribution of stars with detections in V and I in the Sagdig field compared to the the distribution in the CF1 field scaled by the ratios found Table 10.

feature can be identified with the tip of the red giant branch, and has been used by Hoessel and Mould (1982) to estimate distances. The tip of the Population II, first giant branch would be expected to be at $M_{bol} = -3.5$ (Frogel, Persson and Cohen 1980); for a V−I of 1.5 the bolometric correction is 0.97. This feature would then have $M_I = -4.0$. If the feature at I = 21.5 is really the first giant branch tip, then the distance modulus of Sagdig can be estimated to be 25.5. These corrected luminosity functions also show the presence of the blue stars in Sagdig starting at $V = 19$ and they show an over abundance of stars at $I = 18$.

Bright Blue Stars

Sagdig exhibits a well populated blue supergiant region seen in the color magnitude diagram at $V - I \approx 0$ and $V \approx 20$. These stars are probably supergiants; previous distance estimates as well as those I will make give these stars $M_V \lesssim -5$. Such stars are clearly young and represent recent star formation. A traditional exercise for photometers of resolved blue supergiants is the calculation of the mean magnitude and color of the three brightest, blue stars. It also seems to be traditional to do this using different assumptions about the membership of the brightest stars in the system at hand. While a star with $V - I \approx 0.43$ is not likely to be a foreground star (and in fact none are seen in the control field), it is not so unlikely that such an occurrence can be ignored. Table 11 presents data on the ten, brightest blue stars and averages derived from them. The average of stars 2, 3 and 5 does not use the bright but redder stars 1 and 4, and still yields essentially the same mean.

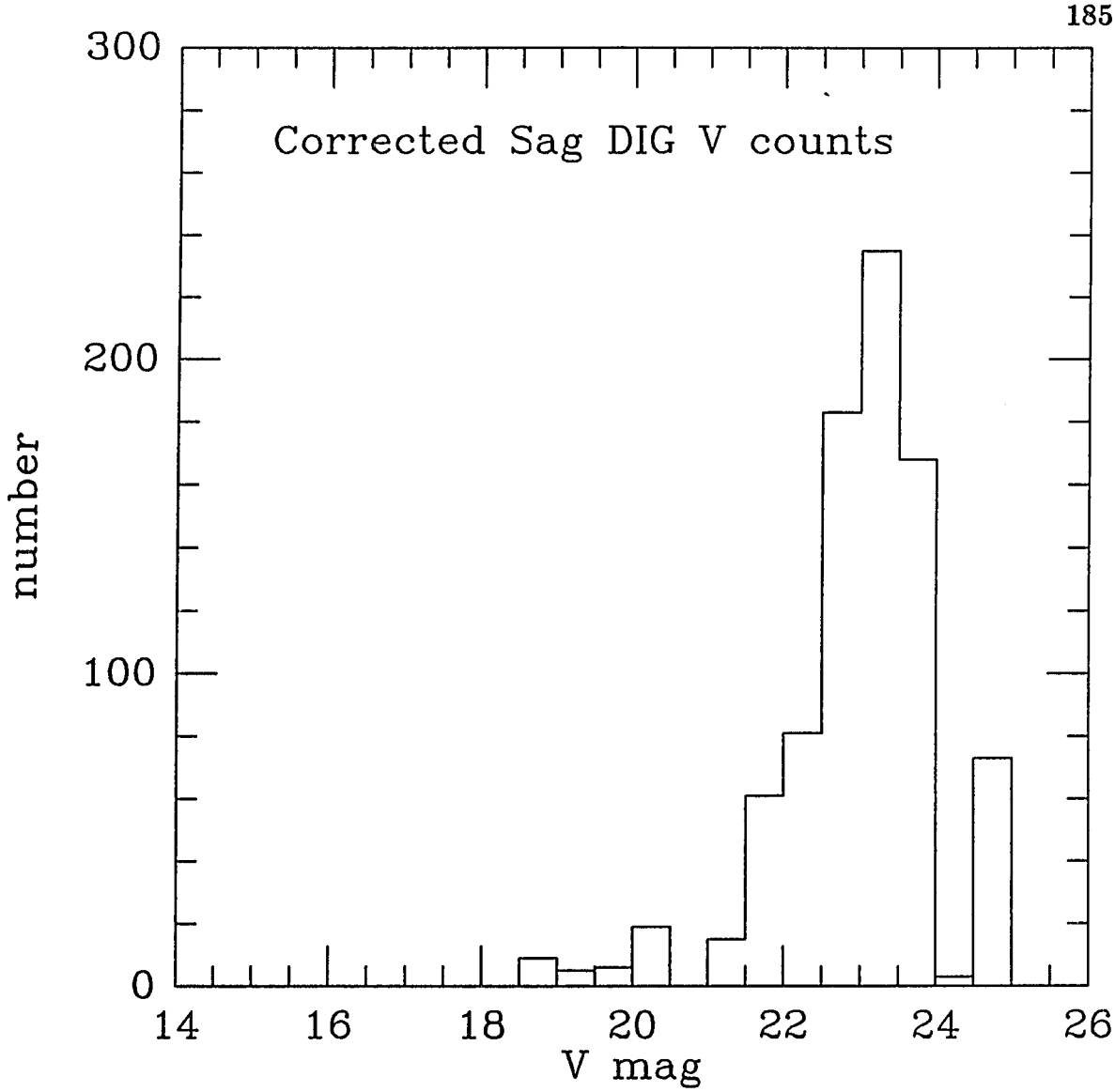

Figure 45. Corrected Differential V Luminosity Function of Sagdig

The scaled, dereddend, CF1, V luminosity distribution was subtracted from the dereddend Sagdig field luminosity distribution to correct for foreground contamination.

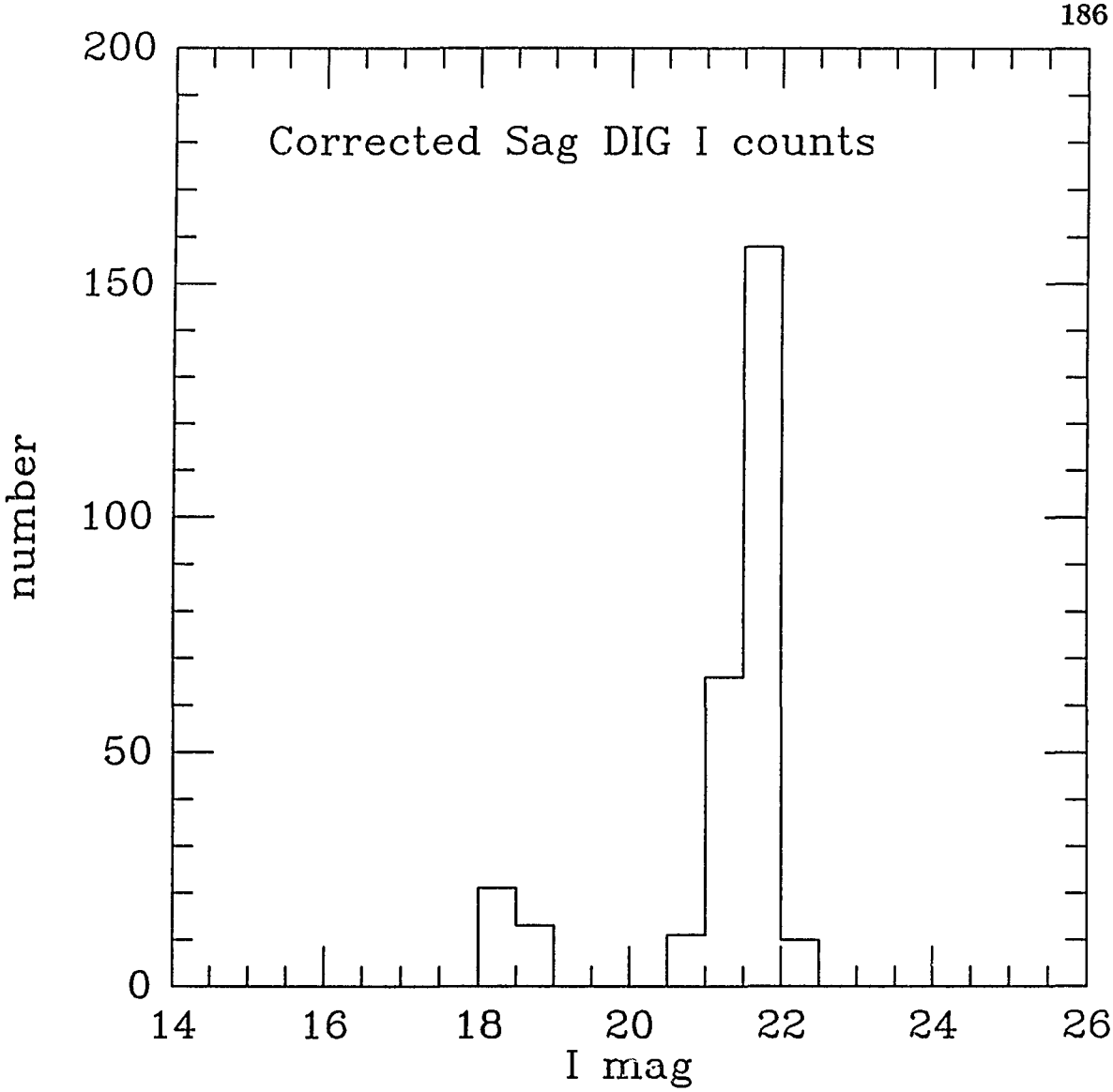

Figure 46. Corrected Differential I Luminosity Function of Sagdig

The scaled, dereddened, CF1, I luminosity distribution was subtracted from the dereddened Sagdig field luminosity distribution to correct for foreground contamination.

Table 11. Sagdig Brightest Blue Stars

						Errors		
Rank	X	Y	V[a]	V−I[a]	77-81[a]	V	V−I	77-81
1	158.0	332.9	19.08	0.43	−.02	0.02	0.02	0.05
2	166.9	327.2	19.44	0.01	0.05	0.02	0.03	0.07
3	113.6	360.7	19.68	0.07	−.04	0.03	0.04	0.06
4	122.8	333.4	19.75	0.25	−.00	0.02	0.03	0.07
5	79.4	382.1	19.81	−.11	0.26	0.04	0.15	0.13
6	101.1	355.3	19.85	0.06	0.07	0.03	0.04	0.07
7	103.1	362.3	20.03	0.00	0.04	0.03	0.04	0.08
8	69.5	365.7	20.16	0.04	−.08	0.03	0.05	0.11
9	109.9	357.0	20.16	−.04	0.03	0.02	0.04	0.11
10	110.6	342.7	20.24	0.08	−.12	0.04	0.06	0.09

Averages	<V>	<V−I>	<B>[b]	<B−V>[b]
stars 1,2,3	19.40	0.17	19.53	0.13
stars 2,3,4	19.62	0.11	19.71	0.09
stars 2,3,5	19.74	−.01	19.62	−.02

Notes:

(a) The V, V−I and 77−81 values are dereddened.

(b) B and B−V have been calculated from V and V−I using the the relations in Cousins (1978).

Figure 47 shows the positions for all of the blue stars from the color-magnitude diagram, i.e. those images which were matched on the V and I frame. Figure 48 shows the positions of the blue stars from the color-color diagram; these stars had images which were matched on frames taken through all four filters.

The blue stars are mostly situated in the region with the highest density of stars. There is also a tail of blue stars which points toward the central, western portion of the field. The bluest of these stars are not found in the central portion of the galaxy's body, but are found away from it. This is suggestive of some internal reddening for the central portion of the galaxy. If de Vaucouleurs, de Vaucouleurs and Corwin's (1976) precepts for calculating internal reddening are used to estimate Sagdig's internal reddening, it would be estimated as about $A_B \approx 0.3$. This value would make the bright blue stars in the central body ≈ 0.13 mag bluer at V−I. It seems likely, on the basis of their apparent position in the galaxy and their observed blue colors (which are too blue to belong to a significant number of foreground stars) that the brightest blue stars do belong to Sagdig.

The estimate of $< V >_3$ is not very sensitive to the choice of stars for this galaxy. Although the inclusion of star 1 does increase $< V >_3$ by 0.2 mag, other subsets of the stars shown in Table 11 yield about the same $< V >_3$. The measured quantities can be converted to the traditional $< B >_3$ and $<B-V>_3$ using Cousin's (1978) measurement of intrinsic lines for his VI system. When converted to $< B >_3$, some of the differences become less between different sets of stars since the brighter stars are somewhat redder.

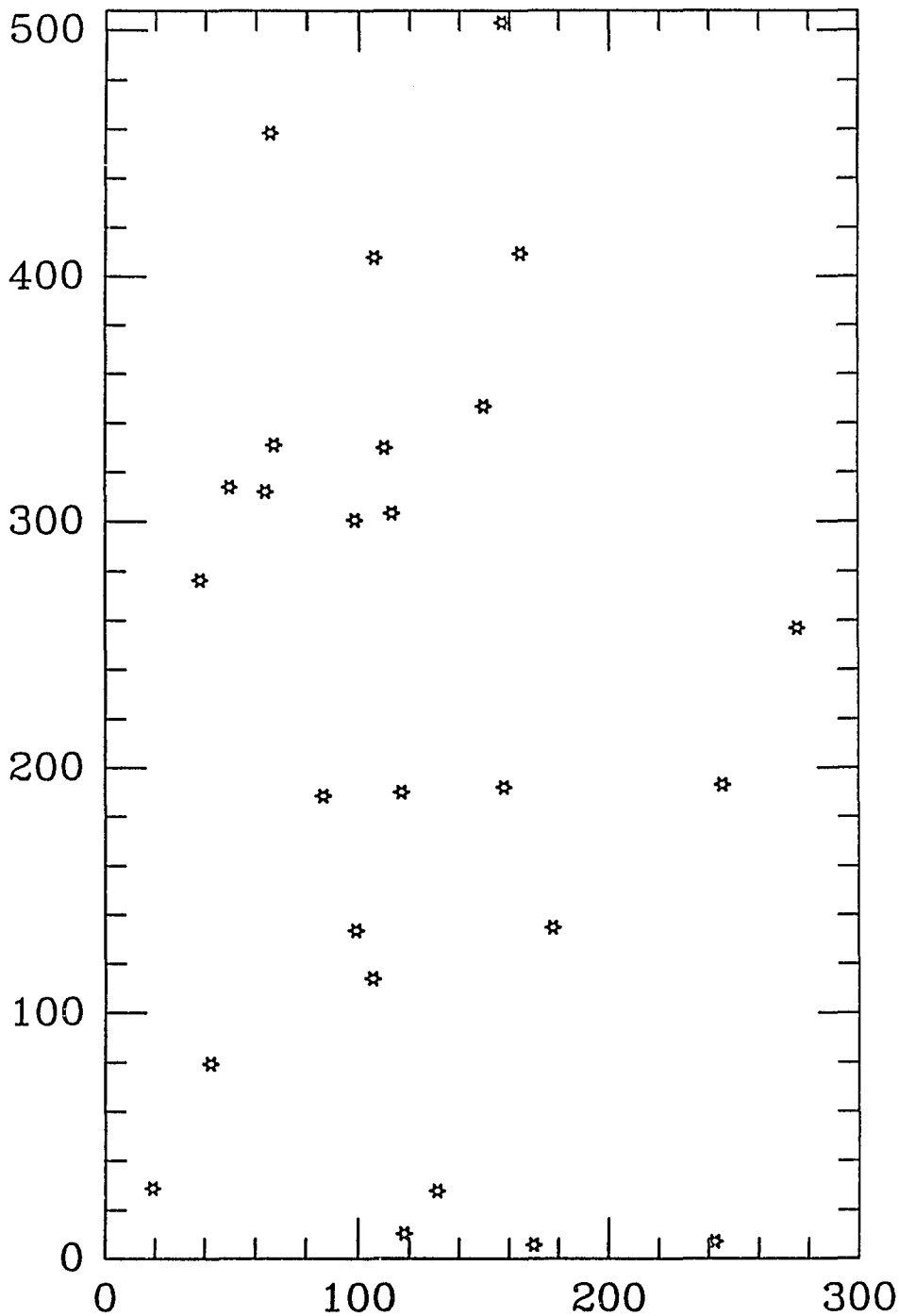

Figure 47. Positions of Blue Stars in the Sagdig Field

This figure shows the positions of stars with $(V-I) < 0.5$ which were detected in the broad bands. This figure should be compared to Figure 33 which is the CCD image of the Sagdig field and is the same scale.

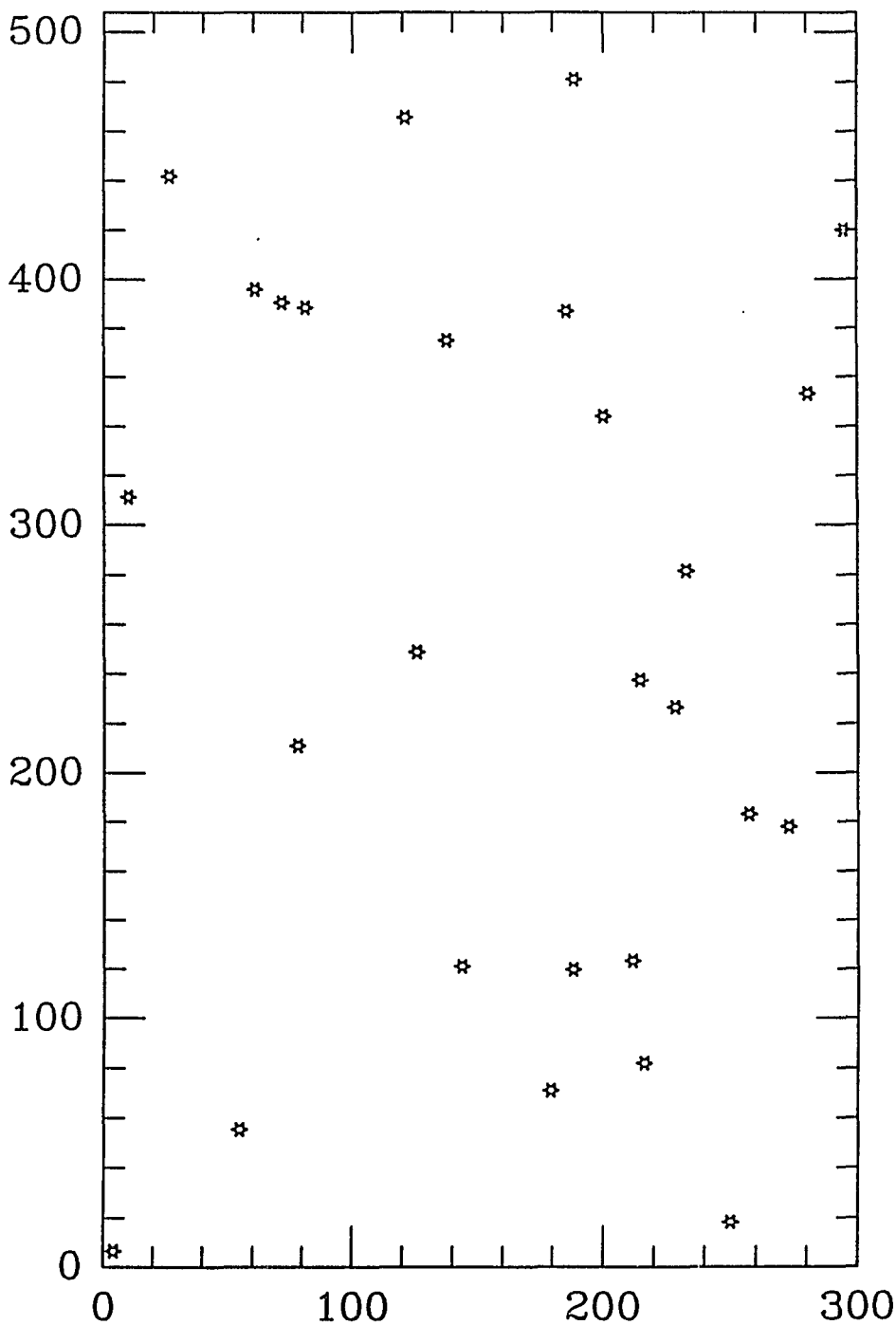

Figure 48. Positions of the Brightest Blue Stars in Sagdig

This figure shows the positions of stars with $(V-I) < 0.5$ which were detected in all four passbands. This figure should be compared to Figure 33 which is the CCD image of the Sagdig field and is the same scale.

The brightest blue stars can be used to estimate the distance of their parent galaxy if the total magnitude of the galaxy is known (Sandage and Tammann 1974). This relationship is known to be almost degenerate for low luminosity parent galaxies (Sandage and Carlson 1985; hereafter SC), but it does provide an estimate of the distance to Sagdig. The empirically measured relation between $< B >_3$ and parent galaxy luminosity found by SC is presented in Figure 49. For a galaxy of unknown distance, a line is constructed by plotting points assuming different distance modulii for the galaxy. This line is the locus of derived absolute galaxy magnitude and derived absolute brightest-blue-star magnitude using the assumed distance modulii to correct the apparent magnitudes. The line has a slope of 1 mag $< B >_3$ per mag M_{B_T} and its intersection with the empirical line yields values for the true $< B >_3$ and M_{B_T}. Even if the empirical relation had very little scatter, a distance determined for low luminosity galaxies will be quite uncertain due to the fact that the slope of the empirical relation is quite close to one and small errors in luminosity would result in large errors in distance. The empirical relation does, however, have significant intrinsic scatter. With these caveats in mind, the present data suggest a distance modulus of $(m - M)_0 = 25.3 \pm 0.5$.

Figure 50 shows an evolutionary track for a 15 $M_\odot$ star with $Z = 0.01$ that has been transformed to the V, V−I plane. The track is one from Brunish and Truran (1982) and includes the effect of mass loss. The transformation to the observational plane was made using the tables of Flower (1977) to obtain bolometric corrections and B−V colors. These were transformed to V, V−I using the tables of Cousins (1979). The track

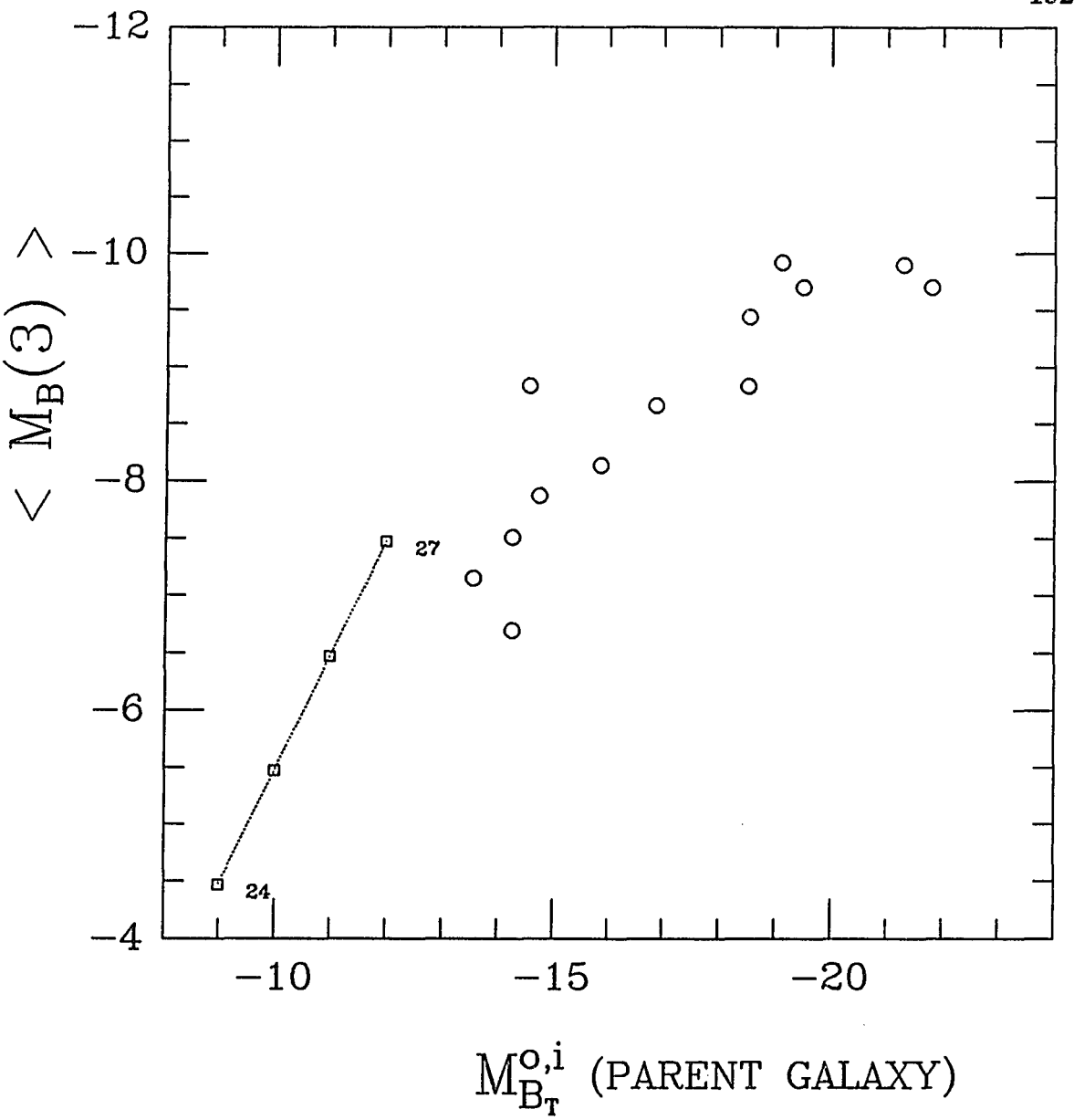

Figure 49. $< M_B(3) >$ as a Function of Parent Galaxy Luminosity

The data points are from Sandage (1986) for the average M_B of the three brightest blue stars in nearby galaxies with distances determined using Cepheids. Also plotted is the locus of points generated for the Sagdig data assuming different distance modulii. The four boxes represent integer modulii, the extremes of which are labelled.

is shown assuming a distance modulus of 25.3 as estimated from the three brightest blue stars. Brunish and Truran (1982) tracks are some of the few which include sub-solar metallicity models for massive stars. The Z = 0.01 model was chosen because of the rather red value of the red supergiants (discussed in the next section). This track is quite close to the observed blue turnup. A 15 $M_\odot$ turnoff would suggest star formation as recently as 10 million years ago. This track may seem bright, but to produce a track one magnitude fainter will still require a 10 $M_\odot$ model and the most recent star formation epoch would have been about 20 million years ago.

Bright Red Stars

An outstanding feature of the Sagdig color-magnitude diagram (Figure 40) is the presence of a clump of stars at $I \approx 13.5$ and $V-I \approx 2$. Stars of this magnitude and color are clearly not present in the control field, and these stars stand out in the V−I distribution of Sagdig compared to CF1 (see Figure 44). There are 27 stars in the region outlined in Figure 40 in the Sagdig field and there are 6 in the control field ($1.7 < V - I < 2.5, 17.7 < I < 18.7$). This means that about 18 are not expected from estimates of foreground contamination. These are the brightest red stars in Sagdig. Investigations of other dwarf irregular galaxies show stars of this type to generally be present (Sandage 1986). These investigations find the brightest red stars to be about the same V magnitude as the brightest blue stars and to have B-$V \sim 1.5$ which corresponds to $V - I \sim 2.1$. These stars are sometimes referred to as red supergiants and Sandage and Tammann (1974) have accumulated an empirical relation between the brightest red stars and the parent galaxy

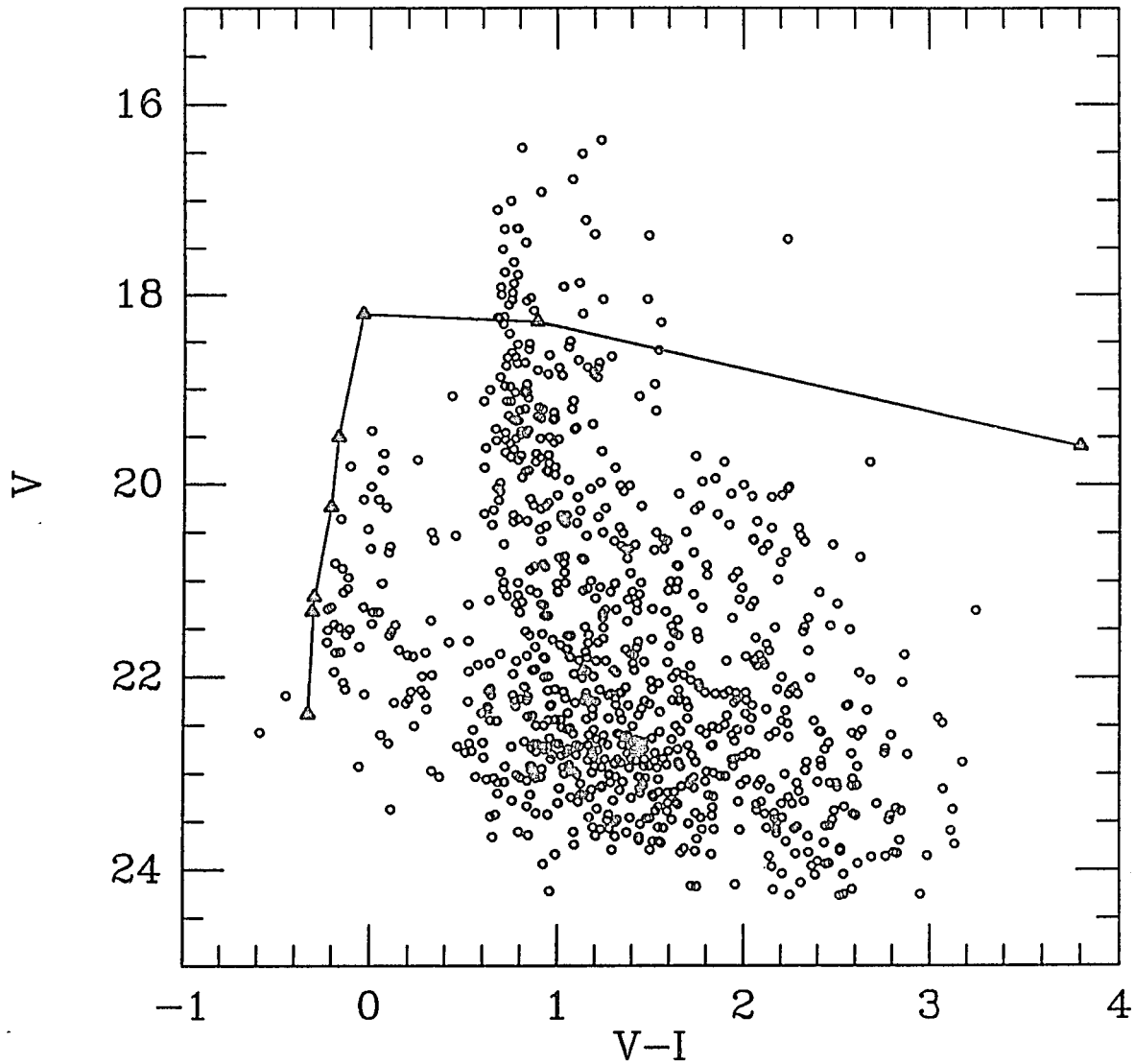

Figure 50. $15M_\odot$ Evolutionary Track Compared to the Sagdig Data

The dereddend, color-magnitude data for the Sagdig field is presented with the evolutionary track for an $15M_\odot$ star with [Fe/H] = −0.3 (Brunish and Truran 1982) assuming $(m - M)_0 = 25.3$.

luminosity in a manner similar to that for the brightest blue stars. This red relation apparently suffers even more scatter than the blue relation (Hoessel and Danielson 1983) and may be completely degenerate for faint galaxies. If the brightest red star game is played for Sagdig using the mean magnitude of stars in the red supergiant portion of the color-magnitude diagram ($V = 20.3$), the data suggest a distance modulus of about 26 as can be seen in Figure 51.

The Sagdig, brightest red stars are found in the color-color plot to occupy the TiO track at the positions of M1 to M4 stars (see Chapter 3 for the empirical calibration). They form a TiO track which is redder in V−I than the mean TiO track and this implies that the metallicity of Sagdig is lower than that of the foreground stars. The positions of these stars in the color-color diagram is shown in Figure 52.

This figure also plots the colors of the stars found in the control field color magnitude diagram in the supergiant region. A least squares fit of a line to the Sagdig red supergiant locus in the color-color plane yields a slope of 3.52 and a $(V - I)_{0.2} = 2.01$ which suggests a metallicity for these star of −0.45 (see Chapter 3, Figure 23a). A line fit to the CF1 stars in this region of the color magnitude plane yields a $(V-I)_{0.2}$ of 1.93 and roughly solar metallicity. The value for the CF1 stars metallicity is about what would be expected. The value for Sagdig may seem high for such a low luminosity dwarf, but this value applies only to the very young stellar population. These metallicity estimates are quite sensitive to the reddening correction and so must be viewed as provisional, but the metallicity of these stars is certainly less than the mean metallicity of the foreground stars. Using the corrected number of 18 Sagdig stars, their integrated V magnitude

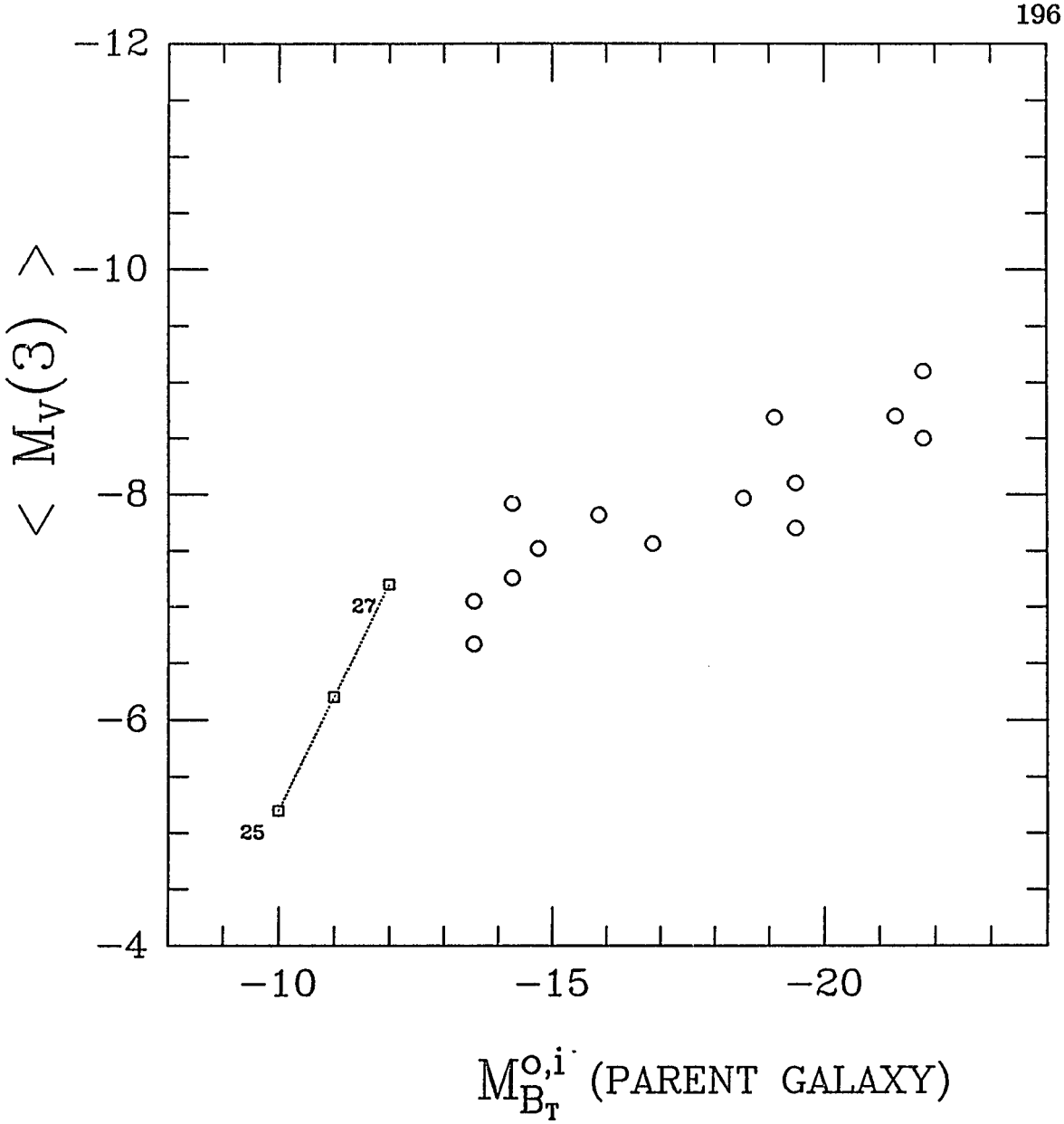

Figure 51. $< M_V(3) >$ as a Function of Parent Galaxy Luminosity

The average M_V of the three brightest red stars in nearby galaxies with distances determined from measurements of Cephieds. The line represents the Sagdig data assuming different distance modulii. The boxes are integer modulus points.

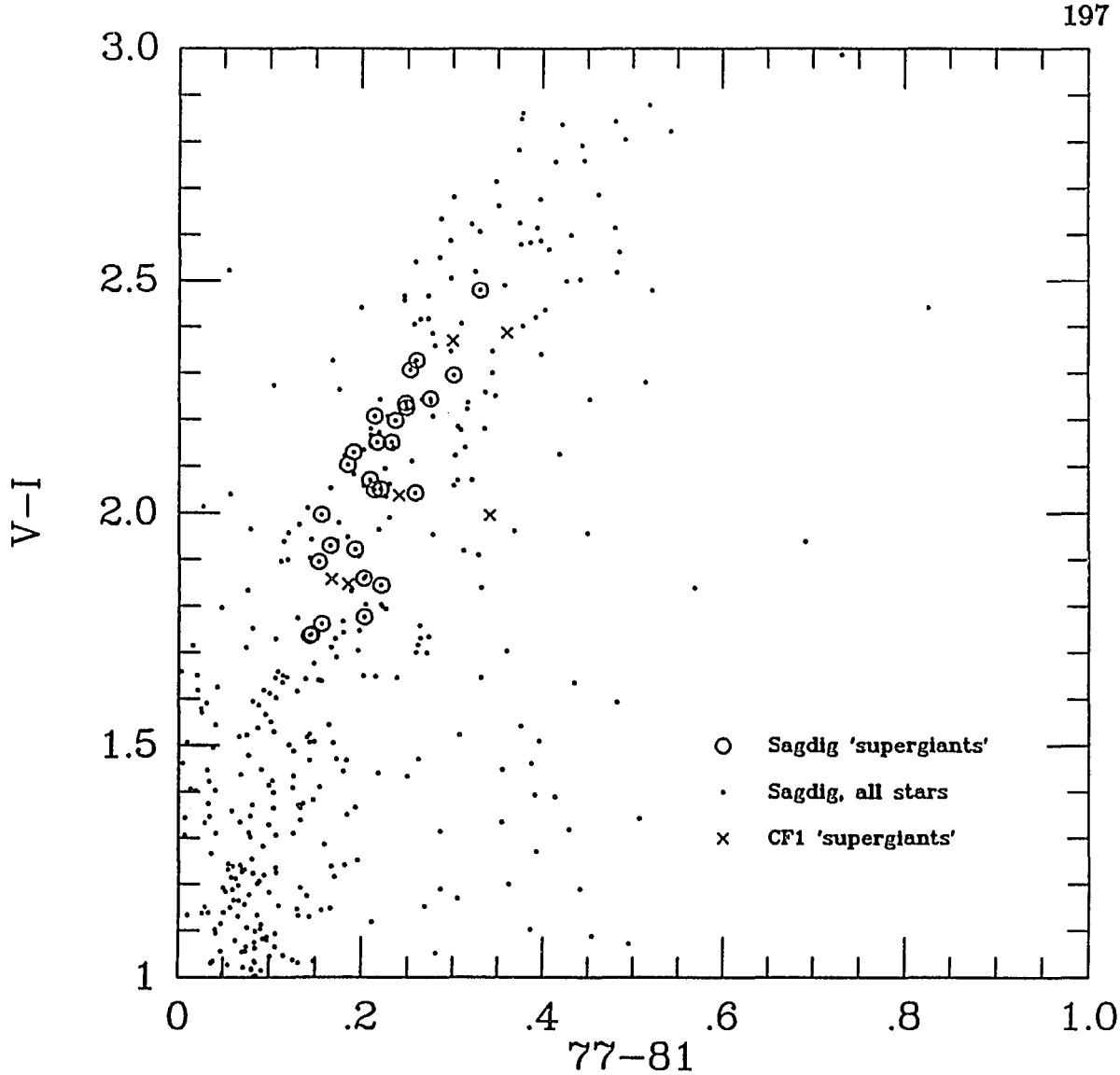

Figure 52. Color-Color Diagram for the Brightest Red Stars in Sagdig

The brightest red star points from the Sagdig field are shown circled. The stars from CF1 in the same region of the color-magnitude diagram are shown as x's. The points are all of the data from the Sagdig field and represent foreground stars as well as Sagdig stars. The colors have been dereddened.

is roughly 17 (compared to Sagidg's 14.7); their mean V−I is 2.06 and their mean I magnitude is 18.25 (which is roughly $M_I = -7$).

A further check on the membership of these stars can be made using a theoretical model for the distribution of Galactic stars. Ratnatunga and Bahcall (1985) have used the BS model to estimate the number of Galactic stars in various color ranges toward a field appropriately symmetric to the Sagdig field ($l^{II} = 32°$, $b^{II} = -16°$) and they predict 29 stars in the range V = 18.9 to 20.9 with B−V greater than 1.41 (equivalent to V − I = 1.4). For this range of color and magnitude, the Sagdig field had 45 stars and the control field had 24. Using my calculated ratio of 1.5 to correct the CF1 counts to the Sagdig field, I would estimate 36 foreground stars which is larger than the Ratnatunga and Bahcall prediction, but is close to the prediction considering the small number statistics. This concentration of stars in the Sagdig field is not expected theoretically nor is it seen in the control field.

There are two problems with having found these red "supergiants" in Sagdig. The first problem is that there are about the same number of them as there are blue supergiants, and the second is that these stars' positions are not correlated with the main body of Sagdig. The fact that there are so many red supergiants is disturbing because the red supergiants are supposed to evolve from the blue and to have significantly shorter lifetimes (Brunish and Truann 1982a). Although the theoretical analysis of the red to blue supergiant ratio does not match the observed ratios in dwarf irregulars, Brunish and Truran point out that if the theoretical analysis of the AGB maximum luminosity (Iben and Truran (1978) is correct, then the ratio of

the brightest red to blue stars can be about one if they are less luminous than $M_{bol} = -7.5$. This is due to the contribution of the AGB stars. It should be noted that the Sagdig stars are more than a magnitude brighter than the carbon stars found in Sagdig (discussed in the following section). If a significant number of them are Sagdig AGB stars, then there may not be a theoretical deficit of luminous AGB stars in Sagdig, but there will be a different problem. Either there are a few hundred AGB stars which are up to two magnitudes less luminous than the red supergiants (see Reid and Mould 1984 for expected luminosity functions), or there is a deficit of less luminous AGB stars. There is no evidence for a few hundred AGB stars in the two magnitudes below the red supergiants as demonstrated by the luminosity function of this field (see Figure 45). These stars are not likely to be AGB stars.

More disturbing than the quantity of bright red stars in this field is their distribution. Plotted in Figure 53 are the positions of the 25 "red supergiants". These stars are scattered about the frame with no real concentration toward the body of Sagdig. If these stars are members of Sagdig, then it is not surprising that their numbers do not correlate well with the brightest blue stars since their spatial distribution does not.

Carbon Stars in Sagdig

The presence of field star contamination in the Sagdig data should not materially affect the measurement of carbon star numbers. As pointed out earlier, there should be no faint, Galactic, carbon stars in a field this size. The control field color-color plot suggests that there may be a few. There

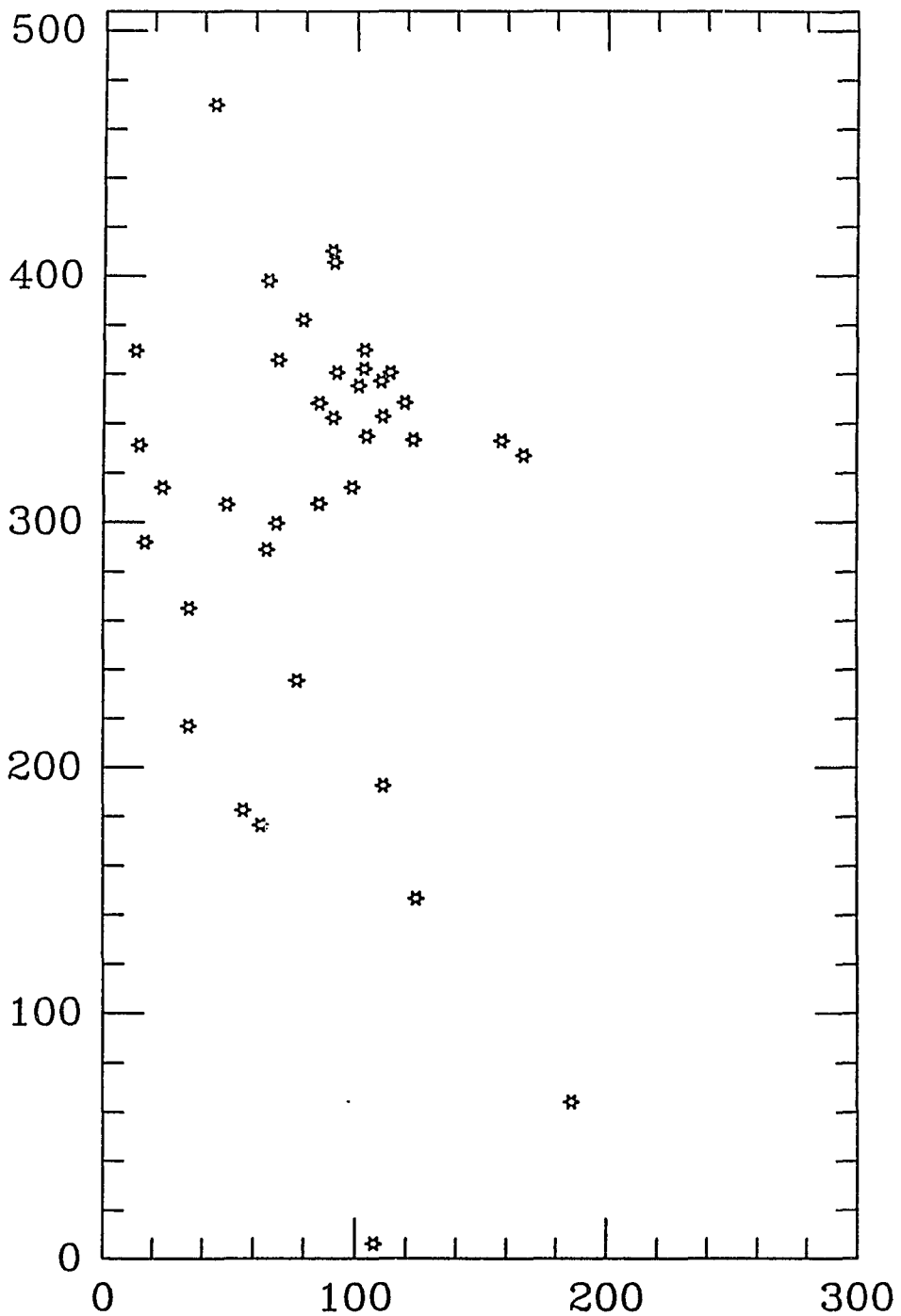

Figure 53. Positions of the Brightest Red Stars in the Sagdig Field

Positions of all of the stars in the region $1.7 < V - I < 2.5$ and $17.7 < I < 18.7$ of the Sagdig color-magnitude diagram.

is only a small magnitude difference which distinguishes carbon stars from K and M stars at the beginning of the carbon star track in the color-color plot. If only a few stars occupy this region, it is important to examine the measurement errors for each candidate before drawing any conclusions based upon these measurements. Because of the far greater number of Sagdig carbon stars, the presence of a few foreground carbon stars in the Sagdig field will not affect any of the conclusions reached here. It would, none-the-less, be amazing if there were ten or so dwarf carbon stars in the control field. A conservative requirement for a star to be unambiguously labelled a carbon star would be for its 77−81 error to be smaller than the 77−81 blue excess which puts it in the carbon star region of the color-color plot. Reasonable limits for the carbon star region are $77-81 < 0.05$ and $V-I > 1.24$. These limits include the full 77−81 range of observed known carbon stars; they do not, however, go as blue, in V−I , as known carbon stars. There is so much overlap from K stars at the bluer colors and most carbon stars are much redder that little is lost by this lower limit for V−I . Pruning the CCDs in this way produces Figures 54 and 55. In these figures, carbon star candidates whose estimated errors lie within the carbon star region are plotted with their 77−81 error bars and all of the rest of the stars measured are plotted as points. In CF1, there are two, quite blue stars which could easily be dwarfs which have strong Na I absorption at 8183,8195Å. Later type dwarfs would not appear in the carbon star region because the Na I absorption would be overcome by TiO absorption. The reddest of the CF1 carbon star candidates was poorly fit in all of the passbands, i.e. high chi values returned from DAOPHOT. Inspection of the image reveals that it is

composed of a blend of at least three images and the photometry cannot be trusted.

The Sagdig field contains 26 stars whose 77–81 errors are contained within the carbon star region, and all are fit quite well. The CF1 carbon star results suggest that as many as three of the bluer candidates may be foreground stars. Table 12 lists their measured properties; Figure 56 shows their positions. These stars exhibit a small concentration in the body of Sagdig, but they also spread across the field. In fact there seems to be a region two minutes of arc west of the main body where they are just as dense. This region is the region pointed to by the 'tail' of blue stars. The distribution of the carbon stars seems to be intermediate between the brightest blue stars and the brightest red stars in terms of being centrally concentrated.

Figure 57 is a color magnitude diagram of the carbon stars whose errors lie within the carbon star region. There is a slight correlation of magnitude with color as would be expected, and there is a definite concentration of points at the blue end of this asymptotic giant branch. The luminosity function of these stars is presented in Figure 58. The concentration of blue carbon stars is seen here as a peak of fainter stars. This is clearly demonstrated by the luminosity function for the redder $(V - I > 2)$ carbon stars also presented in Figure 58. For all carbon stars, $< I >= 20.69 \pm 0.7$, while for the redder ones, $< I >= 20.22 \pm 0.4$. Blanco, McCarthy and Blanco (1980; hereafter BMB) found the carbon star luminosity distribution in the Clouds to be almost gaussian with a mean of $M_I = -4.2$ (if one uses the short LMC distance of $(m - M)_0 = 18.2$). If this type of

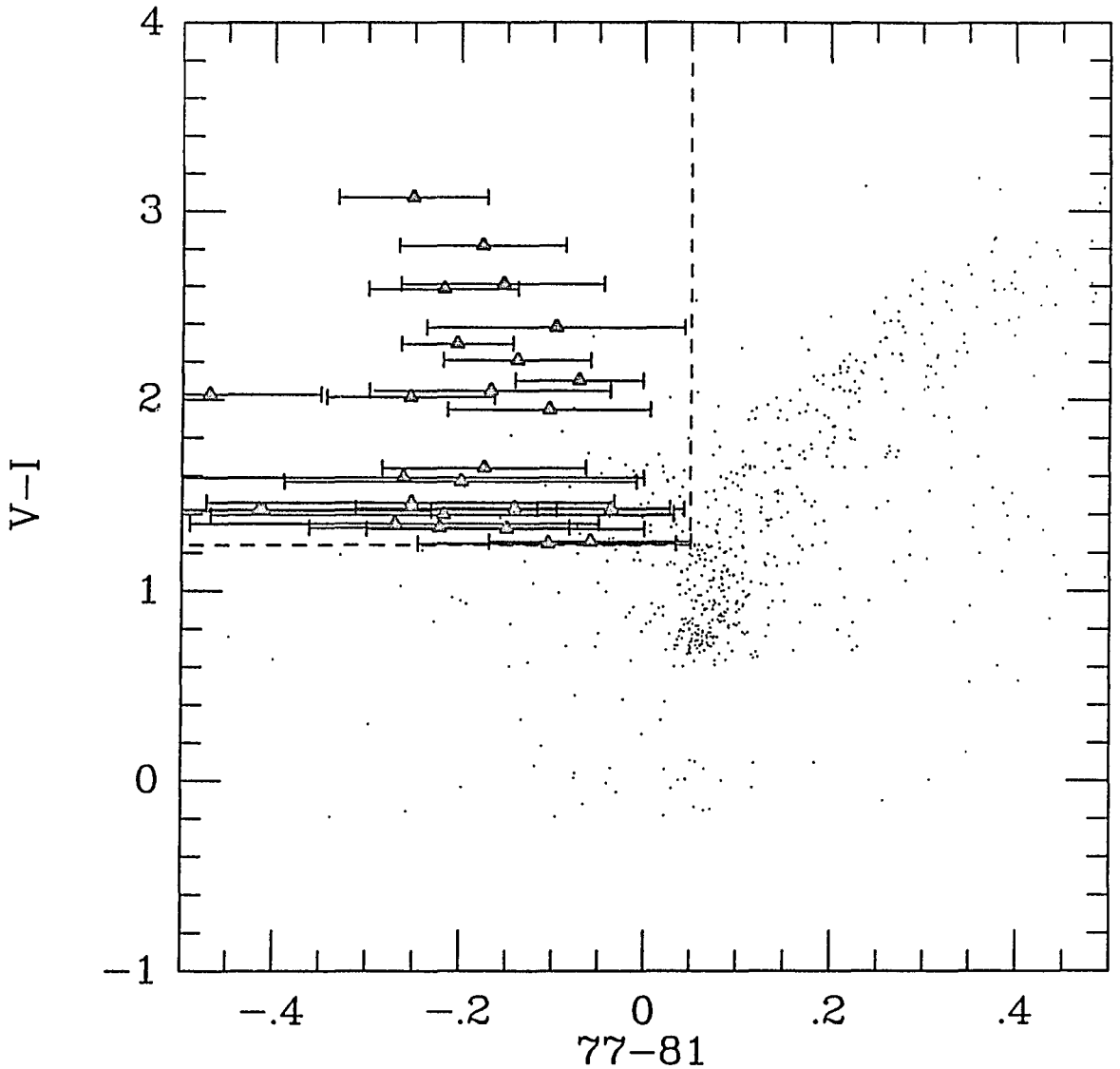

Figure 54. The Color-Color Diagram of the Likely Carbons Stars in Sagdig

The probable carbon stars in the Sagdig field are plotted as filled triangles in the color-color diagram with their error bars in 77−81. The dotted line outlines the adopted carbon star region. All of the stars in the Sagdig field are shown as points.

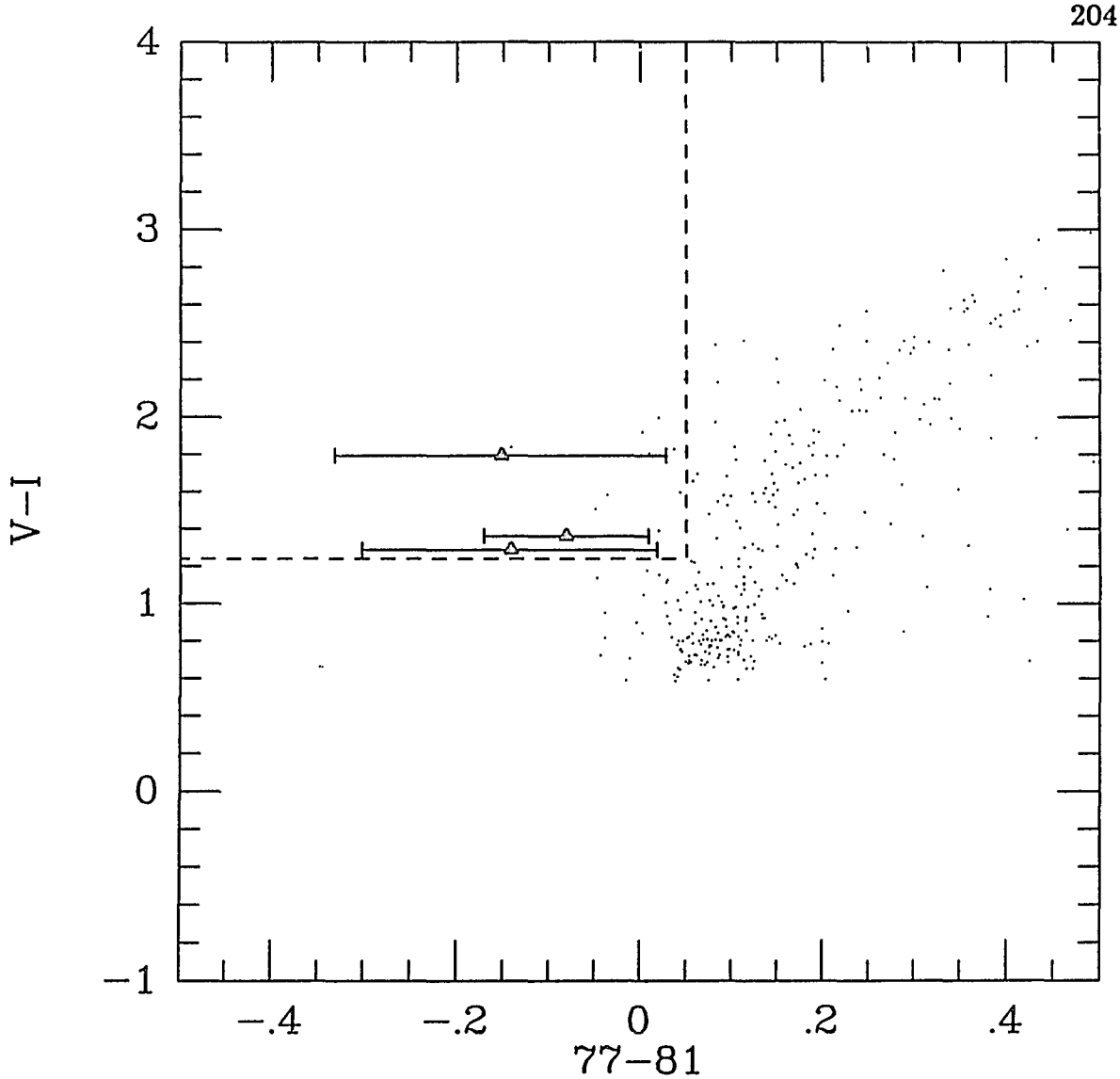

Figure 55. The Color-Color Diagram of Possible Carbon Stars in CF1

All of the stars in the CF1 field are plotted as points and the likely carbon stars are plotted as filled triangles with their error bars in 77−81. The adopted carbon star region is outlined with a dotted line.

Table 12. Sagdig Carbon Stars

X	Y	I[a]	V−I[a]	77−81[a,b]	Errors I	Errors V−I	Errors 77−81
242.6	6.8	19.81	1.43	−.04	0.03	0.04	0.08
110.5	330.0	20.57	1.26	−.06	0.04	0.06	0.11
86.4	188.4	19.73	2.10	−.07	0.08	0.09	0.07
117.1	190.0	20.07	2.38	−.10	0.04	0.22	0.14
245.5	192.9	20.97	1.95	−.10	0.08	0.14	0.11
131.1	27.8	21.36	1.25	−.11	0.07	0.11	0.14
98.6	300.5	19.80	2.21	−.14	0.03	0.06	0.08
158.0	192.1	21.36	1.43	−.14	0.11	0.13	0.17
38.2	276.4	21.53	1.32	−.15	0.11	0.14	0.15
99.3	133.5	20.32	2.61	−.16	0.04	0.10	0.11
106.3	407.5	20.25	2.05	−.17	0.05	0.09	0.13
18.9	28.9	19.36	1.64	−.17	0.11	0.18	0.11
49.8	313.8	20.54	2.82	−.18	0.04	0.16	0.09
169.9	5.6	21.28	1.57	−.20	0.09	0.16	0.19
67.4	331.1	19.88	2.29	−.20	0.03	0.07	0.06
113.3	303.3	21.86	1.40	−.22	0.14	0.18	0.25
156.9	503.2	20.00	2.58	−.22	0.03	0.11	0.08
275.6	257.0	20.84	1.33	−.22	0.08	0.09	0.14
65.5	458.4	20.09	3.07	−.25	0.04	0.10	0.08
177.7	134.7	21.63	1.46	−.25	0.17	0.22	0.22
149.9	346.9	20.22	2.01	−.25	0.04	0.07	0.09
105.5	114.1	21.80	1.59	−.26	0.12	0.19	0.26
42.1	79.3	21.28	1.35	−.27	0.10	0.15	0.22
164.6	409.3	21.23	1.42	−.41	0.15	0.17	0.18
117.9	10.2	21.44	1.42	−.42	0.14	0.17	0.33
64.0	312.1	20.75	2.03	−.47	0.05	0.11	0.12

Notes:

(a) The V, V−I and 77−81 values are dereddened.

(b) These are the stars whose 77−81<0.05 and V−I>1.24 with 77−81 errors which do not extend beyond 77−81=0.05.

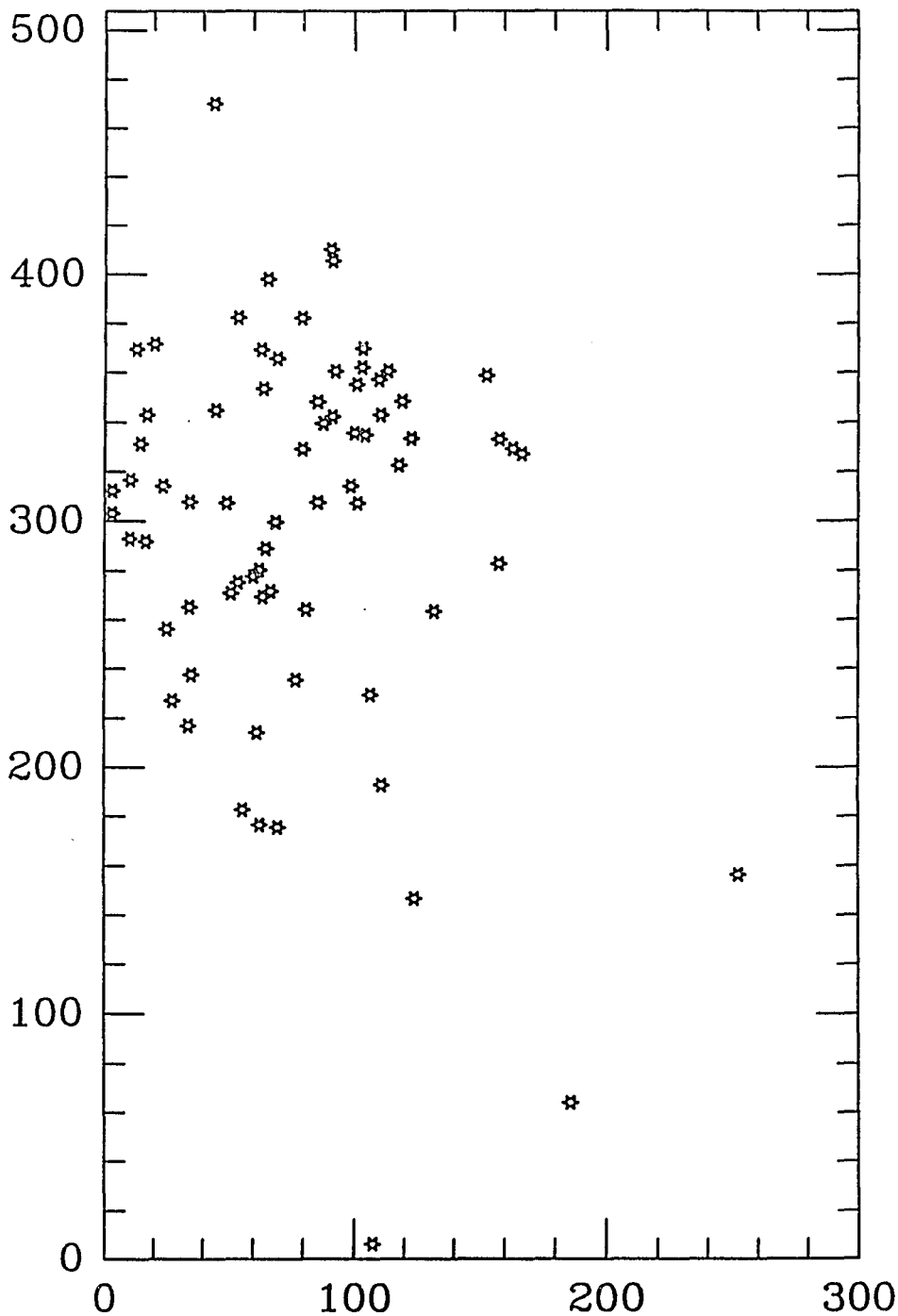

Figure 56. Positions of the Carbon Stars in the Sagdig Field

Positions of the 26 "good" carbon stars in the Sagdig field. This figure should be compared to the CCD frame in Figure 33 which is the same scale.

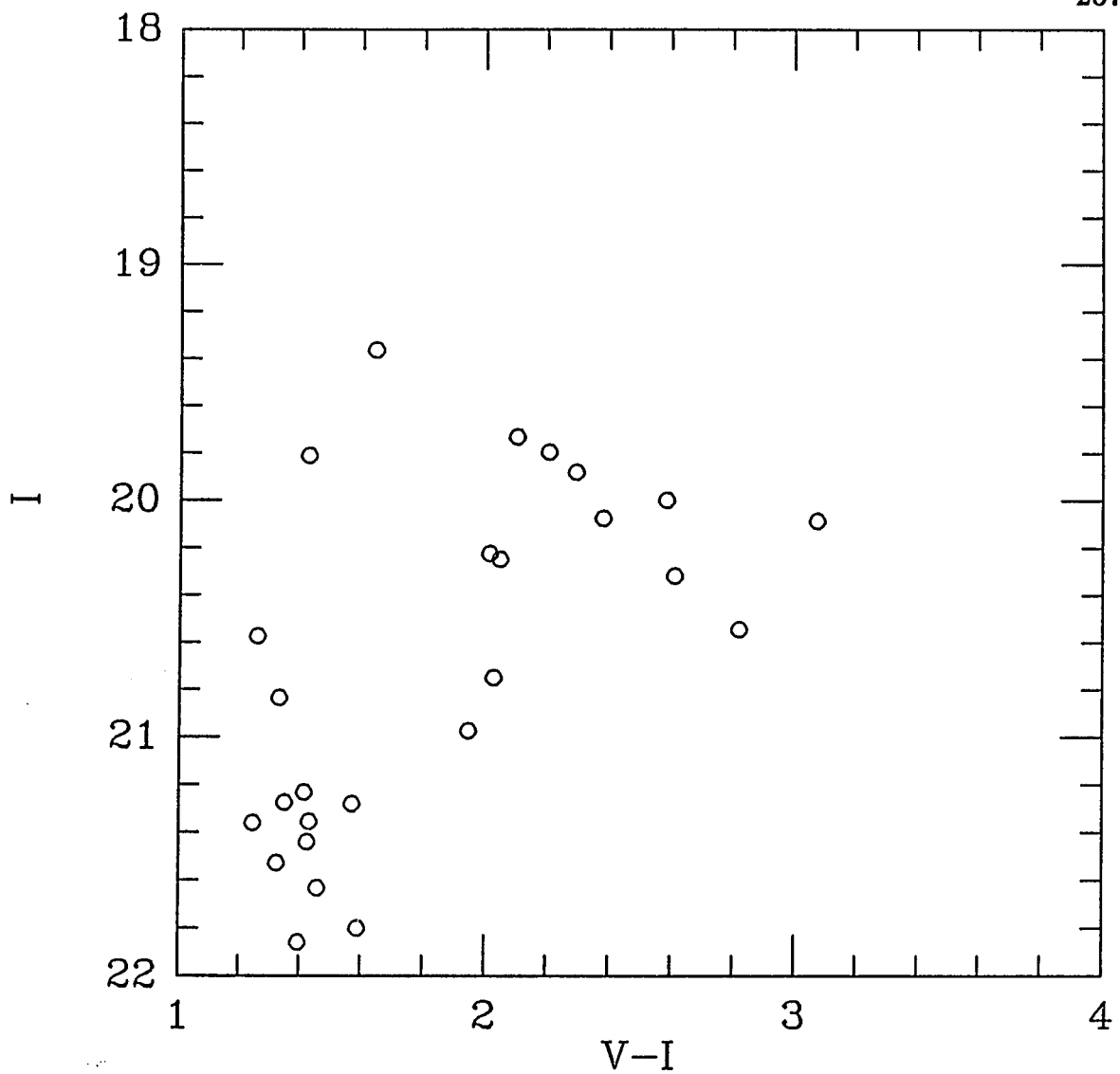

Figure 57. Color-Magnitude Diagram of the Sagdig Carbon Stars These values have been dereddened.

distribution holds for Sagdig, then the distance modulus can be estimated as $(m-M)_0 = 24.4$ to 24.9. These modulii become 25.1 and 25.6 if the Sandage and Carlson (1985) modulus for the LMC is used so that these modulii can be compared to the brightest star estimates. The longer estimate is quite close to the giant branch tip estimate. This longer estimate is probably the better one since for the SMC, BMB found the carbon stars to have $R-I = 0.93$ in the bluest region of the galaxy. This region is probably most similar to Sagdig in stellar population, and this $R-I$ color is equivalent to $V-I = 1.8$ which is the mean color of all the carbon stars in Sagdig used to produce the longer distance estimate.

The total number of carbon stars in the Sagdig field can be estimated from the actual number of stars measured in the carbon star region corrected with the CF1 counts. Such a correction serves two purposes. It would correct for real, Galactic, carbon stars (if any). It would also correct for the measurement errors which placed stars in the carbon star region when they are not really carbon stars. There are 13 CF1 stars in the carbon star region of the color-color diagram and there are 78 Sagdig stars. A reasonable estimate for the total number of Sagdig carbon stars in thus 58 (i.e. $78-13*1.5$). This estimate does not include any correction for incompleteness. For the frame as a whole, I have previously estimated that the data become seriously incomplete at $V \approx 23.5$ and $I \approx 21.5$. Consequently, the number found applies only to carbon stars brighter than $I \approx 21.5$ ($M-I \approx -3.5$ to -4.0). This lower luminosity limit will also serve to limit the pollution of the carbon star region by Sagdig first giant branch stars whose colors are in error since the RGB tip seems to be at $I = 21.5$. For brighter stars,

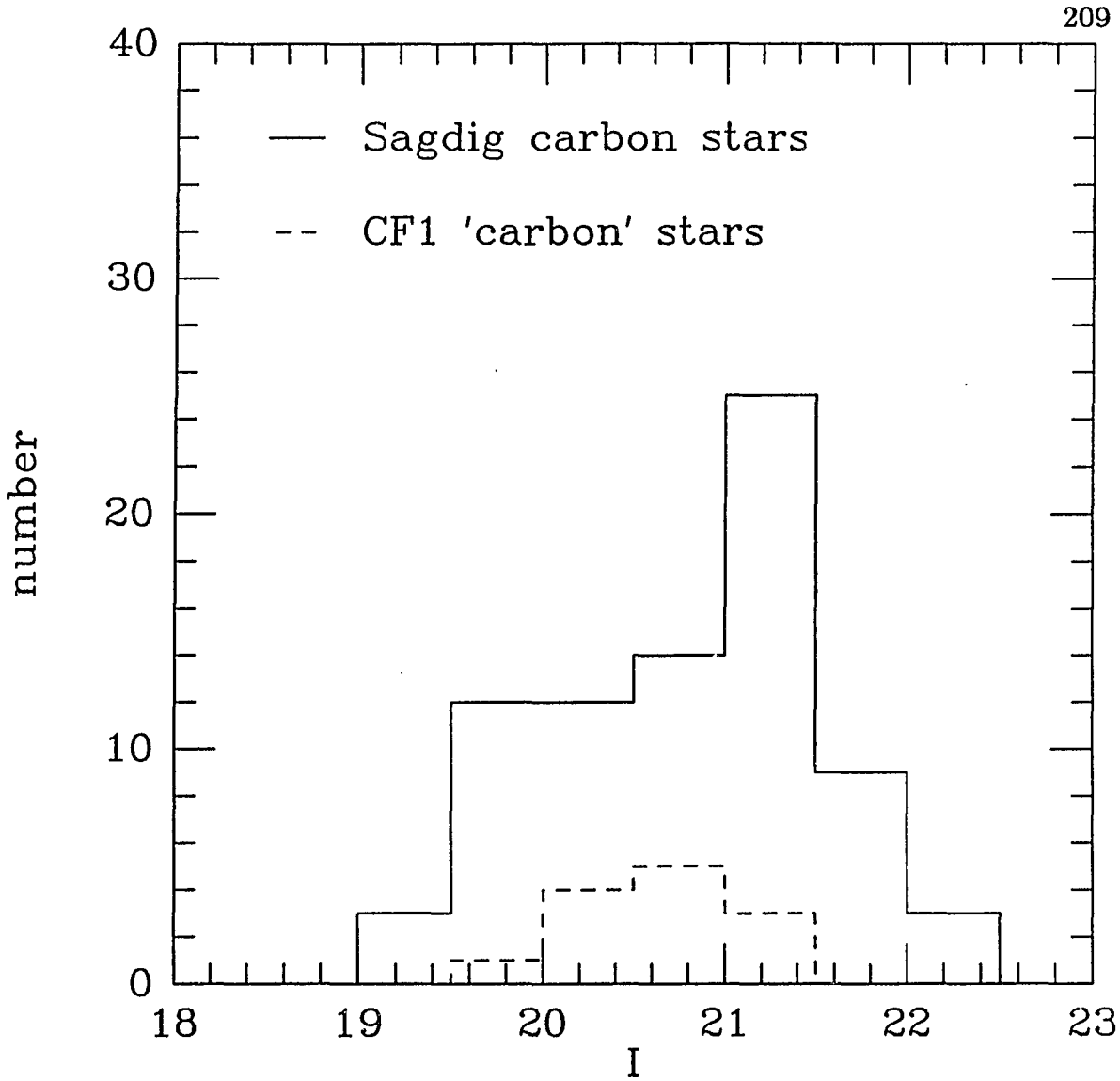

Figure 58. Luminosity Distribution of the Sagidg Carbon Stars

The dereddened luminosity distribution for the 26 'good' carbon stars in the Sagdig field is shown as the solid line and the dashed line is the luminosity distribution for those with $V - I > 1.7$.

the actual number should be corrected upward by about 10% as estimated by the artificial star tests. The total number also must be increased by some unknown factor since our Sagdig field probably did not cover the whole galaxy as evidenced by the lack of a clear drop in carbon star density away from the galaxy body and the rather uniform distribution of the brightest red stars.

The total number of carbon stars in a galaxy was found by BMB to scale as the parent galaxy luminosity. They found 11000 carbon stars in the LMC and 2900 for the SMC. If this relation holds for Sagdig, then its total luminosity can be estimated to be greater than $M_B = -12.2$. Such an estimate would not fit well with the estimate from the brightest blue stars of -10.5. If only the 12 red, carbon stars are considered to be Sagdig's carbon star population, then scaling this number yields a galaxy magnitude of -10.4. Of course, the brightest star estimate for Sagdig's absolute magnitude was derived from the visual estimate of apparent magnitude made by CLLSW and LHWM who also estimated a 'small' size.

A luminosity function for all stars in the carbon star region of the color-color diagrams for Sagdig and CF1 (corrected) is shown in Figure 59. In Figure 60, the color distribution for these stars is presented. As was clear from the unambiguous carbon star data, the brighter carbon stars tend to be redder and the fainter ones are bluer. This would be expected from simple evolution along the AGB following a Hayashi track. It is also interesting to speculate on the possible existence of two distinct populations of carbon stars as evidence by their luminosity distribution. An older, lower metallicity population would produce fainter, bluer carbon stars and a younger, higher

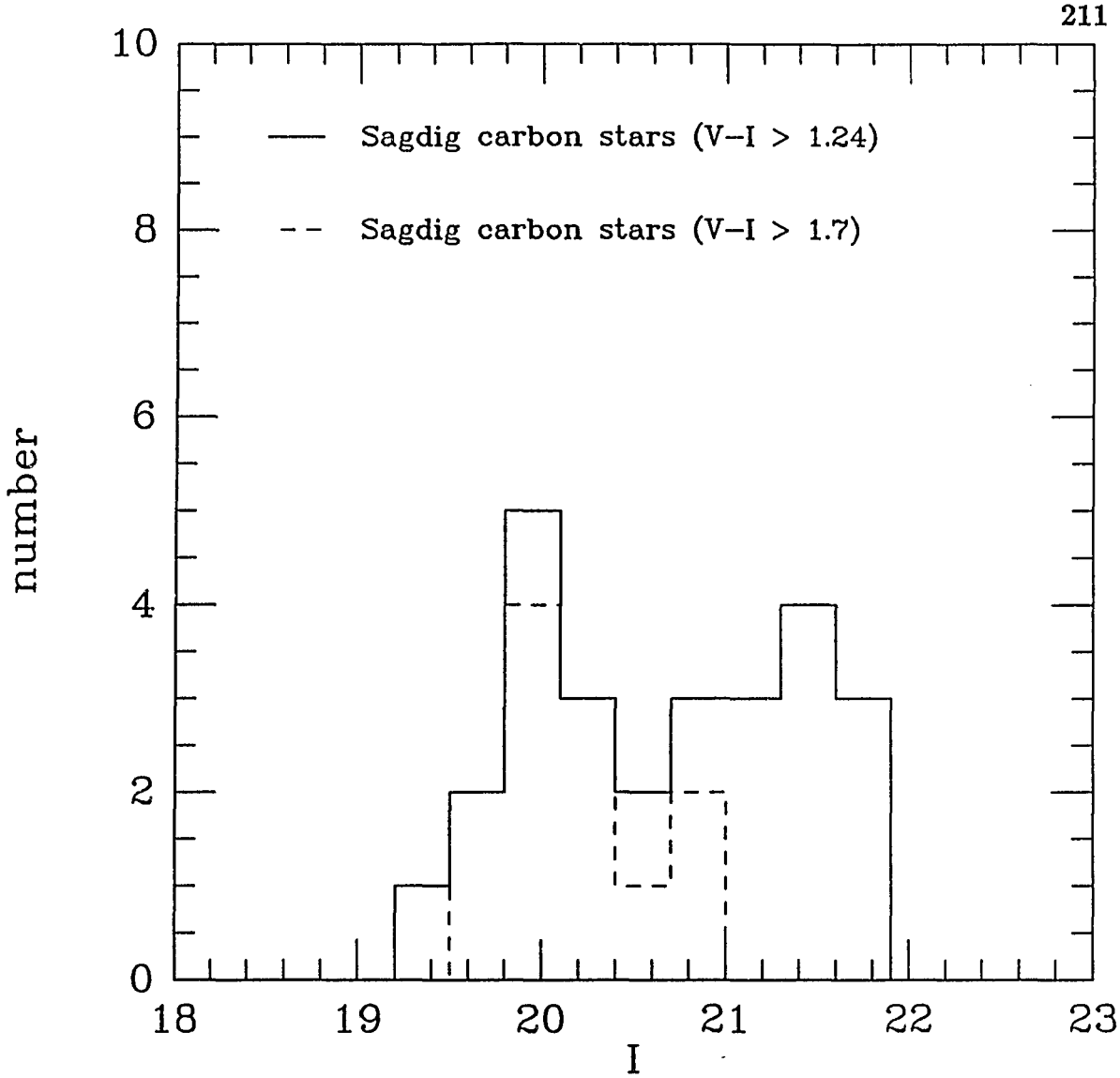

Figure 59. Luminosity Distribution of all Carbon Stars in Sagdig and CF1

The dereddend luminosity distribution for the stars in the carbon star region of the color-color diagram of Sagdig (solid line) is compared to the scaled luminosity distribution for those from the CF1 field (dotted line).

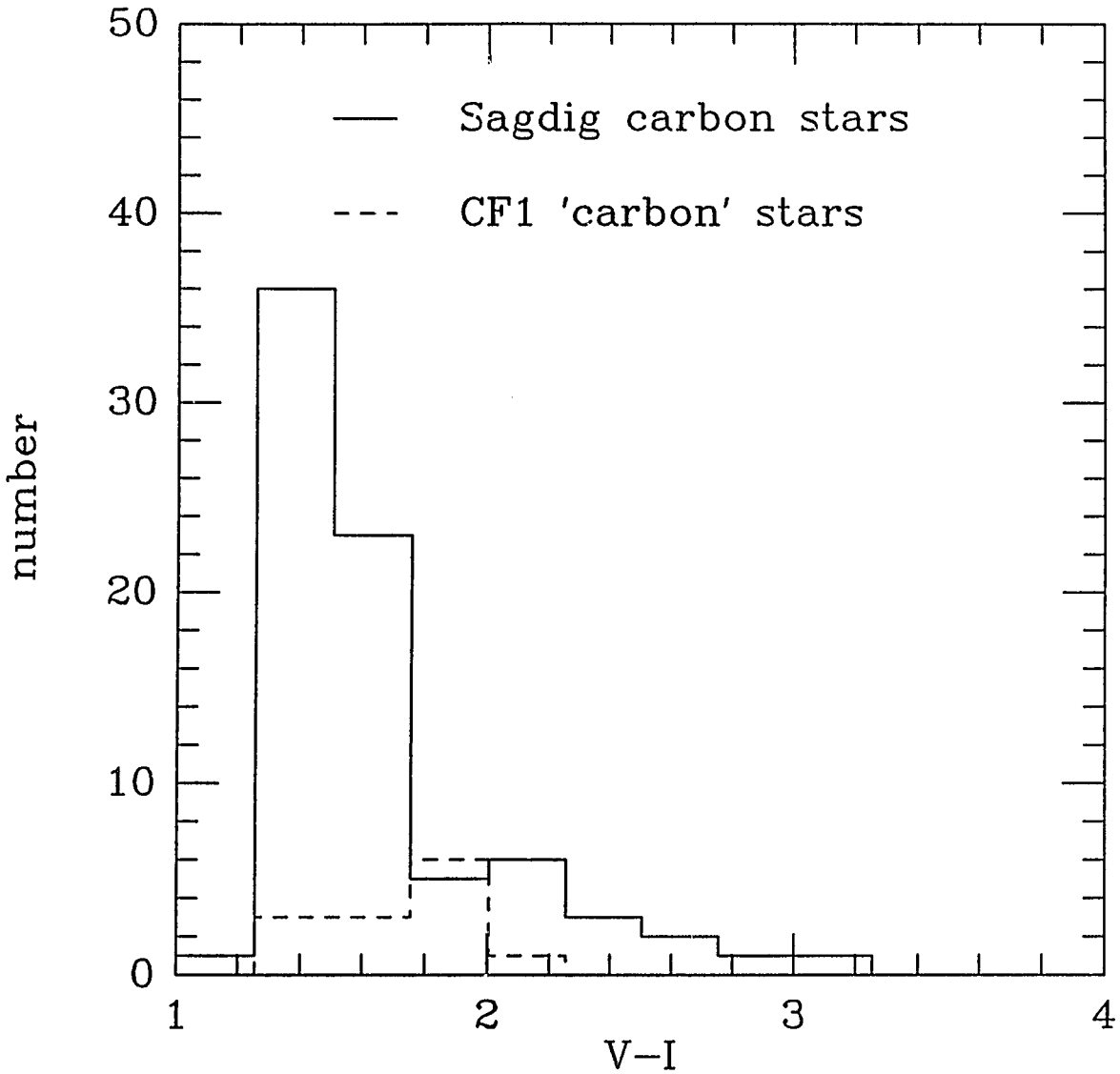

Figure 60. V−I Distribution of all Carbon Stars in Sagdig and CF1

The V−I distribution of all stars from the carbon star region of the color-color diagram for the Sagdig field (solid line) and from the CF1 field (dotted line).

metallicity population would produce brighter, redder carbon stars. A two population model could explain the peak in the carbon star luminosity function at I = 20. The lower luminosity population would correspond to the very base of the AGB, since an $M_I = 21$ gives an Mbol = −4. As Aaronson and Mould (1985) have pointed out, this seems to be the threshold for the production of carbon stars in the dwarf spheroidal companions of the Galaxy and there seems to be a tail which extends to $M_{bol} = -3$. If $M_{bol} = -4$ is correct for these stars then the AGB tip luminosity-age relation found by Aaronson and Mould (1985) in Cloud clusters suggests an age of about 10 Gyr. The redder carbon stars are about 1.5 mag brighter and the Cloud correlation would make these stars, in the mean, about 1 Gyr old. There is no reasonable way to estimate a metallicity for this system using the correlation found by Cook, Aaronson and Norris (1986) because AGB, M stars in Sagdig cannot be identified by this investigation because of the foreground contamination. It is clear that the C/M ratio cannot be significantly less than one or the AGB, M stars would be apparent in the corrected, luminosity function and they are not.

Distance

The giant branch tip and the brightest blue stars suggest that Sagdig has a distance modulus of about 25.5 and 25.3 respectively; the less certain, brightest red star calibration suggests a distance modulus of about 26; the carbon star luminosity function suggests a value of about 25. A simple average of the four methods yields 25.4 and I will adopt this value for the current discussion. This distance places Sagdig on the outer boundary of the

Local Group. Its radial velocity suggests that it could easily be bound to the Local Group following Yahil, Tammann and Sandage's (1977) kinematical analysis of the Local Group. Sagdig is a probable Local Group member.

Summary

Reddening toward Sagdig has been estimated to be $E(B-V) = 0.07$. This value comes from an analysis of field star colors and is roughly half that expected from the Burstein and Heiles maps. These maps are apparently of limited use so near the Galactic plane as demonstrated by this result and the factor of two underestimate of the reddening toward NGC 6822 (McAlary et al. 1983).

Sagdig has both red and blue supergiants so that this system has undergone relatively recent star formation. The apparent magnitudes of these stars suggest that Sagdig's distance modulus is between $(m-M)_0 = 25.4$ and $(m-M)_0 = 26$.

This dwarf galaxy is apparently more extended than the blue body of the galaxy. The red supergiants, and the carbon stars both extend well beyond the region containing the bright blue stars and the region of higher surface brightness on my CCD frames. Part of the larger body for Sagdig is a 'tail' like region which is well defined by a concentration of carbon stars.

If the late-type star distribution and the number of carbon stars point to a brighter parent galaxy luminosity, then the brightest star estimates of the distance would put the galaxy farther away. This would make the carbon stars more than a magnitude too bright compared to those found in the Magellanic Clouds. Of course there is considerable scatter in the brightest

star calibration and there is no reason to think that Sagdig should not add to this scatter.

The asymptotic giant branch population of this galaxy contains carbon stars. The luminosities of Sagidg's carbon stars suggest $(m-M)_0 = 25.6$ (using the Sandage and Carlson LMC modulus). The total number of carbon stars found in Sagdig is quite high for the parent galaxy's luminosity. These carbon stars appear to belong to two populations which are distinguished by color and luminosity. The existence of two distinct C star populations suggests distinct bursts of star formation in the intermediate past. The brighter, redder population of carbon stars most resembles that found in the Magellanic Clouds. The fainter, bluer population most resembles that found in the dwarf spheroidal companions of the Galaxy.

CHAPTER 5

CONCLUSIONS

The primary purpose of this dissertation was the establishment of a 77–81 system. This has been accomplished. The 77–81 system has been defined well enough to allow the direct comparison of data from diverse telescope-instrument combinations. The 77–81 system has three primary standards and these can be used in the future to establish a more comprehensive and accessible set of secondary standards. This system has proven to be capable of distinguishing carbon from M stars in an efficient manner.

The 77–81 colors of carbon stars clearly distinguish them from other types for V–I colors greater than about 1.6. For earlier carbon stars, there is an overlap of colors with K giants. This is due to the presence of cyanogen absorption in many K giants with normal carbon and oxygen abundances. The 77–81 color of a carbon star is reasonably correlated with its carbon abundance class as determined by Yamashita (1972). There is scatter in this relation which is presumably due to the effect of nitrogen abundance, as well as carbon abundance, on the cyanogen concentration in a star's atmosphere.

The 77–81 colors of M stars are well correlated with the M-types of Morgan and Keenan, and so with TiO band strength. From M-types 1.5 to about 6, there is a linear relation between 77–81 color and M-type. For earlier stars, the effect of the continuum slope on the 77–81 color and the

possibility of TiO and CN absorption in late K giants and early M giants renders typing with the 77−81 color less certain. For giants later than M7, there is, as yet, little data. There is a hint in the Baade's Window data that the 77−81 color may reach a maximum. This could be due to contamination of the 81 filter's passband with VO begining at about M7.

The 77−81 color is linearly related to the 7120Å TiO band strength for all ranges of band strength measured. This establishes the 77−81 color as a single-side-band TiO band strength. Because the 77−81 color is a true measure of the TiO band strength, it can be used in conjunction with a temperature indicator as a metallicity measure by analogy with the work of Mould and his collaborators (see Chapter 3). Because the 77−81 system uses broad band V and I colors to aid in the discrimination of late types, the V−I color was chosen as the temperature indicator. The metallicity calibration was shown to work by ranking field giants and seven globular clusters in a reasonable order of metal abundance. The 77−81 rankings are most closely correlated with the metallicity scale of Zinn and West (1984). The sensitivity of the calibration is such that a change of 0.1 mag in the color of the TiO track corresponds to a 0.5 dex change in [Fe/H]. Of course, to be applicable, there must be stars which are cool enough to exhibit TiO absorption which limits the use of the 77−81 metallicity measure to systems more metal rich than about [Fe/H] = −1.3. There is the need to calibrate the system for [Fe/H] > 0.

An examination of the Galaxy's bulge with the 77−81 system proved fruitfull. The mean metallicity of the M giants in Baade's Window was found to be about [Fe/H] = +0.3, if the metallicity calibration is valid

for [Fe/H] > 0. There is, however, considerable width to the bulge TiO track which suggests a range of metallicties which may extend to even higher metallicities. Very few of the M giants found in the bulge could be considered to have [Fe/H] < 0, but this does not directly relate to the relative numbers of stars in different metallicity ranges because of the smaller likelyhood of producing M giants in a metal poor population. No carbon stars were found in the 15 square arcmin field examined in Baade's Window. This means the C/M ratio for this population is smaller than 0.02 because more than 40 M giants were found in this field.

The 77–81 system was used to examine a recent addition to the list of probable Local Group galaxies—the dwarf irregular in Sagittarius (Sagdig). The investigation of Sagdig proved a challenge because of its low Galactic latitude. The estimation of foreground contamination toward Sagdig and the comparison of star counts in a control field with the Bachall and Soneira Galaxy model (1980) showed this model to seriously underestimate the number of stars fainter than $V \approx 21$. These data may provide support for the existence of a thick disk. A new method for the estimation of reddening toward well populated fields was created to measure the reddening toward Sagdig. Observationally, Galactic foreground contamination appears in a color-magnitude diagram as a strongly peaked ridge of stars with a mean, intrinsic color of about $V - I = 0.75$ which tails away to the red. The reddening toward Sagdig was estimated by dereddening the foreground stars' colors to produce this intrinsic color.

Sagdig was found to be similar to other resolved dwarf irregulars in that the presence of bright, blue stars is evidence of relatively recent star

formation. It also seems to contain red "supergiants" as do most other such dwarf irregulars. These bright red stars have a mean metallicity estimated by the 77–81 system to be about [Fe/H] = −0.5. There are AGB carbon stars in Sagdig which means that there has been star formation before the most recent burst but within about 10 Gyr. There is strong evidence that there are two populations of carbon stars in Sagdig. A redder, more luminous set of carbon stars is representative of more massive stars that are about 1 Gyr old. There is also a set of less luminous and bluer carbon stars which may represent a lower metallicity, less massive, population which is about 10 Gyr old. The total number of carbon stars in Sagdig is higher than would be expected from an extrapolation of the Blanco, McCarthy and Blanco (1980) study of the Magellanic Clouds unless this galaxy is two magnitudes brighter than its discoverers estimated. In this regard, it should be noted there is evidence that Sagdig is much more extended than previously thought. Both the carbon stars and the brightest red stars extend well beyond the body of the galaxy detailed by the discoverers.

Estimates of the distance modulus to Sagdig using the brightest star correlation with galaxy luminosity, the luminosity of the giant branch tip and the luminosity of the carbon stars all suggest that the modulus is $(m - M)_0 = 25.4$. If the distance modulus is greater than 26, then the carbon star luminosity distribution will present theorists with the longed for $M_{bol} = -7$ carbon star. The carbon star numbers and luminosity distribution can be reconciled only if the galaxy is much larger but not farther away. If Sagdig is much brighter, but not farther away, then the brightest star correlation with parent galaxy luminosity suffers.

There is much to be done now that the 77–81 system is a proven workhorse. The surface distribution of AGB stars in Local Group dwarf irregulars should be investigated. It will be important to discover whether variations in the AGB luminosity function across a galaxy such as that found by Reid and Mould (1984) in the LMC are typical of dwarf irregulars. The AGB population of all resolvable galaxies should be searched for the very luminous AGB stars which seem to be so rare in the populations investigated so far. The potential of the 77–81 system for the identification of S star candidates (Mould, Aaronson and Cook 1985) should be more fully developed. The characteristics of this supposed, transition object in systems of various metallicities and ages should help resolve some of the current theoretical questions about envelope burning and s-process element production (particularly in lower mass stars).

The AGB population of M31 and M33 as a function of distance from the nucleus should be determined. There is evidence for a radial metallicity gradient in both systems (Blair and Kirshner 1985). A 77–81 investigation will produce two types of data on the metallicity of the AGB populations within this gradient, the C/M ratio and a direct measure of the M star metallicities. These data will probe the metallicity gradient, if any, at the time of formation of the AGB stars. This may allow discrimination between the effect of a pre-existing gradient on AGB evolution and the effect of AGB evolution on the gradient. There is also ongoing research into the interstellar dust in M31 (Searle and Thompson 1987). Mass loss from cool AGB giants is a likely source for dust, and the dust composition should reflect the carbon to M star ratio. A correlation of variations in the reddening law through

M31 and the appropriate surface distribution of AGB stars will lead to a better understanding of the chemical evolution of stellar systems.

APPENDIX A

The following table presents the photometric data for the Baade's Window Field discussed in Chapter 3. This field is roughly centered on BMB's star 140 whose coordinates are $18^h00^m20.9^s, -29°59'19''$ (1950). This star is located at X = 143.6 and Y = 271.4 with an I magnitude of 12.40. The stars are listed in order of increasing I magnitude. The brightest star is the first entry in the left column, the second brightest star is the first entry in the right column, and so on. North is toward increasing X, east is toward increasing Y and the pixels are ≈ 0.59 arcsec in both X and Y. The positions presented in this appendix are for the I frame shown in Figure 24.

Baade's Window Photometry															
					Errors								Errors		
X	Y	I	V−I	77−81	I	V−I	77−81	X	Y	I	V−I	77−81	I	V−I	77−81
186.4	223.4	11.31	1.56	0.14	0.07	0.07	0.07	12.1	243.1	11.42	3.73	0.76	0.04	0.04	0.05
183.5	106.4	11.52	4.10	0.92	0.06	0.06	0.04	243.7	312.9	11.60	2.10	0.19	0.06	0.06	0.06
227.7	198.6	11.65	3.24	0.55	0.05	0.05	0.06	203.4	209.7	11.82	2.33	0.25	0.05	0.05	0.04
7.0	264.3	12.10	0.73	0.07	0.05	0.05	0.04	221.4	397.6	12.23	2.57	0.28	0.05	0.05	0.04
12.6	218.3	12.26	2.64	0.34	0.04	0.04	0.04	168.7	208.4	12.28	1.31	0.10	0.06	0.06	0.04
239.9	82.0	12.32	3.04	0.45	0.03	0.03	0.04	284.6	462.9	12.35	2.10	0.24	0.06	0.06	0.05
182.0	32.5	12.40	2.17	0.23	0.07	0.07	0.05	143.6	271.4	12.40	4.62	0.96	0.04	0.04	0.05
79.0	95.0	12.44	4.09	0.93	0.04	0.04	0.04	185.1	353.2	12.44	2.13	0.18	0.05	0.05	0.04
48.8	64.7	12.44	3.29	0.53	0.05	0.05	0.04	173.0	27.4	12.47	3.41	0.59	0.05	0.05	0.05
51.5	479.7	12.48	2.87	0.40	0.04	0.04	0.05	132.6	90.6	12.56	3.77	0.76	0.04	0.04	0.05
23.5	354.4	12.60	0.36	0.08	0.05	0.05	0.05	259.9	79.4	12.61	2.85	0.43	0.04	0.04	0.04
63.5	290.3	12.64	5.40	1.09	0.05	0.06	0.04	158.1	222.6	12.75	4.77	1.05	0.06	0.07	0.05
148.6	136.3	12.75	1.84	0.18	0.04	0.04	0.04	278.7	104.9	12.76	2.79	0.41	0.04	0.04	0.06
184.9	413.6	12.79	2.57	0.29	0.05	0.05	0.04	17.2	369.8	12.85	0.95	0.10	0.05	0.05	0.04
198.6	213.0	12.88	0.74	0.11	0.05	0.05	0.04	282.4	248.8	12.90	3.23	0.50	0.04	0.04	0.04
115.8	55.6	12.94	2.20	0.22	0.04	0.04	0.04	80.4	310.0	13.02	3.49	0.67	0.05	0.05	0.04
166.3	331.2	13.08	4.11	0.89	0.06	0.06	0.04	256.3	36.5	13.09	1.62	0.10	0.04	0.04	0.04
44.2	378.6	13.09	1.45	0.12	0.04	0.04	0.04	129.8	454.2	13.10	2.83	0.42	0.05	0.05	0.04
96.0	261.8	13.10	2.75	0.34	0.05	0.05	0.04	271.3	355.4	13.13	1.61	0.09	0.08	0.08	0.05

Baade's Window Photometry (continued)

					Errors								Errors		
X	Y	I	V−I	77−81	I	V−I	77−81	X	Y	I	V−I	77−81	I	V−I	77−81
75.4	212.9	13.14	2.35	0.25	0.06	0.06	0.04	166.4	379.1	13.15	2.37	0.24	0.04	0.04	0.06
217.9	398.7	13.20	1.91	0.17	0.05	0.05	0.05	168.9	149.3	13.20	1.58	0.17	0.04	0.04	0.04
210.3	128.6	13.20	2.28	0.21	0.05	0.05	0.04	248.2	473.7	13.21	2.65	0.31	0.05	0.05	0.07
107.1	286.2	13.22	0.63	0.12	0.06	0.06	0.04	193.2	164.3	13.24	1.90	0.19	0.05	0.05	0.04
74.0	397.9	13.24	2.17	0.20	0.05	0.05	0.04	120.6	20.1	13.25	2.74	0.35	0.04	0.04	0.04
288.7	353.5	13.27	2.79	0.35	0.04	0.04	0.06	252.3	418.8	13.27	2.01	0.18	0.06	0.06	0.08
16.4	86.9	13.28	2.08	0.17	0.04	0.04	0.04	164.5	159.6	13.30	2.80	0.30	0.05	0.05	0.05
24.9	334.0	13.32	2.05	0.21	0.04	0.04	0.04	32.5	128.7	13.33	0.89	0.09	0.04	0.04	0.04
29.4	150.8	13.35	2.04	0.17	0.04	0.04	0.04	152.3	209.7	13.37	1.92	0.16	0.04	0.04	0.04
80.0	406.1	13.38	2.14	0.19	0.04	0.04	0.04	244.1	272.9	13.39	1.72	0.19	0.06	0.06	0.04
288.7	361.4	13.45	2.79	0.37	0.04	0.04	0.05	267.0	79.9	13.51	2.55	0.28	0.05	0.05	0.04
165.8	481.2	13.51	2.23	0.22	0.04	0.04	0.05	21.1	260.2	13.52	1.26	0.12	0.05	0.05	0.04
15.3	255.8	13.53	1.65	0.18	0.05	0.05	0.05	60.0	317.1	13.57	2.12	0.20	0.03	0.03	0.04
107.3	410.1	13.59	1.65	0.16	0.04	0.04	0.04	116.2	113.2	13.59	1.71	0.17	0.04	0.04	0.04
289.7	265.6	13.62	2.15	0.19	0.04	0.04	0.05	224.6	188.3	13.62	2.01	0.19	0.06	0.06	0.04
262.0	9.6	13.63	1.61	0.14	0.05	0.05	0.06	74.2	449.3	13.65	1.87	0.18	0.05	0.05	0.05
145.2	428.8	13.66	2.04	0.17	0.04	0.04	0.05	225.4	23.3	13.69	2.46	0.22	0.06	0.06	0.04
44.8	497.5	13.71	1.51	0.15	0.05	0.05	0.05	225.8	411.0	13.71	1.58	0.13	0.05	0.05	0.04
222.7	89.4	13.72	1.76	0.17	0.05	0.05	0.04	223.3	120.0	13.72	1.68	0.11	0.04	0.04	0.04
183.5	52.8	13.73	1.59	0.12	0.06	0.06	0.05	285.0	163.9	13.74	1.88	0.22	0.04	0.04	0.05
148.4	312.1	13.77	1.92	0.13	0.04	0.04	0.03	87.6	100.6	13.77	1.82	0.17	0.05	0.05	0.04
143.7	235.8	13.78	2.00	0.16	0.05	0.05	0.05	80.4	17.9	13.79	2.29	0.20	0.04	0.04	0.04
227.3	259.8	13.81	1.88	0.16	0.04	0.04	0.05	91.8	233.7	13.82	1.98	0.15	0.04	0.04	0.04
189.9	65.1	13.84	1.66	0.15	0.04	0.04	0.04	290.9	60.8	13.85	2.14	0.18	0.04	0.04	0.05
3.7	120.1	13.86	2.08	0.17	0.05	0.05	0.04	255.4	323.6	13.88	1.65	0.14	0.08	0.09	0.08
209.9	135.4	13.89	1.74	0.14	0.04	0.04	0.05	36.1	196.3	13.90	2.29	0.19	0.04	0.04	0.04
124.8	139.8	13.91	1.71	0.11	0.06	0.06	0.04	48.8	382.4	13.91	1.89	0.14	0.04	0.04	0.04
248.3	243.5	13.92	1.87	0.17	0.05	0.05	0.04	248.6	183.4	13.93	2.18	0.18	0.06	0.06	0.04
65.9	438.6	13.94	1.51	0.15	0.05	0.05	0.06	180.7	297.3	13.95	1.90	0.14	0.06	0.06	0.04
233.2	285.7	13.97	0.90	0.13	0.05	0.05	0.04	279.9	449.0	13.98	1.72	0.14	0.06	0.06	0.05
239.5	22.3	13.98	2.12	0.16	0.04	0.04	0.04	245.4	459.7	13.99	1.88	0.18	0.06	0.06	0.05
59.3	147.3	13.99	1.28	0.13	0.04	0.04	0.04	208.6	379.7	14.02	2.09	0.15	0.05	0.05	0.03
76.0	172.8	14.03	1.73	0.17	0.04	0.04	0.04	126.1	285.6	14.04	1.36	0.14	0.05	0.05	0.04
216.2	423.5	14.06	1.87	0.15	0.06	0.06	0.05	283.8	251.9	14.08	1.78	0.17	0.04	0.04	0.04
233.1	33.5	14.09	1.96	0.18	0.05	0.05	0.04	277.5	457.6	14.09	1.68	0.17	0.06	0.06	0.05
113.3	155.7	14.10	1.83	0.16	0.04	0.04	0.05	69.4	190.3	14.10	1.90	0.17	0.04	0.04	0.04
55.7	463.0	14.11	1.80	0.17	0.04	0.04	0.05	195.2	489.9	14.13	2.13	0.20	0.04	0.04	0.06
243.3	98.7	14.13	2.21	0.15	0.03	0.03	0.04	67.9	499.3	14.13	2.13	0.20	0.06	0.06	0.04
96.2	491.6	14.14	1.70	0.20	0.07	0.07	0.06	224.0	276.3	14.15	1.96	0.17	0.03	0.03	0.04
67.1	29.1	14.15	2.08	0.17	0.04	0.04	0.04	17.5	99.6	14.15	2.27	0.21	0.05	0.05	0.05
221.1	45.7	14.17	2.69	0.29	0.04	0.04	0.05	90.9	206.2	14.18	1.06	0.12	0.04	0.04	0.04
19.8	410.7	14.19	1.49	0.17	0.05	0.05	0.04	181.8	230.2	14.23	1.41	0.15	0.06	0.08	0.06
66.1	310.7	14.23	2.29	0.21	0.05	0.05	0.04	112.0	259.5	14.24	2.15	0.18	0.05	0.05	0.06
32.3	87.2	14.24	0.92	0.09	0.05	0.05	0.03	157.2	466.7	14.25	2.01	0.17	0.05	0.05	0.05

Baade's Window Photometry (continued)

					Errors								Errors		
X	Y	I	V−I	77−81	I	V−I	77−81	X	Y	I	V−I	77−81	I	V−I	77−81
33.3	219.7	14.26	2.22	0.22	0.05	0.05	0.06	153.5	135.1	14.27	2.26	0.21	0.04	0.04	0.04
39.2	460.9	14.32	1.80	0.21	0.05	0.05	0.04	130.2	309.4	14.34	2.21	0.18	0.04	0.04	0.05
14.6	168.0	14.35	1.54	0.15	0.05	0.05	0.04	90.9	412.4	14.36	1.75	0.16	0.05	0.05	0.04
32.3	298.5	14.36	2.12	0.19	0.05	0.05	0.04	265.3	499.2	14.38	2.10	0.17	0.06	0.06	0.06
194.5	61.2	14.38	1.73	0.16	0.04	0.04	0.05	53.2	338.8	14.39	0.89	0.09	0.05	0.05	0.05
143.3	48.6	14.40	1.73	0.13	0.04	0.04	0.04	230.3	203.9	14.40	1.46	0.14	0.05	0.05	0.07
23.5	280.5	14.42	1.98	0.14	0.07	0.07	0.04	274.3	19.4	14.42	0.77	0.08	0.06	0.06	0.05
212.3	56.3	14.43	2.14	0.14	0.05	0.05	0.04	244.6	432.5	14.43	1.75	0.15	0.05	0.05	0.05
213.4	204.6	14.45	2.05	0.14	0.06	0.06	0.06	63.5	164.8	14.45	1.86	0.14	0.05	0.05	0.05
109.8	240.3	14.45	1.65	0.17	0.05	0.05	0.04	170.0	23.9	14.45	1.82	0.20	0.05	0.05	0.05
51.3	265.1	14.46	1.93	0.14	0.05	0.05	0.04	144.0	490.0	14.47	0.97	0.16	0.04	0.04	0.05
78.9	336.1	14.48	2.27	0.21	0.04	0.04	0.04	110.8	399.2	14.48	1.77	0.18	0.05	0.05	0.04
7.8	225.2	14.49	1.75	0.17	0.04	0.04	0.04	267.2	207.7	14.50	2.39	0.25	0.05	0.09	0.05
126.5	334.7	14.50	2.07	0.12	0.06	0.06	0.06	28.2	410.9	14.51	1.54	0.18	0.05	0.05	0.04
266.6	181.9	14.52	1.45	0.14	0.03	0.03	0.05	274.5	420.1	14.52	1.91	0.17	0.06	0.06	0.06
205.9	114.6	14.54	1.96	0.19	0.05	0.05	0.05	25.7	504.4	14.54	1.71	0.19	0.06	0.06	0.04
179.6	94.4	14.55	1.82	0.14	0.06	0.06	0.04	128.8	162.6	14.55	2.17	0.19	0.04	0.04	0.04
200.2	335.3	14.58	1.05	0.34	0.06	0.06	0.08	244.1	118.6	14.60	1.81	0.24	0.05	0.05	0.06
135.1	353.6	14.60	1.58	0.14	0.08	0.08	0.06	157.3	397.7	14.61	2.14	0.18	0.04	0.04	0.05
169.0	285.0	14.61	1.64	0.11	0.05	0.05	0.04	151.9	172.0	14.62	1.71	0.14	0.05	0.05	0.04
282.2	262.2	14.62	2.09	0.16	0.06	0.06	0.05	249.2	157.9	14.62	1.67	0.19	0.06	0.06	0.05
11.3	316.7	14.63	1.59	0.23	0.05	0.05	0.06	95.3	231.0	14.64	1.93	0.14	0.04	0.04	0.04
292.9	451.2	14.64	1.54	0.19	0.07	0.07	0.06	215.7	320.8	14.64	1.76	0.18	0.05	0.05	0.04
159.6	436.1	14.66	1.70	0.17	0.05	0.05	0.05	244.6	463.0	14.67	1.52	0.18	0.06	0.06	0.05
261.2	83.2	14.67	1.62	0.16	0.04	0.04	0.04	252.7	141.8	14.67	1.79	0.13	0.04	0.04	0.04
219.5	361.9	14.67	0.83	0.07	0.06	0.06	0.05	182.1	62.1	14.67	1.59	0.15	0.04	0.04	0.04
236.7	84.3	14.68	1.83	0.16	0.04	0.04	0.04	159.8	372.7	14.68	1.64	0.16	0.05	0.05	0.05
51.7	76.0	14.69	1.56	0.14	0.05	0.05	0.05	3.7	233.0	14.69	1.59	0.13	0.04	0.04	0.04
50.6	183.2	14.70	0.88	0.10	0.05	0.05	0.04	127.6	267.4	14.70	1.84	0.16	0.06	0.06	0.05
218.9	368.2	14.72	0.98	0.11	0.05	0.05	0.05	110.4	79.8	14.72	2.28	0.23	0.05	0.05	0.04
294.0	481.9	14.72	1.82	0.17	0.05	0.05	0.06	170.0	338.3	14.72	1.84	0.14	0.05	0.05	0.05
72.9	196.1	14.72	1.70	0.12	0.04	0.04	0.04	170.5	295.4	14.72	1.75	0.10	0.05	0.05	0.04
70.6	84.7	14.73	1.87	0.16	0.05	0.05	0.04	103.3	401.8	14.74	1.84	0.12	0.05	0.05	0.04
95.4	505.1	14.74	1.51	0.22	0.05	0.05	0.08	105.9	243.2	14.75	1.79	0.11	0.05	0.05	0.04
76.8	124.7	14.76	1.52	0.14	0.04	0.04	0.04	70.3	254.2	14.76	1.69	0.12	0.06	0.06	0.04
117.7	400.6	14.76	1.58	0.16	0.05	0.05	0.05	227.3	235.2	14.76	1.67	0.13	0.05	0.05	0.04
292.8	42.4	14.77	1.76	0.17	0.04	0.04	0.04	19.6	255.4	14.78	1.55	0.16	0.06	0.07	0.05
221.7	500.1	14.78	1.88	0.14	0.07	0.07	0.08	73.9	224.4	14.79	1.69	0.16	0.05	0.05	0.05
290.5	355.8	14.79	1.56	0.16	0.06	0.06	0.08	102.6	282.9	14.79	0.92	0.12	0.06	0.06	0.04
96.0	400.7	14.80	1.52	0.13	0.04	0.04	0.04	82.8	406.3	14.80	1.53	0.19	0.05	0.05	0.04
93.3	67.8	14.81	1.86	0.17	0.05	0.06	0.05	87.2	301.9	14.82	1.80	0.10	0.04	0.05	0.04
216.0	413.1	14.82	1.68	0.09	0.05	0.07	0.04	136.7	25.9	14.83	1.75	0.11	0.05	0.05	0.05
110.3	199.6	14.83	1.65	0.15	0.05	0.06	0.05	270.8	222.3	14.84	1.67	0.15	0.04	0.04	0.06
178.1	171.9	14.84	1.82	0.14	0.04	0.04	0.04	190.1	67.7	14.84	1.40	0.12	0.05	0.05	0.05

Baade's Window Photometry (continued)

					Errors								Errors		
X	Y	I	V−I	77−81	I	V−I	77−81	X	Y	I	V−I	77−81	I	V−I	77−81
244.3	75.9	14.85	1.54	0.13	0.04	0.04	0.05	5.3	319.6	14.85	1.82	0.16	0.05	0.06	0.06
41.5	221.8	14.85	1.52	0.15	0.05	0.05	0.06	185.0	308.1	14.85	2.06	0.13	0.05	0.05	0.04
110.2	169.8	14.85	0.92	0.12	0.04	0.04	0.04	199.8	31.5	14.85	1.48	0.15	0.04	0.04	0.04
137.5	237.3	14.86	0.84	0.10	0.05	0.05	0.05	60.1	222.2	14.87	1.74	0.11	0.04	0.04	0.05
92.1	65.1	14.87	1.58	0.15	0.05	0.05	0.04	168.1	362.6	14.87	1.54	0.14	0.05	0.05	0.05
246.9	323.9	14.87	1.81	0.11	0.05	0.05	0.06	28.1	429.2	14.88	1.63	0.16	0.04	0.04	0.04
195.7	263.0	14.88	0.89	0.15	0.05	0.05	0.05	224.3	65.8	14.88	1.71	0.14	0.05	0.05	0.06
115.9	502.5	14.89	1.91	0.10	0.05	0.05	0.05	61.3	429.0	14.89	1.73	0.12	0.04	0.04	0.04
291.9	90.2	14.91	1.46	0.14	0.04	0.05	0.04	114.0	127.4	14.91	1.70	0.12	0.06	0.06	0.06
198.2	146.6	14.91	0.99	0.12	0.04	0.04	0.04	129.2	346.2	14.91	0.88	0.10	0.05	0.05	0.04
22.3	156.6	14.92	1.59	0.16	0.05	0.05	0.04	103.4	405.0	14.92	1.50	0.19	0.05	0.05	0.04
233.2	382.8	14.92	1.80	0.11	0.05	0.05	0.06	59.4	141.0	14.93	1.81	0.11	0.05	0.05	0.04
289.5	25.1	14.93	1.63	0.14	0.03	0.03	0.05	199.4	239.8	14.93	1.69	0.20	0.05	0.05	0.07
17.1	241.6	14.94	1.91	0.17	0.06	0.06	0.06	232.6	203.1	14.94	2.02	0.16	0.06	0.07	0.09
122.8	246.2	14.94	1.53	0.20	0.05	0.05	0.04	41.0	320.9	14.95	1.51	0.15	0.04	0.04	0.04
234.3	26.5	14.95	1.91	0.14	0.08	0.08	0.04	172.9	367.9	14.96	1.72	0.11	0.04	0.05	0.05
167.6	189.8	14.96	1.74	0.10	0.04	0.04	0.05	293.5	172.9	14.96	1.75	0.12	0.05	0.05	0.05
246.1	172.9	14.97	1.68	0.18	0.05	0.05	0.06	18.4	366.1	14.98	1.49	0.15	0.05	0.05	0.05
39.8	361.8	14.98	1.49	0.15	0.06	0.06	0.04	156.8	367.4	14.98	1.46	0.17	0.05	0.05	0.04
90.2	186.4	14.98	1.60	0.18	0.05	0.05	0.04	94.8	210.9	14.98	1.83	0.12	0.05	0.05	0.04
96.0	463.3	14.98	1.43	0.16	0.05	0.05	0.05	249.4	15.7	14.99	1.65	0.09	0.05	0.05	0.05
228.2	90.6	15.00	1.68	0.15	0.05	0.05	0.04	185.5	176.5	15.00	1.76	0.08	0.08	0.08	0.04
68.4	384.4	15.00	1.79	0.11	0.07	0.07	0.05	221.4	335.2	15.00	1.71	0.14	0.07	0.07	0.04
71.3	204.2	15.01	2.13	0.18	0.04	0.04	0.04	235.2	397.3	15.01	1.57	0.15	0.06	0.06	0.06
28.7	21.0	15.01	1.79	0.15	0.04	0.06	0.05	205.3	409.6	15.01	1.51	0.14	0.07	0.09	0.06
173.9	291.2	15.01	0.93	0.11	0.04	0.04	0.04	145.6	247.9	15.01	1.73	0.15	0.06	0.06	0.06
124.9	290.2	15.01	1.52	0.16	0.05	0.05	0.06	78.4	331.4	15.01	1.67	0.14	0.05	0.05	0.04
175.6	474.2	15.02	1.82	0.19	0.07	0.07	0.05	65.0	428.2	15.02	1.75	0.12	0.04	0.04	0.05
139.9	303.8	15.02	1.60	0.15	0.04	0.04	0.04	29.6	327.1	15.02	1.78	0.13	0.05	0.05	0.05
145.7	500.1	15.02	1.66	0.11	0.05	0.05	0.06	223.2	39.3	15.02	1.85	0.10	0.05	0.05	0.04
52.7	359.8	15.02	1.62	0.16	0.05	0.05	0.05	16.4	43.4	15.03	1.72	0.14	0.05	0.05	0.04
157.9	327.8	15.03	1.81	0.15	0.05	0.05	0.05	286.2	308.6	15.03	1.70	0.14	0.06	0.06	0.07
61.8	146.8	15.03	1.76	0.22	0.05	0.06	0.07	76.9	70.5	15.03	2.10	0.13	0.05	0.05	0.04
238.3	209.9	15.04	1.91	0.14	0.06	0.06	0.05	107.4	211.4	15.04	1.80	0.15	0.05	0.05	0.04
195.8	102.6	15.04	1.96	0.17	0.07	0.07	0.05	178.6	177.3	15.04	1.92	0.13	0.05	0.05	0.04
70.5	389.9	15.05	0.94	0.09	0.06	0.06	0.06	192.5	98.6	15.05	1.71	0.13	0.08	0.08	0.04
239.8	186.0	15.05	1.85	0.17	0.05	0.06	0.06	247.4	264.9	15.06	1.90	0.10	0.06	0.06	0.05
156.9	104.6	15.06	0.95	0.11	0.05	0.05	0.05	38.4	182.4	15.06	1.72	0.17	0.05	0.05	0.05
50.9	293.4	15.06	1.64	0.14	0.05	0.05	0.06	118.1	34.0	15.07	1.89	0.13	0.04	0.04	0.05
207.0	188.4	15.07	1.84	0.13	0.05	0.05	0.06	17.3	143.7	15.08	1.76	0.27	0.08	0.09	0.06
164.8	397.0	15.08	1.51	0.16	0.05	0.05	0.04	136.0	333.3	15.09	1.64	0.17	0.05	0.06	0.06
249.6	445.4	15.09	1.39	0.13	0.07	0.07	0.05	38.9	97.4	15.10	1.35	0.16	0.05	0.05	0.04
196.1	439.5	15.10	1.67	0.14	0.05	0.05	0.06	195.8	40.0	15.10	1.66	0.13	0.05	0.05	0.04
235.5	338.2	15.11	1.72	0.12	0.07	0.09	0.06	29.9	244.3	15.11	1.48	0.20	0.05	0.05	0.05

Baade's Window Photometry (continued)																	
					Errors								Errors				
X	Y	I	V−I	77−81	I	V−I	77−81	X	Y	I	V−I	77−81	I	V−I	77−81
52.6	420.5	15.12	1.83	0.12	0.05	0.05	0.06	46.9	151.7	15.12	1.96	0.18	0.04	0.04	0.04
297.3	458.9	15.12	0.87	0.11	0.07	0.07	0.06	271.6	40.3	15.12	1.71	0.09	0.06	0.06	0.05
238.1	456.8	15.13	1.56	0.12	0.07	0.07	0.09	140.4	119.3	15.13	1.57	0.14	0.05	0.05	0.05
107.2	113.7	15.13	1.07	0.08	0.05	0.05	0.04	148.5	5.7	15.13	1.75	0.06	0.05	0.05	0.05
135.6	430.3	15.14	1.81	0.15	0.08	0.08	0.05	129.7	373.1	15.14	1.60	0.12	0.06	0.07	0.06
39.2	175.4	15.14	1.65	0.16	0.05	0.05	0.05	138.0	341.5	15.14	1.82	0.09	0.06	0.06	0.05
142.6	248.6	15.14	1.63	0.11	0.06	0.06	0.06	181.1	385.1	15.14	1.73	0.11	0.05	0.05	0.04
191.6	342.7	15.15	1.63	0.12	0.06	0.06	0.06	48.6	203.6	15.15	2.04	0.13	0.05	0.05	0.05
28.7	155.7	15.15	1.84	0.13	0.04	0.04	0.04	149.1	470.3	15.15	1.69	0.16	0.05	0.05	0.05
9.9	213.5	15.15	0.94	0.16	0.05	0.05	0.05	224.3	472.2	15.15	1.72	0.10	0.06	0.06	0.06
114.2	361.8	15.15	1.64	0.17	0.06	0.06	0.07	100.3	280.4	15.16	1.60	0.11	0.06	0.07	0.05
287.0	99.2	15.16	1.68	0.12	0.05	0.05	0.06	91.6	73.7	15.16	1.85	0.14	0.04	0.04	0.05
13.7	184.1	15.16	1.63	0.17	0.05	0.06	0.05	205.8	280.4	15.16	2.10	0.16	0.05	0.07	0.05
147.8	31.5	15.16	1.67	0.16	0.04	0.04	0.05	220.9	256.3	15.16	1.73	0.13	0.04	0.04	0.05
131.0	183.9	15.17	1.52	0.17	0.05	0.05	0.08	200.3	298.2	15.17	1.43	0.17	0.05	0.05	0.05
164.6	356.0	15.17	1.59	0.09	0.06	0.06	0.06	191.9	90.8	15.18	1.93	0.16	0.05	0.05	0.05
206.1	385.5	15.18	1.63	0.15	0.06	0.06	0.06	69.5	13.8	15.18	1.79	0.08	0.04	0.04	0.04
56.9	39.5	15.18	1.62	0.12	0.06	0.06	0.08	48.7	191.7	15.18	1.52	0.15	0.04	0.04	0.05
270.9	227.7	15.18	1.11	0.16	0.04	0.04	0.06	6.7	468.9	15.19	1.59	0.24	0.05	0.06	0.06
116.7	320.5	15.19	1.52	0.17	0.05	0.05	0.05	104.5	229.9	15.19	1.03	0.12	0.05	0.05	0.04
94.2	368.9	15.19	1.36	0.18	0.05	0.05	0.06	166.3	270.4	15.19	1.70	0.12	0.05	0.06	0.04
73.8	287.0	15.19	1.49	0.19	0.05	0.05	0.06	160.5	350.3	15.20	1.63	0.16	0.05	0.05	0.05
130.7	11.6	15.20	1.80	0.24	0.06	0.07	0.07	201.5	309.4	15.20	1.56	0.14	0.06	0.06	0.05
83.9	298.4	15.20	1.68	0.11	0.04	0.04	0.04	103.7	133.8	15.20	1.37	0.15	0.05	0.05	0.05
160.8	185.2	15.21	0.89	0.12	0.05	0.05	0.06	171.1	305.2	15.21	1.80	0.11	0.04	0.04	0.05
167.6	255.6	15.21	1.67	0.09	0.08	0.08	0.06	97.5	422.3	15.22	1.55	0.15	0.05	0.05	0.06
15.4	409.0	15.22	1.77	0.12	0.05	0.05	0.04	246.5	81.5	15.22	1.55	0.15	0.04	0.04	0.04
175.6	274.9	15.23	1.75	0.14	0.04	0.04	0.04	268.5	310.9	15.23	1.88	0.13	0.05	0.05	0.06
220.2	474.2	15.23	1.95	0.13	0.06	0.06	0.06	31.1	84.9	15.23	1.97	0.15	0.06	0.07	0.04
49.6	53.5	15.23	1.85	0.11	0.05	0.05	0.04	43.6	411.8	15.23	1.47	0.09	0.05	0.05	0.05
193.4	295.8	15.24	1.69	0.16	0.05	0.05	0.05	45.8	326.4	15.24	1.62	0.14	0.04	0.04	0.04
111.6	134.6	15.24	1.73	0.09	0.05	0.05	0.06	245.7	451.0	15.25	0.95	0.08	0.07	0.07	0.07
293.7	85.1	15.25	1.38	0.23	0.05	0.06	0.04	164.7	348.6	15.25	1.18	0.07	0.05	0.05	0.06
59.1	436.9	15.26	1.39	0.17	0.05	0.05	0.05	148.3	112.0	15.26	1.73	0.03	0.05	0.05	0.05
170.1	133.7	15.26	1.68	0.21	0.05	0.05	0.05	32.8	427.0	15.26	1.33	0.17	0.04	0.04	0.04
90.2	116.9	15.27	1.65	0.14	0.07	0.08	0.08	228.3	119.2	15.27	1.61	0.18	0.04	0.04	0.04
26.5	160.2	15.27	0.88	0.10	0.04	0.04	0.04	177.1	160.1	15.27	1.65	0.14	0.04	0.04	0.05
239.5	343.6	15.27	1.63	0.14	0.06	0.06	0.06	65.3	183.6	15.28	1.84	0.15	0.05	0.05	0.04
42.5	37.7	15.28	1.90	0.13	0.05	0.05	0.05	61.5	479.0	15.28	0.97	0.11	0.05	0.05	0.06
35.6	222.6	15.29	1.72	0.18	0.06	0.06	0.06	204.0	56.1	15.30	1.89	0.14	0.05	0.05	0.05
282.1	243.3	15.30	1.79	0.19	0.05	0.06	0.04	98.8	214.5	15.30	1.73	0.08	0.04	0.04	0.04
111.9	10.9	15.31	1.78	0.17	0.05	0.06	0.06	226.0	64.2	15.31	1.71	0.19	0.05	0.06	0.07
291.8	438.5	15.31	1.81	0.17	0.08	0.08	0.06	290.6	397.4	15.31	1.58	0.13	0.07	0.07	0.06
105.9	232.3	15.31	1.54	0.18	0.05	0.05	0.04	38.1	493.5	15.31	1.56	0.19	0.05	0.05	0.06

Baade's Window Photometry (continued)																
					Errors								Errors			
X	Y	I	V−I	77−81	I	V−I	77−81	X	Y	I	V−I	77−81	I	V−I	77−81
26.4	36.7	15.31	1.61	0.12	0.05	0.05	0.05	115.1	67.7	15.31	1.01	0.08	0.06	0.06	0.06
209.0	215.6	15.31	1.45	0.13	0.05	0.06	0.06	163.7	445.8	15.31	1.45	0.16	0.04	0.04	0.04
52.3	99.6	15.32	1.56	0.16	0.07	0.07	0.04	125.5	260.7	15.32	1.78	0.09	0.07	0.07	0.06
16.9	324.9	15.33	1.62	0.11	0.04	0.04	0.05	106.8	33.8	15.33	1.57	0.17	0.05	0.05	0.07
244.7	429.3	15.34	1.56	0.14	0.05	0.05	0.05	19.8	236.9	15.34	1.08	0.20	0.06	0.06	0.06
72.9	337.0	15.35	1.74	0.10	0.05	0.06	0.04	287.7	481.5	15.35	1.76	0.21	0.06	0.07	0.06
287.5	22.6	15.36	1.44	0.10	0.04	0.04	0.05	117.8	298.8	15.36	1.55	0.13	0.04	0.04	0.04
206.5	437.8	15.36	1.19	0.11	0.05	0.05	0.06	226.8	211.7	15.36	1.75	0.22	0.06	0.07	0.08
147.2	352.3	15.36	1.66	0.12	0.07	0.07	0.07	27.1	100.2	15.37	1.90	0.24	0.05	0.05	0.05
146.1	312.3	15.37	1.83	0.14	0.07	0.10	0.07	296.4	232.6	15.38	1.51	0.08	0.06	0.06	0.06
59.2	399.6	15.38	1.49	0.13	0.05	0.05	0.05	57.1	328.6	15.38	1.34	0.11	0.04	0.04	0.06
91.6	281.5	15.39	1.54	0.16	0.05	0.05	0.06	149.8	48.2	15.40	1.91	0.12	0.04	0.04	0.04
164.8	238.5	15.40	1.82	0.13	0.06	0.06	0.05	132.4	298.2	15.40	1.56	0.19	0.05	0.08	0.05
204.0	405.1	15.40	1.66	0.01	0.07	0.10	0.07	172.2	449.6	15.41	1.71	0.13	0.07	0.07	0.06
215.7	430.4	15.41	1.85	0.10	0.06	0.06	0.06	262.1	185.2	15.41	1.66	0.05	0.04	0.05	0.06
173.6	130.8	15.42	1.86	0.13	0.05	0.05	0.05	180.3	203.3	15.42	1.82	0.15	0.07	0.09	0.05
250.4	296.8	15.43	1.10	0.14	0.08	0.08	0.06	104.2	443.6	15.43	1.65	0.09	0.05	0.06	0.05
60.0	474.8	15.43	1.77	0.10	0.04	0.04	0.06	59.1	46.5	15.43	1.65	0.08	0.06	0.06	0.07
162.9	229.0	15.44	1.55	0.20	0.05	0.06	0.05	145.6	5.3	15.44	1.76	0.07	0.06	0.07	0.05
78.4	256.8	15.45	1.90	0.09	0.07	0.08	0.05	32.9	67.1	15.47	1.57	0.15	0.06	0.06	0.05
174.5	401.7	15.48	1.24	0.14	0.05	0.05	0.06	130.0	408.7	15.48	1.66	0.14	0.05	0.05	0.06
6.9	233.8	15.49	1.60	0.14	0.04	0.05	0.04	71.6	282.4	15.49	1.65	0.10	0.05	0.06	0.06
245.1	12.7	15.49	1.10	0.13	0.05	0.05	0.04	139.7	258.0	15.50	1.91	0.17	0.05	0.05	0.06
201.4	277.3	15.50	1.84	0.16	0.05	0.05	0.05	233.7	368.7	15.50	1.67	0.09	0.06	0.07	0.06
193.9	388.7	15.50	1.74	0.17	0.06	0.07	0.06	150.7	449.3	15.51	1.17	0.16	0.06	0.06	0.05
134.0	141.5	15.51	1.78	0.11	0.05	0.06	0.04	22.3	294.1	15.52	1.55	0.17	0.06	0.06	0.06
158.2	303.0	15.52	1.62	0.10	0.05	0.05	0.06	235.4	394.4	15.53	1.90	0.13	0.06	0.07	0.07
193.1	256.7	15.53	1.69	0.16	0.05	0.05	0.05	72.6	50.3	15.53	1.56	0.12	0.06	0.06	0.04
59.8	206.9	15.54	1.76	0.08	0.05	0.05	0.06	217.3	453.6	15.55	1.77	0.12	0.07	0.08	0.07
162.9	112.1	15.56	1.68	0.13	0.04	0.05	0.06	233.9	139.1	15.56	1.73	0.13	0.04	0.04	0.05
165.9	427.8	15.56	1.70	0.14	0.05	0.06	0.06	216.0	247.2	15.56	1.93	0.15	0.05	0.06	0.07
267.4	146.7	15.56	1.72	0.11	0.05	0.05	0.06	234.5	481.6	15.56	1.69	0.13	0.07	0.08	0.08
36.2	283.5	15.57	1.64	0.13	0.05	0.05	0.05	108.6	388.7	15.57	1.83	0.12	0.07	0.07	0.06
279.0	122.8	15.57	1.85	0.13	0.04	0.05	0.05	143.8	305.2	15.57	1.60	0.10	0.05	0.06	0.05
289.3	75.0	15.57	1.52	0.14	0.07	0.08	0.05	156.5	241.5	15.57	1.66	0.12	0.06	0.06	0.06
190.1	121.7	15.57	1.94	0.13	0.05	0.06	0.05	232.1	379.8	15.58	1.59	0.12	0.05	0.06	0.06
24.7	455.9	15.58	1.61	0.16	0.05	0.05	0.06	173.0	101.4	15.58	1.52	0.17	0.06	0.06	0.06
68.5	4.7	15.59	1.77	0.14	0.04	0.05	0.05	75.6	74.3	15.59	1.86	0.13	0.05	0.06	0.04
129.3	232.9	15.59	1.60	0.17	0.05	0.05	0.05	234.7	276.5	15.60	1.59	0.22	0.06	0.06	0.05
239.3	9.8	15.60	1.64	0.10	0.05	0.05	0.05	276.4	364.8	15.60	1.58	0.11	0.06	0.07	0.07
237.8	196.1	15.60	1.60	0.25	0.06	0.07	0.07	140.5	378.3	15.60	1.44	0.17	0.05	0.05	0.06
105.3	274.1	15.60	1.14	0.12	0.06	0.06	0.06	52.0	180.0	15.60	1.67	0.25	0.05	0.06	0.06
159.6	477.1	15.61	1.67	0.16	0.05	0.05	0.06	219.2	293.9	15.61	0.89	0.06	0.05	0.05	0.07
248.0	385.2	15.61	0.98	0.11	0.09	0.09	0.06	238.3	312.4	15.61	1.65	0.23	0.07	0.08	0.07

Baade's Window Photometry (continued)															
					Errors								Errors		
X	Y	I	V−I	77−81	I	V−I	77−81	X	Y	I	V−I	77−81	I	V−I	77−81
60.6	241.8	15.62	1.47	0.13	0.06	0.06	0.05	215.7	416.3	15.62	0.96	0.11	0.06	0.06	0.06
92.3	97.0	15.62	1.07	0.10	0.05	0.05	0.04	85.9	41.0	15.62	1.85	0.13	0.04	0.05	0.05
83.9	440.5	15.63	1.71	0.20	0.05	0.05	0.06	237.1	137.0	15.65	1.13	0.09	0.04	0.04	0.05
106.8	87.3	15.65	1.78	0.19	0.05	0.05	0.05	270.2	19.7	15.65	1.85	0.12	0.05	0.06	0.05
280.7	425.4	15.66	1.11	0.14	0.09	0.09	0.06	267.0	379.4	15.66	1.68	0.14	0.07	0.08	0.06
217.3	125.5	15.66	1.01	0.08	0.05	0.05	0.04	7.6	72.3	15.66	1.66	0.18	0.05	0.06	0.05
231.3	320.0	15.66	1.34	0.21	0.08	0.09	0.09	166.6	503.9	15.66	1.22	0.04	0.08	0.09	0.06
210.9	422.6	15.67	1.71	0.22	0.05	0.05	0.06	85.4	65.8	15.67	1.96	0.14	0.06	0.07	0.06
298.2	314.6	15.67	1.75	0.06	0.07	0.08	0.09	59.6	130.4	15.68	1.59	0.17	0.06	0.06	0.04
29.4	282.3	15.68	1.72	0.16	0.05	0.06	0.04	253.8	212.0	15.68	1.80	0.13	0.05	0.06	0.08
116.7	45.3	15.68	1.65	0.15	0.05	0.05	0.05	7.4	51.8	15.69	1.47	0.17	0.05	0.05	0.06
8.9	475.8	15.69	1.61	0.05	0.08	0.09	0.06	32.5	358.4	15.70	0.92	0.00	0.06	0.07	0.06
264.9	401.0	15.70	1.13	0.05	0.07	0.08	0.07	271.0	368.3	15.70	1.68	0.12	0.05	0.06	0.06
24.5	291.3	15.71	1.50	0.17	0.06	0.06	0.06	192.6	104.0	15.71	1.67	0.17	0.07	0.08	0.06
37.8	281.2	15.71	1.44	0.18	0.05	0.05	0.06	131.3	27.2	15.71	1.69	0.14	0.04	0.05	0.04
280.7	36.0	15.72	1.96	0.15	0.05	0.06	0.05	285.2	84.3	15.72	1.02	0.21	0.08	0.09	0.06
271.8	232.7	15.73	1.62	0.06	0.06	0.07	0.06	8.3	489.0	15.73	1.66	0.15	0.04	0.05	0.05
140.4	492.2	15.73	1.07	0.13	0.05	0.05	0.06	282.1	296.2	15.73	1.66	0.15	0.06	0.06	0.06
122.1	179.0	15.73	1.51	0.10	0.06	0.07	0.06	186.1	76.7	15.74	1.10	0.06	0.05	0.05	0.06
145.5	306.9	15.74	1.04	0.07	0.05	0.06	0.05	166.8	277.3	15.74	1.65	0.21	0.05	0.05	0.05
70.4	248.9	15.75	1.23	0.16	0.07	0.07	0.06	60.5	454.0	15.76	1.62	0.21	0.05	0.05	0.05
129.7	420.1	15.76	1.79	0.14	0.05	0.06	0.04	268.4	131.9	15.76	1.65	0.12	0.06	0.06	0.06
170.9	362.1	15.76	0.86	0.16	0.06	0.06	0.06	42.8	257.9	15.76	1.70	0.13	0.06	0.07	0.05
181.8	396.8	15.77	1.00	0.12	0.08	0.08	0.06	276.2	241.1	15.77	0.77	0.13	0.06	0.07	0.08
226.9	39.3	15.77	1.55	0.11	0.05	0.05	0.04	211.6	381.5	15.77	1.82	0.19	0.06	0.07	0.04
132.7	412.2	15.77	1.63	0.14	0.05	0.06	0.06	135.2	418.5	15.78	1.52	0.15	0.05	0.06	0.05
204.3	167.5	15.78	1.74	0.15	0.06	0.07	0.05	279.5	403.2	15.79	1.68	0.15	0.09	0.09	0.07
47.0	425.9	15.79	1.02	0.11	0.05	0.05	0.04	25.2	200.1	15.79	1.55	0.10	0.06	0.07	0.06
189.6	150.2	15.79	1.30	0.08	0.04	0.05	0.05	201.1	50.2	15.79	1.14	0.06	0.05	0.05	0.06
12.1	214.6	15.80	1.87	0.09	0.06	0.09	0.07	221.3	41.3	15.80	1.59	0.11	0.06	0.07	0.04
279.8	346.6	15.80	1.52	0.11	0.08	0.09	0.07	157.9	356.1	15.80	1.42	0.19	0.05	0.06	0.06
213.7	191.3	15.80	1.53	0.15	0.07	0.07	0.06	221.0	389.0	15.80	1.66	0.25	0.06	0.07	0.06
78.6	367.4	15.81	1.73	0.13	0.07	0.08	0.08	290.4	5.5	15.81	1.56	0.08	0.04	0.05	0.06
233.2	429.0	15.81	1.65	0.19	0.08	0.09	0.07	282.4	225.1	15.81	1.65	0.15	0.06	0.07	0.07
7.2	228.7	15.81	1.78	0.11	0.04	0.06	0.04	190.2	428.2	15.81	1.75	0.18	0.05	0.05	0.06
109.3	32.9	15.82	1.36	0.30	0.05	0.06	0.10	44.1	419.9	15.82	1.23	0.09	0.05	0.05	0.04
77.7	304.5	15.82	1.65	0.16	0.05	0.06	0.04	110.3	217.7	15.82	1.59	0.10	0.05	0.06	0.06
283.0	207.0	15.83	1.66	0.10	0.06	0.06	0.06	62.6	103.6	15.83	1.89	0.15	0.05	0.06	0.06
32.9	103.9	15.83	1.18	0.13	0.05	0.05	0.05	86.4	182.8	15.83	1.61	0.16	0.05	0.07	0.06
252.7	263.7	15.83	1.85	0.16	0.06	0.07	0.06	294.9	110.4	15.84	1.59	0.15	0.05	0.05	0.06
103.5	160.1	15.84	1.59	0.16	0.04	0.05	0.04	127.9	374.4	15.84	1.70	0.15	0.08	0.10	0.08
158.9	137.0	15.84	1.64	0.17	0.06	0.06	0.06	31.7	293.6	15.85	1.72	0.13	0.05	0.06	0.05
188.6	275.6	15.86	1.61	0.20	0.05	0.06	0.06	217.2	487.5	15.86	1.68	0.15	0.06	0.07	0.07
105.1	447.8	15.86	1.13	0.00	0.04	0.04	0.05	182.1	313.0	15.86	1.89	0.10	0.06	0.08	0.06

Baade's Window Photometry (continued)

					Errors								Errors		
X	Y	I	V−I	77−81	I	V−I	77−81	X	Y	I	V−I	77−81	I	V−I	77−81
265.3	493.9	15.87	1.11	0.09	0.07	0.08	0.07	194.4	299.6	15.87	1.61	0.17	0.06	0.07	0.06
178.4	479.3	15.87	1.02	0.14	0.08	0.08	0.06	146.1	297.1	15.88	1.65	0.10	0.05	0.06	0.06
194.8	450.8	15.88	1.72	0.18	0.07	0.08	0.06	188.2	391.0	15.88	1.88	0.09	0.06	0.07	0.06
220.0	205.6	15.89	1.60	0.12	0.07	0.08	0.06	56.3	378.4	15.89	1.49	0.12	0.07	0.08	0.05
66.2	10.1	15.89	1.78	0.13	0.05	0.06	0.05	137.7	101.1	15.89	1.51	0.11	0.05	0.06	0.06
109.7	430.3	15.91	1.48	0.11	0.05	0.05	0.06	194.3	334.9	15.91	1.75	0.17	0.06	0.07	0.06
121.3	168.9	15.92	1.89	0.13	0.05	0.06	0.06	39.5	426.7	15.93	1.41	0.17	0.05	0.05	0.04
38.9	117.2	15.93	1.30	0.15	0.05	0.05	0.04	290.5	413.9	15.93	1.48	0.10	0.06	0.06	0.06
97.8	297.8	15.93	1.55	0.15	0.06	0.07	0.06	295.6	276.0	15.94	1.45	0.14	0.05	0.05	0.06
4.5	224.3	15.94	1.13	0.05	0.05	0.06	0.04	41.3	132.2	15.95	1.49	0.11	0.06	0.06	0.06
156.7	443.1	15.95	1.91	0.09	0.06	0.07	0.06	98.8	333.8	15.95	1.80	0.16	0.06	0.07	0.06
212.7	31.1	15.95	1.88	0.11	0.07	0.08	0.07	12.3	357.5	15.96	1.72	0.13	0.06	0.07	0.06
51.4	354.2	15.96	1.66	0.12	0.06	0.07	0.06	10.8	93.1	15.96	1.82	0.12	0.05	0.06	0.05
216.5	318.2	15.97	1.01	0.09	0.06	0.06	0.06	27.4	38.7	15.97	1.73	0.20	0.07	0.09	0.06
30.4	430.9	15.97	1.52	0.09	0.06	0.07	0.06	25.1	79.1	15.97	1.70	0.19	0.05	0.06	0.05
227.1	187.5	15.98	0.80	0.14	0.09	0.09	0.09	201.4	38.2	15.98	1.67	0.10	0.06	0.07	0.06
112.5	340.5	15.99	1.84	0.08	0.06	0.07	0.07	137.6	286.8	15.99	1.56	0.16	0.06	0.06	0.09
132.7	314.4	15.99	1.55	0.09	0.05	0.06	0.09	206.5	165.9	15.99	1.63	0.09	0.06	0.07	0.05
4.4	300.4	15.99	1.78	0.13	0.06	0.07	0.04	76.1	158.7	15.99	1.80	0.08	0.07	0.08	0.06
128.3	313.0	16.00	1.63	0.11	0.05	0.06	0.06	293.1	6.7	16.01	1.78	0.16	0.05	0.06	0.06
50.1	339.1	16.01	1.50	0.26	0.07	0.09	0.07	36.7	420.8	16.01	0.91	0.12	0.05	0.05	0.04
144.0	23.5	16.01	1.25	0.12	0.05	0.05	0.05	42.7	151.8	16.01	1.04	0.15	0.05	0.05	0.06
40.7	418.7	16.02	1.38	0.15	0.05	0.06	0.05	20.2	449.8	16.02	1.32	0.08	0.05	0.05	0.05
46.0	382.9	16.02	1.38	0.07	0.06	0.07	0.07	70.7	317.7	16.02	1.49	0.15	0.06	0.07	0.06
283.8	125.9	16.02	1.78	0.11	0.05	0.09	0.06	219.8	188.1	16.02	1.74	0.08	0.07	0.08	0.06
15.9	40.3	16.02	1.66	0.13	0.05	0.06	0.06	278.6	466.9	16.03	1.63	0.13	0.07	0.08	0.06
228.6	405.2	16.03	1.13	0.05	0.07	0.08	0.06	43.3	172.7	16.03	1.58	0.17	0.05	0.06	0.05
269.8	375.2	16.04	1.08	0.18	0.07	0.07	0.07	59.4	284.0	16.04	1.56	0.22	0.06	0.07	0.06
47.5	368.6	16.05	2.16	0.15	0.06	0.08	0.07	222.6	30.6	16.05	1.70	0.13	0.06	0.07	0.06
256.0	107.5	16.05	1.76	0.20	0.05	0.06	0.06	29.2	238.6	16.05	1.58	0.12	0.06	0.07	0.06
167.5	307.4	16.05	1.81	0.11	0.06	0.07	0.05	50.6	388.9	16.06	1.61	0.11	0.05	0.06	0.05
280.6	47.6	16.06	1.68	0.04	0.06	0.07	0.06	45.8	273.8	16.06	1.51	0.15	0.07	0.07	0.05
139.9	446.2	16.06	1.28	0.12	0.05	0.06	0.05	236.7	190.4	16.06	1.57	0.11	0.07	0.08	0.06
153.7	416.8	16.06	1.51	0.17	0.05	0.05	0.06	118.6	381.3	16.07	1.48	0.15	0.06	0.07	0.06
289.5	466.7	16.07	1.55	0.07	0.08	0.09	0.07	103.2	156.2	16.07	1.81	0.10	0.04	0.05	0.05
247.9	436.5	16.07	1.83	0.14	0.05	0.06	0.06	176.8	14.7	16.08	1.83	0.12	0.06	0.08	0.05
274.8	156.7	16.08	1.07	0.09	0.05	0.05	0.06	165.2	370.1	16.08	1.41	0.07	0.06	0.07	0.07
236.3	431.1	16.08	1.68	0.18	0.08	0.09	0.07	17.4	13.1	16.09	0.67	0.29	0.07	0.07	0.09
177.9	103.2	16.10	1.10	0.29	0.07	0.07	0.06	27.1	57.4	16.10	1.67	0.11	0.04	0.05	0.06
290.3	346.1	16.10	1.71	0.15	0.09	0.10	0.08	292.0	410.1	16.11	1.76	0.11	0.06	0.07	0.06
100.8	271.5	16.11	0.95	0.01	0.06	0.06	0.08	145.1	493.6	16.11	1.75	0.11	0.05	0.07	0.06
156.9	424.4	16.12	1.43	0.20	0.05	0.06	0.06	89.6	106.1	16.12	1.55	0.14	0.08	0.08	0.06
68.6	329.4	16.12	1.59	0.13	0.07	0.08	0.07	287.1	252.6	16.12	1.44	0.22	0.05	0.06	0.06
231.7	277.3	16.13	1.65	0.18	0.06	0.07	0.06	41.3	490.1	16.13	0.98	0.15	0.05	0.05	0.06

Baade's Window Photometry (continued)

					Errors								Errors		
X	Y	I	V−I	77−81	I	V−I	77−81	X	Y	I	V−I	77−81	I	V−I	77−81
21.3	87.1	16.13	1.57	0.14	0.05	0.06	0.05	40.6	25.7	16.13	1.70	0.14	0.06	0.07	0.06
89.1	303.2	16.13	1.41	0.32	0.07	0.09	0.07	49.0	90.6	16.14	1.26	0.13	0.05	0.06	0.06
35.1	294.0	16.14	1.75	0.16	0.05	0.07	0.05	178.9	491.9	16.14	1.64	0.19	0.06	0.07	0.07
21.8	440.4	16.15	1.84	0.13	0.05	0.06	0.06	228.7	10.6	16.15	1.13	0.09	0.05	0.05	0.06
156.1	17.4	16.16	1.72	0.11	0.05	0.06	0.06	196.4	276.1	16.16	1.55	0.16	0.05	0.06	0.06
61.1	226.3	16.16	1.28	0.15	0.05	0.05	0.06	131.9	105.3	16.16	0.84	0.02	0.05	0.05	0.06
52.6	483.5	16.16	1.30	0.08	0.08	0.09	0.09	153.4	104.2	16.18	1.53	0.19	0.06	0.07	0.06
34.9	172.2	16.18	0.71	0.09	0.05	0.05	0.06	172.1	75.5	16.19	1.53	0.13	0.06	0.07	0.08
234.6	45.0	16.20	1.60	0.09	0.06	0.09	0.06	199.7	136.9	16.20	1.84	0.14	0.07	0.08	0.06
253.3	357.3	16.20	1.69	0.07	0.07	0.08	0.09	222.9	217.8	16.21	1.59	0.12	0.07	0.08	0.06
148.4	443.8	16.21	1.16	0.17	0.07	0.07	0.06	186.6	4.5	16.21	1.66	0.09	0.07	0.08	0.06
176.9	400.8	16.21	1.71	0.17	0.06	0.08	0.07	289.1	205.6	16.21	0.89	0.07	0.06	0.06	0.07
22.7	48.0	16.22	1.41	0.21	0.06	0.07	0.06	288.2	237.0	16.22	1.12	0.13	0.06	0.06	0.06
135.3	500.7	16.22	0.87	0.17	0.06	0.06	0.08	293.3	19.3	16.22	1.57	0.26	0.04	0.05	0.07
216.3	354.3	16.23	1.75	0.11	0.08	0.09	0.08	60.1	54.1	16.23	1.18	0.17	0.06	0.07	0.06
273.5	24.7	16.23	1.24	0.16	0.06	0.06	0.07	120.5	378.8	16.24	1.14	0.34	0.06	0.06	0.07
181.8	271.4	16.24	1.10	0.13	0.07	0.07	0.08	19.0	462.3	16.24	1.28	0.22	0.05	0.05	0.06
231.4	44.3	16.25	1.42	0.14	0.06	0.07	0.06	271.5	217.6	16.25	1.75	0.07	0.06	0.08	0.06
32.6	274.7	16.25	1.58	0.18	0.06	0.07	0.05	152.0	296.3	16.25	1.71	0.11	0.06	0.07	0.06
164.8	409.8	16.25	1.71	0.20	0.06	0.07	0.07	85.7	91.9	16.26	1.33	0.18	0.06	0.06	0.06
202.4	477.1	16.26	1.44	0.17	0.07	0.08	0.06	49.7	108.6	16.26	2.03	0.09	0.05	0.07	0.06
121.0	181.1	16.27	1.21	0.12	0.07	0.08	0.07	53.8	429.7	16.27	1.62	0.16	0.06	0.07	0.06
18.5	476.8	16.28	1.42	0.09	0.07	0.07	0.06	229.1	286.5	16.28	1.10	0.16	0.06	0.07	0.06
59.9	71.5	16.29	1.89	0.13	0.05	0.06	0.05	153.8	159.0	16.29	1.71	0.16	0.06	0.07	0.06
142.8	231.6	16.29	1.14	-0.04	0.06	0.07	0.06	139.9	54.0	16.30	1.58	0.14	0.05	0.06	0.06
8.1	332.1	16.30	1.12	0.13	0.07	0.08	0.08	141.9	227.1	16.30	1.23	0.21	0.06	0.07	0.06
198.4	301.1	16.30	1.09	0.14	0.06	0.07	0.06	138.6	488.9	16.30	1.62	0.15	0.05	0.06	0.06
29.0	462.5	16.31	1.60	0.17	0.09	0.09	0.09	197.4	385.9	16.31	1.89	0.03	0.06	0.08	0.06
271.5	306.6	16.31	1.55	0.18	0.07	0.08	0.08	251.8	145.1	16.31	1.88	0.16	0.05	0.07	0.06
72.5	104.4	16.32	1.15	0.11	0.05	0.05	0.06	145.5	369.1	16.33	1.66	0.18	0.06	0.07	0.06
241.6	142.8	16.33	1.77	0.08	0.04	0.10	0.06	114.7	103.8	16.34	1.55	0.05	0.06	0.07	0.10
280.6	244.9	16.34	1.25	0.17	0.07	0.09	0.07	224.7	440.6	16.34	1.47	0.16	0.07	0.09	0.08
148.9	90.0	16.34	1.57	0.18	0.06	0.07	0.09	128.1	159.9	16.35	1.70	0.19	0.06	0.07	0.07
161.0	191.7	16.35	1.67	0.10	0.07	0.08	0.06	139.5	19.7	16.35	1.39	0.13	0.07	0.08	0.09
102.8	37.1	16.35	1.60	0.10	0.05	0.06	0.08	186.3	209.4	16.35	1.45	0.19	0.08	0.09	0.08
232.8	37.6	16.36	1.41	0.19	0.06	0.07	0.05	133.4	85.8	16.36	1.55	0.14	0.06	0.07	0.07
200.5	178.7	16.36	1.55	0.06	0.07	0.08	0.06	168.8	351.1	16.37	1.56	-0.04	0.06	0.08	0.08
136.7	248.9	16.37	1.01	0.14	0.07	0.07	0.06	247.1	505.6	16.38	1.23	0.16	0.09	0.09	0.09
240.7	206.4	16.38	1.11	0.11	0.08	0.09	0.07	81.9	469.0	16.38	1.18	-0.13	0.07	0.08	0.09
91.2	379.2	16.38	1.28	0.08	0.07	0.08	0.08	191.5	397.2	16.38	1.77	0.23	0.08	0.09	0.09
287.9	388.3	16.39	1.46	0.13	0.08	0.09	0.08	196.7	160.0	16.39	1.53	-0.04	0.06	0.08	0.06
293.0	369.3	16.40	1.48	0.27	0.07	0.08	0.08	7.0	304.3	16.40	1.17	0.05	0.06	0.07	0.06
143.4	257.4	16.40	1.78	0.06	0.06	0.07	0.06	200.7	61.4	16.41	1.65	0.19	0.05	0.06	0.06
87.5	339.3	16.42	1.25	0.13	0.08	0.09	0.06	11.6	487.9	16.42	1.42	0.11	0.05	0.06	0.06

Baade's Window Photometry (continued)

					Errors								Errors		
X	Y	I	V−I	77−81	I	V−I	77−81	X	Y	I	V−I	77−81	I	V−I	77−81
232.6	357.5	16.42	1.44	-0.12	0.08	0.09	0.10	275.7	42.4	16.43	1.54	0.18	0.06	0.07	0.06
63.1	63.5	16.43	1.09	0.03	0.07	0.08	0.08	288.9	400.3	16.43	1.12	0.19	0.09	0.09	0.09
83.8	394.9	16.43	1.53	0.11	0.06	0.08	0.07	294.1	71.1	16.43	1.17	0.14	0.06	0.07	0.06
35.7	425.2	16.43	1.10	0.11	0.05	0.06	0.06	158.0	503.0	16.43	1.77	0.19	0.08	0.10	0.08
9.7	172.8	16.44	1.53	0.17	0.06	0.08	0.06	177.2	193.5	16.45	1.59	0.07	0.07	0.08	0.07
255.9	148.9	16.45	1.13	0.17	0.05	0.06	0.05	11.0	456.6	16.45	1.53	0.24	0.06	0.07	0.06
174.7	285.1	16.46	1.69	0.13	0.06	0.07	0.06	297.0	210.7	16.46	1.79	0.16	0.07	0.08	0.09
127.8	8.6	16.47	1.24	0.09	0.07	0.08	0.07	175.4	367.4	16.47	1.56	0.08	0.06	0.10	0.08
57.3	296.0	16.47	1.56	0.10	0.06	0.08	0.07	72.7	490.4	16.47	1.47	0.06	0.06	0.08	0.06
189.5	336.6	16.47	1.71	0.12	0.07	0.08	0.07	169.4	503.6	16.48	1.05	0.05	0.09	0.10	0.09
176.9	185.0	16.48	1.57	0.17	0.06	0.07	0.09	216.7	287.1	16.49	1.54	0.10	0.06	0.07	0.06
253.6	122.3	16.49	2.01	0.01	0.06	0.08	0.08	201.0	54.3	16.49	1.01	0.17	0.06	0.07	0.06
90.4	391.9	16.50	1.67	0.22	0.07	0.09	0.08	128.4	78.6	16.50	1.52	0.12	0.05	0.06	0.07
183.1	92.7	16.50	2.06	0.23	0.08	0.10	0.06	159.9	24.4	16.50	1.05	0.21	0.06	0.07	0.07
117.4	198.8	16.50	1.71	0.11	0.06	0.08	0.06	202.3	192.7	16.50	1.44	0.22	0.06	0.08	0.09
63.8	222.9	16.50	1.05	0.17	0.05	0.06	0.07	141.9	459.9	16.50	1.62	0.19	0.08	0.09	0.09
272.2	125.0	16.50	1.54	0.03	0.09	0.10	0.07	235.0	89.9	16.51	1.81	0.11	0.06	0.08	0.07
146.9	273.8	16.51	1.87	0.27	0.07	0.10	0.09	159.6	21.6	16.51	1.58	0.13	0.06	0.08	0.07
89.0	405.8	16.51	1.60	0.06	0.06	0.09	0.07	240.9	294.9	16.51	1.18	0.05	0.08	0.09	0.07
124.7	226.5	16.51	1.23	-0.02	0.08	0.09	0.10	92.3	427.0	16.52	1.34	0.22	0.06	0.07	0.07
92.8	295.2	16.52	1.52	0.19	0.06	0.08	0.07	96.9	470.4	16.52	1.72	0.20	0.05	0.09	0.07
11.4	117.6	16.53	1.56	0.04	0.07	0.09	0.07	14.6	432.6	16.53	1.26	0.06	0.06	0.07	0.08
269.9	284.2	16.53	1.53	0.11	0.07	0.09	0.07	146.3	318.9	16.53	1.64	0.20	0.06	0.08	0.09
94.2	77.8	16.54	1.20	0.12	0.05	0.06	0.06	269.7	164.2	16.54	1.55	0.16	0.06	0.08	0.08
116.8	177.8	16.54	1.65	0.09	0.06	0.08	0.07	138.2	241.3	16.54	1.53	0.14	0.06	0.08	0.06
56.8	339.5	16.54	1.21	0.14	0.08	0.09	0.07	119.7	347.5	16.55	0.99	0.06	0.07	0.08	0.08
38.7	314.8	16.56	1.55	0.19	0.05	0.06	0.09	34.9	334.1	16.56	1.35	0.22	0.05	0.06	0.07
223.1	369.5	16.57	1.13	0.13	0.08	0.09	0.06	106.5	490.3	16.57	1.45	0.18	0.08	0.09	0.09
235.6	414.2	16.57	1.45	-0.02	0.09	0.10	0.09	103.1	21.8	16.57	1.71	0.08	0.06	0.07	0.06
126.1	416.2	16.57	1.32	0.11	0.06	0.08	0.07	230.8	140.6	16.57	1.63	0.18	0.04	0.06	0.06
49.9	162.0	16.58	1.77	0.06	0.05	0.07	0.06	130.2	460.8	16.58	1.08	0.08	0.06	0.07	0.07
11.2	334.1	16.58	1.66	0.21	0.08	0.10	0.07	134.6	77.8	16.59	1.18	0.06	0.05	0.06	0.07
230.9	175.4	16.59	1.83	0.14	0.07	0.09	0.06	112.3	85.1	16.60	1.14	0.11	0.06	0.07	0.06
297.8	390.7	16.60	1.64	0.06	0.08	0.09	0.09	12.0	20.5	16.61	1.55	0.16	0.05	0.07	0.06
200.1	42.2	16.61	1.22	0.18	0.06	0.07	0.06	19.0	437.4	16.61	1.30	0.13	0.06	0.07	0.08
107.6	225.2	16.61	1.08	0.01	0.07	0.09	0.09	71.8	24.0	16.61	1.22	0.09	0.06	0.07	0.06
98.2	68.0	16.61	1.62	0.06	0.06	0.08	0.07	260.8	41.2	16.62	1.17	0.00	0.08	0.09	0.08
77.1	470.1	16.62	1.25	0.15	0.08	0.09	0.09	64.6	457.0	16.63	1.03	-0.04	0.07	0.08	0.08
101.9	339.3	16.63	1.62	0.20	0.07	0.09	0.07	19.3	376.8	16.63	1.25	0.17	0.07	0.08	0.07
170.3	458.4	16.63	1.05	0.24	0.09	0.10	0.09	31.0	47.1	16.63	1.65	0.10	0.06	0.07	0.06
123.6	10.4	16.64	1.18	0.07	0.07	0.08	0.08	59.9	466.7	16.64	1.08	0.12	0.05	0.06	0.06
63.6	54.5	16.64	1.80	0.15	0.07	0.10	0.07	116.4	13.0	16.64	1.78	0.16	0.06	0.08	0.07
102.5	393.8	16.64	1.15	0.28	0.07	0.09	0.09	278.5	314.3	16.65	1.06	0.13	0.06	0.07	0.09
26.2	342.4	16.65	1.48	0.18	0.06	0.08	0.08	9.9	284.6	16.65	1.31	0.12	0.07	0.08	0.09

Baade's Window Photometry (continued)

					Errors								Errors		
X	Y	I	V−I	77−81	I	V−I	77−81	X	Y	I	V−I	77−81	I	V−I	77−81
297.1	218.8	16.65	1.24	0.14	0.07	0.08	0.06	194.3	310.2	16.65	1.50	0.14	0.07	0.08	0.09
296.3	306.4	16.66	1.52	0.13	0.08	0.10	0.08	60.0	291.9	16.66	1.40	0.11	0.09	0.10	0.09
278.4	139.3	16.66	1.61	0.07	0.07	0.08	0.08	20.4	337.0	16.66	0.99	0.02	0.07	0.09	0.08
154.8	307.3	16.66	1.29	0.18	0.06	0.08	0.08	148.5	248.2	16.66	1.37	0.13	0.08	0.09	0.08
204.4	191.6	16.67	1.15	0.07	0.07	0.09	0.09	103.1	102.9	16.67	1.22	0.04	0.07	0.09	0.06
138.2	255.1	16.67	1.16	0.19	0.08	0.09	0.07	87.1	357.2	16.68	1.32	0.21	0.08	0.09	0.07
43.6	429.0	16.68	1.18	0.10	0.06	0.07	0.06	26.0	380.0	16.68	1.64	0.22	0.06	0.08	0.06
128.1	214.7	16.69	1.27	0.05	0.07	0.09	0.08	295.0	43.6	16.69	1.42	0.17	0.07	0.09	0.09
148.1	156.7	16.69	1.31	0.06	0.07	0.09	0.07	270.7	120.1	16.69	1.73	0.11	0.06	0.08	0.06
262.1	106.9	16.69	1.04	0.13	0.06	0.06	0.09	65.3	430.6	16.69	1.40	0.16	0.07	0.09	0.08
147.8	243.9	16.70	1.27	0.00	0.07	0.09	0.08	20.0	225.2	16.70	1.13	0.29	0.08	0.09	0.08
39.1	77.2	16.70	1.88	0.04	0.06	0.08	0.07	285.9	417.8	16.71	1.33	0.14	0.08	0.09	0.08
134.5	299.7	16.71	0.47	0.13	0.07	0.10	0.07	157.2	463.2	16.71	1.21	0.05	0.08	0.09	0.08
155.8	23.5	16.72	1.56	0.13	0.06	0.08	0.08	248.0	391.8	16.72	1.63	0.08	0.09	0.10	0.08
225.7	381.6	16.72	1.30	0.08	0.09	0.10	0.10	252.6	97.1	16.73	1.62	0.23	0.06	0.07	0.06
97.3	253.0	16.73	1.13	0.05	0.09	0.10	0.10	75.4	152.8	16.73	1.30	0.22	0.07	0.09	0.08
123.4	489.9	16.74	1.12	0.24	0.09	0.09	0.08	50.0	324.8	16.74	1.07	0.10	0.06	0.07	0.07
193.6	143.6	16.74	1.23	0.08	0.05	0.06	0.06	186.7	431.5	16.74	1.57	0.16	0.07	0.09	0.09
209.7	152.8	16.75	1.50	0.13	0.07	0.10	0.08	30.7	451.0	16.75	1.20	0.17	0.06	0.07	0.07
150.3	177.7	16.75	1.49	0.25	0.07	0.09	0.06	39.7	430.1	16.76	1.37	0.09	0.06	0.08	0.06
70.4	297.9	16.76	0.52	-0.01	0.06	0.07	0.08	158.9	415.4	16.77	1.19	0.19	0.06	0.07	0.08
217.4	110.1	16.77	1.57	0.13	0.08	0.10	0.07	167.9	408.5	16.78	1.65	0.11	0.08	0.10	0.08
100.3	97.6	16.78	1.76	0.19	0.07	0.09	0.06	231.3	180.8	16.78	1.70	0.16	0.07	0.10	0.07
144.9	468.4	16.79	1.42	0.06	0.08	0.10	0.08	146.0	54.5	16.79	1.32	0.11	0.07	0.08	0.06
87.5	161.6	16.79	1.69	0.09	0.07	0.09	0.09	11.5	309.7	16.79	1.11	0.08	0.07	0.08	0.06
52.5	384.7	16.79	1.48	0.09	0.06	0.07	0.06	29.8	440.5	16.80	1.17	0.16	0.06	0.06	0.07
61.5	460.8	16.80	1.42	0.00	0.06	0.07	0.07	87.6	270.1	16.80	1.60	0.17	0.08	0.09	0.08
247.7	230.2	16.80	1.07	0.18	0.08	0.09	0.08	84.2	433.0	16.81	1.08	0.35	0.07	0.08	0.08
132.9	226.4	16.81	1.26	0.26	0.07	0.08	0.09	220.1	410.3	16.81	1.13	0.16	0.08	0.09	0.07
87.7	16.2	16.82	1.67	0.09	0.07	0.09	0.07	93.5	40.1	16.82	1.75	0.03	0.06	0.08	0.07
39.5	204.2	16.82	1.68	0.03	0.05	0.07	0.09	64.2	252.0	16.82	1.13	0.27	0.09	0.10	0.08
185.6	289.9	16.83	1.65	0.18	0.06	0.08	0.08	172.1	108.6	16.83	1.72	0.17	0.08	0.09	0.07
196.9	28.0	16.84	1.40	0.12	0.07	0.08	0.07	153.9	53.9	16.84	0.98	0.19	0.07	0.08	0.07
271.4	320.3	16.85	1.17	0.22	0.08	0.09	0.10	83.5	178.1	16.85	1.55	0.07	0.05	0.07	0.08
293.5	249.1	16.85	1.24	-0.05	0.06	0.07	0.08	201.9	394.1	16.85	1.09	0.15	0.08	0.09	0.08
75.6	178.1	16.85	1.67	0.03	0.06	0.08	0.08	55.5	207.4	16.86	1.40	0.16	0.06	0.08	0.09
261.3	52.3	16.86	1.32	0.16	0.08	0.09	0.08	297.6	160.1	16.87	1.50	0.06	0.09	0.10	0.08
85.0	186.8	16.87	1.58	0.24	0.06	0.08	0.09	131.4	154.4	16.87	1.22	0.14	0.09	0.10	0.07
97.2	478.3	16.87	1.29	0.09	0.07	0.09	0.09	175.7	261.2	16.88	1.32	0.08	0.07	0.08	0.10
113.4	392.5	16.89	1.18	0.25	0.08	0.09	0.07	251.3	7.3	16.89	1.72	0.14	0.06	0.09	0.06
251.3	369.7	16.89	1.76	0.13	0.08	0.09	0.09	149.3	257.2	16.89	1.14	-0.02	0.07	0.08	0.07
133.1	238.8	16.90	1.15	0.01	0.08	0.09	0.08	40.4	185.8	16.91	1.47	0.32	0.07	0.09	0.08
248.5	331.9	16.91	1.44	0.10	0.08	0.09	0.09	66.2	316.9	16.91	1.14	0.17	0.08	0.09	0.08
6.6	94.9	16.91	1.70	0.15	0.07	0.09	0.07	105.3	78.3	16.92	1.55	0.20	0.06	0.08	0.08

Baade's Window Photometry (continued)																
					Errors								Errors			
X	Y	I	V−I	77−81	I	V−I	77−81	X	Y	I	V−I	77−81	I	V−I	77−81
190.9	125.1	16.92	1.16	0.12	0.07	0.09	0.08	200.3	86.4	16.92	1.20	0.19	0.06	0.08	0.09
226.9	122.3	16.93	1.36	0.20	0.06	0.08	0.08	73.3	136.9	16.93	1.68	0.11	0.08	0.09	0.06
89.7	273.5	16.93	1.19	0.19	0.08	0.09	0.08	23.3	152.3	16.95	1.46	0.13	0.06	0.08	0.06
161.6	65.5	16.96	1.18	-0.04	0.07	0.08	0.09	102.9	117.1	16.96	1.73	0.22	0.07	0.09	0.07
56.9	478.2	16.96	1.24	0.60	0.07	0.08	0.09	167.6	171.9	16.97	1.58	0.02	0.06	0.08	0.08
144.6	39.1	16.97	1.03	0.11	0.05	0.06	0.08	204.6	25.4	16.98	1.36	0.08	0.07	0.09	0.08
175.7	112.2	16.98	1.31	0.18	0.08	0.09	0.08	38.8	53.0	16.99	1.23	0.16	0.07	0.08	0.07
187.6	239.9	16.99	1.65	-0.14	0.07	0.10	0.09	69.4	206.8	16.99	1.50	0.03	0.06	0.08	0.07
44.8	265.0	16.99	1.20	0.20	0.07	0.09	0.08	242.1	394.7	17.00	1.15	0.21	0.07	0.08	0.10
182.3	406.6	17.00	1.70	0.11	0.07	0.09	0.09	7.8	357.7	17.00	1.53	0.16	0.08	0.10	0.09
153.5	27.3	17.00	1.50	0.09	0.07	0.09	0.09	267.0	7.1	17.00	1.49	0.33	0.08	0.10	0.09
79.0	112.3	17.01	1.30	0.17	0.06	0.08	0.09	52.1	446.5	17.01	1.16	-0.03	0.06	0.07	0.09
166.6	401.6	17.02	1.29	-0.05	0.07	0.08	0.09	149.4	260.5	17.03	1.66	0.12	0.07	0.09	0.07
182.3	280.0	17.03	1.51	0.18	0.06	0.08	0.08	32.0	336.3	17.03	1.77	0.23	0.06	0.09	0.09
135.9	225.4	17.04	1.34	0.16	0.08	0.09	0.09	227.9	15.0	17.05	1.77	0.14	0.06	0.09	0.08
85.8	232.7	17.05	1.50	0.17	0.08	0.10	0.09	129.0	224.5	17.05	1.23	0.00	0.08	0.09	0.08
284.5	64.6	17.05	1.18	0.19	0.08	0.09	0.08	222.6	54.0	17.05	1.27	0.10	0.07	0.09	0.09
117.0	151.7	17.06	1.67	0.01	0.07	0.09	0.08	37.4	185.3	17.07	1.41	-0.07	0.07	0.09	0.10
169.4	394.9	17.08	1.32	0.05	0.07	0.08	0.09	220.5	56.9	17.08	1.67	0.05	0.07	0.10	0.10
194.6	35.9	17.08	1.39	0.26	0.08	0.09	0.07	69.5	321.2	17.09	1.15	-0.01	0.08	0.09	0.08
22.1	232.4	17.09	1.17	0.19	0.08	0.09	0.10	255.6	242.8	17.09	1.49	0.10	0.08	0.09	0.09
171.4	272.5	17.10	1.18	0.15	0.07	0.09	0.08	198.1	143.0	17.11	1.74	0.02	0.06	0.09	0.07
107.7	179.9	17.12	0.88	0.14	0.07	0.08	0.08	151.5	107.5	17.12	1.18	0.06	0.08	0.10	0.08
198.7	343.4	17.12	1.21	0.09	0.08	0.09	0.09	42.0	279.1	17.15	1.11	0.22	0.07	0.08	0.08
153.2	21.3	17.15	0.97	0.08	0.07	0.08	0.10	36.0	179.6	17.16	1.67	0.13	0.07	0.10	0.09
117.6	427.1	17.16	1.35	0.21	0.08	0.10	0.10	296.1	250.8	17.17	1.36	0.11	0.07	0.08	0.08
14.6	157.7	17.17	1.16	0.31	0.08	0.09	0.09	37.7	209.3	17.18	1.43	0.07	0.06	0.09	0.09
186.8	61.0	17.18	1.11	0.15	0.07	0.09	0.08	98.6	107.9	17.23	1.25	0.13	0.08	0.09	0.09
131.2	417.7	17.24	1.20	-0.13	0.08	0.10	0.09	95.3	103.5	17.27	1.46	0.02	0.08	0.09	0.08
78.4	432.7	17.28	1.08	0.13	0.07	0.09	0.09	267.7	155.6	17.29	0.88	0.04	0.08	0.09	0.10
69.8	73.2	17.29	1.30	0.05	0.07	0.09	0.09	38.3	487.7	17.30	1.37	0.19	0.08	0.10	0.10
20.4	398.6	17.31	1.50	0.28	0.08	0.10	0.08	173.6	125.8	17.31	1.10	0.21	0.08	0.09	0.09
275.6	27.2	17.32	1.14	0.22	0.08	0.09	0.10	59.7	77.3	17.34	1.25	0.04	0.08	0.10	0.09
91.6	29.8	17.35	1.37	-0.02	0.08	0.10	0.10	27.5	45.7	17.40	1.36	0.16	0.08	0.10	0.09

APPENDIX B

The following table presents the photometric data for the Sagittarius Dwarf Irregular discussed in Chapter 4. This field is roughly centered on the coordinates $19^h27^m38.3^s, -17°46'27''$ (1950). The stars are listed in order of increasing I magnitude. The brightest star is the first entry in the right column, and so on. North is toward increasing X, east is toward increasing Y and the pixels are ≈ 0.59 arcsec in both X and Y. The positions presented in this appendix are for the V frame shown in Figure 33.

Sagdig Photometry															
					Errors								Errors		
X	Y	I	V−I	77−81	I	V−I	77−81	X	Y	I	V−I	77−81	I	V−I	77−81
97.3	9.6	15.25	1.32	0.08	0.03	0.09	0.06	243.0	309.8	15.28	2.32	0.28	0.01	0.02	0.07
23.4	361.5	15.50	1.22	0.14	0.01	0.07	0.06	79.3	499.9	15.76	0.89	0.08	0.01	0.06	0.06
284.9	105.2	15.81	1.17	0.11	0.02	0.04	0.05	200.6	330.9	15.99	1.58	0.14	0.01	0.02	0.09
281.9	348.3	16.12	1.00	0.08	0.01	0.02	0.06	275.6	372.7	16.17	1.24	0.04	0.01	0.03	0.08
283.4	9.7	16.27	1.28	0.08	0.01	0.03	0.04	171.6	296.4	16.37	0.83	0.06	0.01	0.03	0.05
60.6	292.3	16.54	0.76	0.06	0.01	0.03	0.06	169.6	38.8	16.62	0.87	0.05	0.02	0.04	0.04
251.5	157.5	16.63	0.87	0.08	0.01	0.04	0.05	96.4	97.2	16.68	1.57	0.09	0.01	0.03	0.05
67.0	415.0	16.70	0.80	0.08	0.01	0.03	0.05	215.7	409.7	16.73	0.91	0.06	0.01	0.03	0.07
197.1	185.9	16.85	1.64	0.11	0.04	0.05	0.06	265.9	97.6	16.87	1.20	0.10	0.01	0.02	0.06
164.8	42.5	16.92	1.33	0.07	0.01	0.02	0.04	88.1	39.1	16.93	0.79	0.06	0.02	0.03	0.04
133.6	240.4	17.00	1.12	0.06	0.01	0.03	0.05	15.1	418.2	17.01	0.85	0.08	0.01	0.02	0.06
151.4	369.2	17.12	0.87	0.07	0.01	0.03	0.06	9.2	501.9	17.16	0.80	0.06	0.01	0.02	0.04
48.7	197.4	17.17	1.62	0.10	0.01	0.03	0.05	289.6	420.5	17.18	1.22	0.10	0.02	0.04	0.04
192.2	469.0	17.20	2.76	0.41	0.02	0.03	0.07	294.7	178.3	17.23	0.85	0.07	0.01	0.02	0.06
241.6	354.5	17.30	0.94	0.05	0.01	0.03	0.06	31.9	286.5	17.34	0.78	0.04	0.02	0.04	0.05
97.1	147.7	17.34	0.84	0.09	0.01	0.03	0.05	207.0	338.7	17.35	0.92	0.06	0.01	0.02	0.04
273.3	243.8	17.41	0.96	0.03	0.01	0.03	0.05	116.6	456.3	17.41	0.84	0.05	0.01	0.02	0.04
294.2	453.9	17.42	0.78	0.07	0.01	0.02	0.06	166.2	376.7	17.49	1.37	0.10	0.01	0.02	0.05
181.1	277.6	17.49	0.82	0.06	0.01	0.02	0.04	287.9	366.5	17.54	1.61	0.15	0.01	0.03	0.09
60.2	16.4	17.54	1.15	0.09	0.01	0.02	0.04	200.6	196.9	17.61	1.14	0.08	0.01	0.02	0.04
182.9	477.2	17.62	1.31	0.10	0.01	0.02	0.04	167.8	385.5	17.64	0.80	0.07	0.01	0.02	0.04

Sagdig Photometry (continued)																
					Errors								Errors			
X	Y	I	V−I	77−81	I	V−I	77−81	X	Y	I	V−I	77−81	I	V−I	77−81
189.0	374.4	17.67	1.30	0.07	0.02	0.04	0.05	144.3	76.4	17.68	0.76	0.06	0.01	0.03	0.04
44.0	337.7	17.69	0.77	0.10	0.01	0.04	0.06	23.9	481.6	17.70	1.19	0.09	0.01	0.03	0.05
69.8	21.5	17.72	1.24	0.08	0.01	0.03	0.05	266.7	455.8	17.72	0.79	0.08	0.02	0.03	0.06
179.5	296.2	17.73	1.28	0.07	0.01	0.03	0.05	125.2	492.4	17.75	1.52	0.14	0.01	0.03	0.05
51.7	182.9	17.77	1.28	0.06	0.01	0.02	0.04	124.5	273.0	17.78	1.29	0.10	0.01	0.02	0.07
110.3	418.3	17.79	0.93	0.10	0.02	0.04	0.06	93.1	212.8	17.79	0.82	0.07	0.01	0.02	0.05
148.6	292.0	17.80	1.04	0.06	0.01	0.02	0.05	236.1	474.1	17.82	1.61	0.15	0.02	0.03	0.07
44.6	135.9	17.85	0.93	0.06	0.01	0.03	0.04	212.0	421.9	17.86	0.87	0.08	0.01	0.02	0.07
154.2	489.3	17.88	1.09	0.09	0.01	0.02	0.04	71.7	390.5	17.90	2.33	0.28	0.01	0.02	0.06
179.1	71.1	17.92	2.32	0.26	0.01	0.04	0.06	104.8	286.3	17.94	1.11	0.08	0.01	0.03	0.06
159.2	297.5	17.98	0.84	0.08	0.01	0.02	0.05	188.5	481.0	17.99	1.98	0.16	0.01	0.03	0.06
86.9	47.7	18.00	1.03	0.06	0.01	0.02	0.05	149.5	76.9	18.01	0.86	0.07	0.01	0.02	0.04
242.5	83.6	18.01	0.91	0.07	0.01	0.03	0.06	256.9	183.1	18.02	2.29	0.22	0.02	0.04	0.06
189.2	235.5	18.02	0.98	0.10	0.01	0.03	0.05	193.4	358.4	18.05	0.81	0.10	0.01	0.03	0.06
151.4	445.4	18.06	0.87	0.06	0.01	0.03	0.04	60.8	396.0	18.08	1.83	0.15	0.01	0.03	0.05
200.1	344.0	18.09	2.24	0.24	0.02	0.03	0.12	143.6	121.1	18.12	2.08	0.17	0.02	0.04	0.05
28.9	279.6	18.15	0.81	0.07	0.01	0.03	0.05	15.5	49.0	18.15	1.17	0.07	0.01	0.03	0.05
227.1	124.9	18.17	3.34	0.54	0.02	0.04	0.06	294.7	419.9	18.19	2.13	0.27	0.02	0.04	0.04
77.7	210.9	18.21	1.93	0.23	0.02	0.04	0.06	161.7	41.0	18.23	0.92	0.06	0.02	0.03	0.05
213.0	131.4	18.24	2.71	0.38	0.01	0.03	0.06	244.1	33.5	18.25	1.16	0.09	0.02	0.04	0.06
26.4	441.9	18.26	2.57	0.34	0.01	0.03	0.06	9.8	311.4	18.27	2.38	0.31	0.01	0.03	0.06
250.3	18.2	18.28	2.02	0.17	0.01	0.03	0.05	164.5	83.7	18.29	0.78	0.03	0.02	0.04	0.04
61.2	183.6	18.30	1.27	0.11	0.01	0.02	0.04	18.3	166.3	18.31	0.91	0.10	0.02	0.04	0.07
121.9	262.5	18.31	0.92	0.08	0.01	0.03	0.06	121.1	465.7	18.31	1.86	0.21	0.01	0.04	0.06
137.7	375.0	18.34	2.39	0.26	0.02	0.04	0.06	35.5	248.2	18.34	0.91	0.06	0.01	0.02	0.06
203.7	391.9	18.34	0.83	0.07	0.02	0.04	0.07	167.5	354.8	18.36	0.80	0.04	0.01	0.03	0.04
62.6	414.4	18.37	0.93	0.02	0.01	0.03	0.05	32.3	13.2	18.38	0.86	0.08	0.01	0.03	0.04
280.3	353.3	18.38	2.41	0.27	0.01	0.03	0.07	24.9	237.2	18.38	1.06	0.07	0.01	0.02	0.05
23.2	179.9	18.41	1.01	0.03	0.01	0.03	0.12	257.9	62.1	18.41	0.98	0.08	0.02	0.03	0.06
54.6	55.3	18.41	2.24	0.23	0.02	0.04	0.04	258.2	371.6	18.42	1.18	0.05	0.01	0.04	0.09
185.4	387.0	18.43	2.16	0.22	0.03	0.04	0.05	270.4	425.3	18.44	1.07	0.07	0.02	0.04	0.07
156.5	11.7	18.44	1.17	0.11	0.01	0.03	0.06	27.0	137.6	18.46	1.06	0.10	0.01	0.02	0.05
220.0	71.1	18.49	0.72	0.06	0.02	0.02	0.06	140.1	238.1	18.50	0.91	0.14	0.03	0.09	0.06
243.3	174.1	18.50	0.83	0.05	0.01	0.01	0.06	102.9	382.6	18.51	0.98	0.11	0.01	0.02	0.05
88.6	227.1	18.51	0.99	0.08	0.02	0.03	0.06	242.6	276.6	18.51	0.81	0.09	0.01	0.03	0.06
175.6	419.0	18.53	1.32	0.08	0.04	0.04	0.06	5.7	492.3	18.54	0.88	0.07	0.02	0.03	0.06
111.0	284.8	18.56	1.74	0.12	0.01	0.02	0.06	232.7	281.7	18.57	1.95	0.21	0.01	0.03	0.06
216.0	82.0	18.58	1.85	0.17	0.01	0.02	0.05	214.4	237.5	18.60	2.31	0.26	0.02	0.04	0.06
81.2	388.4	18.61	2.22	0.20	0.02	0.04	0.05	211.4	123.3	18.61	2.01	0.20	0.02	0.04	0.06
187.7	119.8	18.63	2.14	0.22	0.01	0.02	0.05	268.3	143.7	18.63	1.39	0.12	0.02	0.03	0.04
46.5	35.1	18.64	0.69	0.04	0.02	0.03	0.04	4.0	6.4	18.64	2.14	0.23	0.02	0.04	0.06
154.1	289.4	18.64	1.09	0.12	0.02	0.03	0.05	125.6	248.8	18.64	1.82	0.15	0.01	0.03	0.05
99.1	504.3	18.66	0.86	0.04	0.02	0.03	0.06	145.7	55.1	18.66	0.87	0.05	0.02	0.04	0.06
159.4	268.0	18.66	0.82	0.06	0.01	0.02	0.06	284.5	455.4	18.67	1.04	0.09	0.02	0.04	0.05

Sagdig Photometry (continued)																
					Errors								Errors			
X	Y	I	V−I	77−81	I	V−I	77−81	X	Y	I	V−I	77−81	I	V−I	77−81
122.8	158.7	18.68	0.84	0.08	0.01	0.02	0.06	27.9	240.3	18.68	0.86	0.07	0.01	0.02	0.05
228.3	226.7	18.70	2.19	0.19	0.02	0.04	0.06	37.4	318.0	18.70	1.06	0.12	0.01	0.02	0.06
230.3	144.3	18.71	0.92	0.09	0.02	0.03	0.05	272.5	177.9	18.72	2.28	0.25	0.02	0.04	0.05
222.3	376.2	18.73	0.99	0.08	0.01	0.02	0.08	120.1	395.3	18.74	1.47	0.16	0.01	0.02	0.07
200.2	266.5	18.75	0.92	0.01	0.01	0.02	0.12	288.8	11.6	18.75	0.89	0.06	0.02	0.04	0.04
158.0	332.9	18.76	0.52	-.01	0.01	0.02	0.05	28.1	453.7	18.79	1.42	0.08	0.02	0.04	0.07
84.9	77.5	18.80	0.88	0.07	0.02	0.04	0.06	129.8	18.3	18.83	2.49	0.32	0.02	0.04	0.06
110.3	456.5	18.84	1.44	0.19	0.01	0.02	0.05	279.7	421.5	18.85	2.59	0.31	0.01	0.04	0.07
171.0	298.6	18.86	0.80	0.06	0.07	0.11	0.13	142.2	206.4	18.86	1.03	0.08	0.02	0.04	0.05
136.6	207.1	18.83	0.86	0.06	0.01	0.03	0.05	43.0	98.3	18.86	1.31	0.12	0.02	0.03	0.06
124.0	355.2	18.87	0.75	0.13	0.01	0.03	0.08	89.8	47.7	18.89	1.54	0.10	0.01	0.03	0.06
142.2	312.1	18.91	0.97	0.09	0.02	0.04	0.06	66.2	345.7	18.91	2.27	0.31	0.01	0.05	0.06
208.3	45.1	18.92	1.78	0.18	0.03	0.04	0.04	129.9	249.1	18.93	0.99	0.10	0.01	0.02	0.05
79.6	108.6	18.93	0.80	0.07	0.01	0.03	0.05	224.6	215.4	18.94	1.04	0.25	0.02	0.03	0.09
267.0	234.1	18.95	1.07	0.12	0.03	0.04	0.06	21.0	211.7	18.95	0.83	0.06	0.01	0.03	0.06
184.1	432.3	18.99	0.85	0.14	0.01	0.02	0.06	61.2	468.6	18.99	1.26	0.15	0.01	0.02	0.06
227.6	480.6	18.99	0.75	0.06	0.01	0.04	0.07	154.1	495.4	19.00	0.97	0.07	0.01	0.02	0.06
106.9	359.6	19.01	1.14	0.08	0.01	0.02	0.06	238.6	73.8	19.01	0.89	0.06	0.02	0.04	0.05
35.9	198.4	19.02	2.95	0.39	0.01	0.04	0.06	260.4	175.7	19.03	1.07	0.05	0.01	0.02	0.05
281.8	265.8	19.04	1.03	0.11	0.02	0.04	0.07	133.8	486.1	19.04	1.02	0.09	0.02	0.03	0.06
89.1	304.2	19.05	2.65	0.41	0.04	0.06	0.06	14.8	12.5	19.06	2.05	0.23	0.02	0.04	0.07
180.9	45.0	19.06	0.80	0.05	0.07	0.08	0.09	190.6	201.9	19.08	0.87	0.01	0.01	0.02	0.05
77.6	366.4	19.08	0.83	1.38	0.02	0.04	0.39	144.2	327.0	19.09	1.62	0.11	0.02	0.04	0.06
168.6	293.3	19.09	1.82	0.12	0.02	0.04	0.06	164.8	284.9	19.11	1.34	0.09	0.02	0.04	0.06
77.0	345.1	19.11	1.67	0.10	0.01	0.03	0.06	154.9	59.2	19.11	2.55	0.28	0.02	0.04	0.06
122.1	232.3	19.11	1.65	0.10	0.01	0.02	0.07	7.9	60.2	19.12	0.70	0.09	0.02	0.04	0.06
62.0	273.0	19.12	0.93	0.09	0.01	0.02	0.08	283.5	405.0	19.14	2.03	0.15	0.02	0.03	0.07
180.2	222.1	19.14	1.19	0.10	0.03	0.04	0.07	173.4	339.6	19.15	2.43	0.31	0.02	0.04	0.06
31.4	256.2	19.15	1.89	0.23	0.02	0.04	0.06	108.0	198.8	19.16	0.91	0.05	0.01	0.02	0.06
184.8	117.4	19.20	2.08	0.24	0.02	0.04	0.07	95.2	273.4	19.21	1.66	0.03	0.01	0.02	0.07
74.6	355.3	19.23	1.42	0.11	0.02	0.04	0.18	47.4	152.3	19.23	1.08	0.08	0.02	0.04	0.06
264.4	396.6	19.23	0.89	0.10	0.03	0.04	0.06	211.5	217.1	19.24	1.30	0.07	0.02	0.03	0.06
93.6	365.2	19.25	1.89	0.23	0.02	0.04	0.07	84.5	454.4	19.27	2.41	0.27	0.02	0.04	0.07
265.7	141.8	19.27	2.14	0.17	0.02	0.04	0.05	177.6	285.1	19.27	1.61	0.08	0.02	0.04	0.06
119.7	470.8	19.27	1.43	0.09	0.02	0.03	0.06	291.1	376.8	19.31	1.73	0.17	0.03	0.04	0.08
86.3	238.0	19.32	1.73	0.13	0.02	0.04	0.07	268.1	70.0	19.32	2.94	0.38	0.03	0.09	0.08
187.4	475.0	19.32	1.50	0.11	0.02	0.03	0.06	167.8	369.1	19.33	0.69	0.05	0.02	0.03	0.06
58.7	8.9	19.33	2.06	0.14	0.03	0.05	0.06	76.6	215.5	19.35	2.12	0.23	0.04	0.06	0.07
48.1	408.4	19.36	1.04	0.10	0.02	0.04	0.08	61.2	340.5	19.37	1.33	0.08	0.02	0.04	0.06
195.0	430.7	19.40	1.47	0.01	0.02	0.04	0.10	18.9	139.7	19.40	1.13	0.11	0.02	0.03	0.05
217.7	321.4	19.40	1.39	0.09	0.02	0.04	0.06	9.3	469.7	19.40	1.02	0.11	0.02	0.04	0.07
76.1	358.1	19.41	1.19	0.09	0.02	0.04	0.19	204.9	488.3	19.41	0.77	0.17	0.02	0.03	0.06
14.1	262.0	19.41	0.94	0.06	0.02	0.04	0.06	120.2	243.3	19.41	1.43	0.14	0.02	0.04	0.06
240.0	9.4	19.42	1.45	0.11	0.02	0.04	0.07	112.7	454.8	19.42	1.10	0.09	0.02	0.03	0.06

Sagdig Photometry (continued)																	
					Errors								Errors				
X	Y	I	V−I	77−81	I	V−I	77−81	X	Y	I	V−I	77−81	I	V−I	77−81
167.6	393.5	19.42	1.45	0.07	0.03	0.04	0.09	30.8	371.7	19.43	2.25	0.22	0.02	0.09	0.11
168.6	461.4	19.43	1.12	0.16	0.02	0.04	0.07	38.0	149.0	19.44	2.71	0.33	0.04	0.06	0.06
209.9	284.8	19.46	1.11	0.09	0.03	0.04	0.07	248.4	489.8	19.46	2.77	0.31	0.03	0.08	0.10
188.9	366.7	19.46	0.99	0.06	0.02	0.04	0.07	201.3	14.4	19.46	0.95	0.09	0.03	0.04	0.12
201.0	401.5	19.47	1.13	-.11	0.03	0.04	0.10	19.0	29.0	19.48	1.73	-.17	0.11	0.18	0.11
264.2	177.3	19.48	1.12	0.14	0.02	0.03	0.06	280.3	243.4	19.48	0.76	0.07	0.03	0.04	0.09
135.0	194.4	19.48	0.76	0.09	0.01	0.03	0.06	62.8	18.7	19.49	3.13	0.50	0.02	0.06	0.05
293.0	504.5	19.49	2.43	0.35	0.03	0.06	0.10	73.0	80.5	19.50	1.24	0.12	0.03	0.04	0.06
118.9	334.2	19.50	0.78	0.08	0.02	0.03	0.07	145.5	347.0	19.51	1.46	0.14	0.02	0.04	0.07
52.2	228.5	19.51	3.16	0.54	0.02	0.07	0.07	51.1	458.2	19.52	1.69	0.12	0.03	0.04	0.07
136.8	415.4	19.52	1.82	0.18	0.02	0.04	0.06	166.9	327.2	19.55	0.09	0.05	0.02	0.03	0.07
36.4	359.2	19.56	2.03	0.18	0.02	0.04	0.09	66.8	122.3	19.56	1.72	0.12	0.03	0.04	0.07
199.7	291.3	19.60	0.77	0.13	0.03	0.04	0.12	289.3	406.3	19.61	1.02	0.02	0.04	0.04	0.09
122.8	333.4	19.61	0.34	0.01	0.02	0.03	0.07	83.5	163.5	19.62	1.68	0.09	0.03	0.05	0.07
294.4	318.3	19.62	1.86	0.14	0.02	0.04	0.08	51.2	342.7	19.64	1.48	0.42	0.04	0.05	0.15
194.4	200.5	19.65	2.15	0.24	0.02	0.04	0.05	89.0	484.6	19.65	2.21	0.31	0.03	0.06	0.07
196.1	366.3	19.66	0.92	0.11	0.03	0.04	0.07	97.9	261.3	19.67	0.85	0.09	0.02	0.03	0.08
76.2	291.3	19.68	0.99	0.11	0.03	0.05	0.07	57.2	306.5	19.68	1.53	0.19	0.03	0.04	0.07
98.3	396.4	19.69	0.87	0.12	0.02	0.03	0.07	185.9	407.2	19.70	2.22	0.21	0.03	0.05	0.07
77.8	186.3	19.73	0.74	0.13	0.03	0.04	0.06	113.6	360.7	19.73	0.15	-.03	0.02	0.04	0.06
191.6	327.9	19.74	0.85	0.05	0.03	0.04	0.08	83.2	358.9	19.75	1.22	0.15	0.05	0.06	0.07
131.4	371.1	19.75	1.23	0.04	0.02	0.04	0.07	156.7	252.2	19.76	2.45	0.29	0.02	0.06	0.08
116.5	279.3	19.79	1.00	0.03	0.02	0.04	0.07	117.3	436.2	19.79	2.75	0.36	0.03	0.06	0.07
279.0	298.5	19.80	2.17	0.20	0.03	0.06	0.09	92.3	245.9	19.82	0.69	0.39	0.08	0.09	0.11
61.7	333.5	19.82	1.52	0.08	0.03	0.05	0.06	265.9	161.7	19.82	3.26	0.37	0.03	0.12	0.09
104.9	282.8	19.82	1.49	0.11	0.02	0.04	0.08	45.7	273.9	19.83	1.12	0.09	0.02	0.04	0.06
110.7	399.7	19.83	1.39	0.02	0.02	0.04	0.06	195.8	259.3	19.83	2.65	0.49	0.03	0.06	0.07
86.4	188.4	19.84	2.19	-.06	0.08	0.09	0.07	85.3	476.8	19.86	1.67	0.03	0.03	0.05	0.10
222.9	402.8	19.86	2.64	0.29	0.04	0.09	0.09	136.6	189.5	19.87	2.14	0.31	0.02	0.04	0.07
163.8	239.5	19.87	1.09	0.06	0.07	0.08	0.08	238.2	414.6	19.87	2.20	0.26	0.03	0.11	0.10
9.9	46.2	19.88	1.73	0.15	0.04	0.06	0.07	121.5	482.0	19.89	0.74	0.13	0.03	0.04	0.07
243.1	380.9	19.89	2.10	0.15	0.04	0.07	0.09	6.9	330.5	19.89	2.14	0.21	0.03	0.07	0.07
221.4	97.1	19.89	1.12	0.09	0.03	0.04	0.08	195.4	332.0	19.90	1.83	0.21	0.04	0.06	0.14
55.5	309.2	19.90	1.60	0.16	0.03	0.05	0.06	101.1	355.3	19.90	0.15	0.08	0.02	0.04	0.07
98.6	300.5	19.91	2.29	-.13	0.03	0.06	0.08	180.4	271.9	19.92	2.16	0.33	0.03	0.05	0.06
266.2	201.0	19.92	2.88	0.45	0.03	0.09	0.07	242.6	6.8	19.92	1.51	-.03	0.03	0.04	0.08
46.7	449.7	19.93	1.46	0.04	0.02	0.04	0.09	151.1	266.2	19.93	1.26	0.09	0.03	0.05	0.09
42.4	246.7	19.96	1.31	0.08	0.02	0.04	0.06	4.4	167.4	19.96	1.84	0.09	0.03	0.07	0.07
262.8	371.1	19.97	1.70	0.11	0.03	0.06	0.10	46.3	462.6	19.98	2.35	0.34	0.03	0.07	0.08
67.4	331.1	19.99	2.38	-.19	0.03	0.07	0.06	42.8	258.9	19.99	1.12	0.05	0.03	0.05	0.06
231.2	284.9	20.00	1.51	0.04	0.02	0.04	0.09	110.0	273.9	20.02	1.71	0.00	0.03	0.05	0.07
45.7	14.2	20.02	1.01	0.12	0.03	0.04	0.08	20.0	398.4	20.02	0.80	-.08	0.05	0.05	0.08
158.9	187.4	20.03	1.25	0.00	0.03	0.04	0.08	79.4	382.0	20.03	-.02	0.27	0.14	0.15	0.13
288.2	385.1	20.03	2.72	0.30	0.04	0.11	0.12	44.1	399.1	20.03	1.71	0.05	0.04	0.06	0.07

Sagdig Photometry (continued)																	
					Errors								Errors				
X	Y	I	V−I	77−81	I	V−I	77−81	X	Y	I	V−I	77−81	I	V−I	77−81
264.3	335.8	20.03	1.02	0.12	0.03	0.04	0.09	283.1	157.5	20.03	2.97	0.53	0.03	0.08	0.08
237.3	145.2	20.04	1.73	0.25	0.04	0.06	0.07	189.7	243.9	20.04	1.99	0.21	0.04	0.06	0.08
235.1	297.1	20.04	2.33	0.23	0.04	0.08	0.09	206.1	265.2	20.06	2.27	0.22	0.03	0.09	0.11
124.4	224.9	20.07	1.23	0.04	0.03	0.04	0.07	124.9	240.1	20.09	0.96	0.09	0.03	0.04	0.08
181.5	196.3	20.09	1.29	0.10	0.05	0.07	0.09	112.6	481.0	20.09	2.85	0.46	0.04	0.08	0.09
194.2	276.3	20.10	1.13	0.14	0.04	0.06	0.13	212.2	155.1	20.10	2.70	0.40	0.04	0.12	0.08
23.7	332.2	20.10	1.40	0.05	0.03	0.05	0.08	157.0	503.2	20.11	2.67	-.21	0.03	0.11	0.08
103.1	362.3	20.14	0.09	0.05	0.03	0.04	0.08	175.8	347.6	20.14	1.09	-.03	0.02	0.03	0.08
293.4	108.2	20.14	2.84	0.42	0.03	0.09	0.09	141.7	467.3	20.15	0.94	0.09	0.03	0.05	0.10
239.0	409.5	20.16	1.46	0.09	0.03	0.10	0.11	135.1	282.4	20.16	1.34	0.20	0.05	0.15	0.14
117.2	190.0	20.19	2.47	-.09	0.04	0.22	0.14	62.8	477.9	20.19	1.69	0.00	0.04	0.06	0.08
107.3	6.3	20.20	0.54	-.07	0.06	0.11	0.10	65.6	458.5	20.20	3.16	-.24	0.04	0.10	0.08
117.8	377.6	20.21	1.33	0.19	0.04	0.05	0.09	74.0	278.3	20.22	1.59	0.18	0.04	0.07	0.09
29.8	413.5	20.22	1.09	0.09	0.04	0.05	0.09	69.5	365.7	20.23	0.13	-.07	0.04	0.05	0.11
195.4	167.1	20.25	1.33	0.18	0.03	0.07	0.10	11.2	449.3	20.27	2.50	0.28	0.02	0.08	0.10
60.3	76.9	20.27	2.49	0.27	0.03	0.08	0.07	110.6	342.6	20.27	0.17	-.11	0.04	0.06	0.09
14.4	331.4	20.29	0.41	-.12	0.08	0.09	0.14	202.2	201.5	20.29	1.80	0.18	0.04	0.06	0.07
109.9	357.0	20.31	0.05	0.04	0.03	0.04	0.11	205.9	357.7	20.32	2.05	0.13	0.04	0.06	0.09
78.7	150.9	20.33	2.21	0.19	0.06	0.10	0.09	113.2	276.7	20.33	2.67	0.38	0.03	0.09	0.08
44.9	45.4	20.33	0.78	0.06	0.06	0.07	0.08	289.5	396.1	20.34	2.54	0.25	0.05	0.09	0.11
149.9	346.9	20.34	2.10	-.25	0.04	0.07	0.09	65.1	161.1	20.34	2.01	0.32	0.04	0.14	0.08
33.8	312.6	20.35	0.87	0.12	0.03	0.05	0.09	141.4	120.1	20.35	0.98	0.10	0.08	0.09	0.13
2.0	16.4	20.36	0.94	0.05	0.04	0.06	0.11	80.6	184.1	20.36	2.32	0.32	0.04	0.06	0.08
48.3	395.9	20.36	1.33	0.06	0.05	0.06	0.07	1.9	479.1	20.36	2.29	0.24	0.04	0.07	0.10
106.4	407.6	20.36	2.13	-.16	0.05	0.09	0.13	108.6	303.1	20.36	3.21	0.50	0.04	0.14	0.11
88.7	258.5	20.37	1.68	0.04	0.03	0.06	0.10	165.9	298.9	20.38	2.05	0.38	0.04	0.10	0.07
102.3	184.9	20.39	1.51	0.11	0.05	0.06	0.11	94.2	47.4	20.40	1.98	0.12	0.04	0.07	0.08
52.0	99.8	20.41	1.76	0.16	0.04	0.06	0.08	8.0	64.9	20.42	0.80	-.04	0.04	0.05	0.08
232.4	486.3	20.42	1.84	0.27	0.04	0.07	0.11	19.6	395.2	20.43	2.52	0.41	0.05	0.09	0.09
51.8	286.0	20.43	1.73	0.16	0.06	0.08	0.08	211.4	88.6	20.43	2.04	0.19	0.17	0.20	0.08
189.3	404.2	20.43	1.80	0.02	0.05	0.07	0.09	99.3	133.6	20.43	2.70	-.15	0.04	0.10	0.11
200.6	103.8	20.44	1.01	0.08	0.04	0.06	0.07	258.9	125.5	20.44	1.00	0.14	0.05	0.06	0.10
78.7	228.5	20.44	1.23	0.14	0.04	0.06	0.09	108.9	366.1	20.46	1.45	0.20	0.03	0.05	0.08
116.2	174.4	20.47	0.87	0.01	0.04	0.05	0.09	27.3	476.2	20.48	1.88	0.23	0.04	0.06	0.09
150.2	43.1	20.48	1.50	0.13	0.07	0.09	0.11	253.5	399.9	20.49	1.48	-.03	0.06	0.08	0.13
128.8	31.0	20.49	2.33	0.28	0.03	0.10	0.07	284.7	166.3	20.49	1.55	0.01	0.05	0.09	0.13
22.8	298.1	20.50	1.71	0.03	0.04	0.07	0.09	241.5	451.6	20.50	2.13	0.07	0.06	0.10	0.14
11.2	337.7	20.50	0.79	0.24	0.06	0.08	0.09	61.0	85.1	20.51	2.26	0.23	0.05	0.08	0.11
70.0	275.5	20.51	1.25	0.07	0.04	0.05	0.10	221.6	222.6	20.53	1.03	0.07	0.07	0.08	0.12
288.0	284.4	20.54	1.30	0.18	0.05	0.07	0.16	163.7	484.1	20.54	0.81	0.08	0.04	0.05	0.12
164.2	183.9	20.55	1.01	0.07	0.05	0.06	0.11	108.9	165.3	20.56	2.50	0.27	0.06	0.13	0.11
271.9	445.6	20.57	1.49	0.03	0.06	0.08	0.13	129.0	361.6	20.58	2.67	0.31	0.05	0.13	0.14
238.8	428.3	20.58	0.86	0.12	0.06	0.08	0.17	59.4	282.3	20.59	2.23	0.24	0.05	0.11	0.09
285.9	64.5	20.59	3.20	0.39	0.05	0.16	0.13	14.8	480.2	20.59	1.74	0.21	0.06	0.08	0.14

Sagdig Photometry (continued)																
					Errors								Errors			
X	Y	I	V−I	77−81	I	V−I	77−81	X	Y	I	V−I	77−81	I	V−I	77−81
103.3	369.9	20.60	0.07	-.03	0.03	0.04	0.09	36.4	505.7	20.60	1.25	0.08	0.07	0.09	0.11
229.7	337.0	20.60	2.00	0.34	0.05	0.07	0.16	269.4	467.3	20.61	2.51	0.40	0.09	0.13	0.14
258.8	81.5	20.62	1.15	0.08	0.05	0.06	0.10	105.2	71.3	20.63	2.69	0.34	0.06	0.15	0.12
288.5	134.2	20.63	1.50	0.16	0.06	0.07	0.10	104.2	334.9	20.63	-.07	0.07	0.04	0.04	0.09
16.0	362.6	20.64	1.63	0.38	0.04	0.10	0.13	189.9	212.3	20.64	0.88	0.05	0.05	0.06	0.08
100.0	164.1	20.65	1.59	0.13	0.06	0.12	0.13	175.7	147.5	20.65	2.43	0.41	0.04	0.10	0.09
247.9	272.1	20.66	2.67	0.40	0.05	0.12	0.10	49.8	313.8	20.66	2.91	-.17	0.04	0.16	0.09
168.7	22.2	20.66	2.93	0.49	0.05	0.14	0.13	90.7	409.9	20.66	0.19	0.06	0.04	0.04	0.11
91.6	29.8	20.67	1.78	-.03	0.05	0.07	0.10	119.1	381.3	20.68	0.72	0.09	0.05	0.06	0.10
133.6	160.2	20.68	1.75	0.12	0.06	0.08	0.12	110.5	330.0	20.69	1.35	-.05	0.04	0.06	0.11
195.3	87.6	20.70	2.05	0.09	0.06	0.11	0.09	150.0	413.0	20.70	1.24	0.07	0.06	0.09	0.13
40.3	188.1	20.71	1.99	0.13	0.06	0.09	0.08	115.0	426.6	20.71	2.80	0.36	0.05	0.12	0.10
161.3	146.3	20.71	1.74	0.03	0.03	0.06	0.11	140.9	494.2	20.71	3.32	0.25	0.07	0.19	0.16
275.9	36.0	20.72	2.59	0.44	0.06	0.14	0.11	182.8	275.7	20.72	1.79	0.27	0.08	0.13	0.16
34.3	216.8	20.72	0.18	0.13	0.04	0.04	0.08	181.6	314.3	20.73	1.60	0.02	0.04	0.07	0.11
114.4	346.5	20.73	1.71	0.10	0.06	0.08	0.10	169.8	231.6	20.74	1.39	-.06	0.08	0.10	0.12
158.8	341.8	20.74	1.29	0.00	0.06	0.07	0.13	38.4	18.2	20.75	2.55	0.25	0.05	0.12	0.09
84.9	246.9	20.75	2.42	-.05	0.04	0.10	0.12	239.3	488.1	20.75	1.00	0.00	0.06	0.08	0.14
278.4	119.2	20.75	2.59	0.45	0.11	0.16	0.13	138.9	30.3	20.75	1.40	0.09	0.04	0.06	0.08
75.1	196.6	20.75	1.06	0.12	0.06	0.07	0.11	37.7	244.6	20.76	1.24	-.12	0.05	0.06	0.09
58.8	225.7	20.76	1.10	0.10	0.04	0.06	0.10	151.2	410.6	20.77	1.14	0.29	0.06	0.08	0.13
98.0	184.5	20.77	2.03	0.12	0.08	0.09	0.14	16.7	291.9	20.78	0.09	0.09	0.06	0.07	0.08
6.5	298.8	20.78	1.95	0.21	0.05	0.08	0.11	220.1	449.9	20.80	1.92	-.08	0.08	0.11	0.18
198.0	498.7	20.80	2.49	0.39	0.06	0.11	0.12	186.6	107.2	20.81	2.87	0.38	0.08	0.26	0.11
48.7	132.3	20.81	0.91	0.11	0.06	0.07	0.07	74.4	409.9	20.82	2.04	0.29	0.05	0.08	0.09
16.6	302.5	20.82	1.20	0.06	0.06	0.07	0.09	101.1	333.1	20.83	0.93	0.08	0.04	0.06	0.11
220.6	132.6	20.84	1.79	0.28	0.08	0.11	0.11	282.8	15.2	20.84	1.15	0.12	0.07	0.11	0.08
11.9	180.6	20.86	1.45	0.14	0.04	0.07	0.11	64.0	312.2	20.86	2.12	-.46	0.05	0.11	0.12
36.4	255.8	20.89	1.23	0.06	0.06	0.07	0.13	34.0	413.9	20.89	1.86	0.19	0.07	0.10	0.12
24.2	409.6	20.89	1.56	0.15	0.08	0.10	0.14	290.5	392.7	20.89	1.24	-.03	0.08	0.09	0.13
259.9	19.7	20.90	1.58	0.05	0.07	0.10	0.08	88.7	395.4	20.90	2.31	0.32	0.06	0.13	0.16
216.7	424.3	20.91	1.28	0.14	0.08	0.09	0.13	193.6	370.9	20.92	2.63	0.27	0.08	0.15	0.11
216.7	52.6	20.92	0.96	0.02	0.08	0.09	0.11	41.9	278.1	20.92	1.22	0.08	0.07	0.09	0.08
229.8	499.3	20.93	1.43	0.52	0.11	0.14	0.19	250.6	46.4	20.94	2.67	0.41	0.10	0.19	0.13
279.0	477.1	20.95	2.69	0.44	0.06	0.24	0.20	275.6	257.0	20.95	1.42	-.21	0.08	0.09	0.14
128.4	434.6	20.97	2.92	0.43	0.07	0.23	0.13	264.7	89.5	20.98	3.08	0.74	0.06	0.18	0.13
129.3	325.3	20.98	1.01	0.36	0.06	0.07	0.13	161.7	386.4	20.98	1.72	0.44	0.08	0.12	0.10
24.5	476.7	20.98	1.92	0.09	0.06	0.10	0.13	152.9	355.2	20.98	1.22	0.02	0.08	0.09	0.14
180.0	181.5	20.99	1.54	0.00	0.08	0.09	0.16	39.2	308.9	20.99	1.02	0.09	0.05	0.07	0.11
287.5	404.8	20.99	1.17	0.46	0.13	0.14	0.18	247.6	27.3	21.00	1.37	0.17	0.08	0.11	0.16
257.0	111.8	21.00	2.04	0.46	0.08	0.12	0.18	284.9	340.4	21.00	2.39	0.35	0.08	0.15	0.13
139.4	102.3	21.01	2.58	0.37	0.08	0.15	0.18	169.6	383.5	21.01	1.75	-.01	0.11	0.16	0.17
80.0	297.4	21.02	1.40	0.14	0.07	0.09	0.15	292.9	241.8	21.02	1.31	0.09	0.09	0.11	0.16
235.8	313.6	21.03	2.03	0.70	0.12	0.18	0.21	242.3	360.6	21.03	1.36	0.40	0.09	0.11	0.13

Sagdig Photometry (continued)																	
					Errors								Errors				
X	Y	I	V−I	77−81	I	V−I	77−81	X	Y	I	V−I	77−81	I	V−I	77−81
101.8	234.6	21.05	0.92	0.23	0.08	0.10	0.12	59.6	228.4	21.07	1.52	0.26	0.05	0.08	0.24
139.0	336.8	21.07	2.41	0.18	0.08	0.18	0.21	23.8	314.1	21.08	0.15	0.03	0.08	0.09	0.15
35.1	464.5	21.08	1.40	0.29	0.09	0.13	0.14	245.6	193.0	21.08	2.03	-.09	0.08	0.14	0.11
11.1	67.1	21.09	2.18	0.23	0.08	0.14	0.13	245.5	209.9	21.11	2.57	0.53	0.08	0.22	0.16
19.9	196.9	21.11	2.33	0.46	0.06	0.13	0.14	80.2	93.0	21.12	1.79	0.37	0.09	0.16	0.14
227.1	52.0	21.12	2.91	0.55	0.09	0.29	0.14	124.1	146.7	21.12	-.10	-.09	0.09	0.10	0.11
243.9	100.6	21.13	2.89	0.50	0.09	0.26	0.18	205.9	119.7	21.13	1.24	0.28	0.06	0.12	0.15
193.3	77.4	21.13	2.23	0.22	0.08	0.17	0.19	223.8	427.1	21.13	1.64	-.10	0.09	0.12	0.18
92.4	360.7	21.13	-.06	0.08	0.08	0.09	0.11	44.3	198.3	21.14	1.70	-.04	0.08	0.11	0.13
76.7	316.8	21.15	1.42	0.36	0.06	0.10	0.12	50.6	256.5	21.16	1.04	0.15	0.06	0.08	0.12
255.8	137.4	21.16	2.35	0.19	0.11	0.20	0.18	126.5	330.7	21.16	2.10	0.04	0.07	0.11	0.14
44.1	5.5	21.17	0.87	-.04	0.12	0.13	0.17	128.8	371.0	21.17	1.24	0.17	0.08	0.09	0.13
31.1	125.1	21.17	1.27	0.06	0.06	0.08	0.14	123.2	398.3	21.18	0.95	-.01	0.08	0.09	0.12
126.6	445.4	21.18	0.78	0.23	0.08	0.09	0.11	46.0	350.2	21.19	1.01	0.19	0.08	0.10	0.13
284.2	32.3	21.20	1.81	-.05	0.05	0.09	0.16	65.6	398.0	21.21	0.41	0.03	0.13	0.14	0.13
287.6	355.1	21.21	1.43	0.02	0.08	0.15	0.16	20.8	22.8	21.21	1.73	0.12	0.06	0.12	0.14
118.8	104.8	21.22	2.53	0.21	0.07	0.17	0.14	39.5	167.8	21.22	1.49	0.05	0.12	0.15	0.16
106.5	238.4	21.22	1.23	0.17	0.08	0.10	0.13	227.5	393.4	21.22	2.29	0.29	0.09	0.22	0.16
177.9	109.2	21.23	1.12	0.05	0.08	0.10	0.19	265.9	48.2	21.24	1.99	0.15	0.11	0.17	0.22
56.9	62.2	21.24	1.59	0.15	0.10	0.16	0.18	48.3	434.9	21.25	1.83	0.19	0.09	0.11	0.10
70.1	128.4	21.25	1.07	0.05	0.07	0.08	0.19	86.9	208.4	21.26	1.28	-.32	0.07	0.11	0.24
86.0	253.3	21.26	1.36	-.03	0.07	0.09	0.16	76.6	470.1	21.27	1.93	0.34	0.07	0.09	0.18
19.9	64.2	21.28	1.68	-.01	0.12	0.14	0.21	71.8	163.0	21.29	1.18	0.12	0.06	0.08	0.12
287.1	95.6	21.29	2.77	0.47	0.09	0.32	0.19	23.3	44.3	21.29	1.89	0.21	0.09	0.14	0.17
73.0	241.4	21.29	1.13	-.04	0.10	0.12	0.22	190.2	445.2	21.30	1.04	0.16	0.09	0.11	0.14
12.8	369.7	21.31	-.03	-.06	0.08	0.11	0.15	214.3	289.1	21.32	0.85	-.44	0.11	0.13	0.17
68.2	207.0	21.33	1.28	0.29	0.11	0.13	0.20	111.2	192.6	21.34	0.50	0.03	0.07	0.09	0.15
9.9	435.6	21.34	1.46	0.14	0.11	0.14	0.22	20.8	332.1	21.34	1.52	-.02	0.09	0.13	0.18
164.7	409.4	21.34	1.50	-.40	0.15	0.17	0.18	2.8	209.8	21.34	1.53	0.04	0.09	0.12	0.22
209.0	15.5	21.34	1.74	0.22	0.10	0.13	0.18	45.2	204.8	21.36	1.47	-.15	0.12	0.14	0.26
11.8	446.8	21.36	2.16	0.31	0.06	0.15	0.16	182.2	256.6	21.37	2.61	0.33	0.11	0.26	0.24
56.0	182.5	21.37	-.05	0.06	0.08	0.09	0.11	42.2	117.7	21.38	1.61	0.08	0.11	0.12	0.23
96.0	406.1	21.38	1.42	-.06	0.08	0.09	0.15	189.5	163.4	21.38	1.75	0.01	0.07	0.15	0.18
42.2	79.3	21.39	1.44	-.26	0.10	0.15	0.22	169.9	5.6	21.39	1.66	-.19	0.09	0.16	0.19
190.5	132.7	21.39	1.56	0.18	0.12	0.14	0.21	150.6	136.7	21.39	0.91	0.11	0.08	0.11	0.14
110.1	118.3	21.40	1.88	0.06	0.08	0.15	0.13	117.6	296.1	21.40	0.91	-.14	0.12	0.16	0.17
156.6	112.7	21.40	2.61	0.06	0.11	0.26	0.17	92.6	103.1	21.41	1.54	0.36	0.14	0.18	0.18
74.1	50.8	21.42	2.36	0.11	0.10	0.21	0.15	85.5	348.1	21.42	0.05	0.13	0.17	0.17	0.17
173.6	336.1	21.42	1.82	0.28	0.10	0.16	0.15	1.8	230.1	21.42	1.54	-.07	0.20	0.26	0.19
91.1	342.2	21.42	0.10	-.07	0.11	0.12	0.20	22.9	84.7	21.43	2.70	0.49	0.09	0.37	0.21
64.3	461.6	21.43	1.05	0.22	0.11	0.12	0.17	108.1	224.0	21.44	2.27	0.34	0.12	0.18	0.21
89.8	386.6	21.46	1.61	0.32	0.09	0.13	0.14	10.8	236.5	21.46	1.28	-.06	0.12	0.14	0.22
137.6	25.9	21.47	1.80	0.27	0.07	0.11	0.11	158.0	192.1	21.47	1.52	-.13	0.11	0.13	0.17
109.6	377.2	21.47	1.43	0.04	0.10	0.13	0.17	131.1	27.9	21.47	1.33	-.10	0.07	0.11	0.14

Sagdig Photometry (continued)																	
					Errors								Errors		
X	Y	I	V−I	77−81	I	V−I	77−81	X	Y	I	V−I	77−81	I	V−I	77−81
16.2	379.3	21.47	0.93	0.34	0.14	0.18	0.23	34.6	55.0	21.50	1.56	0.19	0.09	0.13	0.20
105.4	303.4	21.50	1.49	0.02	0.10	0.13	0.23	100.9	223.8	21.51	1.93	0.58	0.12	0.18	0.23
2.7	73.8	21.52	1.80	0.08	0.12	0.16	0.18	34.7	481.3	21.52	0.92	0.18	0.13	0.14	0.23
220.1	12.5	21.52	1.90	-.14	0.13	0.26	0.23	120.9	67.1	21.53	1.82	0.27	0.09	0.12	0.18
119.4	348.4	21.53	0.20	0.06	0.11	0.12	0.17	154.6	441.0	21.54	0.85	0.23	0.12	0.13	0.15
76.6	193.5	21.54	1.26	0.31	0.12	0.13	0.16	108.6	232.8	21.54	0.89	0.22	0.11	0.12	0.16
112.4	142.1	21.55	1.30	-.23	0.09	0.13	0.19	67.4	168.9	21.55	1.35	0.05	0.09	0.13	0.18
56.2	220.7	21.55	1.33	-.02	0.08	0.11	0.13	68.9	299.5	21.55	0.09	0.32	0.11	0.12	0.18
118.0	10.2	21.55	1.51	-.41	0.14	0.17	0.33	247.3	77.7	21.56	2.21	0.43	0.10	0.20	0.20
3.3	69.3	21.56	2.27	0.32	0.14	0.21	0.19	9.9	301.3	21.56	1.48	0.40	0.11	0.13	0.23
66.0	173.1	21.56	1.08	-.08	0.09	0.11	0.14	77.0	235.5	21.57	0.38	0.71	0.13	0.15	0.32
49.3	307.3	21.58	0.19	0.19	0.08	0.09	0.16	63.8	360.6	21.59	0.73	0.10	0.17	0.18	0.23
71.9	255.3	21.60	1.04	-.19	0.10	0.13	0.19	259.8	90.6	21.61	2.53	0.83	0.11	0.21	0.17
61.0	479.1	21.61	1.11	-.25	0.16	0.18	0.20	57.7	74.1	21.62	1.17	0.10	0.11	0.13	0.13
257.8	278.9	21.63	1.63	-.19	0.14	0.21	0.26	271.9	272.5	21.64	1.92	0.20	0.12	0.19	0.22
38.2	276.5	21.64	1.41	-.14	0.11	0.14	0.15	235.9	195.2	21.65	0.95	0.09	0.09	0.10	0.19
115.5	308.7	21.66	1.30	-.02	0.10	0.14	0.25	65.3	443.4	21.66	1.43	-.04	0.13	0.17	0.14
8.0	285.7	21.67	2.37	0.52	0.16	0.26	0.16	105.5	152.5	21.68	0.93	-.22	0.11	0.14	0.15
186.4	64.1	21.68	0.24	0.36	0.13	0.14	0.12	83.8	251.2	21.68	1.02	0.20	0.10	0.12	0.19
31.4	302.3	21.68	1.56	0.27	0.11	0.14	0.18	64.5	241.4	21.69	1.28	0.45	0.14	0.16	0.19
289.3	34.5	21.71	1.21	0.22	0.08	0.11	0.21	235.0	73.1	21.72	2.07	0.18	0.12	0.21	0.17
24.6	268.8	21.72	1.68	0.49	0.14	0.18	0.23	129.0	353.1	21.73	0.97	-.01	0.11	0.14	0.20
177.7	134.8	21.75	1.55	-.24	0.17	0.22	0.22	98.6	314.3	21.75	-.10	-.33	0.16	0.16	0.22
135.0	314.8	21.76	1.63	0.17	0.15	0.21	0.25	96.2	295.6	21.78	1.55	0.40	0.14	0.20	0.23
225.4	463.4	21.78	2.47	0.29	0.18	0.36	0.24	76.4	107.2	21.79	1.73	0.34	0.13	0.21	0.22
128.5	199.7	21.79	0.71	-.12	0.10	0.13	0.19	57.9	253.4	21.80	1.14	0.06	0.12	0.14	0.29
141.9	145.4	21.81	1.25	0.00	0.13	0.17	0.22	49.9	216.9	21.81	1.32	0.12	0.11	0.13	0.19
65.3	225.0	21.81	0.72	0.00	0.10	0.12	0.16	90.3	456.5	21.82	1.19	0.40	0.14	0.16	0.21
104.2	193.9	21.82	1.60	0.41	0.13	0.22	0.27	108.1	56.2	21.82	1.53	0.23	0.13	0.20	0.24
154.6	72.4	21.83	2.23	0.32	0.15	0.25	0.28	59.1	158.6	21.84	1.29	0.37	0.13	0.16	0.32
99.7	249.9	21.84	0.61	0.36	0.14	0.16	0.21	91.2	295.4	21.85	1.13	0.12	0.14	0.16	0.23
222.9	57.3	21.85	1.37	-.03	0.19	0.22	0.23	62.7	176.4	21.86	0.03	-.02	0.12	0.13	0.19
113.6	210.4	21.86	2.61	0.49	0.16	0.33	0.28	105.5	114.2	21.91	1.68	-.25	0.12	0.19	0.26
270.8	89.6	21.92	1.63	-.07	0.15	0.27	0.26	180.5	83.0	21.92	0.73	-.39	0.17	0.18	0.21
159.4	61.9	21.92	1.79	0.20	0.15	0.22	0.19	183.8	67.0	21.94	1.02	-.18	0.17	0.19	0.19
103.5	505.7	21.95	1.42	0.04	0.20	0.22	0.19	113.3	303.4	21.97	1.48	-.21	0.14	0.18	0.25
19.1	208.2	21.98	1.70	0.14	0.17	0.23	0.28	176.7	372.8	22.00	1.05	-.20	0.26	0.28	0.28
85.6	307.4	22.01	-.07	-.25	0.18	0.18	0.17	7.5	387.8	22.02	1.32	0.06	0.15	0.25	0.46
38.0	214.5	22.02	1.19	0.05	0.12	0.14	0.20	65.1	288.8	22.04	-.09	0.03	0.20	0.21	0.20
201.0	88.6	22.12	2.34	0.36	0.21	0.39	0.23	91.4	405.3	22.15	0.39	-.29	0.17	0.18	0.27
81.1	336.6	22.19	0.69	-.14	0.18	0.20	0.19	44.2	469.9	22.20	0.28	-.10	0.21	0.22	0.36
134.8	113.2	22.22	0.94	0.44	0.31	0.33	0.32	47.6	239.8	22.27	0.61	0.41	0.20	0.22	0.27
69.5	166.2	22.27	1.41	0.44	0.17	0.22	0.27	210.9	83.0	22.28	1.63	0.05	0.20	0.26	0.26
289.8	305.3	22.29	1.16	0.50	0.31	0.35	0.24	243.1	458.8	22.31	2.04	-.07	0.27	0.37	0.19
34.5	265.1	22.32	0.05	-.19	0.26	0.26	0.20	101.8	120.3	22.35	1.46	-.04	0.28	0.34	0.42

APPENDIX C

The following table presents the photometric data for the NGC 6822 control field, CF1, discussed in Chapter 4. This field is roughly centered on the coordinates $19^h40^m55^s, -15°46'59''$ (1950). The stars are listed in order of increasing I magnitude. The brightest star is the first entry in the left column, the second brightest star is the first entry in the right column, and so on. North is toward increasing X, east is toward increasing Y and the pixels are ≈ 0.59 arcsec in both X and Y. The positions presented in this appendix are for the V frame shown in Figure 35.

CF1 Photometry															
					Errors								Errors		
X	Y	I	V−I	77−81	I	V−I	77−81	X	Y	I	V−I	77−81	I	V−I	77−81
66.4	395.4	15.89	0.98	0.13	0.02	0.04	0.03	293.9	339.0	15.96	1.30	0.10	0.02	0.04	0.02
257.4	73.5	16.00	1.21	0.10	0.02	0.03	0.02	253.6	31.6	16.00	1.28	0.11	0.02	0.03	0.01
30.1	190.7	16.13	1.01	0.09	0.02	0.03	0.02	68.8	501.1	16.27	1.30	0.12	0.02	0.04	0.03
232.2	210.1	16.28	0.97	0.08	0.02	0.03	0.03	6.9	170.0	16.32	0.96	0.10	0.02	0.02	0.03
187.0	249.6	16.56	1.09	0.11	0.02	0.03	0.02	69.3	23.9	16.63	0.98	0.09	0.02	0.03	0.01
162.1	66.3	16.68	1.13	0.09	0.01	0.01	0.03	2.9	326.7	16.70	1.39	0.10	0.02	0.03	0.03
251.2	499.8	16.79	1.09	0.12	0.02	0.03	0.05	246.9	319.3	16.80	1.12	0.08	0.01	0.02	0.02
30.0	209.6	16.88	1.24	0.09	0.02	0.03	0.02	263.1	9.0	17.05	1.07	0.07	0.02	0.02	0.03
295.8	236.0	17.07	1.10	0.10	0.02	0.03	0.02	219.2	133.1	17.10	1.08	0.09	0.01	0.01	0.03
280.1	406.7	17.10	1.27	0.12	0.02	0.02	0.04	3.8	6.1	17.17	1.11	0.12	0.02	0.02	0.02
180.1	397.7	17.20	2.04	0.20	0.02	0.02	0.04	169.2	464.7	17.23	1.23	0.16	0.03	0.03	0.03
288.5	56.0	17.23	1.70	0.14	0.02	0.03	0.03	165.8	31.0	17.30	1.02	0.09	0.02	0.03	0.02
207.6	185.9	17.31	1.43	0.14	0.01	0.02	0.01	178.6	450.2	17.33	1.00	0.12	0.01	0.02	0.02
186.8	64.7	17.34	1.06	0.10	0.01	0.02	0.01	89.2	424.8	17.34	1.17	0.12	0.02	0.03	0.04
68.6	137.9	17.38	0.88	0.10	0.02	0.03	0.03	93.7	287.0	17.39	0.98	0.10	0.02	0.03	0.03
93.9	67.6	17.41	2.96	0.44	0.02	0.03	0.02	11.8	389.2	17.42	1.31	0.11	0.01	0.02	0.02
187.4	392.1	17.45	1.03	0.14	0.01	0.02	0.04	23.2	12.2	17.46	0.90	0.07	0.01	0.01	0.03
132.6	267.4	17.50	1.34	0.14	0.02	0.04	0.04	51.8	295.6	17.50	1.18	0.09	0.01	0.02	0.03
173.1	498.5	17.59	1.20	0.12	0.02	0.03	0.04	25.8	84.8	17.61	1.10	0.11	0.02	0.02	0.02
6.4	7.9	17.68	1.15	0.15	0.02	0.02	0.03	77.8	102.8	17.72	3.27	0.52	0.02	0.03	0.02

CF1 Photometry (continued)																	
					Errors									Errors			
X	Y	I	V−I	77−81	I	V−I	77−81	X	Y	I	V−I	77−81	I	V−I	77−81
15.5	143.4	17.74	1.04	0.07	0.02	0.03	0.03	99.3	372.6	17.77	0.89	0.14	0.01	0.01	0.03
273.6	457.4	17.81	1.37	0.14	0.02	0.03	0.03	279.9	185.9	17.92	1.03	0.08	0.01	0.02	0.04
86.3	393.6	17.99	1.05	0.13	0.03	0.04	0.04	265.2	401.7	18.02	1.07	0.14	0.02	0.04	0.04
166.6	141.3	18.05	1.05	0.11	0.01	0.02	0.03	81.0	435.8	18.06	1.11	0.13	0.02	0.03	0.04
26.1	227.0	18.06	1.01	0.13	0.02	0.03	0.04	44.0	292.2	18.08	1.01	0.08	0.01	0.01	0.04
29.5	83.1	18.09	2.68	0.39	0.02	0.02	0.03	23.9	86.6	18.09	1.88	0.15	0.03	0.04	0.03
180.5	9.4	18.12	0.99	0.08	0.02	0.04	0.04	219.9	221.4	18.14	1.03	0.10	0.02	0.03	0.03
142.9	485.9	18.15	0.98	0.08	0.01	0.02	0.03	65.9	471.8	18.16	0.95	0.11	0.02	0.03	0.04
7.8	444.9	18.24	1.02	0.14	0.02	0.03	0.03	143.6	460.3	18.27	1.10	0.14	0.02	0.03	0.02
27.5	200.8	18.27	1.05	0.13	0.02	0.02	0.03	205.1	403.0	18.28	1.71	0.18	0.02	0.03	0.04
131.4	277.0	18.28	1.59	0.24	0.02	0.04	0.04	212.6	436.8	18.30	1.09	0.15	0.03	0.04	0.03
245.6	390.4	18.32	1.04	0.13	0.01	0.02	0.04	263.2	155.6	18.33	1.20	0.11	0.03	0.04	0.03
248.1	103.3	18.35	1.10	0.10	0.01	0.02	0.04	189.0	482.5	18.35	1.09	0.17	0.01	0.02	0.03
198.4	370.6	18.35	1.77	0.20	0.02	0.03	0.04	270.4	300.2	18.37	1.77	0.10	0.02	0.04	0.03
243.9	339.1	18.38	1.81	0.18	0.01	0.01	0.04	89.3	289.8	18.38	1.49	0.15	0.02	0.03	0.04
242.1	79.3	18.43	1.47	0.04	0.01	0.02	0.04	144.2	181.2	18.43	1.49	0.14	0.01	0.01	0.02
8.6	138.3	18.44	1.16	0.11	0.02	0.03	0.02	247.7	143.3	18.53	2.15	0.20	0.02	0.04	0.03
293.9	52.2	18.58	1.02	0.10	0.01	0.02	0.04	178.7	322.2	18.58	1.14	0.13	0.02	0.03	0.04
98.2	259.0	18.59	1.09	0.12	0.02	0.02	0.04	12.4	93.4	18.60	1.12	0.10	0.02	0.03	0.04
292.0	67.2	18.66	2.66	0.33	0.01	0.03	0.03	97.9	366.3	18.67	1.21	0.16	0.01	0.01	0.03
223.6	272.1	18.72	1.27	0.13	0.02	0.03	0.03	276.4	459.1	18.72	0.96	0.10	0.02	0.03	0.04
241.0	286.5	18.73	1.43	-.02	0.03	0.04	0.12	8.9	209.9	18.77	1.10	0.10	0.03	0.04	0.03
127.0	219.6	18.78	1.06	0.11	0.02	0.02	0.03	204.6	313.5	18.79	1.21	0.12	0.01	0.02	0.03
49.3	440.7	18.79	2.33	0.27	0.02	0.03	0.04	97.2	146.2	18.86	0.88	0.07	0.01	0.01	0.04
108.7	479.5	18.90	1.12	0.14	0.02	0.03	0.03	132.5	433.2	18.92	2.29	0.37	0.02	0.05	0.04
64.3	126.9	18.92	3.07	0.36	0.02	0.05	0.04	272.2	316.2	18.95	1.46	0.09	0.02	0.04	0.04
210.1	170.4	18.96	1.05	0.07	0.02	0.03	0.04	73.5	129.1	18.99	1.38	0.13	0.02	0.03	0.04
114.4	185.9	19.01	2.81	0.42	0.02	0.04	0.05	238.9	252.3	19.01	1.41	0.19	0.02	0.03	0.09
25.2	402.9	19.01	2.14	0.22	0.02	0.03	0.04	109.4	382.8	19.02	1.10	0.17	0.03	0.04	0.04
229.7	328.2	19.02	1.02	0.12	0.02	0.03	0.04	249.3	301.1	19.04	3.42	0.53	0.02	0.08	0.04
42.8	233.0	19.06	1.07	0.10	0.02	0.03	0.03	205.2	109.3	19.13	1.98	0.12	0.02	0.04	0.04
110.6	105.4	19.13	2.09	0.22	0.03	0.05	0.05	144.4	428.2	19.13	1.37	0.18	0.02	0.03	0.04
148.7	454.0	19.15	1.91	0.17	0.02	0.04	0.05	182.9	372.0	19.15	2.38	0.25	0.02	0.04	0.04
139.9	397.5	19.16	2.98	0.47	0.03	0.05	0.05	66.6	45.4	19.18	1.29	0.16	0.02	0.04	0.02
122.0	222.6	19.18	1.26	0.13	0.03	0.03	0.03	200.9	33.4	19.20	1.09	0.09	0.02	0.04	0.03
209.1	326.1	19.22	1.22	0.14	0.01	0.02	0.04	244.7	274.7	19.23	1.40	0.14	0.02	0.04	0.04
72.6	459.3	19.23	1.09	0.08	0.03	0.04	0.03	187.9	296.2	19.24	2.04	0.19	0.02	0.04	0.04
212.0	63.2	19.26	1.26	0.07	0.03	0.04	0.04	19.4	120.0	19.27	1.84	0.17	0.01	0.02	0.03
100.6	414.4	19.27	1.18	0.06	0.02	0.03	0.04	152.5	325.8	19.27	1.59	0.14	0.03	0.04	0.04
4.2	129.5	19.29	1.53	0.22	0.02	0.04	0.06	35.9	33.0	19.30	1.52	0.09	0.02	0.04	0.04
47.0	417.7	19.31	1.83	0.22	0.02	0.04	0.06	85.1	25.5	19.38	2.44	0.27	0.02	0.04	0.04
194.5	391.9	19.40	2.65	0.24	0.03	0.05	0.12	216.6	65.8	19.40	2.84	0.42	0.03	0.05	0.04
62.3	80.3	19.41	0.94	0.07	0.02	0.03	0.05	20.6	55.3	19.43	2.85	0.44	0.02	0.04	0.04
51.7	166.9	19.45	1.11	0.08	0.03	0.04	0.06	170.6	375.0	19.47	1.82	0.13	0.02	0.03	0.04

CF1 Photometry (continued)

					Errors								Errors		
X	Y	I	V−I	77−81	I	V−I	77−81	X	Y	I	V−I	77−81	I	V−I	77−81
208.7	351.4	19.47	1.57	0.16	0.03	0.04	0.04	10.9	11.1	19.48	1.87	0.13	0.02	0.03	0.04
131.6	470.3	19.49	1.60	0.18	0.02	0.04	0.04	247.0	244.4	19.50	0.99	0.14	0.03	0.04	0.06
65.4	330.8	19.51	3.22	0.60	0.02	0.07	0.03	152.6	443.1	19.54	1.11	0.06	0.03	0.04	0.06
140.4	482.0	19.59	2.06	0.17	0.02	0.04	0.06	30.1	180.5	19.59	1.01	0.15	0.02	0.05	0.05
177.6	186.6	19.59	0.94	0.15	0.03	0.03	0.04	172.5	175.1	19.61	0.99	0.10	0.02	0.04	0.04
6.7	32.9	19.61	0.89	0.23	0.04	0.04	0.06	94.2	107.7	19.62	1.87	0.17	0.03	0.04	0.04
137.8	111.4	19.63	2.14	0.25	0.02	0.04	0.04	77.2	210.3	19.64	1.22	0.15	0.03	0.04	0.04
195.0	313.0	19.68	1.12	0.13	0.02	0.03	0.05	109.7	205.8	19.69	2.81	0.50	0.04	0.10	0.06
261.1	134.0	19.70	1.61	0.15	0.02	0.04	0.06	145.2	492.1	19.73	1.11	0.17	0.02	0.04	0.06
190.0	280.0	19.74	1.99	0.17	0.02	0.04	0.05	23.0	251.8	19.74	1.84	0.12	0.02	0.04	0.05
91.6	350.7	19.74	2.87	0.37	0.04	0.08	0.05	251.5	393.5	19.75	2.85	0.38	0.02	0.08	0.05
108.2	7.3	19.75	2.86	0.44	0.03	0.08	0.06	17.1	382.7	19.75	2.72	0.33	0.03	0.06	0.04
112.2	401.6	19.77	1.77	0.23	0.03	0.04	0.04	164.1	373.4	19.77	1.25	0.26	0.02	0.03	0.04
49.3	305.4	19.80	1.53	0.14	0.03	0.04	0.06	60.6	305.0	19.81	1.22	0.06	0.03	0.04	0.05
241.9	68.3	19.81	2.91	0.40	0.03	0.07	0.05	17.4	387.3	19.82	2.79	0.41	0.03	0.06	0.05
288.6	79.5	19.82	2.28	0.19	0.04	0.06	0.05	126.5	328.0	19.84	2.21	0.31	0.03	0.05	0.05
191.4	115.1	19.85	1.35	0.08	0.04	0.05	0.06	43.6	180.8	19.85	1.33	0.16	0.03	0.04	0.07
51.9	394.5	19.85	2.32	0.26	0.03	0.05	0.06	253.2	220.2	19.85	1.24	-.01	0.04	0.05	0.13
63.2	11.1	19.87	2.78	0.42	0.03	0.06	0.06	14.3	104.9	19.88	0.94	0.15	0.03	0.04	0.05
236.8	355.0	19.89	3.23	0.47	0.03	0.13	0.06	91.2	212.2	19.89	0.91	0.07	0.03	0.04	0.05
262.1	39.7	19.90	2.10	0.04	0.04	0.06	0.09	45.5	171.4	19.91	2.22	0.22	0.03	0.04	0.06
254.6	433.0	19.91	1.80	0.20	0.03	0.05	0.06	190.8	338.8	19.91	1.28	0.12	0.04	0.05	0.06
203.6	252.0	19.91	1.50	0.20	0.02	0.05	0.06	282.6	409.5	19.93	1.07	0.22	0.04	0.04	0.09
25.9	99.5	19.94	3.04	0.45	0.03	0.07	0.06	14.2	342.4	19.95	2.28	0.34	0.02	0.04	0.06
239.8	120.8	19.97	1.98	0.22	0.03	0.05	0.06	186.3	505.8	19.98	1.37	0.09	0.05	0.06	0.06
137.4	407.9	19.99	1.59	0.27	0.03	0.04	0.05	236.4	404.3	20.01	3.54	0.73	0.03	0.12	0.07
88.5	133.1	20.01	1.64	0.11	0.02	0.04	0.07	107.6	92.5	20.03	1.73	0.14	0.03	0.05	0.05
34.3	491.8	20.03	2.19	0.19	0.03	0.06	0.05	177.7	299.5	20.04	1.98	0.23	0.03	0.05	0.07
34.1	442.4	20.04	2.08	0.25	0.04	0.05	0.06	56.7	191.5	20.06	1.36	0.16	0.02	0.04	0.05
272.1	92.9	20.08	1.94	0.20	0.04	0.06	0.07	242.0	330.4	20.12	2.65	0.37	0.03	0.08	0.07
269.0	113.2	20.13	1.30	0.06	0.04	0.05	0.08	40.1	442.4	20.15	1.44	0.24	0.04	0.04	0.06
118.0	49.2	20.15	1.07	0.11	0.03	0.04	0.06	92.0	85.3	20.17	1.48	0.12	0.02	0.04	0.04
287.5	232.0	20.17	1.09	0.07	0.05	0.06	0.08	232.5	23.4	20.18	1.40	0.11	0.03	0.04	0.06
82.9	401.9	20.18	1.19	0.14	0.03	0.04	0.06	262.9	81.5	20.18	1.31	0.07	0.04	0.05	0.07
145.6	12.2	20.19	1.42	0.06	0.04	0.05	0.07	153.9	175.7	20.20	1.22	0.17	0.04	0.05	0.08
150.1	23.0	20.20	1.33	0.12	0.03	0.04	0.06	238.0	325.1	20.20	1.16	0.23	0.04	0.05	0.08
187.2	105.6	20.21	1.88	0.17	0.04	0.06	0.06	94.6	141.8	20.21	1.90	0.18	0.03	0.04	0.06
86.1	199.5	20.22	1.13	0.13	0.03	0.04	0.07	279.7	63.9	20.23	2.45	0.25	0.05	0.09	0.07
176.4	131.0	20.24	2.08	0.23	0.03	0.07	0.06	263.8	75.9	20.25	1.39	0.14	0.04	0.05	0.07
285.9	150.0	20.25	1.41	0.16	0.03	0.04	0.06	70.7	69.4	20.26	2.49	0.27	0.04	0.10	0.08
266.0	272.5	20.27	2.65	0.31	0.03	0.10	0.07	103.8	457.7	20.27	1.00	0.02	0.03	0.04	0.09
120.0	360.2	20.27	2.33	0.21	0.04	0.07	0.08	252.4	236.8	20.28	1.58	0.16	0.05	0.06	0.08
218.8	199.4	20.32	1.15	0.10	0.03	0.04	0.08	199.3	208.0	20.33	1.39	0.09	0.05	0.06	0.09
121.9	280.8	20.34	1.78	0.28	0.04	0.12	0.09	147.3	264.4	20.36	2.87	0.39	0.04	0.13	0.09

CF1 Photometry (continued)																
					Errors								Errors			
X	Y	I	V−I	77−81	I	V−I	77−81	X	Y	I	V−I	77−81	I	V−I	77−81
4.5	368.6	20.38	2.69	0.35	0.04	0.12	0.08	54.1	338.0	20.40	1.13	0.12	0.05	0.06	0.07
58.0	431.9	20.41	1.84	0.16	0.04	0.06	0.08	184.8	70.6	20.41	1.27	0.15	0.04	0.05	0.06
4.2	75.6	20.42	1.38	0.34	0.05	0.08	0.10	294.4	166.0	20.42	2.91	0.38	0.04	0.14	0.10
44.6	405.5	20.44	1.12	0.18	0.04	0.06	0.10	211.9	260.2	20.45	2.94	0.39	0.04	0.13	0.09
119.9	401.4	20.46	1.06	0.21	0.04	0.05	0.08	219.6	270.0	20.47	1.11	-.01	0.04	0.04	0.13
121.8	101.5	20.48	1.65	-.05	0.03	0.05	0.09	214.6	143.1	20.48	1.01	-.01	0.05	0.06	0.08
221.6	266.1	20.52	2.26	0.11	0.04	0.06	0.08	21.0	213.3	20.53	1.48	0.20	0.05	0.08	0.09
64.3	130.0	20.54	2.07	0.13	0.04	0.08	0.09	205.9	468.9	20.54	0.99	0.15	0.05	0.05	0.08
198.1	182.7	20.54	1.72	0.30	0.04	0.06	0.07	159.4	431.1	20.56	1.55	0.21	0.04	0.05	0.09
128.6	149.1	20.56	2.13	0.13	0.04	0.08	0.09	34.1	57.7	20.57	2.47	0.37	0.03	0.08	0.08
222.3	149.4	20.59	1.40	0.06	0.03	0.04	0.09	142.1	50.9	20.60	2.29	0.05	0.06	0.10	0.08
17.7	465.2	20.61	2.08	0.54	0.04	0.07	0.11	155.8	21.8	20.66	2.39	0.29	0.04	0.09	0.08
128.8	378.9	20.67	2.21	0.23	0.06	0.10	0.18	282.5	149.5	20.69	1.10	0.11	0.04	0.05	0.09
249.2	128.6	20.69	2.60	0.18	0.06	0.13	0.10	3.6	456.8	20.70	1.08	0.18	0.08	0.11	0.11
266.9	332.6	20.70	1.08	0.24	0.06	0.08	0.11	199.0	256.6	20.70	2.32	0.28	0.04	0.14	0.11
70.6	184.6	20.71	2.09	0.30	0.05	0.10	0.13	169.2	289.2	20.71	2.23	0.38	0.05	0.07	0.13
81.7	225.3	20.72	2.91	0.65	0.05	0.14	0.09	35.3	233.6	20.74	2.11	0.18	0.05	0.10	0.12
288.1	159.1	20.74	1.99	0.09	0.05	0.08	0.12	87.2	482.0	20.75	1.20	0.14	0.05	0.07	0.10
41.4	221.1	20.78	2.70	0.32	0.04	0.13	0.11	73.5	147.4	20.82	2.21	0.03	0.06	0.09	0.10
35.2	62.1	20.82	1.50	0.20	0.04	0.06	0.09	284.9	205.3	20.82	1.51	0.09	0.04	0.06	0.14
290.8	499.8	20.83	1.45	0.05	0.10	0.12	0.14	294.1	371.6	20.84	0.98	0.23	0.06	0.07	0.11
64.6	222.9	20.85	2.20	0.17	0.05	0.09	0.09	19.8	222.9	20.86	2.67	0.45	0.05	0.13	0.12
97.6	493.4	20.86	1.34	0.03	0.06	0.07	0.10	54.2	142.7	20.86	2.50	0.29	0.06	0.14	0.09
222.6	334.2	20.87	2.13	-.11	0.09	0.12	0.20	155.0	478.0	20.87	2.58	0.30	0.06	0.18	0.13
227.0	90.1	20.87	1.45	0.19	0.04	0.06	0.09	240.3	65.5	20.87	1.19	0.03	0.06	0.07	0.11
123.2	416.4	20.89	2.07	0.31	0.27	0.29	0.09	32.5	133.7	20.91	2.51	0.41	0.05	0.17	0.11
95.3	396.3	20.93	2.49	0.23	0.05	0.15	0.11	53.1	451.3	20.93	2.65	0.24	0.06	0.18	0.13
194.1	436.8	20.95	2.70	0.14	0.08	0.19	0.13	193.4	145.0	20.95	2.26	0.18	0.06	0.11	0.11
215.9	267.0	20.95	1.13	0.03	0.06	0.07	0.11	220.7	19.7	20.98	2.78	0.25	0.05	0.15	0.12
159.9	180.0	21.01	2.39	0.32	0.05	0.11	0.13	156.7	161.4	21.02	2.85	0.66	0.05	0.12	0.14
254.7	20.8	21.03	2.86	0.28	0.06	0.21	0.19	236.0	495.0	21.04	2.08	-.12	0.13	0.19	0.18
12.3	325.4	21.05	0.98	0.45	0.09	0.10	0.16	60.4	307.9	21.09	2.02	0.20	0.06	0.11	0.14
25.7	108.7	21.10	3.13	0.43	0.05	0.25	0.13	88.9	90.1	21.12	2.39	0.35	0.05	0.14	0.10
10.0	292.7	21.13	1.87	0.12	0.05	0.11	0.12	3.1	360.4	21.13	1.67	0.22	0.08	0.11	0.16
38.7	37.6	21.14	2.68	0.11	0.06	0.19	0.14	43.2	434.7	21.15	2.69	0.46	0.18	0.22	0.11
36.3	111.7	21.15	1.58	0.22	0.06	0.10	0.14	281.9	194.8	21.17	2.12	0.07	0.08	0.18	0.18
272.2	57.8	21.17	2.48	0.11	0.09	0.21	0.15	140.9	120.7	21.17	2.25	0.35	0.07	0.13	0.11
143.9	242.9	21.19	2.15	0.22	0.05	0.10	0.15	197.2	300.3	21.20	1.94	0.18	0.06	0.10	0.15
93.2	292.8	21.20	1.65	0.34	0.08	0.12	0.13	166.4	196.0	21.22	2.36	0.34	0.08	0.16	0.16
218.0	388.5	21.26	1.93	0.32	0.07	0.09	0.13	142.9	200.1	21.27	1.87	-.01	0.07	0.11	0.15
144.4	374.8	21.31	1.68	0.05	0.08	0.11	0.18	110.1	96.1	21.32	2.70	0.28	0.08	0.20	0.14
152.9	92.6	21.32	1.31	0.45	0.07	0.09	0.13	255.6	371.5	21.32	2.38	0.36	0.11	0.19	0.14
95.5	30.1	21.34	1.60	0.39	0.05	0.10	0.17	18.3	153.3	21.34	0.88	0.01	0.06	0.10	0.15
102.7	22.0	21.35	3.16	0.56	0.04	0.37	0.18	236.1	225.7	21.35	2.48	0.18	0.08	0.22	0.22

CF1 Photometry (continued)															
					Errors								Errors		
X	Y	I	V−I	77−81	I	V−I	77−81	X	Y	I	V−I	77−81	I	V−I	77−81
242.6	326.1	21.36	1.96	0.21	0.09	0.14	0.18	171.3	143.6	21.37	1.14	0.32	0.08	0.09	0.13
9.7	232.5	21.37	1.89	0.07	0.10	0.16	0.17	230.1	184.0	21.37	1.22	0.41	0.09	0.12	0.18
79.6	380.6	21.44	1.37	0.41	0.10	0.13	0.15	181.0	62.8	21.45	1.40	0.20	0.08	0.11	0.14
236.3	502.2	21.47	1.09	0.23	0.17	0.19	0.19	188.6	81.8	21.48	2.49	0.08	0.07	0.14	0.19
21.6	42.0	21.49	1.58	-.11	0.09	0.12	0.16	38.3	217.7	21.59	0.95	0.07	0.07	0.09	0.18
255.6	223.3	21.66	1.95	0.09	0.11	0.16	0.18	19.1	241.0	21.71	1.80	-.02	0.07	0.13	0.28
191.1	153.7	21.73	1.90	0.38	0.11	0.17	0.21	73.4	36.9	21.77	2.63	0.33	0.12	0.31	0.20
206.5	180.6	21.84	2.05	0.52	0.12	0.22	0.18	60.6	350.7	21.85	1.69	0.50	0.09	0.17	0.27
55.1	185.0	22.02	2.18	0.46	0.09	0.20	0.24	276.4	200.1	22.34	2.18	0.41	0.16	0.32	0.31

REFERENCES

Aaronson, M. 1986, in *Stellar Populations*, ed. C. A. Norman, A. Renzini, and M. Tosi (Cambridge: Cambridge), p. 45.

Aaronson, M., Da Costa, G. S., Hartigan, P., Mould, J. R., Norris, J., and Stockman, H. S. 1984, *Ap. J. (Letters)*, **277**, L9.

Aaronson, M., and Mould, J. 1985, *Ap. J.*, **288**, 551.

Aaronson, M., and Mould, J. 1985, *Ap. J.*, **290**, 191.

Aaronson, M., Mould, J., and Cook, K. H. 1985, *Ap. J. (Letters)*, **291**, L41.

Aaronson, M., Olszewski, E. W., and Hodge, P. W. 1983, *Ap. J.*, **267**, 271.

Alcaino, G. 1975, *Astr. Ap. Suppl.*, **21**, 5.

Arp, H. C. 1955, *Ap. J.*, **60**, 317.

Arp, H. C. 1965, *Ap. J.*, **141**, 43.

Arp, H. C., Baum, W. A., and Sandage, A. R. 1953, *Astr. J.*, **58**, 4.

Arp, H. C., and Hartwick, F. D. A. 1971, *Ap. J.*, **167**, 499.

Bahcall, J. N., and Soneira, R. M. 1980, *Ap. J. Suppl.*, **44**, 73.

Baumert, J. H. 1974, Ph.D. Thesis, Ohio State University.

Bessel, M S., Wood, P. R., and Lloyd Evans, T. 1983, *M. N. R. A. S.*, **202**, 59.

Bessel, M. S. 1979, *Publ. A. S. P.*, **91**, 589.

Blanco, B. M., Blanco, V. M., and McCarthy, M. F. 1978, *Nature*, **271**, 639.

Blanco, V. M. 1986, *Astr. J.*, **91**, 290.

Blanco, V. M., Frogel, J. A., and McCarthy, M. F. 1981, *Publ. A. S. P.*, **93**, 532.

Blanco, V. M., McCarthy, M. F., and Blanco, B. M. 1980, *Ap. J.*, **242**, 938.

Blanco, V. M., and Blanco, B. M. 1984, *Publ. A. S. P.*, **96**, 603.

Blanco, V. M., and McCarthy, M. F. 1983, *Astr. J.*, **88**, 1442.

Blanco, V. M., and McCarthy, M. F., and Blanco, B. M. 1984, *Astr. J.*, **89**, 636.

Branch, D., Lambert, D. L., and Tomkin, J. 1980, *Ap. J. (Letters)*, **241**, L83.

Brunish, W. M., and Truran, J. W. 1982, *Ap. J. Suppl.*, **49**, 447.

Burbidge, E. M., Burbidge, G. R., Fowler, W. A., and Hoyle, F. 1957, *Rev. Mod. Phys.*, **29**, 547.

Burstein, D., and Heiles, C. 1984, *Ap. J. Suppl.*, **54**, 33.

Cameron, A. G. W. 1955, *Ap. J.*, **121**, 144.

Cesarsky, D. A., Laustsen S., Lequeux, J., Schuster, H-E., and West, R. M. 1977, *Astr. Ap.*, **61**, L31.

Cohen, J. G., Frogel, J. A., Persson, S. E., and Elias, J. H. 1981, *Ap. J.*, **249**, 481.

Clayton, M. L., and Feast, M. W. 1969, *M. N. R. A. S.*, **146**, 411.

Cook, K. H., Aaronson, M., and Norris, J. 1986, *Ap. J.*, **305**, 634.

Cousins, A. W. J. 1973, *M. N. R. A. S.*, **77**, 223.

Cousins, A. W. J. 1976, *M. N. R. A. S.*, **81**, 25.

Cousins, A. W. J. 1978, *M. N. A. S. S. A.*, **37**, 62.

Cudworth, K. M. 1985, *Astr. J.*, **90**, 65.

Dean, J. F., Warren, P. R., and Cousins, A. W. J. 1978, *M. N. R. A. S.*, **183**, 569.

Dearborn, D. S. P., Liebert, J. Aaronson, M., Dahn, C. C., Harrington, R., Mould, J., and Greenstein, J. L. 1986, *Ap. J.*, **300**, 314.

Feast, M. W. 1967, *Observatory*, **87**, 35.

Fisher, J. R., and Tully, R. B. 1975, *Astr. Ap.*, **44**, 151.

Flower, P. J. 1977, *Astr. Ap.*, **54**, 31.

Frogel, J., Cohen, J. G., and Persson, S. E. 1983, *Ap. J.*, **275**, 773.

Fujimoto, M. Y., and Sugimoto, D. 1979, *Publ. Astr. Soc. Japan*, **31**, 1.

Grahm, J. A. 1982, *Publ. A. S. P.*, **94**, 244.

Hardie, R. H. 1962, in *Astronomical Techniques*, ed. W. A. Hiltner (Chicago: University of Chicago Press), p. 178.

Hartwick, F. D. A., and Sandage, A. 1968, *Ap. J.*, **153**, 715.

Hoessel, J. G., and Mould, J. R. 1982, *Ap. J.*, **254**, 38.

Hoffmeister, C., Richter, G., and Wenzel, W. 1985, *Variable Stars* (Berlin: Springer-Verlag), p. 68.

Humphreys, R. m. 1983, *Ap. J.*, **269**, 335.

Iben, I. Jr. 1974, *Ann. Rev. Astr. Ap.*, **12**, 215.

Iben, I. Jr. 1975, *Ap. J.*, **196**, 525.

Iben, I. Jr. 1975, *Ap. J.*, **196**, 549.

Iben, I. Jr., and Renzini, A. 1982, *Ap. J. (Letters)*, **259**, L79.

Iben, I. Jr., and Renzini, A. 1982, *Ap. J. (Letters)*, **263**, L23.

Iben, I. Jr., and Renzini, A. 1983, *Ann. Rev. Astr. Ap.*, **21**, 271.

Johnson, H. R., Mould, J. R., and Bernat, A. P. 1982, *Ap. J.*, **258**, 161.

Keenan, P. C., and Morgan, W. W. 1941, *Ap. J.*, **94**, 501.

Kogon, C. S., and Wehlau, A. 1974, *Astr. J.*, **79**, 387.

Landolt, A. U. 1983, *Astr. J.*, **88**, 439.

Lee, O. J., Baldwin, R. B., Hamlin, D. W., and Kinnaird, R. F. 1940, *Ann. Dearborn Obs.*, **5**, Part 16.

Lloyd Evans, T. 1984, *M. N. R. A. S.*, **208**, 447.

Lloyd Evans, T., and Menzies, J. W. 1977, *M. N. R. A. S.*, **178**, 163.

Longmore, A. J., Hawarden, T. G., Webster, B. L., Goss, W. M., and Mebold, U. 1978, *M. N. R. A. S.*, **184**, 97P.

Mackay, C. D. 1986, *Ann. Rev. Astr. Ap.*, **24**, 255.

McAlary, C. W., Madore, B. F., McGonegal, R., McLaren, R. A., and Welch, D. L. 1983, *Ap. J.*, **273**, 539.

McClure, R. D. 1985, *J. R. A. S. Can.*, **79**, 277.

Morgan, W. W., Keenan, P. C., and Kellman E. 1943, in *An Atlas of Stellar Spectra*, (Chicago: University of Chicago Press), p. 27.

Mould, J. 1983, *Kitt Peak Newsletter*, No. 25, p. 11.

Mould, J., and Aaronson, M. 1986, *Ap. J.*, **303**, 10.

Mould, J. R., and McElroy, D. B. 1978, *Ap. J.*, **221**, 580.

Mould, J. R., and Siegel, M. J. 1982, *Publ. A. S. P.*, **94**, 223.

Mould, J., Stutman D., and McElroy, 1979, *Ap. J.*, **228**, 423.

Muchmore, D. O., Nuth, J. A., and Stencel, R. E. 1987, *Ap. J. (Letters)*, **315**, L141.

Nassau, J. J., and Blanco, V. M. 1954, *Ap. J.*, **120**, 129.

Nassau, J. J., and Blanco, V. M. 1957, *Ap. J.*, **125**, 195.

Nassau, J. J., and Colacevich, A. 1950, *Ap. J.*, **111**, 199.

Nassau, J. J., and van Albada, G. B. 1949, *Ap. J.*, **109**, 391.

Pagel, B. E. J., and Patchett, B. 1975, *M. N. R. A. S.*, **172**, 13.

Palmer, L. G., and Wing, R. F. 1982, *Astr. J.*, **87**, 1739.

Pearse, R. W. B., and Gaydon, A. G. 1963, *The Identification of Molecular Spectra*, (London: Chapman and Hall), p. 304.

Pike, C. D. 1976, *M. N. R. A. S.*, **177**, 257.

Ratnatunga, K. U., and Bahcall, J. N. 1985, *Ap. J. Suppl.*, **59**, 63.

Reid, N., and Mould, J. 1984, *Ap. J.*, **284**, 98.

Reid, N., and Mould, J. 1985, *Ap. J.*, **299**, 236.

Renzini, A., and Voli, M. 1981, *Astr. Ap.*, **94**, 175.

Richer, H. B., Crabtree, D. R., and Pritchet, C. J. 1984, *Ap. J.*, **287**, 138.

Richer, H. B., Pritchet, C. J., and Crabtree, D. R. 1985, *Ap. J.*, **298**, 240.

Richer, H. B., and Crabtree, D. R. 1985, *Ap. J. (Letters)*, **298**, L13.

Sandage, A. 1970, *Ap. J.*, **162**, 841.

Sandage, A. 1983, *Astr. J.*, **88**, 1569.

Sandage, A. 1986, *Astr. J.*, **91**, 496.

Sandage, A. R., and Walker, M. F. 1955, *Astr. J.*, **60**, 230.

Sandage, A., Smith, L. L., and Norton, R. H. 1966, *Ap. J.*, **144**, 894.

Sandage, A., and Carlson, G. 1985, *Astr. J.*, **90**, 1464.

Sandage, A., and Katem, B. 1964, *Ap. J.*, **139**, 1088.

Sandage, A., and Tammann, G. A. 1974, *Ap. J.*, **191**, 603.

Sandage, A., and Walker, M. F. 1966, *Ap. J.*, **143**, 313.

Sandage, A.R. 1953, *Astr. J.*, **58**, 61.

Sargent, W. L. W., and Lo, K-Y. 1986, in *Star Forming Galaxies*, ed. D. Kunth, T. X. Thuan, and J. T. T. Van (Paris: Editions Frontieres), p. 253

Sawyer Hogg, H. 1973, *Publ. David Dunlop Obs.*, **3**, No. 6.

Searle, L., and Thompson, I. 1987, personal commmunication.

Scalo, J. M., and Ross, J. E. 1976, *Astr. Ap.*, **48**, 219.

Schecter, P. L., and Caldwell, J. A. 1986, personal communication.

Schwarzschild, M. and Harm, R. 1965, *Ap. J.*, **142**, 855.

Stephenson, C. B. 1973, *Pub. Warner and Swasey Obs.*, **2**, No. 2.

Stetson, P. B. 1987, *Publ. A. S. P.*, **99**, 191.

Stetson, P. B. 1984, *DAOPHOT User's Manual.*

Ulrich, R. K. 1973, in *Explosive Nucleosynthesis*, ed. D. N. Schramm and W. D. Arnett (Austin: Univ. Texas), p. 139.

Walker and Mack 1986, *M. N. R. A. S.*, **220**, 69.

Walker, M. 1965, in *Stellar Evolution*, ed. R. F. Stein and A. G. W. Cameron (New York: Plenum), p. 403.

Wallerstein, G. 1973, *Ann. Rev. Astr. Ap.*, **11**, 115.

Webbink, R. F. 1985, in *IAU Symposium* No. 113, *Dynamics of Star Clusters*, ed. J. Goodman and P. Hut (Dordrecht: Reidel), p. 541.

Westerlund, B. E. 1960, Uppsala Ann. **4**, 7.

Westerlund, B. E. 1964, in *IAU Symposium* No. 20, *The Galaxy and the Magellanic Clouds*, ed. F. J. Kerr and A. W. Rodgers (Canberra: Aust. Acad. Sci.), p. 239.

Wing, R. F. 1967, Ph.D. Thesis, University of California, Berkeley.

Wing, R. F. 1971, in *Proceedings of the Conference on Late-Type Stars*, KPNO Contrib. No. 554, ed. G. W. Lockwood and H. M. Dyck, p. 145.

Wing, R. F., and Stock, J. 1973, *Ap. J.*, **186**, 979.

Wood, P. R. 1985, in *Cool Stars with Excesses of Heavy Elements*, ed. M. Jaschek and P. C. Keenan (Dordrecht: Reidel), p. 357.

Yahil, A., Tammann, G. A., and Sandage, A. 1977, *Ap. J.*, **217**, 903.

Yamashita, Y. 1972, *Ann. Tokyo Astron. Obs.*, **13**, 169.

Yamashita, Y. 1975, *Ann. Tokyo Astron. Obs.*, **15**, 47.

Zinn, R., and West, M. J. 1984, *Ap. J. Suppl.*, **55**, 45.

de Vaucouleurs, G., de Vaucouleurs, A., and Corwin, H. G. 1976, *The Second Reference Catalog of Bright Galaxies* (Austin: University of Texas Press).

van de Hulst, H. C. 1949, *Recherches Astronomiques de L'Observatoire D'Utrecht*, **11**, Part 2.

van den Bergh, S. 1971, *Ap. J.*, **76**, 1082.